TRACKING THE SOURCES AND FATES OF FLUORESCENT ORGANIC MATTER IN THE EUTROPHIC NEUSE RIVER ESTUARY, NORTH CAROLINA

Alexandria G. Hounshell

A dissertation submitted to the faculty at the University of North Carolina at Chapel Hill in partial fulfillment of the requirements for the degree of Doctor of Philosophy in the Department of Marine Sciences.

Chapel Hill
2019

Approved by:

Hans W. Paerl

Marc Alperin

Nathan S. Hall

Christopher L. Osburn

Michael F. Piehler

ABSTRACT

Alexandria G. Hounshell: Tracking the sources and fates of fluorescent organic matter in the eutrophic Neuse River Estuary, North Carolina
(Under the direction of Hans W. Paerl)

Eutrophication is defined as 'an increase in the rate of supply of organic matter (OM) to an ecosystem'. In estuaries, this can take two forms: an increase in allochthonous and an increase in autochthonous OM. The goal of this dissertation was to use spectrofluorometry, as excitation emission matrices (EEMs), and other measures of OM quantity and quality, to constrain the OM pool in the Neuse River Estuary (NRE) and to assess how climate change and human activities in the watershed are altering the quantity and quality of OM.

EEMs can be coupled with the statistical decomposition technique, parallel factor analysis (PARAFAC), to identify broad classes of fluorescent OM (FOM). The first chapter assessed the use of PARAFAC as applied to fluorescent dissolved OM (FDOM) and base extracted fluorescent particulate OM (BEFPOM) and determined the dominate sources of these two pools were different. The second chapter used multivariate statistics to identify sources of FOM. Results suggest the FDOM pool is composed of terrestrial, humic-like OM while the FPOM pool contains terrestrial, humic-like and autochthonous OM.

In the final chapters, I focused on how anthropogenic activities alter OM in the NRE. A dissolved organic carbon (DOC) source and sink term, under different riverine discharge conditions, was calculated to assess when the estuary acts as a processer versus a pipeline for DOC export. Results indicate the source and sink term was an order of magnitude less than

riverine loading and contained large variability. They do suggest the estuary may act as a pipeline for riverine DOC export to the coastal ocean following extreme events. Finally, I assessed the ability of estuarine phytoplankton and bacterial assemblages to use watershed dissolved organic nitrogen (DON) as a nutrient source. I used DON addition bioassays to assess the impact of wastewater treatment facility effluent, chicken and turkey litter leachate, and river DON on phytoplankton growth. Chicken litter leachate was the only treatment which stimulated phytoplankton growth. This research serves as a baseline for understanding the current FOM pool in the NRE and demonstrates how the OM pool may be changing in response to climatic and anthropogenic pressures.

ACKNOWLEDGEMENTS

Science is not conducted in a bubble and I am indebted to the dozens and dozens of people who have made the work that went into this dissertation possible. I enthusiastically thank all the current and past Paerl Lab members. They are the nuts and bolts of this work and I am forever grateful for the hundreds of ModMon runs, the hours of sample analysis, setting up bioassays, and for just being a vast knowledge base and invaluable resource. To my advisor, Hans Paerl for taking me into his lab, allowing me to pursue my own interests and ideas, and guiding me through this entire process. I thank all of my committee members for the many hours spent in committee meetings, all the comments and critiques, and the numerous nuggets of advice and wisdom: Specifically, Marc Alperin for his eye for detail and for the chance to be a part of his field classes; Nathan Hall for putting up with the barrage of random thoughts and questions; Chris Osburn for the technical know-how to get this all done and for helping me turn rough ideas into finished products; and to Mike Piehler for his abundant advice and for helping me navigate the 'elbow rubbing' side of science. I am incredibly grateful to have learned and watched from the very best and I look forward to continued collaborations in the future. I am also thankful to my family: to my parents for instilling a love of the aquatic world at a young age, for all of the adventures we've shared, and for always pushing me to question the world around me; and to my brother for making sure I reach the top of every mountain I climb. And, finally, thank you to all the wonderful friends I've made along the way: for your un-ending support, willingness to always listen, and the many belly laughs we've shared, have made it all worth it. Thank you!

TABLE OF CONTENTS

LIST OF TABLES

LIST OF FIGURES

LIST OF ABBREVIATIONS AND SYMBOLS

a_{254}	Absorbance at 254 nm
a_{350}	Absorbance at 350 nm
BEFPOM	Base extracted fluorescent particulate organic matter
BIX	Biological Index
C	Carbon
CDOM	Colored Dissolved Organic Matter
Chl *a*	Chlorophyll-*a*
CO_2	Carbon Dioxide
CoIA	Co-Inertia Analysis
DIN	Dissolved Inorganic Nitrogen
DO	Dissolved Oxygen
DOC	Dissolved Organic Carbon
DOM	Dissolved Organic Matter
DON	Dissolved Organic Nitrogen
EEMs	Excitation Emission Matrices
EWE	Extreme weather event
FDOM	Fluorescent Dissolved Organic Matter
FI	Fluorescent Intensity
FOM	Fluorescent Organic Matter
FPOM	Fluorescent Particulate Organic Matter
HCl	Hydrochloric Acid

HIX	Humification Index
ModMon	Neuse River Estuary Modeling and Monitoring Project
N	Nitrogen
NaOH	Sodium hydroxide
NH_4^+	Ammonium
nMDS	Non-metric multidimensional scaling
NO_2^-	Nitrite
NO_3^-	Nitrate
NR	Neuse River
NRE	Neuse River Estuary
OC	Organic Carbon
OM	Organic Matter
ON	Organic Nitrogen
P	Phosphorus
PAR	Photosynthetically Active Radiation
PARAFAC	Parallel Factor Analysis
PCA	Principal Component Analysis
pCO_2	Partial pressure of Carbon Dioxide
PN	Particulate Nitrogen
PO_4^{3-}	Phosphate
POC	Particulate Organic Carbon
POM	Particulate Organic Matter
PP	Primary Productivity

PS	Pamlico Sound
PSC	Pulse Shunt Concept
PSU	Practical Salinity Units
Q	Discharge
Q.S.E.	Quinine Sulfate Equivalents
Q.S.U.	Quinine Sulfate Units
RDA	Redundancy Analysis
RM-ANOVA	Repeated Measures Analysis of Variance
Sal	Salinity
$SUVA_{254}$	Specific Absorption at 254 nm
TCC	Tucker's Congruence Coefficient
TDN	Total Dissolved Nitrogen
tDOC	Terrestrial Dissolved Organic Carbon
Temp	Temperature
TMDLs	Total Maximum Daily Loads
TOC	Total Organic Carbon
Turb	Turbidity
WRTDS	Weighted Regression on Time, Discharge, and Season
WWTF	Wastewater Treatment Facility

CHAPTER 1: INTRODUCTION AND MOTIVATION

Organic matter (OM) plays an important role in regulating key processes in aquatic systems including: light availability (Osburn et al., 2009), the complexation and transport of metals (Bergamaschi et al., 2012), transport of pollutants (Ripszam et al., 2015), a carbon (C) substrate for microbial respiration (Moran et al., 2000) and a nutrient source, as either nitrogen, N or phosphorus, P, to primary production (Boyer et al., 2006; Bronk et al., 2007). Additionally, OM plays an important role in controlling the eutrophication status of an ecosystem. Eutrophication, as defined by Nixon, 1995, is 'an increase in the rate of supply of OM to an ecosystem'. In coastal, aquatic ecosystems, this can either be in the form of terrestrial OM flushed into the system from the watershed (i.e., allochthonous OM) or from autochthonous OM produced when phytoplankton convert inorganic nutrients (as N and P) to biomass *in situ* (Nixon, 1995). Both pathways of eutrophication can lead to negative impacts on affected coastal ecosystems, including bottom water hypoxia/anoxia, fish kills, habitat degradation, and the formation of nuisance or harmful algal blooms, all of which disrupt ecosystem function and can lead to cascading negative impacts up the food web (Cloern, 2001; Nixon, 1995).

Eutrophication has been a widely recognized problem in coastal ecosystems, including estuaries, for several decades and efforts have been enacted in an attempt to reduce eutrophication and its associated negative impacts (Cloern, 2001). These efforts have mainly been aimed at reducing inorganic nutrient loading to limit autochthonously produced OM (i.e., phytoplankton blooms) by controlling N and P loading through nutrient criteria and total maximum daily loads (TMDLs). As such, nutrient reduction efforts have largely focused on

point-sources (i.e., wastewater treatment facilities – WWTF; agricultural operations; industrial inputs) historically high in dissolved inorganic N (Lebo et al., 2012; Paerl et al., 2004). While these efforts have led to a reduction in inorganic N loading, there has been a reported increase in organic N (ON) to riverine and estuarine ecosystems (Pellerin et al., 2006, Lebo et al., 2012, Harrington and Bowen, 2017), including in response to expected increases in precipitation due to climate change (Gabriel et al., 2015). Additionally, chlorophyll *a* (Chl *a*) concentrations, used as a proxy for phytoplankton biomass and as a measure for the effectiveness of enacted nutrient reductions, have not been shown to decrease in response to the decreasing N loading in many of these systems (Cloern, 2001; Paerl et al., 2010, Lebo et al., 2012, Keith, 2014).

Terrestrial OM loading is also an important factor in terms of eutrophication, either as an increase in the rate of supply of terrestrial OM to the system or as a nutrient source, specifically as a N-source, supporting phytoplankton growth (Berman and Bronk, 2003; Bronk et al., 2007; Eom et al., 2017; Seitzinger et al., 2002). Historically, identifying and tracking OM, both as terrestrial and autochthonous OM sources, has been time consuming and expensive. These constraints limited the number of samples that could be collected and used to assess the temporal and spatial variability of OM in an ecosystem, making it difficult to resolve the sources, fates, and role OM plays in eutrophication and its potential role in stimulating phytoplankton growth. More recently, the use of spectrofluorometry (i.e., fluorescence) in conjunction with bulk OM measurements, have been used to rapidly and broadly characterize the OM pool in a variety of aquatic ecosystems, including estuaries (Brym et al., 2014; Coble, 1996; Jaffé et al., 2014; Markager et al., 2011; Osburn et al., 2012; Stedmon and Markager, 2005).

Using a combination of techniques, it is possible to obtain a broad overview of the quantity and quality of OM, as both fluorescent dissolved OM (FDOM) and fluorescent particulate OM

(FPOM), as well as assess the sources and fates of broad classes of fluorescent OM (FOM) *in situ*. Spatially, the sources of OM to many estuaries transition from allochthonous, terrestrial sources in the upper estuary where riverine loading is the main driver of OM to more autochthonous sources of OM produced *in situ* (i.e., phytoplankton and microbial production) (Canuel and Hardison, 2016; Markager et al., 2011). The transition from allochthonous in the upper estuary to autochthonous OM in the mid to lower estuary is due to a combination of physical, chemical, and biological processes including: conservative mixing as the highly concentrated riverine water mixes with less concentrated marine water (Markager et al., 2011); photochemical and microbial degradation which transforms and removes allochthonous and autochthonous sources of OM (McCallister et al., 2006; Osburn et al., 2009; Stedmon and Markager, 2005); and production and consumption of OM *in situ* by phytoplankton and microbial assemblages (McCallister et al., 2006). Temporally, the sources and fates of OM in estuaries are highly variable and are largely driven by seasonal changes occurring in both the watershed (i.e., hydrologic flow path, leaf litter fall, seasonal precipitation patterns) (Singh et al., 2014) and in the estuary (i.e., photochemical and microbial degradation, phytoplankton production) (Canuel and Hardison, 2016). However, in addition to seasonal changes, temporal OM changes are also heavily driven by physical conditions affecting the estuary, including riverine discharge and wind-driven sediment resuspension events (Canuel and Hardison, 2016; Crosswell et al., 2017; Dixon et al., 2014; Osburn et al., 2012).

The OM pool is operationally divided into dissolved OM (DOM) and particulate OM (POM) as defined by filtration, such that anything greater than 0.7 μm is considered POM and anything smaller than 0.7 μm is considered DOM. This operationally defined size classification has important implications for how we think about the sources, fates, and bio-reactivity of the DOM

and POM pools, respectively (Canuel and Hardison, 2016; McCallister et al., 2006; Osburn et al., 2012). The DOM pool is mainly composed of allochthonous and bacterially degraded DOM while the POM pool is generally thought to be comprised of both allochthonous sources and autochthonous POM generated by phytoplankton growth *in situ* (McCallister et al., 2006). The sources, molecular size, and chemical structure of the DOM and POM pools influence its bio-reactivity and ultimate fate in estuarine environments (McCallister et al., 2006; Raymond and Bauer, 2001). McCallister et al., (2006) hypothesized the highly terrestrial and bacterial nature of the DOM pool in estuaries was due to the rapid conversion of autochthonous DOM by bacteria *in situ* while the autochthonous nature of POM is allowed to persist due to its lower bio-reactivity. Studies have also demonstrated transformations between the POM and DOM pool (Asmala et al., 2018), especially along the estuarine turbidity maximum where POM concentrations are high and sediment resuspension events are common (Canuel and Hardison, 2016). However, few studies have simultaneously assessed the quality and quantity of both DOM and POM spatially and temporally in estuarine ecosystems (McCallister et al., 2006; Osburn et al., 2012).

The goal of this study was to better understand the similarities, differences, and linkages between the sources and transformations of the FDOM and FPOM pools in estuarine environments and to provide a baseline and understanding for how the FOM pool in estuaries is changing due to climatic and anthropogenic pressures. This includes how an increasing frequency of extreme precipitation events, as predicted due to climate change (Bender et al., 2009; Janssen et al., 2016) may alter dissolved OC (DOC) cycling in estuarine environments as well as how an increase in dissolved ON (DON) from anthropogenic watershed sources may contribute to continued instances of nuisance phytoplankton blooms. Taken collectively, my research has led to a better understanding of the dominant sources and fates of terrestrial and

autochthonous FOM in a eutrophic estuarine environment, the Neuse River Estuary (NRE), North Carolina, USA, including following an extreme precipitation event. The research will further our understanding of the transport of and role terrestrial and autochthonous OM plays in stimulating and sustaining eutrophication and its negative impacts in coastal, estuarine systems.

The first part of this study, chapter 2 focused on the use of spectrofluorometry as EEMs coupled with PARAFAC (EEM-PARAFAC) to assess the sources and transformations of both the FDOM and base extracted FPOM (BEFPOM) pools simultaneously, in the NRE. The goal of this chapter was to assess the use and utility of PARAFAC modeling to understand differences in the FDOM and BEFPOM pools in estuarine environments as well as to identify and track an estuarine FDOM signal (i.e., phytoplankton and microbial production plus photochemical and microbial degradation of FDOM) *in situ*. Ultimately, the identified estuarine FDOM signal could be incorporated into an existing FDOM source-based PARAFAC model, FluorMod (Osburn et al., 2016), and used to track watershed and autochthonous sources of FDOM through a dynamic, eutrophic estuary. Results from this chapter highlight the differences, in terms of dominate sources, of the FDOM and BEFPOM pools. Additionally, an estuarine FDOM signal was identified using experimental bioassays; however, the signal was not identified in FDOM samples collected from the NRE due to the overwhelming fluorescence intensity of terrestrial FDOM *in situ*.

Chapter 3 continued to assess differences in the FDOM and FPOM pools in the NRE by using a combination of bulk OM analyses as well as fluorescence (EEMs) and absorbance (as colored DOM, CDOM) to characterize the DOM and POM pools, respectively. Multivariate statistical analyses including principal components analysis (PCA), redundancy analysis (RDA) and co-inertia analysis (CoIA) were used not only to understand the sources and transformations

of DOM and POM in the NRE, but also to identify potential linkages and transformations between the DOM and POM pools *in situ*. Results from this chapter demonstrate the utility of using multivariate techniques originally designed for analysis of ecological data sets, as applied to data sets of environmental parameters, DOM, and POM to assess the relationships and drivers between these three sets of measurements.

While chapters 2 and 3 serve as a baseline for understanding the current dynamics of FDOM and FPOM in eutrophic estuaries, Chapter 4 assessed how DOM dynamics in the NRE may change under increasing frequency of extreme precipitation events due to climate change. A non-steady state box model approach was used to constrain flow into and out of the marine end member and to calculate DOC and CDOM (as absorbance measured at 350 nm, a_{350}) source and sink terms under varying riverine discharge conditions, spanning from baseflow to extreme flow (4^{th} to 99^{th} flow quantiles, respectively). The study also incorporated measurements of CO_2 efflux and phytoplankton primary production to provide linkages between observed DOC dynamics and both potential DOC degradation and production processes, as respiration of DOC to CO_2 and primary production, in the estuary. The variability of the resolved values from the salinity and OM box models was high, indicating the coarse spatial and temporal scale used for both the estuarine monitoring effort and box model approach was not able to accurately constrain *in situ* dynamics in this estuary. Following extreme riverine discharge events, however, results indicate the estuary acted as a river system leading to potential export of un-altered riverine OM to the coastal end member, similar to the Pulse-Shunt Concept as applied to stream and river systems (Raymond et al., 2016). This has important implications for the role of estuaries as a pipeline for the export of un-altered, riverine OM especially in light of predicted increases in extreme precipitation events due to climate change (Janssen et al., 2016, Bender et al., 2009).

Finally, chapter 5 focused on the role watershed FDOM sources may play as a nutrient source, specifically as an N (DON) source, for stimulating phytoplankton growth in the NRE. Using a series of experimental watershed DON addition bioassays, I determined chicken litter leachate was capable of stimulating phytoplankton growth in excess of that stimulated by the inorganic nutrients contained in this source alone. Using the EEM-PARAFAC technique, I identified a fluorescence signal which may be responsible for stimulating this excess growth. I demonstrated that other watershed sources of DON (WWTF effluent, turkey litter leachate, concentrated river DON) do not stimulate phytoplankton growth.

Taken collectively, overarching results from this study suggest the FOM pool in the NRE was overwhelmingly dominated by terrestrial FDOM. The DOC pool was 85% of the total organic C (TOC) while the POC pool represented 15% of TOC, as was indicated by bulk concentrations. In terms of OM quality, FDOM results suggest the FDOM pool was almost completely dominated by terrestrial, humic-like FOM (93% allochthonous FDOM; 7% autochthonous FDOM). While FPOM results did indicate the FPOM pool contains compounds from both allochthonous (37%) and autochthonous (63%) sources, the relative amounts of autochthonous FPOM compared to the overall FOM pool, were small (~ 4%). The dominance of terrestrial fluorescent signals, particularly in the FDOM pool, made it difficult to identify fluorescent signatures unique to biological production, degradation, or transformations *in situ* (Murphy et al., 2018; Stedmon and Markager, 2005). While the dominant terrestrial fluorescent signals made it difficult to identify biological fluorescent signals *in situ*, it was possible to identify these signals using experimental techniques, as demonstrated in this study. With the identification of some ‘global’ reference that captures the dominate terrestrial fluorescent signals

and can be subtracted from measured EEMs collected in aquatic ecosystems, it may be possible to capture these same biological signals *in situ* (Murphy et al., 2018).

Results from the last two chapters demonstrated that the OM pool, specifically the DOM pool, in the NRE is changing. This includes changes associated with the increase in recent extreme precipitation events, as predicted in response to climate change (Bender et al., 2009; Janssen et al., 2016), which were shown to alter how the estuary exports DOC to the coastal end member, as well as changes to the sources of watershed nutrients, as DON. Overall, within the time scale of exposure (days to several weeks), sources of watershed DON generally do not appear to stimulate growth of phytoplankton and microbial assemblages in estuarine environments, in excess of the inorganic nutrients contained in these sources. Chicken litter leachate, however, did stimulate phytoplankton growth in excess of growth stimulated by the inorganic nutrients contained in this source, indicating management of watershed sources of DON may benefit from a targeted approach.

REFERENCES

Asmala, E., Haraguchi, L., Markager, S., Massicotte, P., Riemann, B., Staehr, P.A., Carstensen, J., 2018. Eutrophication Leads to Accumulation of Recalcitrant Autochthonous Organic Matter in Coastal Environment. Global Biogeochemical Cycles 32, 1673–1687. https://doi.org/10.1029/2017GB005848

Bender, M.A., Knutson, T.R., Tuleya, R.E., Sirutis, J.J., Vecchi, G.A., Garner, S.T., Held, I.M., 2009. Modeled Impact of Anthropogenic Atlantic Hurricanes. Science 327, 454–458.

Bergamaschi, B.A., Krabbenhoft, D.P., Aiken, G.R., Patino, E., Rumbold, D.G., Orem, W.H., 2012. Tidally Driven Export of Dissolved Organic Carbon, Total Mercury, and Methylmercury from a Mangrove-Dominated Estuary. Environmental Science & Technology 46, 1371-1378. https://doi.org/10.1021/es2029137

Berman, T., Bronk, D.A., 2003. Dissolved organic nitrogen: a dynamic participant in aquatic ecosystems. Aquatic Microbial Ecology 31, 279–305. https://doi.org/10.3354/ame031279

Boyer, J.N., Dailey, S.K., Gibson, P.J., Rogers, M.T., Mir-Gonzalez, D., 2006. The role of dissolved organic matter bioavailability in promoting phytoplankton blooms in Florida Bay. Hydrobiologia 569, 71–85. https://doi.org/10.1007/s10750-006-0123-2

Bronk, D.A., See, J.H., Bradley, P., Killberg, L., 2007. DON as a source of bioavailable nitrogen for phytoplankton. Biogeosciences 4, 283–296.

Brym, A., Paerl, H.W., Montgomery, M.T., Handsel, L.T., Ziervogel, K., Osburn, C.L., 2014. Optical and chemical characterization of base-extracted particulate organic matter in coastal marine environments. Marine Chemistry 162, 96–113. https://doi.org/10.1016/j.marchem.2014.03.006

Canuel, E.A., Hardison, A.K., 2016. Sources, Ages, and Alteration of Organic Matter in Estuaries. Annual Review of Marine Science 8, 409–434. https://doi.org/10.1146/annurev-marine-122414-034058

Cloern, J.E., 2001. Our evolving conceptual model of the coastal eutrophication problem. Marine Ecology Progress Series 210, 223–253. https://doi.org/10.3354/meps210223

Coble, P.G., 1996. Characterization of marine and terrestrial DOM in seawater using excitation-emission matrix spectroscopy. Marine Chemistry 51, 325–346. https://doi.org/10.1016/0304-4203(95)00062-3

Crosswell, J.R., Anderson, I.C., Stanhope, J.W., Dam, B. Van, Brush, M.J., Ensign, S., Piehler, M.F., Mckee, B., Bost, M., Paerl, H.W., 2017. Carbon budget of a shallow, lagoonal estuary: Transformations and source-sink dynamics along the river-estuary-ocean continuum. Limnology and Oceanography 62, S29–S45. https://doi.org/10.1002/lno.10631

Dixon, J.L., Osburn, C.L., Paerl, H.W., Peierls, B.L., 2014. Seasonal changes in estuarine dissolved organic matter due to variable flushing time and wind-driven mixing events. Estuarine, Coastal and Shelf Science 151, 210–220. https://doi.org/10.1016/j.ecss.2014.10.013

Eom, H., Borgatti, D., Paerl, H.W., Park, C., 2017. Formation of Low-Molecular-Weight Dissolved Organic Nitrogen in Predenitrification Biological Nutrient Removal Systems and Its Impact on Eutrophication in Coastal Waters. Environmental Science & Technology 51, 3776–3783. https://doi.org/10.1021/acs.est.6b06576

Gabriel, M., Knightes, C. Cooter, E., Dennis R., 2016. Evaluating relative sensitivity of SWAT-simulated nitrogen discharge to projected climate and land cover changes in two watersheds in North Carolina, USA. Hydrological Processes 30, 1403-1418. https://doi.org/10.1002/hyp.10707

Harrington, N., Bowen, J.D., 2017. Comparing the impact of organic versus inorganic nitrogen loading to the Neuse River Estuary with a mechanistic eutrophication model. Report submitted to NC WRRI. Report no. 470. Raleigh, NC.

Jaffé, R., Cawley, K.M., Yamashita, Y., 2014. Applications of Excitation Emission Matrix Fluorescence with Parallel Factor Analysis (EEM-PARAFAC) in Assessing Environmental Dynamics of Natural Dissolved Organic Matter (DOM) in Aquatic Environments. A Review, in: Advances in the Physiochemical Characterization of Dissolved Organic Matter: Impact on Natural and Engineered Systems. pp. 28–73.

Janssen, E., Sriver, R.L., Wuebbles, D.J., Kunkel, K.E., 2016. Seasonal and regional variations in extreme precipitation event frequency using CMIP5. Geophysical Research Letters 43, 5385–5393. https://doi.org/10.1002/2016GL069151

Keith, D.J., 2014. Satellite remote sensing of chlorophyll *a* in support of nutrient management in the Neuse and Tar-Pamlico river (North Carolina) estuaries. Remote sensing of the environment 153, 61-78. https://doi.org/10.1016/j.rse.2014.05.019

Lebo, M.E., Paerl, H.W., Peierls, B.L., 2012. Evaluation of progress in achieving TMDL mandated nitrogen reductions in the Neuse river basin, North Carolina. Environmental Management 49, 253–266. https://doi.org/10.1007/s00267-011-9774-5

Markager, S., Stedmon, C.A., Søndergaard, M., 2011. Seasonal dynamics and conservative mixing of dissolved organic matter in the temperate eutrophic estuary Horsens Fjord. Estuarine, Coastal and Shelf Science 92, 376–388. https://doi.org/10.1016/j.ecss.2011.01.014

McCallister, S.L., Bauer, J.E., Ducklow, H.W., Canuel, E.A., 2006. Sources of estuarine dissolved and particulate organic matter: A multi-tracer approach. Organic Geochemistry 37, 454–468. https://doi.org/10.1016/j.orggeochem.2005.12.005

Moran, M.A., Sheldon, W.M., Zepp, R.G., 2000. Carbon loss and optical property changes during long-term photochemical and biological degradation of estuarine dissolved organic matter. Limnology and Oceanography 45, 1254–1264.

Murphy, K.R., Timko, S.A., Gonsior, M., Powers, L.C., Wünsch, U.J., Stedmon, C.A., 2018. Photochemistry Illuminates Ubiquitous Organic Matter Fluorescence Spectra. Environmental Science & Technology 52, 11243–11250. https://doi.org/10.1021/acs.est.8b02648

Nixon, S.W., 1995. Coastal marine eutrophication: A definition, social causes, and future concerns. Ophelia 41, 199–219.

Osburn, C.L., Handsel, L.T., Mikan, M.P., Paerl, H.W., Montgomery, M.T., 2012. Fluorescence tracking of dissolved and particulate organic matter quality in a river-dominated estuary. Environmental Science & Technology 46, 8628–8636. https://doi.org/10.1021/es3007723

Osburn, C.L., Handsel, L.T., Peierls, B.L., Paerl, H.W., 2016. Predicting Sources of Dissolved Organic Nitrogen to an Estuary from an Agro-Urban Coastal Watershed. Environmental Science & Technology 50(16), 8473-8484. https://doi.org/10.1021/acs.est.6b00053

Osburn, C.L., O'Sullivan, D.W., Boyd, T.J., 2009. Increases in the longwave photobleaching of chromophoric dissolved organic matter in coastal waters. Limnology and Oceanography 54, 145–159. https://doi.org/10.4319/lo.2009.54.1.0145

Paerl, H.W., Rossignol, K.L., Hall, N.S., Peierls, B.L., Wetz. M.S., 2010. Phytoplankton community indicators of short- and long-term ecological change in the anthropogenically and climatically impacted Neuse River Estuary, North Carolina, USA. Estuaries and Coasts 33(2), 485-497. https://doi.org/10.1007/s12237-009-9137-0

Paerl, H.W., Valdes, L.M., Joyner, A.R., Piehler, M.F., Lebo, M.E., 2004. Solving problems resulting from solutions: Evolution of a dual nutrient management strategy for the eutrophying Neuse River Estuary, North Carolina. Environmental Science & Technology 38, 3068–3073. https://doi.org/10.1021/es0352350

Pellerin, B.A., Kaushal, S.S., McDowell, W.H., 2006. Does anthropogenic nitrogen enrichment increase organic nitrogen concentrations in runoff from forested and human-dominated watersheds? Ecosystems 9, 852-864. https://doi.org/10.1007/s10021-006-0076-3

Raymond, P.A., Bauer, J.E., 2001. Use of ^{14}C and ^{13}C natural abundances for evaluating riverine, estuarine, and coastal DOC and POC sources and cycling: A review and synthesis. Organic Geochemistry 32, 469–485. https://doi.org/10.1016/S0146-6380(00)00190-X

Ripszam, M., Paczkowska, J., Veenaas, C., Haglund, P., 2015. Dissolved Organic Carbon Quality and Sorption of Organic Pollutants in the Baltic Sea in Light of Future Climate Change. Environmental Science & Technology 49, 1445-1452. https://doi.org/10.1021/es504437s

Seitzinger, S.P., Sanders, R.W., Styles, R., 2002. Bioavailability of DON from natural and anthropogenic sources to estuarine plankton. Limnology and Oceanography 47, 353–366. https://doi.org/10.4319/lo.2002.47.2.0353

Stedmon, C. A., Markager, S., 2005. Tracing the production and degradation of autochthonous fractions of dissolved organic matter using fluorescence analysis. Limnology and Oceanography 50, 1415–1426. https://doi.org/10.4319/lo.2005.50.5.1415

Singh, S., Inamdar, S., Mitchell, M., McHale, P, 2014. Seasonal pattern of dissolved organic matter (DOM) in watershed sources: influence of hydrologic flow paths and autumn leaf fall. Biogeochemistry 118(1-3), 321-337. https://doi.org/10.1007/s10533-013-9934-1

CHAPTER 2: USING EXCITATION EMISSION MATRICES COUPLED WITH PARALLEL FACTOR ANALYSIS (EEM-PARAFAC) TO CHARACTERIZE FLUORESCENT ORGANIC MATTER SIGNATURES, SOURCES AND TRANSFORMATIONS IN THE NEUSE RIVER ESTUARY, NORTH CAROLINA

1. Summary

Spectrofluorometric scans, as excitation emission matrices (EEMs), coupled with the statistical decomposition technique, parallel factor analysis (PARAFAC) have been used since the early 2000's to assess the fluorescent organic matter (FOM) pool in a variety of aquatic ecosystems. Originally developed for fluorescent dissolved organic matter (FDOM), the technique has since been applied to base extracts of fluorescent particulate organic matter (FPOM) and can now be used to assess the base extracted fluorescent POM (BEFPOM) pool. The EEM-PARAFAC technique has been used almost exclusively as a sample-based model such that a PARAFAC model is applied to samples collected from an ecosystem of interest. Recently, the application of a source-based PARAFAC model has been explored, such that a PARAFAC model is generated on EEMs of FOM sources (i.e., watershed sources) and then applied to sample EEMs collected from the ecosystem of interest as a means to identify and track different FOM watershed sources *in situ*. The goal of this study was to explore the utility of PARAFAC modeling as applied to FDOM and FPOM samples collected from the eutrophic Neuse River Estuary (NRE), North Carolina, USA to understand FOM signatures, sources, and transformations *in situ*. This was accomplished in two ways: 1. Compare PARAFAC models generated on three sets of data (FDOM, BEFPOM, and FDOM+BEFPOM EEM samples) to understand the similarities and differences between these pools and 2. Experimentally identify a

FDOM estuarine processing signal that could be used as part of a watershed source-based PARAFAC model to track allochthonous and autochthonous sources of FDOM. Results suggest the FDOM and FPOM pools are sufficiently different to warrant separate PARAFAC models, highlighting the different sources between these two pools. Additionally, while an estuarine FDOM signal, which represented both FDOM signals of production and degradation, was identified using seasonal experimental bioassays and was included in a source-based PARAFAC model, when applied to estuarine samples collected *in situ* the source-based model was unable to accurately identify FDOM dynamics. This study highlights some of the potential applications and shortcomings of using PARAFAC modeling to assess the FOM pool, as both FDOM and BEFPOM in a eutrophic estuary, such as the NRE.

2. Introduction

Excitation-emission matrices (EEMs) coupled with Parallel Factor Analysis (PARAFAC) has proven to be a quick, cost-effective, and robust means of analyzing fluorescent organic matter (FOM) in aquatic environments (Murphy et al., 2013). The technique relies on the ability of organic molecules to absorb light and re-emit that light as fluorescence, due to its conjugated molecular structure, most often derived from aromatic rings and multi-bond structure (Aiken, 2014). While the EEM-PARAFAC technique is not capable of directly identifying individual OM molecules or molecular structures, it does provide a robust overview of the dominant patterns in the broader aquatic FOM pool, allowing for the relative sources, transport, and transformations of the FOM pool to be assessed (Stubbins et al., 2014).

While the EEM-PARAFAC technique was originally developed for FDOM samples, it has since been applied to extracts of base-extracted fluorescent particulate organic matter (BEFPOM) (Osburn et al. 2012). This method allows for studies that simultaneously assess both

the FDOM and BEFPOM pools in aquatic ecosystems. Studies that have used the EEM-PARAFAC technique to assess both the FDOM and BEFPOM pools have used a combined PARAFAC model approach, whereby both FDOM and BEFPOM samples are collectively modeled with a single PARAFAC model (Osburn et al., 2015, 2012). However, it is well established in the literature, that the sources, transformations, and reactivity of these two OM pools are different, especially in estuarine environments where there are sources of both allochthonous, terrestrial derived-material and autochthonous OM or OM material produced in the estuary (i.e., via phytoplankton and/or microbial production) (Asmala et al., 2018; McCallister et al., 2006; Osburn et al., 2012; Raymond and Bauer, 2001).

In estuaries, the dissolved OM (DOM) pool is largely composed of terrestrial-like material while the particulate OM (POM) pool is a combination of both terrestrial-like sources as well as POM produced *in situ* by phytoplankton biomass (McCallister et al., 2006; Osburn et al., 2012). While the POM pool is comprised of seemingly more labile material than DOM, it is hypothesized the DOM pool is more biologically reactive and is available for heterotrophic utilization (McCallister et al., 2006; Raymond and Bauer, 2001). The utilization of biologically-reactive components from the DOM pool, rapidly and selectively remove this type of DOM, leaving a more terrestrial, humic-like signature in the overall DOM pool (McCallister et al., 2006). The sources and degradation pathways of DOM and POM, respectively, have important implications for understanding the structure and composition of each pool at any given location in the estuary. In this study, I explore the ability of PARAFAC to model FDOM and BEFPOM samples together in a single model versus individually modeling each FOM pool separately in order to fully capture the variability and transformations of these two pools through estuarine environments.

Additionally, most generated PARAFAC models are sample-based models, such that a PARAFAC model is developed on EEMs collected from samples representative of the ecosystem of interest. However, models, more broadly can either be classified as sample based, as most historical EEM-PARAFAC models developed, or they can be source based models, such that the known sources are characterized and modeled and then applied to samples collected from the ecosystem of interest. Osburn et al., (2016) was the first study to develop a source-based PARAFAC model that was then applied to EEM samples collected in the ecosystem of interest, in this case the Neuse River, to track the various watershed FDOM sources through the river system. How a source based PARAFAC model, however, would be applied to a system, such as an estuary, is unclear. Specifically, in estuarine systems there are several processes which may dilute, obscure, and transform FDOM source signals *in situ*. Compared to riverine systems, estuaries have much longer residence times allowing for the degradation and transformation (i.e., microbial and photo-degradation) of FDOM *in situ* which acts to both obscure and alter FDOM source signals (Stedmon and Markager, 2005a). Additionally, allochthonous FDOM source signals in estuaries are diluted by mixing with the marine end-member (Markager et al., 2011). Thus, the applicability of a source-based model to estuarine samples is unclear and may be limited to systems where allochthonous sources can be accurately constrained and *in situ* OM production and transformations are limited, as in stream or river systems (Osburn et al., 2016).

The main goals of this study were to explore the use of PARAFAC modeling as applied to both FDOM and FPOM samples collected simultaneously from the Neuse River Estuary (NRE), North Carolina (NC), by 1. Exploring the differences and relationships between the FDOM and FPOM pools via PARAFAC modeling and 2. Exploring and potentially expanding the use of a source-based PARAFAC model to track watershed FDOM sources in samples collected from a

dynamic, estuarine ecosystem that contains both autochthonous and allochthonous FOM as well as *in situ* degradation and transformation processes. Additionally, results from this study were used to capture fluorescence signals that could be identified and used as an estuarine FDOM signal *in situ* and for assessing mechanisms controlling the production and degradation of autochthonous FDOM in estuarine ecosystems. The study followed a two-pronged approach:

1. FDOM and BEFPOM PARAFAC modeling: In order to assess the similarities and differences between the FDOM and BEFPOM pools, three separate PARAFAC models (FDOM, BEFPOM, and FDOM+BEFPOM) were applied to samples collected as part of a year-long environmental assessment of FDOM and BEFPOM in the NRE. The three models were compared to assess the relative similarities and differences between each of the models and the respective FDOM and BEFPOM pools. Additionally, modeling results in conjunction with additional environmental parameters collected were used to assess the sources and transformations of these two pools *in situ*. This first section of the study addressed two main questions:
    a. What are the similarities and differences of the BEFPOM and FDOM pools? What do these similarities and differences indicate about the sources of these FOM pools?
    b. During PARAFAC modeling, does one FOM pool (either BEFPOM or FDOM) exert a greater influence on the identified PARAFAC components? Can the two FOM pools be successfully modeled together or do the two FOM pools require separate BEFPOM and FDOM models?
2. Seasonal experimental bioassays: Experimental bioassays were conducted to capture a FDOM signal that was unique to estuarine production and degradation processes. The identified fluorescent signal was then used in conjunction with the previously developed

9-component PARAFAC model (FluorMod) and associated mixing model, developed on Neuse River watershed source samples (Osburn et al., 2016), to track both allochthonous and autochthonous sources through the NRE. The second part of the study addressed the following questions:

a. Can fluorescent signals be identified that are unique to FDOM production and transformation in estuarine environments? And if yes, can these fluorescent signals be accurately identified in samples collected *in situ*?
b. What is the applicability of a source-based model to monitoring FDOM in estuarine waters that contain sources of both allochthonous and autochthonous FDOM?

Results from this study helped to constrain the applicability and limitations of using and developing PARAFAC models on different fractions of the FOM pool in estuarine ecosystems. These results included the differences between the BEFPOM and FDOM pools as well as the applicability of a source based PARAFAC model to estuarine water samples. Additionally, the study addressed important questions about the similarities and differences between the BEFPOM and FDOM pools and helped identify the sources of these two pools in estuarine environments. The study also identified a fluorescent signal unique to the production and degradation of FDOM in estuarine ecosystems and explored potential mechanisms for the production and degradation of this identified signal.

3. Methods

3.1 Sample collection

Samples for PARAFAC model comparisons (FDOM, BEFPOM, FDOM+BEFPOM) were collected from the NRE, located in Eastern NC. A year-long environmental survey was conducted from July 20, 2015 to July 18, 2016 in coordination with the long term (1994 to

present) University of North Carolina-Chapel Hill (UNC-CH) NRE Modeling and Monitoring (ModMon) program (Paerl et al., 2014). Briefly, samples were collected at 11 stations located along the main axis of the estuary from the head of the estuary near Streets Ferry Bridge (Station 0) to a location near the entrance to Pamlico Sound (Station 180) (Figure 2.1). Samples were collected twice monthly in the spring, summer, and fall (March – November) and monthly during the winter (November – February). Temperature (Temp), salinity (Sal), turbidity (Turb), and dissolved oxygen (DO) were measured at surface (0.2 m below surface) and bottom (0.5 m above bottom) depths using a YSI 6600 multi-parameter, water quality sonde (Hall et al., 2013). At each station, water samples were collected from near-surface (0.5 m below surface) and bottom (~0.5 m from bottom) for various biological and chemical analyses. Water samples were returned to the UNC-CH Institute of Marine Sciences (IMS) within ~ 6 hours of collection and filtered through combusted (450^{o}C for 4 hours) glass fiber filters (GF/F) with a 0.7 µm pore size. Filters were collected for particulate analyses (particulate organic carbon, POC; particulate nitrogen, PN; Chlorophyll-*a*, Chl *a*; and FPOM) and the filtrate collected for dissolved analyses (dissolved organic carbon, DOC; dissolved organic nitrogen, DON; and FDOM). Collected filters and filtrate were stored frozen (-20^{o}C) in the dark until analysis.

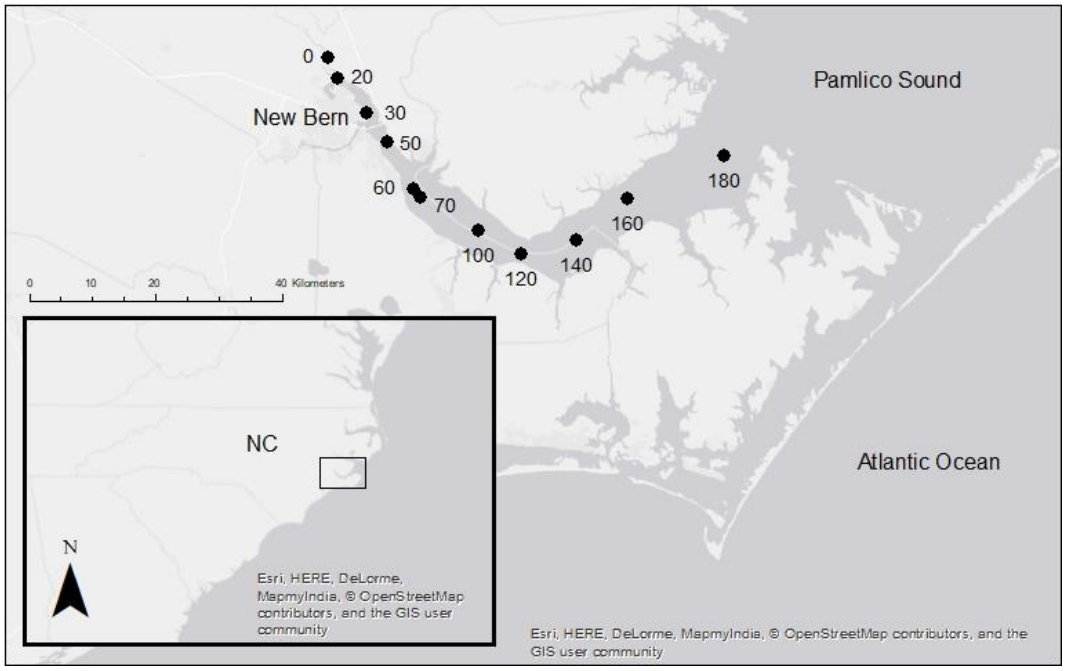

Figure 2-1. Map of the NRE located in eastern NC. Locations of sample collection are labeled as numbered dots from 0 at the head of the estuary to 180 at the outlet to Pamlico Sound.

DOC concentration was measured on collected filtrate via high-temperature catalytic oxidation on a Shimadzu TOC-5000 analyzer (Peierls et al., 2003). Total dissolved nitrogen (TDN), nitrate + nitrite (NO_3^- + NO_2^-), and ammonium (NH_4^+) were determined colorimetrically using a Lachat QuickChem autoanalyzer (Peierls et al., 2003). DON was determined by subtracting the dissolved inorganic nitrogen species (DIN, as NO_3^- + NO_2^- + NH_3^+) from TDN. The molar DOC to DON ratio (DOC:DON) was calculated using measured DOC and DON concentrations. POC and PN were determined on one set of collected filters via high temperature combustion on a Costech ECS 4010 analyzer, after vapor acidification (HCl) to remove carbonates (Paerl et al., 2018). POC and PN concentrations were used to calculate the molar POC:PN ratios.

Phytoplankton biomass was measured as Chl *a* using a modified version of EPA method 445.0 (Arar and Collins, 1997). Briefly, collected filters were extracted overnight in 90% acetone

followed by processing in a tissue grinder. Extracts were analyzed un-acidified on a Turner Designs TD-700 fluorometer with a narrow bandpass filter.

For FDOM and BEFPOM analysis, about 100 mL of collected sample was filtered through a combusted (450^{o}C for 4 hrs.) 0.7 µm porosity glass fiber (GF/F) filter. The filter was collected for BEFPOM analysis (Brym et al., 2014) and the filtrate collected for FDOM analysis (Osburn et al., 2012). FDOM filtrate and BEFPOM filters were stored frozen (-20^{o}C) in the dark, until analysis. Both BEFPOM and FDOM samples were analyzed for fluorescence spectra as EEMs on a Cary Varian Eclipse Spectrofluorometer at 950 V and 750 V, respectively. Excitation wavelengths were measured from 240 to 450 nm every 5 nm and emission wavelengths measured from 300 to 600 nm at 2 nm intervals. Immediately prior to analysis, both FDOM and BEFPOM samples were filtered through a polyethersulfone (PES) 0.2 µm porosity filter. Instrument excitation and emission corrections were applied to each sample EEM as well as corrections for inner-filtering effects, calibrated against the Raman signal of Nanopure water or sodium hydroxide for FDOM and BEFPOM analysis respectively, and standardized to quinine sulfate equivalents (Q.S.E.) (Osburn et al., 2012; Stedmon and Bro, 2008). Absorbance scans used for EEMs correction were analyzed on a Shimadzu UV-1700 PharmaSpec measured from 200 nm to 800 nm. Samples with raw absorbance > 0.4 at 240 nm were diluted for both absorbance and fluorescence scans to limit inner filtering effects, as both primary and secondary inner filtering effects (Ohno, 2002, Osburn et al., 2012). Primary inner filtering effects are classified as the absorption of excitation wavelengths by OM molecules within the sample while secondary inner filtering effects correspond to the absorption of emitted fluorescence by the sample (Ohno, 2002).

Several indicators of OM quality were derived from the absorbance and fluorescence measurements. a_{350} is the absorbance measured at 350 nm converted to Napierian absorption coefficients (Spencer et al., 2013). $SUVA_{254}$ was calculated following Weishaar et al., (2003) by dividing absorbance as measured at 254 nm by the DOC or POC concentration (mg L^{-1}) for DOM and POM, respectively. The humification index (HIX) and biological index (BIX) were calculated according to Huguet et al., (2009) and used as indicators of allochthonous or autochthonous FOM, respectively. The 'peak picking' method was also used to identify specific locations in EEM space (Peak A, C, M, N, T, B) that have been well characterized and previously identified in the literature (Coble, 2007; Fellman et al., 2009) and which can be used to track the sources and quality of FOM through aquatic ecosystems.

3.2 PARAFAC modeling

PARAFAC was applied to sets of collected FDOM and/or BEFPOM EEMs to mathematically identify and separate broad classes of FOM inherent to each set of samples (Murphy et al., 2013; Stedmon and Bro, 2008). By using the coupled EEM-PARAFAC technique, broad classes of FOM can be identified and tracked through aquatic systems and the transport, fate, and bioreactivity of FOM can be assessed (Fellman et al., 2011; Jaffé et al., 2014; Markager et al., 2011). Three PARAFAC models were generated for the FDOM (n = 472) and BEFPOM (n = 476) samples collected from the NRE at all time points, stations, and depths: a FDOM model that contained only FDOM EEMs, a BEFPOM model that only contained BEFPOM EEMs, and a combined FDOM+BEFPOM model that contained both BEFPOM and FDOM EEMs. Each PARAFAC model was developed using the drEEM Toolbox in Matlab R2017b (Murphy et al., 2013). All EEMs were normalized to their total fluorescence (i.e., sum of fluorescence across each sample EEM) prior to modeling (Osburn et al., 2012). Each model was developed using

random initialization on ten separate model runs and was split half validated between at least two sets of four randomly generated subsets of samples. Models with components >3 (n components = 4-7) were eliminated based on visual interpretation of identified components as well as failing split half validation tests. After PARAFAC modeling, the sample component loadings were re-scaled to the total fluorescence of each sample for subsequent data analysis and visualization.

Each PARAFAC model was compared to previously published and identified PARAFAC components on OpenFluor (Murphy et al., 2014). Components with > 95% match using Tucker Congruence Coefficients (TCC) were selected to identify each PARAFAC component. PARAFAC model comparisons (FDOM v. BEFPOM, FDOM v. FDOM+BEFPOM, BEFPOM v. FDOM+BEFPOM) were conducted in-house code in Matlab R2017b to determine if individual components identified in the three PARAFAC models matched with > 95% similarity as determined by TCC (Lorenzo-Seva and Berge, 2006).

3.3 Experimental bioassays

A series of seasonal experimental bioassays were conducted from July 2017 to April 2018 in an effort to isolate a FDOM signal that was unique to estuarine processes and could be used to track the simultaneous production, transformation, and processing of FDOM through eutrophic estuarine ecosystems. Briefly, four experimental bioassays were conducted seasonally: July 2017, October 2017, February 2018, and April 2018 in order to capture any seasonal variability in estuarine FDOM signals. For each experimental bioassay, water was collected from the riverine (Station 0S) and estuarine end member (Station 180S) about 0.5 m below the surface and immediately filtered through 202 µm mesh to remove any zooplankton and large particulates. Collected water was stored at ambient temperature, in the dark during transport to UNC-CH IMS where the water was then stored, overnight in a flow-through seawater pond to maintain ambient

temperature and light conditions. The following morning, collected water was divided into 16 pre-aged 1-L, transparent polyethylene Cubitainers for treatments as described in Table 2.1. Pre-aging of Cubitainers reduces possible leaching of optically-active components (Osburn et al., 2001). Cubitainers have been shown to transmit ~95% of light in the photosynthetically active radiation (PAR) wavelengths (400-700 nm) and 20-35% in the UV-wavelengths (300-400 nm) (Peierls, unpublished results). Controls contained no additions while the nutrient treatments contained nitrogen (N) and phosphorus (P) added as 3 mg L^{-1} nitrate (NO_3^-) and 0.6 mg L^{-1} phosphate (PO_4^{-3}), respectively on Day 0. The goal of the nutrient additions was to ensure the phytoplankton and microbial communities were not nutrient limited. Cubitainers were incubated for a total of seven days under ambient water temperature and light conditions, with samples collected on each day (Day 0, 1, 2, 3, 4, 5, 6). Samples were analyzed for DOM absorbance and fluorescence as well as Chl *a*, DOC, and nutrients ($NO_{2/3}$, NH_4^+, TDN, DON; on Days 0 and 6 only).

Table 2-1. Experimental bioassay treatments used to isolate the estuarine FDOM signal.

Cubitainer number	Treatment	Treatment name	Description
1-4	Riverine control	0S Control	No addition
5-8	Riverine nutrient treatment	0S Nuts	N and P added
9-12	Marine control	180S Control	No addition
13-16	Marine nutrient treatment	180S Nuts	N and P added

3.4 Estuarine FDOM signal identification

To isolate the estuarine FDOM signal produced during the incubation experiment, the EEM collected on day 0 for each respective treatment and replicate was subtracted from the coupled EEM collected from the same treatment, replicate, and seasonal bioassay (July 2017, October 2017, February 2018, April 2018) for the remaining time points (Day 1-6). All EEMs were divided by their total fluorescence prior to subtraction. The subtraction procedure acted as a

sample ‘normalization’ to remove the initial influence of terrestrial, humic-like fluorescence contained in the sample and allowed me to capture any fluorescence signals that were produced during the experiment (Murphy et al., 2018). The subtracted EEMs were then concatenated across treatment, replicate, and seasonal bioassay (n = 378) and a PARAFAC model applied using the drEEM toolbox in Matlab R2017b (Murphy et al., 2013). The single component identified in the global model matched with previously identified components on OpenFluor (Murphy et al., 2014). PARAFAC models were also developed for various subsets of the subtracted EEMs, including by treatment (All treatments, 0S Control, 0S Nutrient, 180S Control, 180S Nutrient) and season (All seasons, July 2017, October 2017, February 2018, April 2018).

3.5 FluorMod

FluorMod is a mixing model based on a 9-comopnent PARAFAC model developed using watershed source samples (reference, wastewater treatment facility – WWTF influent, WWTF effluent, poultry litter leachate, swine lagoon, septic outflow, street runoff, soil leachate) collected from the Neuse River watershed (Osburn et al., 2016). FDOM PARAFAC components identified in the watershed samples contained both humic-like, terrestrial FDOM signatures (FluorMod C1, potential leaf material; C2, natural stream DOM; C4, soil leachate; C6 urban runoff; C7 WWTF effluent; and C9 urban runoff) and protein-like FDOM signatures that are indicative of recent biological activity and are considered biologically reactive (FluorMod C3, protein, tryptophan; C5, protein, tyrosine; and C8, microbial activity) (Osburn et al., 2016).

To develop the FluorMod additive mixing model, Osburn et al. (2016) characterized samples of DON sources collected in the watershed and assigned proportions of the 9 identified PARAFAC components to each source. Eight DON sources from the Neuse River watershed were characterized: reference, WWTF effluent, WWTF influent, poultry leachate, swine lagoon,

septic outflow, street runoff, and soil leachate (Osburn et al., 2016). The additive mixing model, FluorMod, can then be applied to samples collected from the Neuse River and watershed to determine the relative proportion of each identified watershed source within the collected water sample. The application of FluorMod both as a mixing model and as a 9-component PARAFAC model was specifically developed for the Neuse River watershed and river network. The goal of this study was to explore and potentially expand the use of FluorMod, as a source based PARAFAC model and as a mixing model, to estuarine samples collected from the downstream NRE.

In order to apply FluorMod to estuarine samples, an additional estuarine FDOM source was needed to capture processes within the estuary that produce or transform FDOM *in situ*. Application of FluorMod to FDOM estuarine samples was used in conjunction with the 1-component estuarine FDOM model developed using the experimental bioassays. Briefly, FluorMod was applied to FDOM samples collected from the NRE as part of this study. The estuarine FDOM model was then applied to the sample residuals after application of FluorMod. The estuarine FDOM model was also applied to sample residuals after application of the 3-component FDOM PARAFAC model developed on estuarine FDOM samples during the first part of this study.

4. Results and Discussion

4.1 Environmental parameters

Environmental parameters (DOC, DON, POC, PN, Chl *a*) measured during the study were plotted by station down the estuary (Figure 2.2; Appendix 2, Figure A2.1, Table A2.1). DOC and DON generally decreased down estuary, particularly downstream of station 30, and with increasing salinity following conservative mixing (Markager et al., 2011). For the purposes of

this study, we will characterize parameters as following conservative mixing if, 1. The p-value as calculated for the respective component versus salinity is statistically significant ($p < 0.05$) and 2. The r^2 value is greater than 0.1, as defined in Markager et al., (2011). Conservative mixing indicates the river is the main source of DOC and DON to the NRE. Trends for DOC and DON are seasonally consistent (Appendix 2, Figure A2.1) and exhibit a statistically significant negative relationship with salinity (Appendix 2, Table A2.1). DOM parameters, primarily as [DOC], increased between Station 0 and Station 30, prior to following a conservative mixing pattern. This is likely a result of un-gaged and un-characterized streams and rivers, including the Trent River, draining into the upper NRE, and which contribute freshwaters high in DOC and terrestrial-like DOM (Cabaniss and Shuman, 1987; Vähätalo et al., 2005).

Particulate parameters (POC, PN, Chl *a*), however, generally increase in concentration down estuary (Figure 2.2) and with increasing salinity over the study period (July 2015 – July 2016) (Appendix 2, Figure A2.1, Table A2.1), indicating the estuary is a source of particulate material, most likely from phytoplankton production, measured as Chl *a*. Relationships between particulate parameters and salinity in estuaries are often weak due to the Chl *a* maximum where Chl *a* biomass accumulates and rapidly increases at the location where estuarine flushing time is most conducive for phytoplankton growth (Peierls et al., 2012).

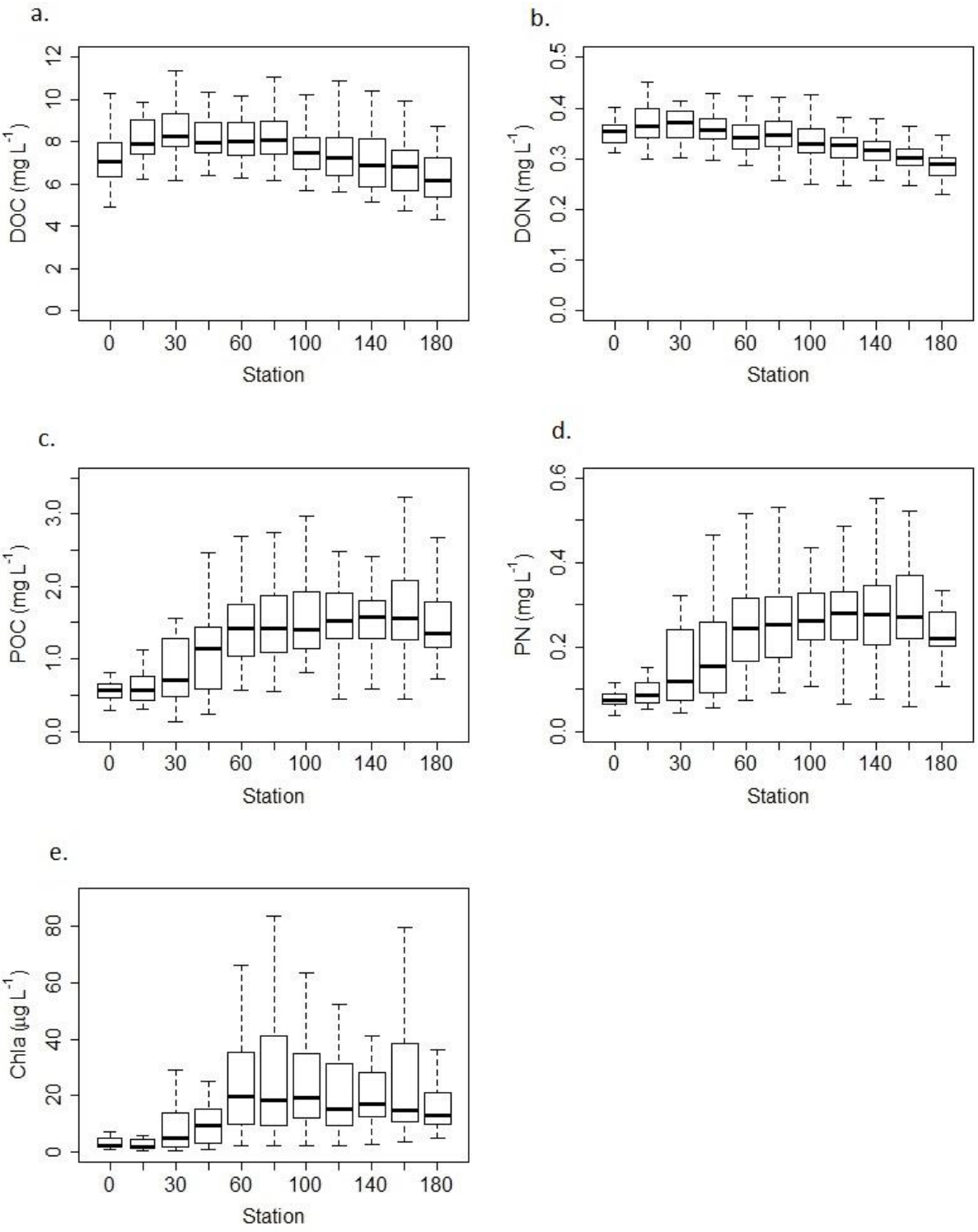

Figure 2-2. Boxplots of various chemical and biological (a. DOC, b. DON, c. POC, d. PN, e. Chl *a*) parameters plotted down estuary by station (Station 0 -180). Each station represents samples collected from both depths (surface and bottom) and at all time points. Outliers for particulate parameters were omitted for visualization.

4.2 FDOM PARAFAC modeling

A three component PARAFAC model was fitted to collected FDOM samples (n = 472). Each component was split half, validated and matched with previously identified components on OpenFluor (Figure 2.3; Appendix 2, Table A2.2, Figure A2.2). FDOM Component 1 (FDOM C1) was identified as a terrestrial, humic-like component similar to Peaks A and C (Coble, 2007). FDOM Component 2 (FDOM C2) was identified as a microbial humic-like component, similar to Peak M, which has been linked to recent biological activity and is prevalent in eutrophic, human-impacted waters (Murphy et al., 2008). The component also contains fluorescence in the peak A region, which is ubiquitous to aquatic environments. This component likely represents fluorescence from both of these regions (Peaks M and A), which are co-occurring and following similar patterns in the estuary. Finally, FDOM Component 3 (FDOM C3) was identified as an additional indicator of terrestrial, humic-like material (Osburn et al., 2018). Results from the FDOM PARAFAC model indicate the FDOM pool is largely composed of humic-like material, mainly derived from terrestrial sources.

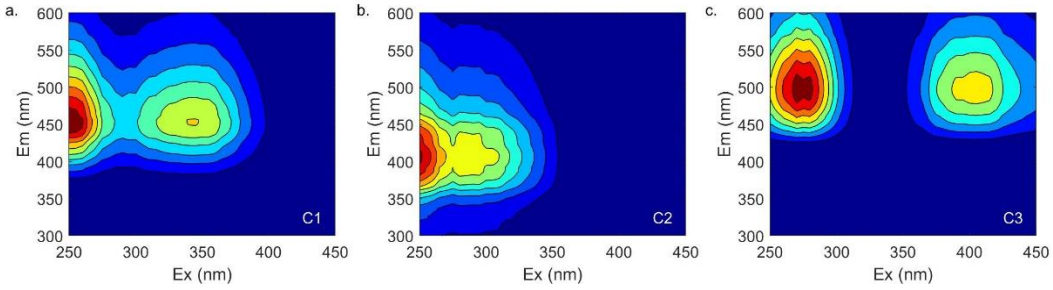

Figure 2-3. Model components (C1-C3) for the 3-component FDOM model.

Table 2-2. OpenFluor matches for the 3-component FDOM model (TCC > 0.95). Matches were made on 01-14-2019. References are only a partial list of matches made on OpenFluor.

	Ex max. (nm)	Em max. (nm)	OpenFluor Matches	Description	Reference
C1	< 250, 345	454	19	Terrestrial, humic-like, fulvic-acid like	Kulkarni et al., 2017; Osburn et al., 2018, 2016
C2	< 250	406	14	Terrestrial and microbial, humic-like, estuarine, eutrophic waters, similar to M-peak	Cawley et al., 2012; Osburn et al., 2012; Yamashita et al., 2013
C3	270, 405	498	5	Terrestrial, humic-like	Gueguen et al., 2014; Osburn et al., 2018; Yamashita et al., 2011

All three identified components (C1 – C3) had a statistically significant positive, linear relationship with DOC and DON (Appendix 2, Figure A2.4, Table A2.2). Therefore, like the dissolved fraction (DOC, DON), the three FDOM components decreased down estuary and with increasing salinity generally following conservative mixing (Figure 2.4; Appendix 2, Figure A2.5, Table A2.3), indicating all three components are of terrestrial origin. There were seasonal variations in the relationship between the various components (FDOM C1-C3) and salinity (Appendix 2, Figure A2.5, Table A2.3) which may reflect seasonally varying sources of terrestrial-like material from the riverine end member.

During the fall, there were elevated FDOM intensities in the upper NRE as compared to other seasons (Appendix 2, Table A2.3), as indicated by the y-intercept values. Similar results have been found for other eutrophic, estuarine environments with forested catchments. Stedmon and Markager, (2005) observed increased FDOM intensity and [DOC] during the fall in estuarine waters draining a forested catchment. In streams and river systems, observed increases in DOC and fluorescence intensity during the fall have been linked to overland flow through leaf litter and shallow soils, especially following fall storm events (Singh et al., 2014). During the fall

2015 study period, there were two identified storm events in the NRE (Hounshell et al., 2019) that could have resulted in the mobilization of watershed DOM from forested catchments leading to the increased fluorescence intensities observed in the estuary.

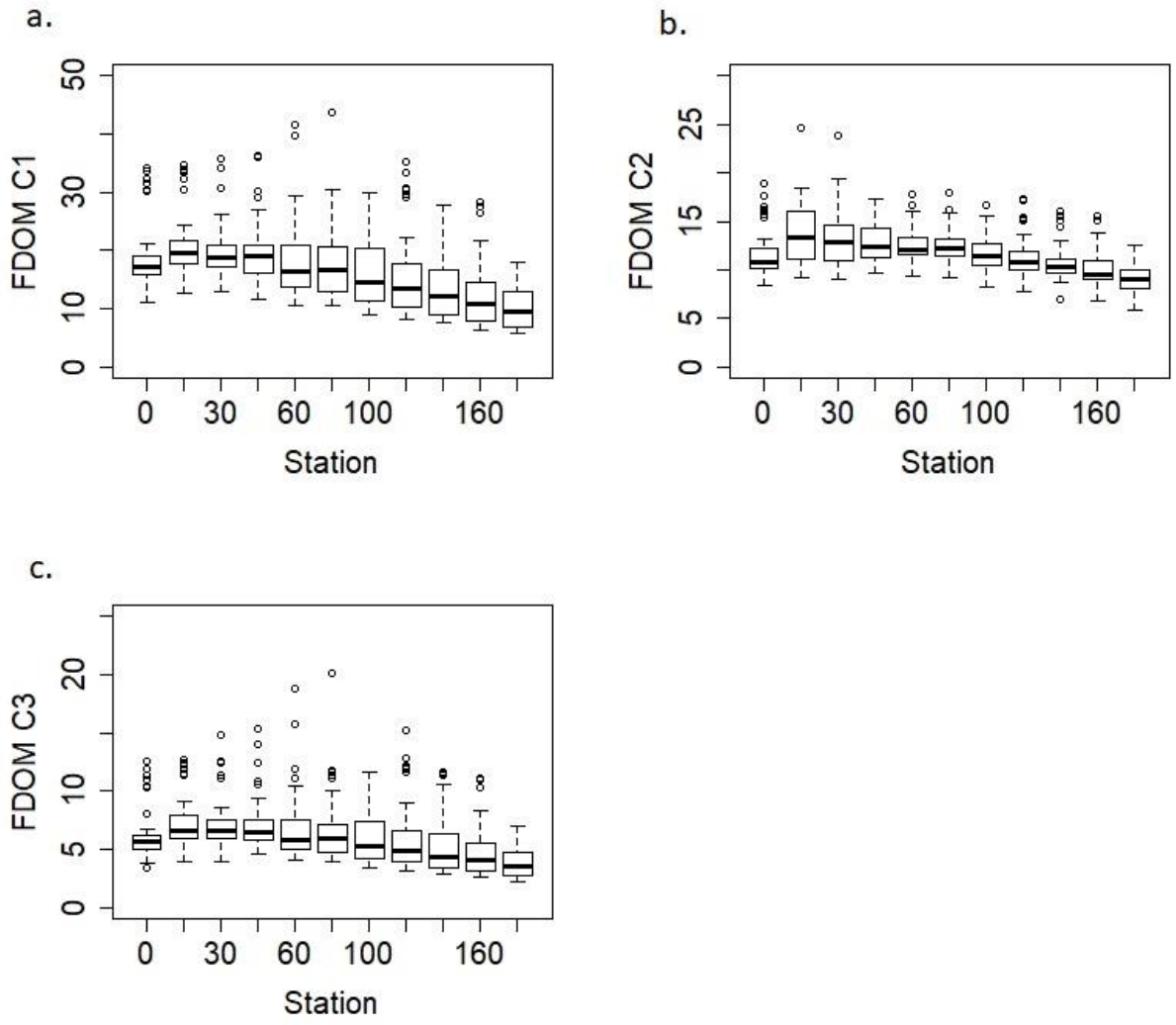

Figure 2-4. Boxplots of each of the three identified FDOM PARAFAC components plotted by station for all time points and depths.

Another way to assess how the three identified FDOM components relate to each other and to environmental parameters, is to use principal components analysis (PCA) to reduce the dimensionality of the data and plot all collected data along two dimensions (Figure 2.5). All three of the identified components (FDOM C1-C3) had positive loadings along PC1 and were

inversely related to salinity, indicating these components were more prevalent at low salinities (i.e., in riverine water). The three FDOM components were also aligned with other fluorescence-derived measurements (Peaks B, T, N, M, A, C, HIX) which are often classified as indicators of terrestrial, humic-like material (Coble, 2007; Huguet et al., 2009). The three FDOM components were plotted opposite of BIX, which is a fluorescence indicator often linked with recent, biological production of FDOM (Huguet et al., 2009). FDOM components were also distributed along PC2 with FDOM C1 and C3 clustered towards zero while FDOM C2 had positive PC2 loadings. FDOM C2 was clustered with fluorescence peaks that are typically indicators of material that are considered more biologically reactive (Coble, 2007), while FDOM C1 and C3 were clustered with fluorescence peaks identified as FDOM that is largely considered recalcitrant. While the components (FDOM C1-C3) were identified as terrestrial in origin, PCA results indicate there were some potential differences in the lability of the FDOM material as identified in the FDOM PARAFAC model.

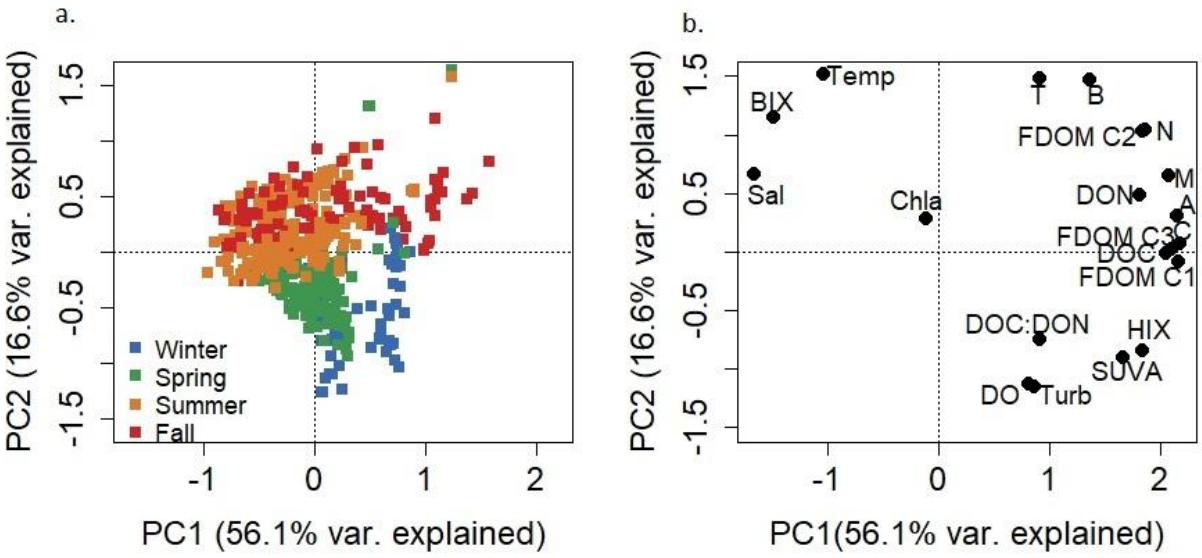

Figure 2-5. PCA results as applied to DOM parameters, including the 3-components identified in the FDOM model. a. Sample scores plotted by season. b. Variable loadings plotted in PCA space. Variables are identified on the graph.

4.3 BEFPOM PARAFAC modeling

A 5-component PARAFAC model was fitted to BEFPOM samples collected from the NRE (n = 476) (Figure 2.6, Table 2.3). Each component was split half validated and the first four components (C1 – C4) matched with several previously identified fluorophores on OpenFluor (Table 2.3; Appendix 2, Figure A2.6). Most of the components matched (C1-C4) with components previously identified in PARAFAC models that included BEFPOM samples (Brym et al., 2014; Osburn et al., 2015, 2012). BEFPOM component 1 (FPOM C1) was identified as a protein-like fluorophore most similar to tryptophan (Osburn et al., 2016). BEFPOM component 2 (BEFPOM C2) matched with components that have only been identified in models that include BEFPOM EEMs and are characteristic of eutrophic estuaries and microbial re-processing of FOM (Brym et al., 2014; Osburn et al., 2015, 2012). This component is essential in the characteristic BEFPOM 'three-peak pattern' (Brym et al., 2014). BEFPOM component 3 (FPOM C3) was classified as a terrestrial, humic-like fluorescence peak that is indicative of fulvic acid-like fluorescence often derived from soil leachates (Graeber et al., 2012; Osburn et al., 2016). BEFPOM component 4 (FPOM C4) was identified as microbial, humic-like fluorescence similar to the previously identified Peak M and has been linked with recent biological production (Coble, 2007; Yamashita et al., 2013). Finally, BEFPOM component 5 (FDOM C5) matched with a single previously identified fluorophore described as terrestrial, humic-like, similar to Peak C (Søndergaard et al., 2003). However, because this component only matched with one identified fluorophore in OpenFluor, we classified this component as 'un-characterized'.

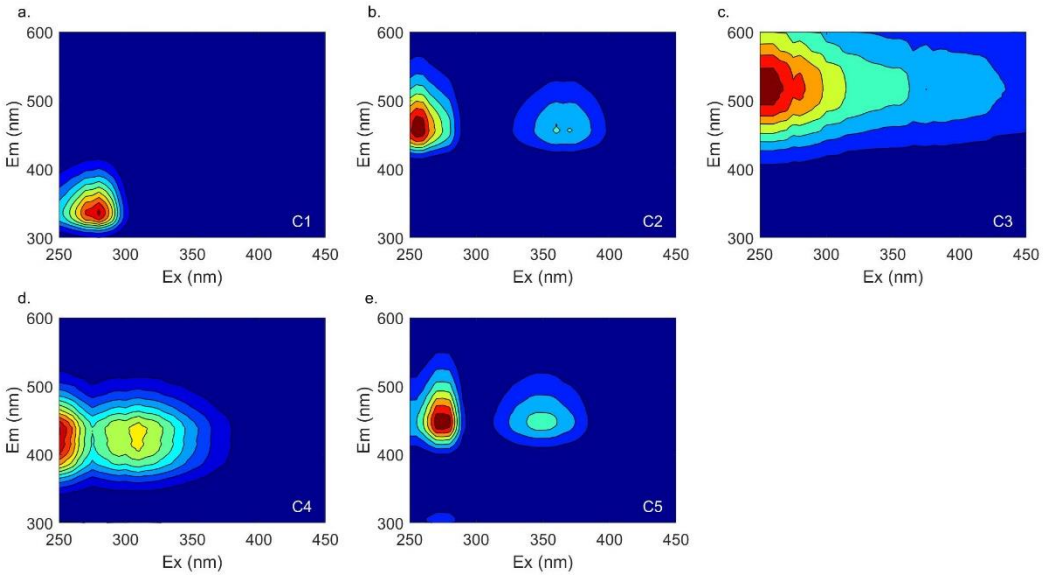

Figure 2-6. 5-component PARAFAC model developed on collected BEFPOM samples.

Table 2-3. OpenFluor matches for the 5-component BEFPOM model (TCC > 0.95). Matches were made on 01-14-2019. References are only a partial list of matches made on OpenFluor.

	Ex max. (nm)	**Em max. (nm)**	**OpenFluor Matches**	**Description**	**Reference**
C1	280	336	21	Protein, tryptophan-like	Brym et al., 2014; Osburn et al., 2016, 2012
C2	255, 360	456	3	FPOM specific, eutrophic estuaries, microbial reprocessing of terrestrial DOM	Brym et al., 2014; Osburn et al., 2015, 2012
C3	260	516	33	Terrestrial, humic-like, fulvic-acid like, soil leachates	Brym et al., 2014; Osburn et al., 2012; Shutova et al., 2014
C4	<250, 310	438	44	Marine and terrestrial humic-like, combination of A and M peaks, possibly photo-labile	Brym et al., 2014; Murphy et al., 2008; Yamashita et al., 2013
C5	265, 345	448	1	Similar to humic peak C, terrestrial-like; un-characterized	Søndergaard et al., 2003

FPOM components plotted down estuary both increased (FPOM C1, C2, C5) and decreased (FPOM C3, C4) in intensity with distance from the riverine end member, indicating a mix of

autochthonous components produced *in situ* as well as terrestrial like-components that are diluted, or potentially removed down estuary (Figure 2.7). Like the FDOM components, FPOM components that were characterized as terrestrial, humic-like decreased down estuary and followed a typical conservative mixing pattern (Markager et al., 2011) (Appendix 2, Figure A2.8, Table A2.5). For the FPOM results, these terrestrial components included C3 which was identified as a terrestrial, humic-like component with similarities to soil leachate and C4 which was classified as a marine/terrestrial humic-like component. The three components (FPOM C1, C2, C5), which increased in intensity down estuary, were most likely produced within the estuary (i.e., microbial or phytoplankton production) (Markager et al., 2011). These components include C1 which was characterized as protein, tryptophan-like, C2 which was characterized as FPOM specific and was indicative of microbial reprocessing of terrestrial DOM, and C5 which was un-characterized. I hypothesized that the previously un-characterized C5 component was likely a biological byproduct that was produced in the estuary and may be unique to BEFPOM samples.

The various BEFPOM components were plotted against measurements of particulate OM (POC, PN, Chl *a*) (Appendix 2, Figure A2.9, Table A2.6). Both FPOM C1 and C5 had strong, statistically significant relationships with POC, PN, and Chl *a*, further indicating these two components are likely produced i*n situ* via phytoplankton or microbial production.

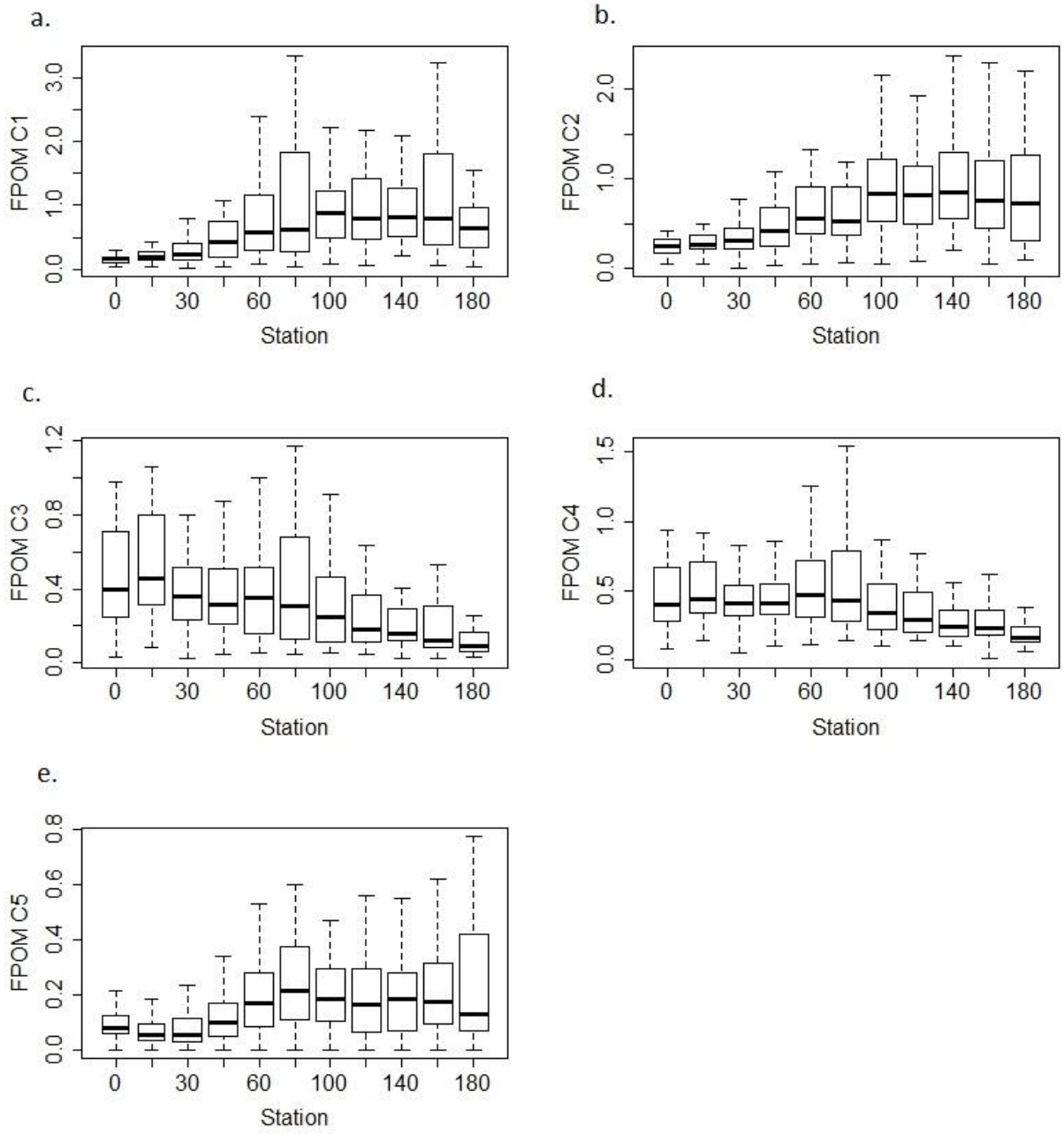

Figure 2-7. Boxplots of the 5 BEFPOM components plotted down estuary by station. Each station includes all samples collected from both depths (surface and bottom) and all time points. Outliers were removed for visualization.

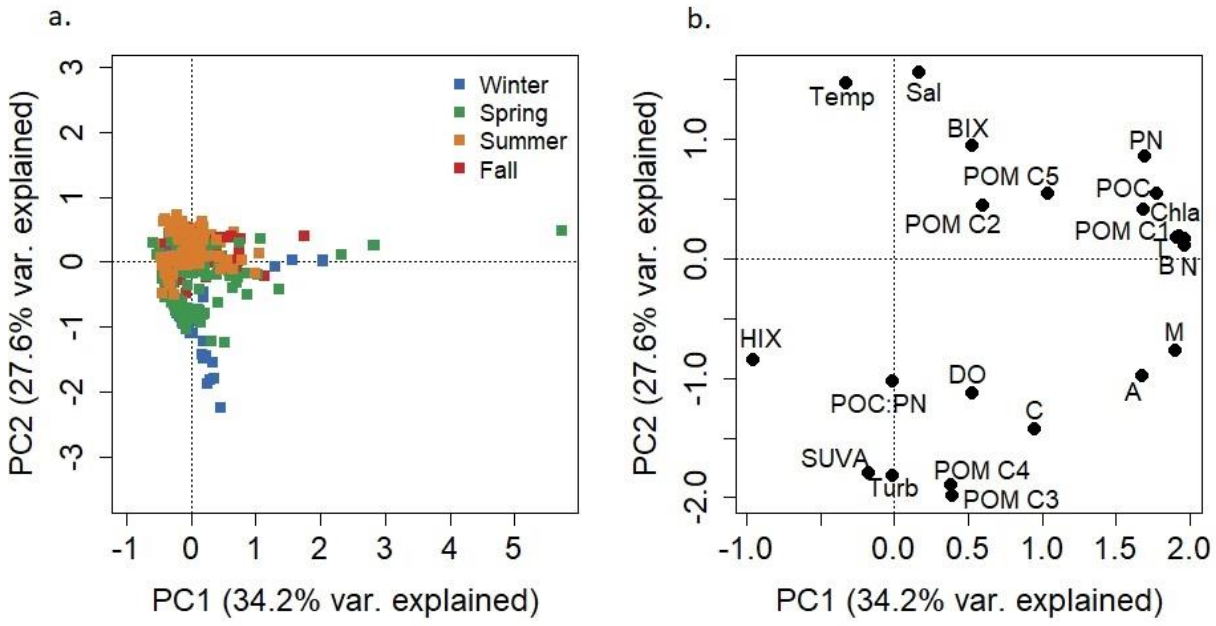

Figure 2-8. PCA results for FPOM parameters. a. Sample scores plotted by season. b. Variable loadings plotted in PCA space. Variables are identified on the plot.

PCA was also applied to FPOM modeling results and associated POM variables (Figure 2.8). The 5 identified BEFPOM components were distributed along principal components axis 2 (PC2), such that components identified as terrestrial, humic-like material had negative PC2 loadings and were clustered with other indicators of terrestrial, humic-like material (SUVA, Peak C). Components characterized as more marine and biologically produced had positive PC2 loadings and were clustered with indicators of more recent, biologically produced OM (BIX). Unlike the FDOM pool which was almost entirely dominated by terrestrial, humic-like FOM, the FPOM pool included FOM sources from both terrestrial and autochthonous sources.

4.4 FDOM+BEFPOM PARAFAC modeling

A 5-component PARAFAC model was fitted to the combined FDOM and BEFPOM samples (n = 948) (Figure 2.9, Table 2.4). All components were split half validated and matched with previously identified components in OpenFluor (Appendix 2, Figure A2.10). The components

identified for the combined (FDOM+BEFPOM) model were almost identical to the components identified for the BEFPOM model. Components included a humic-like, microbial peak (FDOM+BEFPOM C1); a terrestrial, humic-like peak (FDOM+BEFPOM C2); a FPOM specific component (FDOM+BEFPOM C3); a protein-like tryptophan component (FDOM+BEFPOM C4); and an un-characterized component (FDOM+BEFPOM C5) linked to biological production in the BEFPOM model developed for the BEFPOM samples only.

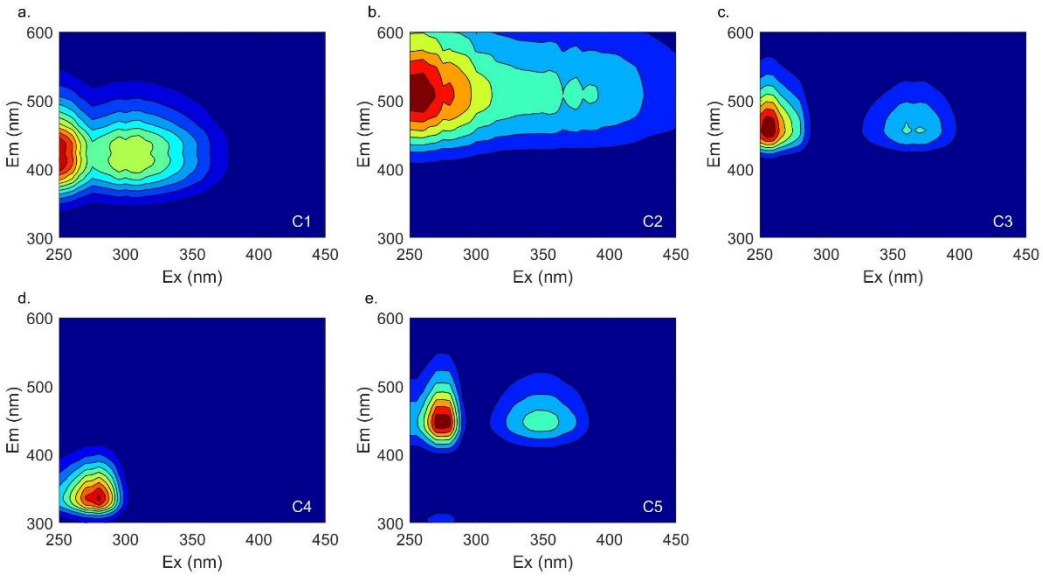

Figure 2-9. 5-component PARAFAC model developed for FDOM+BEFPOM samples.

Table 2-4. OpenFluor matches for the 5-component FDOM+BEFPOM model (TCC > 0.95). Matches were made on 01-22-2019. References are only a partial list of matches made on OpenFluor.

	Ex max. (nm)	Em max. (nm)	OpenFluor Matches	Description	Reference
C1	<250, 310	412	43	Terrestrial, humic-like, similar to marine humic-like M peak	Brym et al., 2014; Murphy et al., 2008; Osburn et al., 2012
C2	260	506	38	Terrestrial, humic-like, fulvic acid-like, soil leachate	Brym et al., 2014; Murphy et al., 2014; Osburn et al., 2016
C3	255, 360	456	3	FPOM specific, microbial re-processing of terrestrial DOM, nutrient impacted estuaries	Brym et al., 2014; Osburn et al., 2015, 2012
C4	280	336	21	Protein-like, tryptophan	Brym et al., 2014; Cawley et al., 2012; Osburn et al., 2012
C5	275, 345	448	1	Similar to humic peak C, terrestrial-like, un-characterized	Søndergaard et al., 2003

When plotted against salinity and by station, the identified FDOM+BEFPOM components as applied to either FDOM or BEFPOM samples showed similar patterns as components identified for the individual FDOM and BEFPOM models (Appendix 2, Figure A2.11, Table A2.7; Appendix 2, Figure A2.14, Table A2.9). For the FDOM samples, this indicates that even though several of the identified components were associated with recent biological activity in the BEFPOM pool (C3, C5), the components as applied to FDOM samples generally followed conservative mixing patterns, indicating these components had terrestrially-derived FDOM sources (Appendix 2, Figure A2.11, Table A2.7). However, for C4, identified as protein-like, tryptophan, the fluorescent intensity remained constant throughout the estuary and across all salinities when applied to FDOM samples. This indicated the fluorescent intensity of this biologically reactive component was dictated by processes occurring in the estuary, as both

production and degradation, more so than mixing processes between the riverine and marine end-members alone (Markager et al., 2011). Additionally, the fluorescent intensity of protein-like components, including tryptophan are often higher in the marine compared to the riverine end member, due to biological production in marine systems (Stedmon and Markager, 2005). Therefore, I expect the source of this component was both production in the estuary (as phytoplankton and microbial production) and mixing with the marine end member (i.e., Pamlico Sound).

For the BEFPOM samples, the patterns were essentially the same for the combined model (FDOM+BEFPOM) and the individual model (BEFPOM), where terrestrial-like components (FDOM+BEFPOM C1, C2) decreased down estuary and biologically reactive components increased down estuary (FDOM+BEFPOM C3, C4, C5) (Appendix 2 Figure A2.14, Table A2.9). Results from the combined model (FDOM+BEFPOM) as applied to the FDOM and BEFPOM samples further highlight the dichotomy between the two pools: the FDOM pool was dominated by terrestrial FDOM while the BEFPOM pool was a combination of terrestrial FOM sources from the watershed (i.e., terrestrial sources) and biological sources (i.e., phytoplankton biomass) produced in the estuary.

PCA was also applied to results from the combined model (FDOM+BEFPOM), as the combined model applied to FDOM samples (Appendix 2, Figure A2.16) and as applied to BEFPOM samples (Appendix 2, Figure A2.17). Results were similar to the respective individual FDOM and BEFPOM models. For FDOM samples the FDOM+BEFPOM C4 component was not clustered with the other DOM fluorescence components, indicating this component was sufficiently different from the other FDOM+BEFPOM components as applied to FDOM

samples. The C4 component was identified as protein-like, specifically tryptophan, and has been identified as a biologically-produced component in the FDOM pool (Coble, 2007).

4.5 PARAFAC model comparisons

Results from TCC comparisons between PARAFAC models (FDOM, BEFPOM, FDOM+BEFPOM) indicated the BEFPOM and FDOM+BEFPOM model contained the exact same components (Table 2.5). This indicated the combined model (FDOM+BEFPOM) was entirely dominated by fluorescence variability in the BEFPOM samples. There was some overlap between the FDOM, BEFPOM, and FDOM+BEFPOM models as all three models contained a fluorophore that was identified as similar to the previously characterized M-peak. While the M-peak has been designated as a potential indicator of recent biological activity in open ocean environments (Murphy et al., 2008), for this study, all models indicate this component was terrestrially-derived. This peak has also been described as ubiquitous to eutrophic, estuarine waters and has been identified in previous PARAFAC models generated for samples collected from the NRE (Osburn et al., 2012).

Table 2-5. Model comparisons between the three PARAFAC models generated for samples collected from the NRE: the 3-component FDOM model, 5-component BEFPOM model, and 5-component FDOM+BEFPOM model. An X indicates components which were > 95% similar.

	FDOM C1	FDOM C2	FDOM C3	BEFPOM C1	BEFPOM C2	BEFPOM C3	BEFPOM C4	BEFPOM C5
BEFPOM C1								
BEFPOM C2								
BEFPOM C3								
BEFPOM C4		X						
BEFPOM C5								
FDOM+BEFPOM C1		X					X	
FDOM+BEFPOM C2						X		
FDOM+BEFPOM C3					X			
FDOM+BEFPOM C4				X				
FDOM+BEFPOM C5								X

All the identified components from the three models (FDOM, BEFPOM, FDOM+BEFPOM applied to FDOM samples, FDOM+BEFPOM applied to BEFPOM samples) were plotted in PCA space (Figure 2.10). Because the BEFPOM model and FDOM+BEFPOM model applied to BEFPOM samples were exactly the same, each of the coupled components from these two models were clustered together in PCA space. Similarly, all FDOM components and FDOM+BEFPOM components applied to FDOM samples were clustered together along the positive loadings of principal component axis 1 (PC1), except for C4d which was more closely associated with the three biologically produced BEFPOM components. C4d was the only component identified as being a biologically produced DOM fluorophore, while all other FDOM components were identified as terrestrial, humic-like components. The two BEFPOM components that were also identified as terrestrial like had positive loadings along PC1. Negative loadings on PC1 indicate components that were considered autochthonous and produced within the estuary.

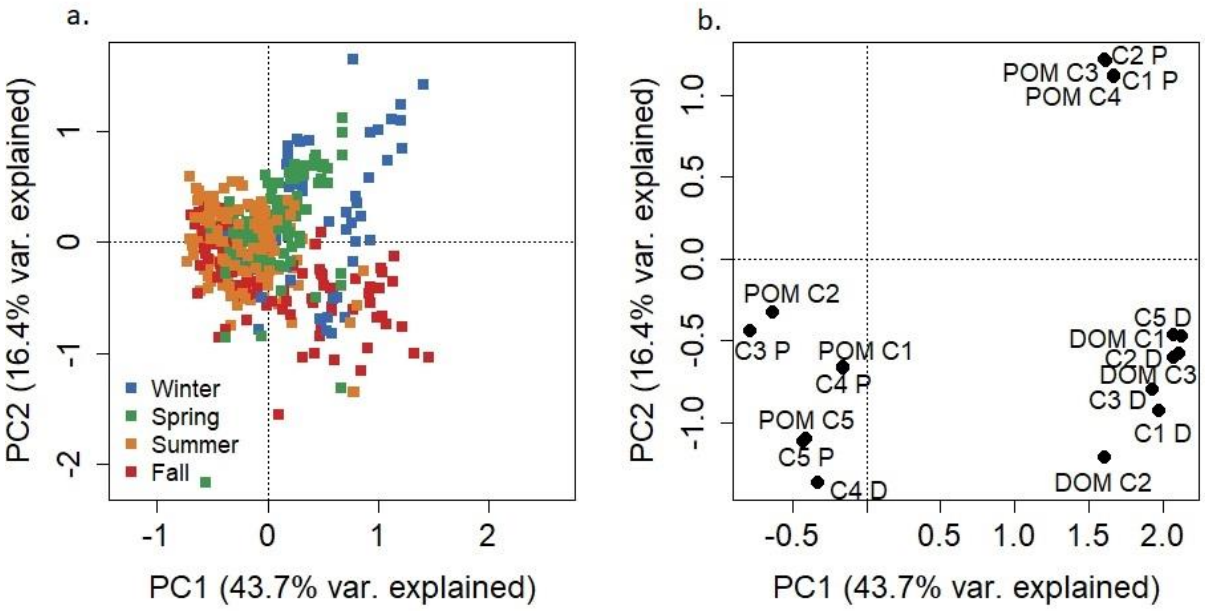

Figure 2-10. PCA results as applied to components from all three models (FDOM, BEFPOM, FDOM+BEFPOM applied to FDOM samples, FDOM+BEFPOM applied to FPOM samples). a. Sample scores plotted by season. b. Variable loadings plotted in PCA space. DOM C1-C3 indicate components identified in the FDOM model. POM C1-C5 indicate components identified in the BEFPOM model. C1-C5 P and C1-C5 D indicate BEFPOM and FDOM components identified in the combined FDOM+BEFPOM model, respectively.

Results from the three models (FDOM, FPOM, FDOM+BEFPOM) and from the model comparisons, suggest the FDOM pool is largely composed of terrestrial, humic-like material while the BEFPOM pool contains fluorophores identified as both terrestrial-like and as autochthonous components produced within the estuary. Model comparisons suggest the combined model (FDOM+BEFPOM) was almost entirely dominated by fluorescence variability in the BEFPOM pool.

4.6 FluorMod estuarine signal

Seasonal experimental bioassays were used to isolate an estuarine FDOM processing signal (production + degradation). Chl *a* was plotted to track phytoplankton biomass during each incubation experiment (Figure 2.11). Chl *a* results were seasonally variable with the lowest

growth during February 2018. In July 2017 there was clear stimulation of phytoplankton biomass in the nutrient addition treatments compared to the respective (0S and 180S) controls. In the October 2017 and April 2018 bioassays, there were differences in phytoplankton responses for station 0S and 180S. For station 0S, Chl *a* biomass was high in both the control and nutrient treatment for the first several days (Days 1-4), before growth became limited, most likely due nutrient limitation (N and P). Around day 5 and 6, the 0S control became nutrient limited, while phytoplankton biomass continued to accumulate in the nutrient treatment. For station 180S, the control was almost immediately growth limited, such that the 180S nutrient treatment resulted in elevated phytoplankton biomass compared to the 180S control for all time points. Chl *a* results suggest phytoplankton growth was stimulated during these experimental bioassays, in excess of average *in situ* concentrations (4.9 µg L^{-1} and 14.9 µg L^{-1} for 0S and 180S, respectively).

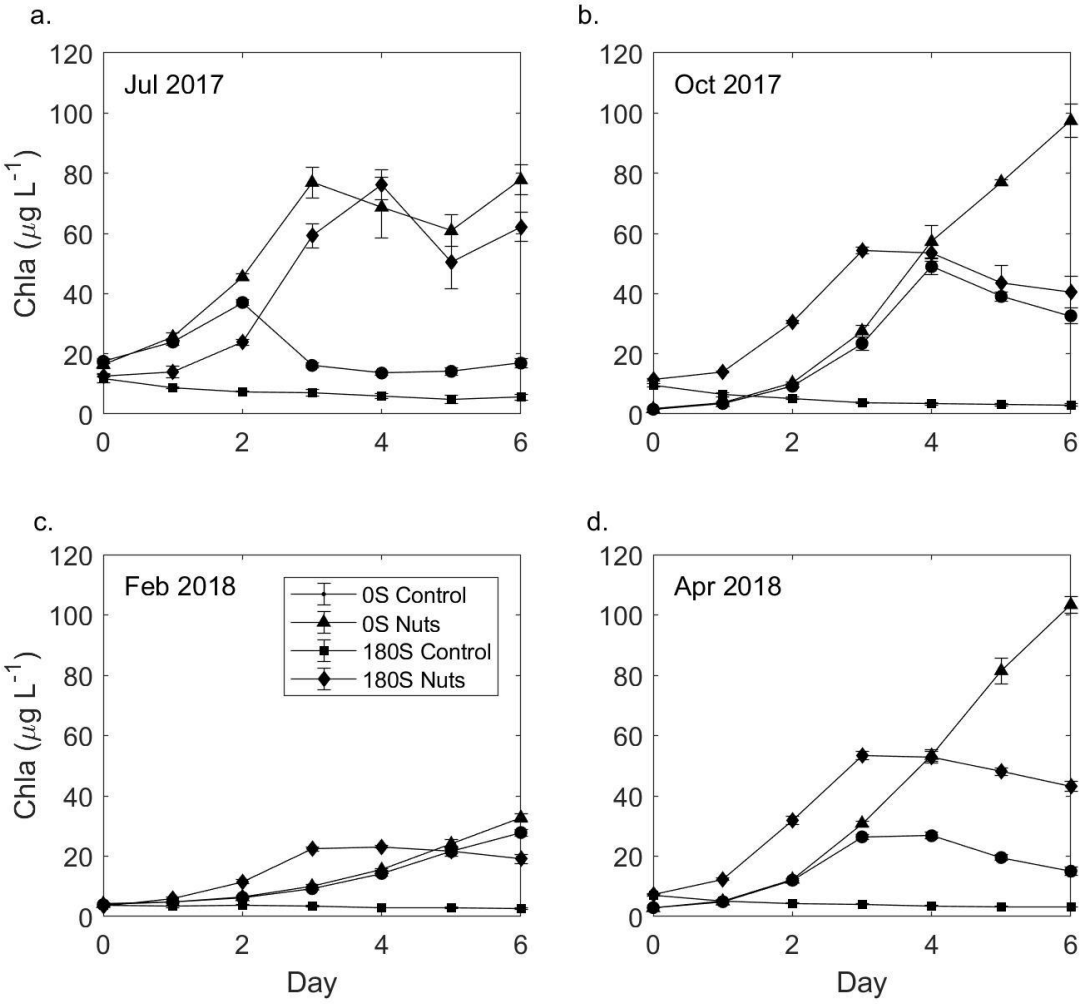

Figure 2-11. Plots of Chl *a* through time for each of the experimental bioassays used to identify an FDOM estuarine processing signal. Results were plotted by bioassay.

A single FDOM component was identified from the subtracted EEMs collected from all experimental bioassays (n = 378) and matched with previously characterized components on OpenFluor (n = 11; TCC > 95%) (Figure 2.12, Table 2.6). Based on matches with the OpenFluor database, the component was identified as a protein-like fluorophore, specifically tryptophan (Lambert et al., 2017; Wheeler et al., 2017). This type of fluorescence has been shown to increase during the exponential phase of phytoplankton growth in other, similarly designed

experimental bioassays using phytoplankton and microbial communities collected from a eutrophic estuary (Stedmon and Markager, 2005).

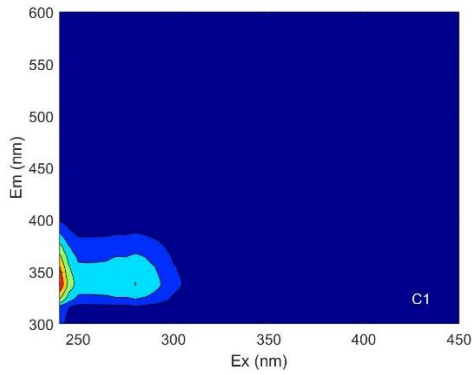

Figure 2-12. Estuarine processing signal identified from samples collected during all of the experimental bioassays (n = 378).

Table 2-6. OpenFluor matches for the 1-component PARAFAC model developed on experimental bioassay FDOM samples. Listed references are only a short subsection of total matches on OpenFluor.

	Ex max. (nm)	**Em max. (nm)**	**OpenFluor Matches**	**Description**	**Reference**
C1	< 250	338	11	Protein-like, tryptophan	Lambert et al., 2017; Murphy et al., 2008; Wheeler et al., 2017

In addition to the OpenFluor database, the 1-component model was compared to the 9-component FluorMod PARAFAC model to assess the uniqueness of the identified estuarine signal to fluorescence signals identified from Neuse River watershed sources (Osburn et al., 2016) using the TuckMatch function in Matlab. The identified 1-component model did not match with any FluorMod components at a similarity > 95%, but did match with FluorMod C3 (identified as protein-like, tryptophan) at > 85% similarity. Comparisons with FluorMod components demonstrate that the estuarine signal identified from the experimental bioassays may be unique enough from watershed sources to be identified and tracked in estuarine samples collected from the NRE.

In order to assess how location (Station 0 vs. 180) and season impacted the evolution of an estuarine fluorescence signal, subtracted samples (day 0 subtracted from subsequent time points, day 1-6) were separated by location (0S, 180S), treatment (control, nutrient addition), and season (Jul 2017, Oct 2017, Feb 2018, Apr 2018) and individual PARAFAC models applied (Table 2.7). July 2017 samples resulted in a 2-component PARAFAC model that was different from the 1-component global model identified for all concatenated samples (Figure 2.13; Table 2.7). The 2-component model matched with previously identified components on OpenFluor. The fitted 2-component model contained both the protein-like, tryptophan fluorescence which was broadly identified in the global experimental bioassay model in addition to a component that has been identified as a microbial, humic-like component indicative of recent biological production, specifically microbial production and has been identified in similar experimental bioassays (Dainard et al., 2015; Stedmon and Markager, 2005). Several of the sample groups did not result in an identified PARAFAC model, indicating there were not sufficient enough or consistent enough fluorescence intensity in the subtracted samples to be accurately modeled by PARAFAC (Table 2.8).

There are clear seasonal differences in the evolution of the estuarine signal for each of the experimental bioassays. The global model developed on all collected samples was largely driven by fluorescence signals from the April 2018 experiment where the same 1-component model was identified for all of the individual treatments (Table 2.8). The global 1-component model was also identified in the combined samples from February 2018, but was not individually identified for each of the treatments. This demonstrates the fluorescence signal from the 1-component model was weak in samples collected from February 2018 and could only be identified when the maximum (n = 96) number of samples were modeled together. For the October 2017 bioassay

samples, no PARAFAC model was identified, despite the relatively high Chl *a* values observed during this incubation (Figure 2.11). As described above, a 2-component model was developed for the July 2017 samples. This model was driven by samples from the riverine treatment (0S), indicating the fluorescence components identified in this experiment were unique to the riverine end member.

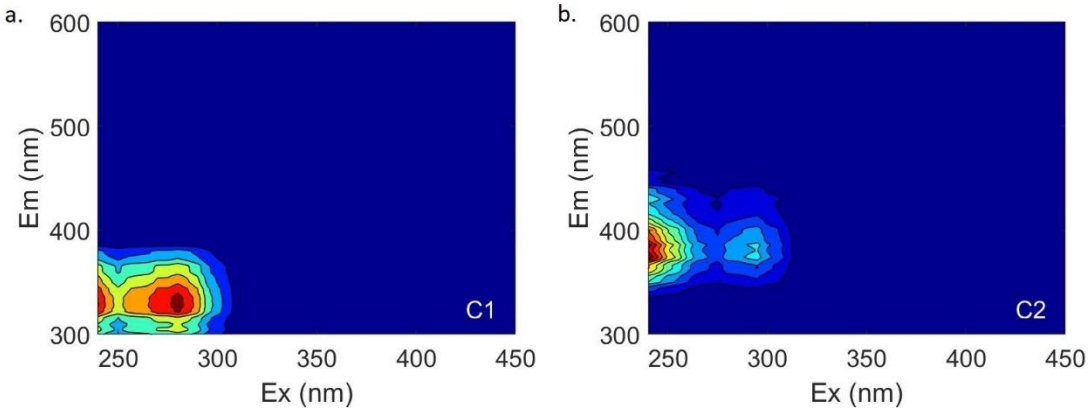

Figure 2-13. 2-component model identified from the July 2017 experiment.

Table 2-7. OpenFluor matches for the 2-component PARAFAC model developed on experimental bioassay FDOM samples from July 2017. The TCC threshold for the 2nd component was set at TCC > 0.90. Listed references are only a short subsection of the total matches on OpenFluor.

	Ex max. (nm)	**Em max. (nm)**	**OpenFluor Matches**	**Description**	**Reference**
C1	<240, 280	328	23	Protein-like, tryptophan	Dainard et al., 2015; Lambert et al., 2016; Podgorski et al., 2018
C2	<240, 295	425	4 (TCC > 0.90)	Humic-like, recent biological production (microbial reprocessing, phytoplankton degradation)	Dainard et al., 2015; Lambert et al., 2017; Podgorski et al., 2018

Table 2-8. Results from applying PARAFAC models to various subsets of subtracted samples collected from the experimental bioassays. Samples were grouped by both location (0S and 180S) and season (July 2017, October 2017, February 2018, April 2018) and PARAFAC models generated.

Treatment	**Season**				
	All	July 2017	October 2017	February 2018	April 2018
All	• 1-component model • 'all' model • characterized as protein-like fluorescence	• 2-component model • 'July 2017' model • Includes protein-like and microbial peak	NONE	• 1-component model • Same as 'all' model	• 1-component model • Same as 'all' model
0S Control	Similar to 'all' model	Same as 'July 2017' model	NONE	NONE	Same as 'all' model
0S Nutrient	Similar to 'all' model	Same as 'July 2017' model	NONE	NONE	Same as 'all' model
180S Control	Similar to 'all' model	NONE	NONE	NONE	Same as 'all' model
180S Nutrient	Similar to 'all' model	NONE	NONE	NONE	Same as 'all' model

Some of the differences between locations (0S vs. 180S) could be explained by the optical properties of the two different water samples used for incubation. The riverine water collected at Station 0S was much darker and had a greater concentration of colored DOM (CDOM) as compared to Station 180S, as measured by absorbance at 350 nm (a_{350}) (Figure 2.14). In more colored, optically dense water, such as in the riverine end member, there are more inner filtering effects which can act to essentially 'protect' FDOM components from photodegradation (Stedmon et al., 2007). Component 2, identified in the July 2017 experimental bioassay, has been shown to be highly photolabile, such that the production of this component by microbial re-processing is often matched by its rate of photodegradation (Stedmon and Markager, 2005). Therefore, in optically clear waters, such as at station 180S, I expect this component to be immediately photodegraded following microbial production. In the riverine water, however, the darker color of the water would allow this component to persist in the environment due to inner filtering effects, in which molecules absorb incoming solar radiation and may serve to protect this component from photodegradation (Stedmon et al., 2007). FDOM centered in the protein-like region has also been shown to be highly photolabile, particularly when exposed to UVA light (Stedmon et al., 2007). Therefore, I hypothesize that it was possible to identify these two biologically reactive components in the riverine water due to inner filtering effects which protected these components from photodegradation, while no components were identified in the optically clear marine water (180S) during the July 2017 experimental bioassay. These results suggest several biologically produced components identified in the experimental bioassays were highly photolabile and once present in the estuary, were quickly removed, particularly in optically clear water such as in the mid- to lower-estuary.

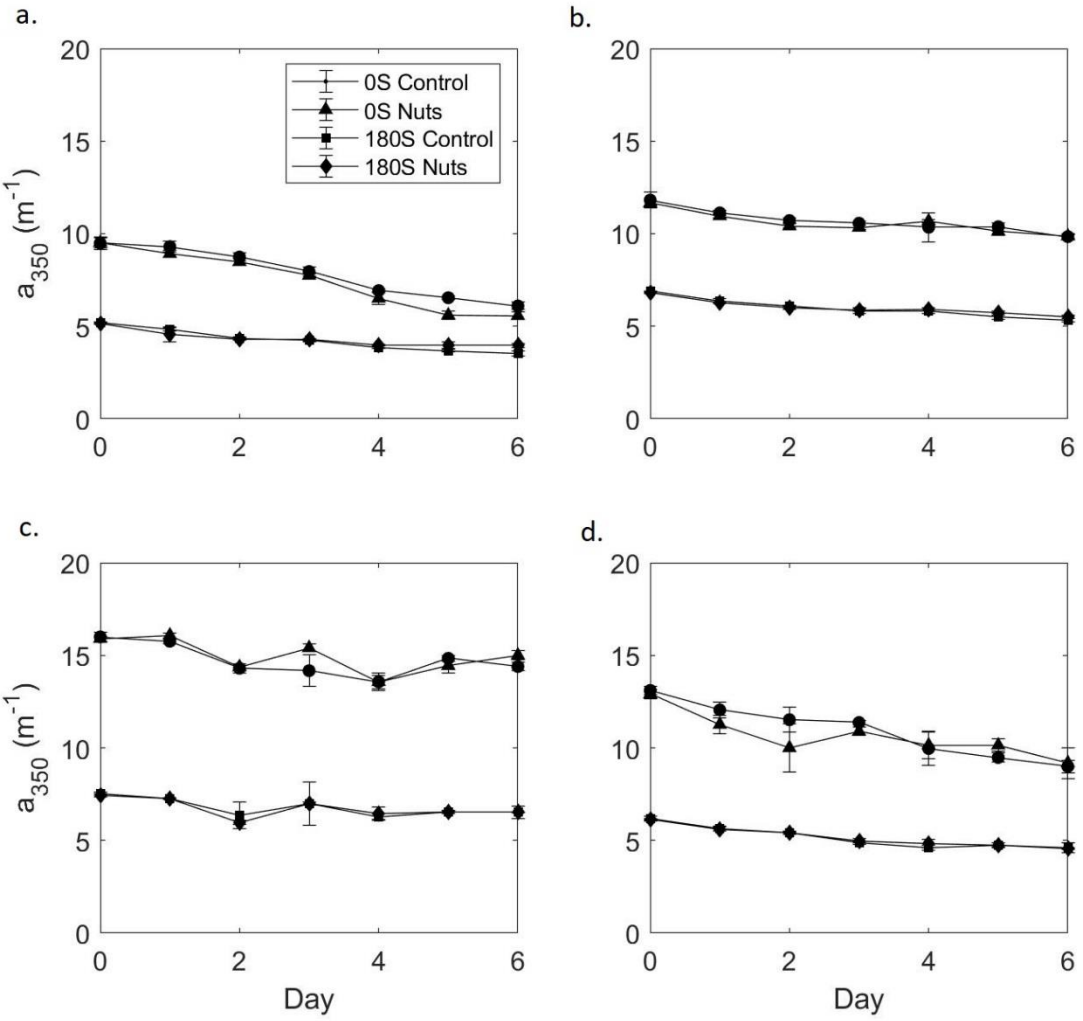

Figure 2-14. Absorbance at 350 nm (a_{350}) plotted for each treatment and experimental bioassay: a. July 2017, b. October 2017, c. February 2018, d. April 2018.

The goal of the experimental bioassays was to identify an estuarine processing signal that could be used to track and assess estuarine FDOM processing, as the combination of FDOM production and degradation, *in situ*. When applied to the un-subtracted EEM samples collected from each experimental bioassay, the 1-component estuarine signal remained constant through all bioassays and treatments (Appendix 2, Figure A2.19). This suggests the FDOM pool in the NRE is overwhelmingly dominated by terrestrial FDOM, even under experimental conditions, masking any potential FDOM production or degradation signals that were present in the estuary

(Murphy et al., 2018; Stedmon and Markager, 2005). This also suggests the planktonic contribution to FDOM in the NRE is small compared to the terrestrial FDOM signal, and likely doesn't affect the overall FDOM pool *in situ*.

In an effort to remove some of the overwhelming influence of terrestrial FDOM in the bioassay samples, a PARAFAC model was fitted to the raw EEM samples collected from all experimental bioassays (n = 441). A 2-component PARAFAC model was identified. The 1-component estuarine processing model was then applied to the sample residuals after application of the 2-component bioassay model. The identified 2-component model was mainly characterized by terrestrial, humic-like fluorescence (Appendix 2, Figure A2.21, Table A2.10). The fluorescent intensity of the three components (2 component bioassay PARAFAC model plus 1 component estuarine processing model) was then plotted through time for each of the seasonal bioassay experiments (Figure 2.15; Appendix 2, Figure A2.23, Figure A2.24, Figure A2.25).

For the July 2018 bioassay (Figure 2.15), the two humic-like, terrestrial components identified decreased during the bioassay, particularly for the 0S treatments, indicating this type of FDOM was removed either via biological or photo-degradation. The estuarine processing signal, however, increased in intensity through the bioassay, for all treatments, indicating production during the experimental bioassay. Results from the other three seasonal bioassays generally follow similar patterns; however, the October 2017, February 2018, and April 2018 bioassays had much greater variability among treatment replicates (Appendix 2, Figure A2.23, Figure A2.24, Figure A2.25). Taken collectively, these results indicate the estuarine processing signal can be identified in experimental bioassay samples after application of a PARAFAC model that acts to 'remove' some of the terrestrial FDOM signals inherent to the samples. The estuarine signal cannot be identified in raw, un-altered EEM samples collected from the bioassay.

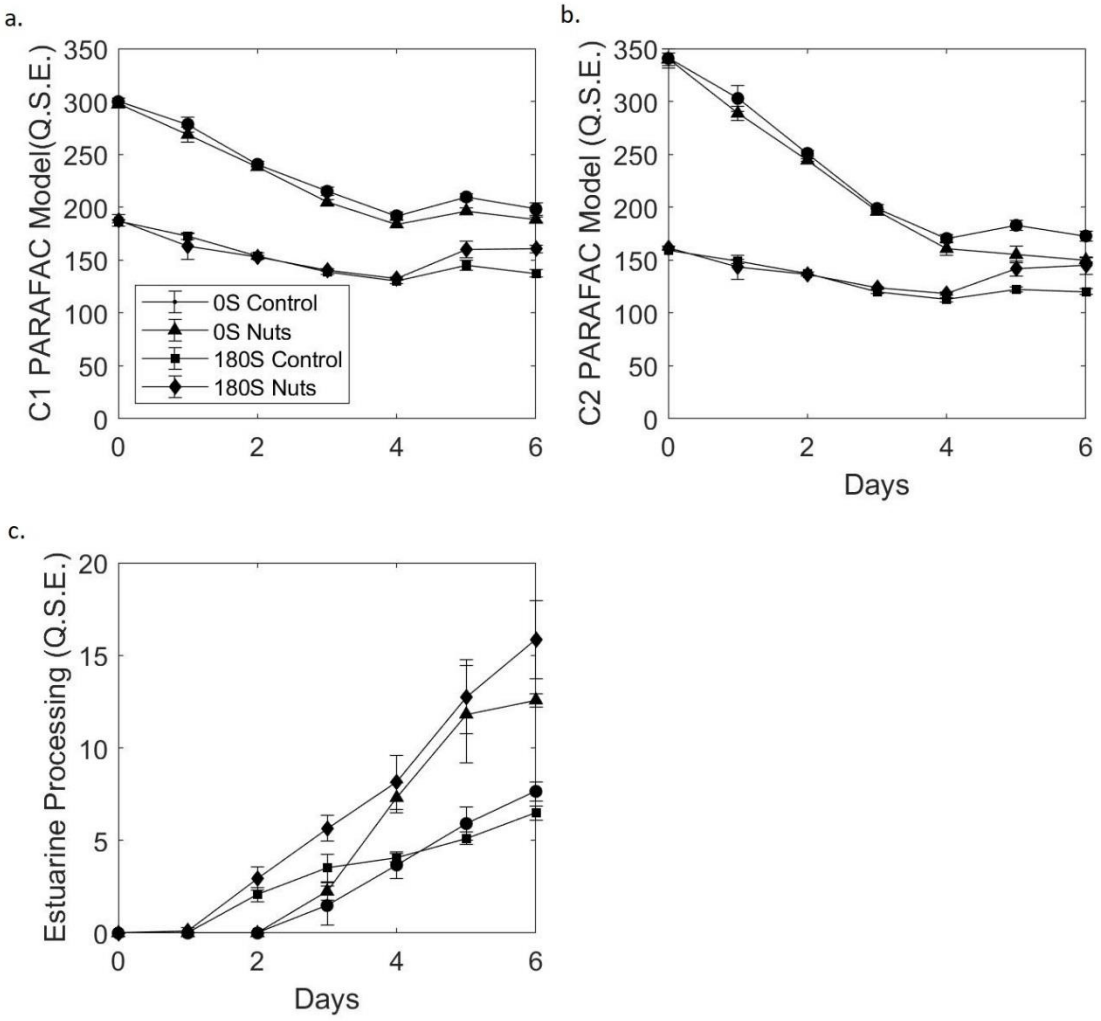

Figure 2-15. Plots of the three experimental bioassay components plotted through time separated by treatment for the July 2017 experimental bioassay. a. Component 1 of the applied PARAFAC model, b. Component 2 of the applied PARAFAC model, and c. 1 component estuarine processing signal.

4.7 Application of FluorMod

To explore the applicability of a PARAFAC model developed on watershed sources to samples collected in an estuarine environment, the FluorMod 9-component PARAFAC model and mixing model (Osburn et al., 2016) were applied to FDOM samples collected in the NRE as part of this year long project. Results from the FluorMod mixing model suggest the estuary was overwhelmingly dominated by background type fluorescence (Reference + Soil leachate) (>

80%) (Figure 2.16; Appendix 2, Figure A2.26). Sources characterized as urban (WWTF influent, WWTF effluent, septic outflow, street runoff) were much smaller in magnitude compared to the background fluorescence (< 10%). Generally, the proportion of summed urban sources increased down estuary while those characterized as agriculture (poultry litter leachate, swine lagoon) remained constant (Figure 2.16; Appendix 2, Figure A2.26). It is somewhat counterintuitive for the urban sources to increase down estuary, as urban development in the NRE watershed is low compared to the upstream river and estuary (Osburn et al., 2016). We suspect several of the sources categorized as 'urban' in FluorMod are identifying potential signals of FDOM production in the NRE. Specifically, the sources associated with human waste (WWTF influent, septic outflow) have relatively high fluorescence in the protein-like region. This region of fluorescence has been linked with biological production *in situ* in estuarine ecosystems, including the NRE (Osburn et al., 2012). Therefore, we expect the urban FluorMod sources which appear to be increasing down estuary, may be due to the production or transformations (i.e., phytoplankton and/or microbial production; photochemical degradation from humic-like FDOM) of FDOM in the NRE.

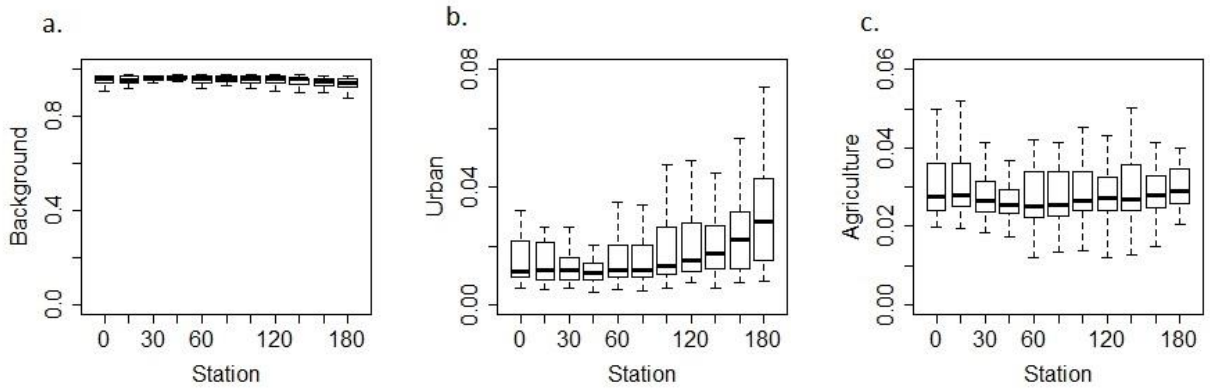

Figure 2-16. Application of the FluorMod mixing model to FDOM samples collected from the NRE plotted by station. FluorMod results as grouped by Background (Reference + Soil), Urban (WWTF effluent, WWTF influent, Septic, Street), and Agriculture (Poultry litter + Swine lagoon). Values represent the proportion of each group in a sample. Each station includes samples collected from both depths (surface and bottom) and all time points.

The applicability of using FluorMod to describe FDOM estuarine samples was assessed by analyzing sample residuals after application of the 9-component FluorMod PARAFAC model (Figure 2.17). FluorMod was unable to capture fluorescence variability of samples between emission wavelengths 450-500 nm. Fluorescence in this region is typically associated with terrestrial, humic-like FDOM (Coble, 2007). This residual signal in the estuary may be a result of the degradation (photochemical, microbial degradation) of terrestrial, humic-like and fulvic-like FDOM that occurs between its source in the watershed and the estuary (Winter et al., 2007), a process which would not be captured by the watershed sources of FDOM used in the development of FluorMod.

The FluorMod 9-component model does appear to capture the majority of the fluorescence variability in the protein-like region of the EEMs (Figure 2.17), which was in a similar area as the estuarine processing signal identified in the experimental bioassays (Figure 2.12). In order to assess this, the 1-component estuarine processing signal was applied to the sample residuals after the application of the 9-component FluorMod PARAFAC model (Figure 2.18). Application of

the estuarine processing signal resulted in low fluorescence intensities (FI < 0.5 Q.S.E.), indicating this type of fluorescence (i.e., protein-like) was already removed from the samples during the initial application of FluorMod. This demonstrates that the estuarine processing signal identified in the experimental bioassays, while unique compared to individual FluorMod components (TCC < 0.95), is overlapped and obscured by competing watershed source components identified in the original FluorMod model.

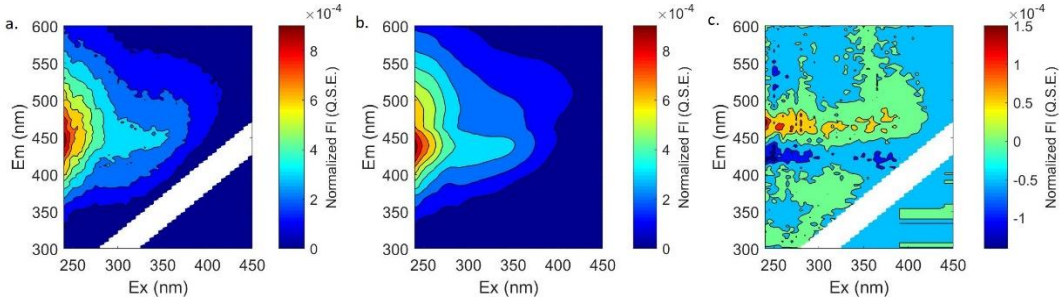

Figure 2-17. FluorMod 9-component model as applied to an FDOM sample collected on 04-06-16 from Station 100 bottom. a. Sample EEM, b. Model EEM, and c. Residual EEM. Colors correspond to normalized fluorescence intensity, as normalized to the total fluorescence of the sample. This sample was representative of samples collected from the NRE.

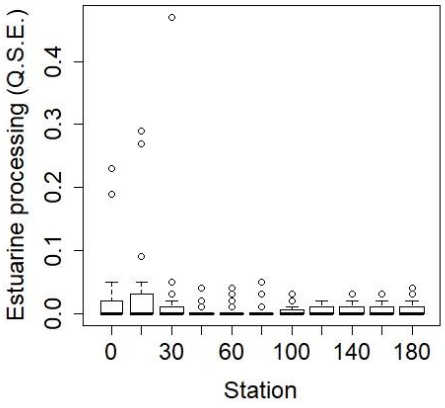

Figure 2-18. Estuarine processing signal plotted down estuary as applied to residual samples after application of FluorMod.

In order to assess if the experimental estuarine processing signal identified during this study occurs *in situ*, the 1-component estuarine processing model was applied to sample residuals from

the FDOM 3-component model (Figure 2.19). Generally, the fluorescent intensity of this component as applied to estuarine samples was low, with a median ~ 0 Q.S.E. However, this estuarine processing signal may be applicable to the NRE when phytoplankton biomass was abnormally high. In fall 2015 there was an exceptionally large phytoplankton bloom at station 30 surface (Chl *a* > 450 µg L^{-1}). This corresponded with the highest fluorescence intensity measured for the estuarine processing signal in the NRE (FI > 5 Q.S.E.). Chl *a* had a statistically significant, but weak positive linear relationship with the estuarine processing signal (Appendix 2, Figure A2.28), which was mainly driven by the anomalously high Chl *a* and FI measured in the fall of 2015.

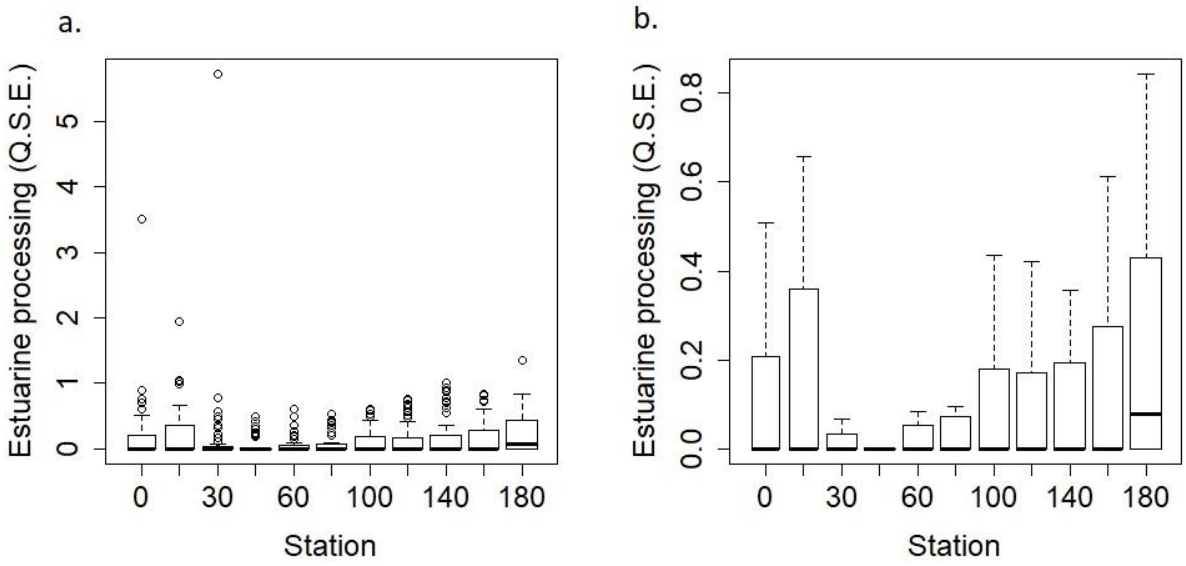

Figure 2-19. Estuarine processing signal applied to sample residuals after the application of the FDOM 3-component model developed for the NRE. Samples are plotted down the estuary by station. a. includes outliers b. outliers are removed for visualization.

While results from the bioassays suggest it is possible to identify a FDOM signal that is unique to estuarine processing in the NRE, when applied to FDOM samples collected *in situ*, it was difficult to identify this component. Application of FluorMod to estuarine samples suggested the need for an estuarine specific processing term, however, when applying the 1-component

estuarine signal identified, it became clear that this signal overlapped with several other, protein-like signals already contained in FluorMod and identified as watershed sources (WWTF influent, septic outflow) (Osburn et al., 2016). When applying the identified estuarine processing signal to residuals of the 3-component FDOM model developed during this study, it was also clear that this signal is not typically identified in the estuary. However, the component was identified in the estuary following a particularly high Chl *a* bloom at station 30S. Results from the bioassays and application of FluorMod indicated the FDOM pool in the estuary was almost overwhelmingly composed of terrestrial, humic-like signals with very few signals indicative of recent *in situ* biological production. Only under extreme circumstances when Chl *a* was highly elevated were there indications of biologically produced FDOM in the estuary which were strong enough to identify over the more ubiquitous terrestrial, humic-like FDOM signals (Murphy et al., 2018; Stedmon and Markager, 2005).

5. Conclusions

This study examined a variety of techniques to develop and apply PARAFAC models to EEM samples collected from an estuarine environment, including developing models generated on specific fractions of the FOM pool (as FDOM and BEFPOM), as well as identifying a potential fluorescent estuarine processing signal, and applying a watershed source-based PARAFAC model to FDOM samples collected from an estuarine ecosystem. Results from this study suggest that PARAFAC modeling was capable of capturing big picture FOM dynamics, such as the dominant sources of FDOM and BEFPOM, as well as identifying an estuarine processing signal in bioassays. However, in the FDOM pool, PARAFAC modeling was unable to resolve any fluorescence signatures of autochthonous FDOM production *in situ.*

Based on modeling results from this chapter, I conclude that the FDOM and BEFPOM pools not only had different sources within the estuary, but also contained fluorescent components that were unique to each pool. The BEFPOM pool contained more distinct fluorescence variability than the FDOM pool, particularly in the protein-like region of fluorescence, and therefore dominated PARAFAC modeling when both FDOM+BEFPOM samples were modeled together. By modeling the two pools separately, it was possible to obtain a better understanding of the degree to which the two pools overlap; in this study, only a single component overlapped between the two pools, indicating these two pools are relatively distinct.

Results from the three PARAFAC models and PCA results also demonstrated that the sources of the FDOM and BEFPOM pools were different, as has been suggested in the literature (Asmala et al., 2018; Osburn et al., 2012; Raymond and Bauer, 2001). The FDOM pool was largely dominated by terrestrial, humic-like material derived from the watershed and follows conservative mixing in the estuary, while the BEFPOM pool was a combination of both terrestrially derived material as well as autochthonous BEFPOM produced in the estuary by phytoplankton and microbial assemblages.

While the PARAFAC models developed for FDOM samples collected in the NRE were unable to identify any type of fluorescent material produced *in situ*, results from the experimental bioassays suggest FDOM is produced and degraded in the estuary; specifically a fluorescent component which resembled the previously characterized protein-like, tryptophan FDOM. However, when applied to either FluorMod residuals or residuals from the 3-component FDOM PARAFAC model developed on estuarine samples, this 1-component estuarine processing signal could not be identified in estuarine samples, suggesting this component was rapidly metabolized in the estuary. Murphy et al., (2018) suggests there may be a handful of certain, ubiquitous

fluorescence signals that could be reliably removed from EEM samples, possibly allowing for the identification and tracking of underlying fluorescence components, such as the estuarine processing signal identified for this study, in samples collected from aquatic environments. However, its ephemeral nature suggests that this component will be difficult to observe *in situ*, except during a phytoplankton bloom.

Without the ability to identify a unique estuarine processing signal *in situ*, the application of a source-based PARAFAC model to estuarine samples is limited. It is likely the transformation of sources from the watershed to estuarine environments are too varied to accurately capture both the original sources and the subsequent *in situ* transformations in a source based model. Therefore, until it is possible to capture *in situ* transformations, a sample-based PARAFAC model appears to be most appropriate for capturing FOM variability in estuarine ecosystems.

REFERENCES

Aiken, G.R., 2014. Fluorescence and dissolved organic matter: A chemist's perspective, in: Coble, P.G., Lead, J., Baker, A., Reynolds, D.M., Spencer, R.G.M. (Eds.), Aquatic Organic Matter Fluorescence. Cambridge University Press, New York, New York, pp. 35–74.

Arar, E.J., Collins, G.B., 1997. In Vitro Determination of Chlorophyll a and Pheophytin a in Marine and Freshwater Algae by Fluorescence. EPA Method 445.0. Technical report for USA-EPA, Cincinnati, Ohio, September 1997.

Asmala, E., Haraguchi, L., Markager, S., Massicotte, P., Riemann, B., Staehr, P.A., Carstensen, J., 2018. Eutrophication Leads to Accumulation of Recalcitrant Autochthonous Organic Matter in Coastal Environment. Global Biogeochemistry Cycles 32, 1673–1687. https://doi.org/10.1029/2017GB005848

Brym, A., Paerl, H.W., Montgomery, M.T., Handsel, L.T., Ziervogel, K., Osburn, C.L., 2014. Optical and chemical characterization of base-extracted particulate organic matter in coastal marine environments. Marine Chemistry 162, 96–113. https://doi.org/10.1016/j.marchem.2014.03.006

Cabaniss, S.E., Shuman, M.W., 1987. Synchronous fluorescence spectra of natural waters: tracing sources of dissolved organic matter. Marine Chemistry, 21, 37-50/

Cawley, K.M., Ding, Y., Fourqurean, J., Jaffe, R., 2012. Characterising the sources and fate of dissolved organic matter in Shark Bay, Australia: a preliminary study using optical properties and stable carbon isotopes. Marine and Freshwater Research 63, 1098–1107.

Coble, P.G., 2007. Marine optical biogeochemistry: The chemistry of ocean color. Chemical Reviews 107, 402–418. https://doi.org/10.1021/cr050350

Dainard, P.G., Guéguen, C., McDonald, N., Williams, W.J., 2015. Photobleaching of fluorescent dissolved organic matter in Beaufort Sea and North Atlantic Subtropical Gyre. Marine Chemistry 177, 630–637. https://doi.org/10.1016/j.marchem.2015.10.004

Fellman, J.B., Miller, M.P., Cory, R.M., D'Amore, D. V., White, D., 2009. Characterizing dissolved organic matter using PARAFAC modeling of fluorescence spectroscopy: A comparison of two models. Environmental Science & Technology 43, 6228–6234. https://doi.org/10.1021/es900143g

Fellman, J.B., Petrone, K.C., Grierson, P.F., 2011. Source, biogeochemical cycling, and fluorescence characteristics of dissolved organic matter in an agro – urban estuary. Limnology and Oceanography 56, 243–256. https://doi.org/10.4319/lo.2011.56.1.0243

Graeber, D., Gelbrecht, J., Pusch, M.T., Anlanger, C.B., von Schiller, D.C., 2012. Agriculture has changed the amount and composition of dissolved organic matter in Central European headwater streams. Science of the Total Environment 438, 435–446. https://doi.org/10.1016/j.scitotenv.2012.08.087

Gueguen, C., Cuss, C.W., Cassels, C.J., Carmack, E.C., 2014. Absorption and fluorescence of dissolved organic matter in the waters of the Canadian Artic Archipelago, Baffin Bay, and the Labrador Sea. Journal of Geophysical Research: Oceans. 119, 2034–2047. https://doi.org/10.1002/2013JC009173.Received

Hall, N.S., Paerl, H.W., Peierls, B.L., Whipple, A.C., Rossignol, K.L., 2013. Effects of climatic variability on phytoplankton community structure and bloom development in the eutrophic, microtidal, New River Estuary, North Carolina, USA. Estuarine, Coastal and Shelf Science 117, 70–82. https://doi.org/10.1016/j.ecss.2012.10.004

Hounshell, A.G., Rudolph, J.C., Van Dam, B.R., Hall, N.S., Osburn, C.L., Paerl, H.W. 2019. Extreme weather events modulate processing and export of dissolved organic carbon in the Neuse River Estuary, NC. Estuarine, Coastal, and Shelf Science 219, 189-200. https://doi.org/10.1016/j.ecss.2019.01.020

Huguet, A., Vacher, L., Relexans, S., Saubusse, S., Froidefond, J.M., Parlanti, E., 2009. Properties of fluorescent dissolved organic matter in the Gironde Estuary. Organic Geochemistry 40, 706–719. https://doi.org/10.1016/j.orggeochem.2009.03.002

Jaffé, R., Cawley, K.M., Yamashita, Y., 2014. Applications of Excitation Emission Matrix Fluorescence with Parallel Factor Analysis (EEM-PARAFAC) in Assessing Environmental Dynamics of Natural Dissolved Organic Matter (DOM) in Aquatic Environments: A Review, in: Advances in the Physiochemical Characterization of Dissolved Organic Matter: Impact on Natural and Engineered Systems. pp. 28–73.

Kulkarni, H. V, Mladenov, N., Johannesson, K.H., Datta, S., 2017. Applied Geochemistry Contrasting dissolved organic matter quality in groundwater in Holocene and Pleistocene aquifers and implications for influencing arsenic mobility. Applied Geochemistry 77, 194–205. https://doi.org/10.1016/j.apgeochem.2016.06.002

Lambert, T., Bouillon, S., Darchambeau, F., Morana, C., Roland, F.A.E., Descy, J.P., Borges, A. V., 2017. Effects of human land use on the terrestrial and aquatic sources of fluvial organic matter in a temperate river basin (The Meuse River, Belgium). Biogeochemistry 136, 191–211. https://doi.org/10.1007/s10533-017-0387-9

Lambert, T., Teodoru, C.R., Nyoni, F.C., Bouillon, S., Darchambeau, F., Massicotte, P., Borges, A. V., 2016. Along-stream transport and transformation of dissolved organic matter in a large tropical river. Biogeosciences 13, 2727–2741. https://doi.org/10.5194/bg-13-2727-2016

Lorenzo-Seva, U., Berge, J.M.F., 2006. Tucker's Congruence Coefficient as a Meaningful Index of Factor Similarity. Methodology. 2, 57–64. https://doi.org/10.1027/1614-1881.2.2.57

Markager, S., Stedmon, C.A., Søndergaard, M., 2011. Seasonal dynamics and conservative mixing of dissolved organic matter in the temperate eutrophic estuary Horsens Fjord. Estuarine, Coastal and Shelf Science 92, 376–388. https://doi.org/10.1016/j.ecss.2011.01.014

McCallister, S.L., Bauer, J.E., Ducklow, H.W., Canuel, E.A., 2006. Sources of estuarine dissolved and particulate organic matter: A multi-tracer approach. Organic Geochemistry 37, 454–468. https://doi.org/10.1016/j.orggeochem.2005.12.005

Murphy, K.R., Stedmon, C. A., Waite, T.D., Ruiz, G.M., 2008. Distinguishing between terrestrial and autochthonous organic matter sources in marine environments using fluorescence spectroscopy. Marine Chemistry 108, 40–58. https://doi.org/10.1016/j.marchem.2007.10.003

Murphy, K.R., Stedmon, C.A., Graeber, D., Bro, R., 2013. Decomposition routines for Excitation Emission Matrices. Analytical Methods 5(23) 1–29. https://doi.org/10.1039/c3ay41160e.drEEM

Murphy, K.R., Stedmon, C.A., Wenig, P., Bro, R., 2014. OpenFluor- An online spectral library of auto-fluorescence by organic compounds in the environment. Analytical Methods 6, 658–661. https://doi.org/10.1039/c3ay41935e

Murphy, K.R., Timko, S.A., Gonsior, M., Powers, L.C., Wünsch, U.J., Stedmon, C.A., 2018. Photochemistry Illuminates Ubiquitous Organic Matter Fluorescence Spectra. Environmental Science & Technology 52, 11243–11250. https://doi.org/10.1021/acs.est.8b02648

Ohno, T., 2002. Fluorescence inner-filtering correction for determining the humification index of dissolved organic matter. Environmental Science & Technology 36, 742-746. https://doi.org/10.1021/es0155276

Osburn, C.L., Boyd, T.J., Montgomery, M.T., Bianchi, T.S., Coffin, R.B., Paerl, H.W., 2016. Optical Proxies for Terrestrial Dissolved Organic Matter in Estuaries and Coastal Waters. Frontiers in Marine Science 2(127). https://doi.org/10.3389/fmars.2015.00127

Osburn, C.L., Handsel, L.T., Mikan, M.P., Paerl, H.W., Montgomery, M.T., 2012. Fluorescence tracking of dissolved and particulate organic matter quality in a river-dominated estuary. Environmental Science & Technology 46, 8628–8636. https://doi.org/10.1021/es3007723

Osburn, C.L., Handsel, L.T., Peierls, B.L., Paerl, H.W., 2016. Predicting Sources of Dissolved Organic Nitrogen to an Estuary from an Agro-Urban Coastal Watershed. Environmental Science & Technology 50, 8473–8484. https://doi.org/10.1021/acs.est.6b00053

Osburn, C.L., Mikan, M.P., Etheridge, J.R., Burchell, M.R., Birgand, F., 2015. Seasonal variation in the quality of dissolved and particulate organic matter exchanged between a salt marsh and its adjacent estuary. Journal of Geophysical Research: Biogeosciences. 120, 1–20. https://doi.org/10.1002/2014JG002897

Osburn, C.L., Morris, D.P., Thorn, K.A., Moeller, R.E., 2001. Chemical and optical changes in freshwater dissolved organic matter exposed to solar radiation. Biogeochemistry 54, 251–278. https://doi.org/10.1023/A:1010657428418

Osburn, C.L., Oviedo-Vargas, D., Barnett, E., Dierick, D., Oberbauer, S.F., Genereux, D.P., 2018. Regional Groundwater and Storms Are Hydrologic Controls on the Quality and Export of Dissolved Organic Matter in Two Tropical Rainforest Streams, Costa Rica. Journal of Geophysical Research: Biogeosciences 123, 850–866. https://doi.org/10.1002/2017JG003960

Paerl, H.W., Crosswell, J.R., Dam, B. Van, Hall, N.S., Rossignol, K.L., Osburn, C.L., Hounshell, A.G., Sloup, R.S., Harding, L.W., 2018. Two decades of tropical cyclone impacts on North Carolina's estuarine carbon, nutrient and phytoplankton dynamics: implications for biogeochemical cycling and water quality in a stormier world. Biogeochemistry 141(3), 307-332. https://doi.org/10.1007/s10533-018-0438-x

Paerl, H.W., Hall, N.S., Peierls, B.L., Rossignol, K.L., 2014. Evolving Paradigms and Challenges in Estuarine and Coastal Eutrophication Dynamics in a Culturally and Climatically Stressed World. Estuaries and Coasts 37, 243-258. https://doi.org/10.1007/s12237-014-9773-x

Peierls, B.L., Christian, R.R., Paerl, H.W., 2003. Water Quality and Phytoplankton as Indicators of Hurricane Impacts on a Large Estuarine Ecosystem. Estuaries 26, 1329–1343. https://doi.org/10.1007/BF02803635

Podgorski, D.C., Zito, P., McGuire, J.T., Martinovic-Weigelt, D., Cozzarelli, I.M., Bekins, B.A., Spencer, R.G.M., 2018. Examining Natural Attenuation and Acute Toxicity of Petroleum-Derived Dissolved Organic Matter with Optical Spectroscopy. Environmental Science & Technology 52, 6157–6166. https://doi.org/10.1021/acs.est.8b00016

Raymond, P.A., Bauer, J.E., 2001. Use of ^{14}C and ^{13}C natural abundances for evaluating riverine, estuarine, and coastal DOC and POC sources and cycling: A review and synthesis. Organic Geochemistry 32, 469–485. https://doi.org/10.1016/S0146-6380(00)00190-X

Shutova, Y., Baker, A., Bridgeman, J., Henderson, R.K., 2014. Spectroscopic characterisation of dissolved organic matter changes in drinking water treatment: From PARAFAC analysis to online monitoring wavelengths. Water Research 54, 159–169. https://doi.org/10.1016/j.watres.2014.01.053

Singh, S., Inamdar, S., Mitchell, M., McHale, P., 2014. Seasonal pattern of dissolved organic matter (DOM) in watershed sources: influence of hydrologic flow paths and autumn leaf fall. Biogeochemistry 118, 321–337. https://doi.org/10.1007/s10533-013-9934-1

Søndergaard, M., Stedmon, C.A., Borch, N.H., 2003. Fate of terrigenous dissolved organic matter (DOM) in estuaries: Aggregation and bioavailability. Ophelia 57, 161–176. https://doi.org/10.1080/00785236.2003.10409512

Spencer, R.G.M., Aiken, G.R., Dornblaser, M.M., Butler, K.D., Holmes, R.M., Fiske, G., Mann, P.J., Stubbins, A., 2013. Chromophoric dissolved organic matter export from U.S. rivers. Geophysical Research Letters 40, 1575-1579. https://doi.org/10.1002/grl.50357.

Stedmon, C.A., Bro, R., 2008. Characterizing dissolved organic matter fluorescence with parallel factor analysis. Limnology and Oceanography Methods 6, 572–579. https://doi.org/10.4319/lom.2008.6.572

Stedmon, C.A., Markager, S., 2005. Tracing the production and degradation of autochthonous fractions of dissolved organic matter using fluorescence analysis. Limnology and Oceanography 50, 1415–1426. https://doi.org/10.4319/lo.2005.50.5.1415

Stedmon, C.A., Markager, S., 2005. Resolving the variability in dissolved organic matter fluorescence in a temperate estuary and its catchment using PARAFAC analysis. Limnology and Oceanography. 50, 686–697.

Stedmon, C.A., Markager, S., Tranvik, L., Kronberg, L., Latis, T., Martinsen, W., 2007. Photochemical production of ammonium and transformation of dissolved organic matter in the Baltic Sea. Marine Chemistry 104, 227–240. https://doi.org/10.1002/2013JC009173.

Stubbins, A., Lapierre, J.F., Berggren, M., Prairie, Y.T., Dittmar, T., Del Giorgio, P.A., 2014. What's in an EEM? Molecular signatures associated with dissolved organic fluorescence in boreal Canada. Environmental Science & Technology 48, 10598–10606. https://doi.org/10.1021/es502086e

Vähätalo, A.V., Wetzel, R.G., Paerl, H.W., 2005. Light absorption by phytoplankton and chromophoric dissolved organic matter in the drainage basin and estuary of the Neuse River, North Carolina (U.S.A.). Freshwater Biology 50, 477–493. https://doi.org/10.1111/j.1365-2427.2004.01335.x

Weishaar, J.L., Fram, M.S., Fujii, R., Mopper, K., 2003. Evaluation of Specific Ultraviolet Absorbance as an Indicator of the Chemical Composition and Reactivity of Dissolved Organic Carbon. Environmental Science & Technology 4702–4708. https://doi.org/10.1021/es030360x

Wheeler, K.I., Levia, D.F., Hudson, J.E., 2017. Tracking senescence-induced patterns in leaf litter leachate using parallel factor analysis (PARAFAC) modeling and self-organizing maps. Journal of Geophysical Research: Biogeosciences 122, 2233–2250. https://doi.org/10.1002/2016JG003677

Winter, A.R., Anne, T., Fish, E., Playle, R.C., Smith, D.S., Curtis, P.J., 2007. Photodegradation of natural organic matter from diverse freshwater sources. Aquatic Toxicology 84, 215–222. https://doi.org/10.1016/j.aquatox.2007.04.014

Wünsch, U., Bro, R., Stedmon, C., Wenig, P., Murphy, K., 2019. Emerging patterns in the global distribution of dissolved organic matter fluorescence. Analytical Methods. https://doi.org/10.1039/C8AY02422G

Yamashita, Y., Boyer, J.N., Jaffé, R., 2013. Evaluating the distribution of terrestrial dissolved organic matter in a complex coastal ecosystem using fluorescence spectroscopy. Continental Shelf Research 66, 136–144. https://doi.org/10.1016/j.csr.2013.06.010

Yamashita, Y., Panton, A., Mahaffey, C., Jaffé, R., 2011. Assessing the spatial and temporal variability of dissolved organic matter in Liverpool Bay using excitation-emission matrix fluorescence and parallel factor analysis. Ocean Dynamics 61, 569–579. https://doi.org/10.1007/s10236-010-0365-4

CHAPTER 3: SPATIAL AND TEMPORAL DISTRIBUTION OF FLUORESCENT ORGANIC MATTER IN THE NEUSE RIVER ESTUARY, NORTH CAROLINA

1. Summary

The importance of estuaries as transformers, producers, and transporters of nutrients and organic matter prior to export to the coastal ocean, is well established in the literature. Due to their location along the fresh- to saltwater gradient, estuaries contain a complex mixture of organic matter which is characteristic of both allochthonous (terrestrial) and autochthonous (produced *in situ*) sources. The composition of the organic matter pool is influenced by spatial (distance down estuary) and temporal (seasonal; riverine discharge) variability, making it difficult to tease apart and assess the organic matter dynamics in hydrologically-complex and variable environments like estuaries. While previous studies have assessed either the dissolved or particulate organic matter pool over short temporal or spatial scales, few studies have simultaneously assessed both the dissolved and particulate organic matter pools in estuarine environments. The goal of this study was to address this gap by simultaneously assessing both the dissolved and particulate organic matter pools spatially, along the full fresh- to saltwater estuarine gradient and temporally, for a full year. The quality and quantity of each organic matter pool (dissolved and particulate) was assessed for a range of parameters (concentration, absorbance and fluorescence indices) resulting in a multivariate data set that spanned temporal and spatial gradients. In order to take advantage of the diverse data collected, multivariate statistical techniques were applied, including principal component, redundancy, and co-inertia analyses used to understand how environmental variables and indicators of dissolved and

particulate organic matter quality and quantity relate to each other. Results indicate organic matter quantity and quality were dominated by terrestrial, humic-like organic matter loaded from the riverine end-member and autochthonous organic matter produced *in situ* by phytoplankton and microbial assemblages in the lower to mid-estuary. The dissolved organic matter pool was largely controlled by riverine discharge throughout the estuary, while the particulate organic matter pool was controlled by riverine discharge in the upper estuary and by phytoplankton organic matter production in the mid- to lower-estuary. By relating the dissolved and particulate organic matter pools directly via co-inertia analysis, it was possible to determine similar sources of organic matter for the two pools and assess how these sources relate to various absorbance and fluorescence indices. Results suggest, indices of organic matter quality can be used across the dissolved and particulate organic matter pools to fully assess organic matter sources and distribution along the freshwater to marine continuum.

2. Introduction

Estuaries represent the transition from freshwater to saltwater and have been shown to be important sites for the production, transformation, and storage of nutrients and organic matter (OM), prior to export to the coastal ocean (Paerl et al., 1998; Raymond and Bauer, 2001; Vlahos and Whitney, 2017). Due to their transitional nature, estuaries represent complex mixtures of both terrestrially-derived and autochthonously produced OM, each of which have unique molecular structures, characteristics, and bio-availabilities (Asmala et al., 2018; Markager et al., 2011; Osburn et al., 2012). OM is often divided into two pools operationally defined by filtration: the dissolved OM (DOM) pool is anything which passes through a 0.7 µm mesh size filter while the particulate OM (POM) pool is anything retained on a 0.7 µm mesh size filter.

Generally, DOM concentrations in estuaries are much greater than POM concentrations while DOM is largely considered to be more bio-available to heterotrophic organisms than POM (McCallister et al., 2006; Raymond and Bauer, 2001). Both DOM and POM can be derived from either terrestrial (allochthonous) or autochthonous sources. The composition, relative dominance, and sources of these two pools changes through the estuary in response to physical, chemical, and biological processes that occur from the upper to lower estuary (Huguet et al., 2009; McCallister et al., 2006). In the upper estuary, the POM pool is largely composed of terrestrial, humic-like material delivered from the river and surrounding watershed. In the lower estuary, the POM pool becomes more characteristic of autochthonous, biological sources of OM as the POM pool shifts from terrestrial dominated particulates (i.e., removal via sedimentation, flocculation) to those produced by phytoplankton (Brym et al., 2014; Osburn et al., 2012). Likewise, the DOM pool also undergoes dilution and transformation from the riverine to marine end members, but appears to retain more of its allochthonous, terrestrial character than the POM pool, lacking major removal processes via bacterial and/or photochemical degradation (McCallister et al., 2006; Osburn et al., 2012). Due to the differing dominance of their sources and lability, the partitioning of the OM pool into POM and DOM has important implications for the ultimate fate and bio-reactivity of OM in estuaries.

Studies have demonstrated how the two pools, despite having different compositions through the estuary, may be linked. Exchange between the POM and DOM pools is mainly due to photodegradation of POM to DOM, such that the photodissolution of POM leads to colored DOM (CDOM) (Huguet et al., 2009; Osburn et al., 2012) but can also be transformed through decomposition via microbial degradation (Asmala et al., 2018) and extracellular release of DOM from phytoplankton (i.e., part of the POM pool) (Carlson and Hansell, 2014). Production of

POM is largely due to phytoplankton growth and the conversion of dissolved nutrients and dissolved inorganic carbon to phytoplankton biomass (Bianchi, 2007). Despite previous studies that have assessed the DOM and/or POM pool in estuaries, few studies have simultaneously assessed the quantity and quality of both the DOM and POM pools over the prominent temporal and spatial gradients characterizing estuaries. The goal of this study was to fill this gap by assessing DOM and POM concentration and composition over a year-long (July 2015 – July 2016) study period in the eutrophic, river-dominated, Neuse River Estuary (NRE), North Carolina (NC), USA.

Using concentration (dissolved organic carbon, [DOC]; particulate organic carbon, [POC]) as well as absorbance and fluorescence measurements, as fluorescence DOM (FDOM) and fluorescence POM (FPOM), the quantity and quality of the two OM pools were assessed. Due to the multiple parameters collected to assess the quantity and quality of both the DOM and POM pools as well as environmental data collected, multivariate statistical analyses were used to fully consider the range of data and measurements collected. The study addressed three key questions:

1. What are the differences in the quantity and quality of the FDOM and FPOM pools along the estuarine continuum in the NRE?
2. What controls FDOM and FPOM composition temporally and spatially?
3. Are these two pools connected? Can we directly relate processes in the FDOM pool to those in the FPOM pool and vice versa?

Results from this study will further our understanding of the controls, processes, and function of the FDOM and FPOM pools in estuarine environments, and enhance our understanding of how the FDOM and FPOM pools may influence carbon and nutrient cycling in eutrophic estuaries.

3. Materials and Methods

3.1 Study site and sampling methods

The NRE is a eutrophic, river-dominated, micro-tidal estuary located in the coastal plain of eastern NC (Figure 3.1). The Neuse River flows through the increasingly urbanized Raleigh-Durham area and several growing, downstream municipalities (Goldsboro, Kinston, and New Bern, NC) before entering the estuary where land use is characterized by agriculture (concentrated animal feeding and row crop operations), wetlands, and forested watersheds (Bhattacharya and Osburn, 2017; Rothenberger et al., 2009; Stow et al., 2001). Due to the mixed land use, a variety of nutrient and OM sources are present within both the Neuse river and NRE (Osburn et al, 2016; Pellerin et al., 2006; Stedmon et al., 2006). The estuary drains into the Albemarle-Pamlico Sound, a semi-lagoonal system which has restricted exchange with the Atlantic Ocean, leading to residence times of ~5-8 weeks in the NRE (Peierls et al., 2012). This provides ample time for phytoplankton and associated microbial assemblages to utilize both inorganic and organic nutrients flushed into the NRE (Christian et al., 1991; Luettich et al., 2000). The NRE is strongly nitrogen (N)-limited (Paerl et al., 1995; Rudek et al., 1991) and can exhibit large phytoplankton blooms in the summer and fall months which exacerbate bottom water hypoxia and can lead to widespread fish kills (Paerl et al., 1998; Paerl et al., 2004).

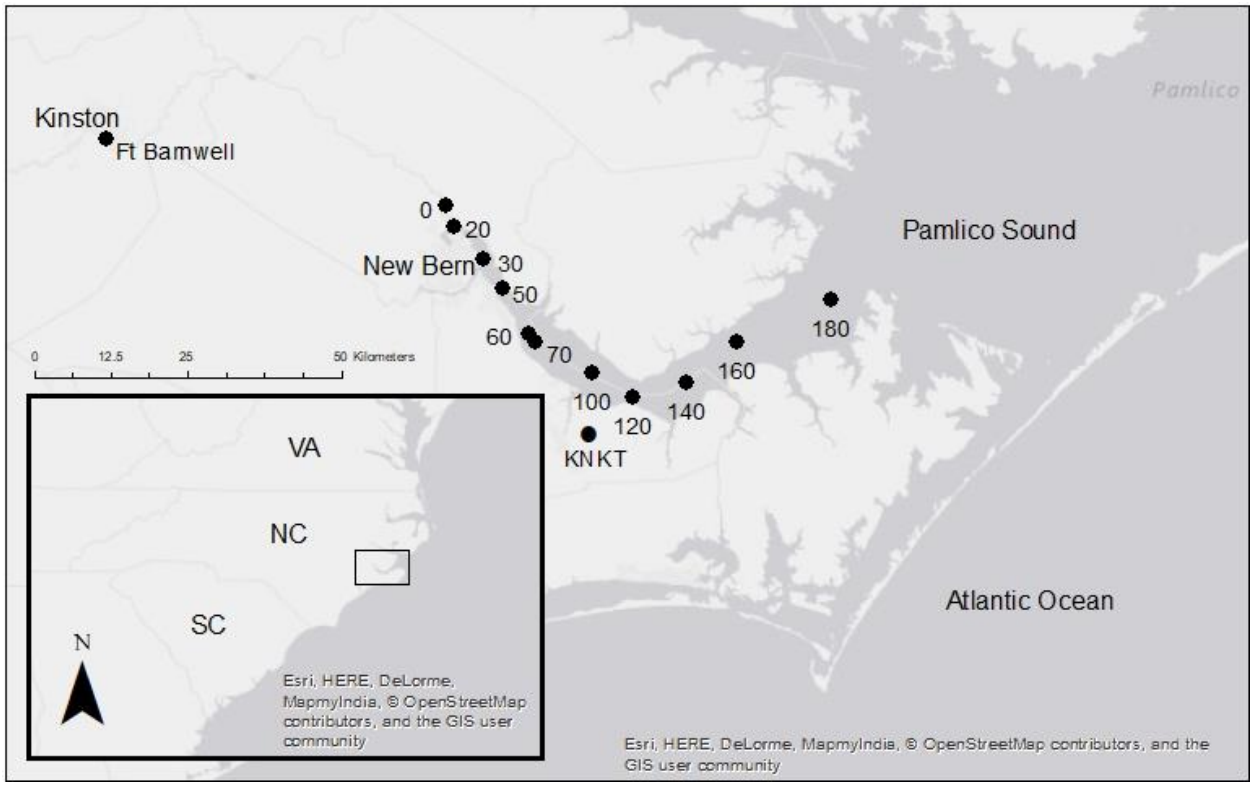

Figure 3-1. Map of the NRE located in Eastern NC. ModMon sampling locations are designated as station 0 -180. The location of the USGS gage used for riverine discharge data is designated as Ft. Barnwell. Wind data was collected at the Cherry Point Marine Corps Air Station (MCAS) weather station, KNKT located in Havelock, NC.

Samples for physical, chemical, biological, and OM analyses were collected as part of the Neuse River Monitoring and Modeling Program (ModMon; http://paerllab.web.unc.edu/projects/modmon/) located at the University of North Carolina – Chapel Hill, Institute of Marine Sciences (UNC-CH IMS) (Paerl et al., 2018). Samples were collected for a full year from July 20, 2015 to July 28, 2016, bi-weekly from March to October and monthly from November to February. For each sampling date (n = 22), samples were collected at 11 stations in the NRE spanning from the upstream-most location of salinity intrusion (Station 0) to the mouth of the estuary (Station 180) (Figure 3.1). Temperature (Temp), salinity (Sal), turbidity (Turb), and dissolved oxygen (DO) were measured at surface (0.2 m below surface) and bottom (0.5 m above bottom) depths using a YSI 6600 multi-parameter,

water quality sonde (Hall et al., 2013). Surface (0.2 m below surface) and bottom (0.5 m above bottom) water samples were collected for various chemical, biological, and OM analyses at each of the 11 stations. Samples were maintained in the dark at ambient temperature and returned to UNC-CH IMS within ~6 hours of collection. Samples were then filtered through combusted (450^{o}C, 4 hours) 0.7 µm mesh size, GF/F glass fiber filters. The filtrate was collected and stored frozen at -20°C in the dark until dissolved nutrient and DOM quantitative and qualitative analysis. Filters were collected and stored frozen at -20^{o}C in the dark until chlorophyll-*a* (Chl *a*) analysis, conducted within one month of collection, and POM quantitative and qualitative analysis, as described below.

3.2 Organic matter analysis

DOC concentration ([DOC]) was measured via high-temperature catalytic oxidation on a Shimadzu TOC-5000 analyzer (Peierls et al., 2003). Total dissolved nitrogen (TDN), nitrate + nitrite (NO_3^- + NO_2^-), and ammonium (NH_4^+) were determined colormetrically using a Lachat QuickChem autoanalyzer (Peierls et al., 2003). Dissolved organic nitrogen ([DON]) was determined by subtracting the dissolved inorganic nitrogen species (DIN, as NO_3^- + NO_2^- + NH_3^+) from TDN. The molar DOC:DON ratio was calculated after converting measured [DOC] and [DON] to molar units. [POC] and particulate nitrogen ([PN]) were determined on one set of collected filters via high temperature combustion on a Costech ECS 4010 analyzer, after vapor acidification (HCl) to remove carbonates (Paerl et al., 2018). [POC] and [PN] were used to calculate the molar POC:PN ratios.

For absorbance and fluorescent OM analyses (FDOM and FPOM), thawed DOM samples were re-filtered through 0.2 µm mesh size, polyethersulfone (PES) filters immediately prior to analysis. Samples for POM analysis were extracted from frozen filters using the base extracted

FPOM (BEFPOM) method, originally developed for extraction of POM from soils and sediments, and later adapted to estuarine seston samples by Osburn et al., 2012. Briefly, seston on collected filters was extracted using 10 mL of 0.1 M NaOH and stored in the dark at 4ºC for 24 hours. Samples were then neutralized with concentrated HCl (~ 100 µL) to measured neutral pH (~ 7.0) and filtered through 0.2 µm mesh size, PES filters. Filtered extracts were immediately analyzed for absorbance and fluorescence as described below.

Absorbance spectra for filtered DOM and extracted BEFPOM samples were measured on a Shimadzu UV-1700 Pharma-Spec spectrophotometer. Absorbance spectra were corrected using a Nanopure water blank collected on the same day as analysis. All samples with > 0.4 raw absorbance units at 240 nm were diluted (Osburn et al., 2012). Absorbance values at 254 nm were converted to Napierian absorbance coefficients (a_λ, m^{-1}) (Spencer et al., 2013). Specific UV absorbance ($SUVA_{254}$) (L mg^{-1} C m^{-1}) was calculated as a_{254}/[OC] (as DOC or POC, respectively) for each sample (Weishaar et al., 2003).

Fluorescence spectra were obtained on a Varian Cary Eclipse spectrofluorometer. Excitation wavelengths were measured from 240 to 450 nm every 5 nm. Emission wavelengths were measured from 300 to 600 nm at 2 nm intervals. Instrument excitation and emission corrections were applied to each sample in addition to corrections for inner-filtering effects, calibrated against the Raman signal of Nanopure water, and standardized to quinine sulfate equivalents (Q.S.E.) (Murphy et al., 2013; Osburn et al., 2012). Excitation and emission scans were concatenated into 151 x 43 Excitation-Emission Matrices (EEMs).

The humification index (HIX) and biological index (BIX) were calculated from measured fluorescence spectra and were used as indicators of the relative quality of OM in estuaries from more terrestrial, humic-like OM to more biological, autochthonously produced OM (Huguet et

al., 2009). HIX is the ratio of the H (435-480 nm) and L (300-345 nm) regions of fluorescence measured at an excitation wavelength of 254 nm. HIX is indicative of the degree of humification and aromaticity of the FOM pool in a sample and generally decreases down estuary (Table 1). BIX is calculated as the ratio between the β (380 nm) (Peak M) and α (430 nm) (Peak C) regions of fluorescence measured at an excitation wavelength of 310 nm. BIX is an indicator of autochthonous, recently produced FOM and generally increases down estuaries (Huguet et al., 2009) (Table 3.1). In addition to fluorescent indicators such as HIX and BIX, peak-picking methods were used to identify previously selected and characterized EEM fluorescent peaks from the literature (Table 3.2) (Coble, 2007; Fellman et al., 2010).

Table 3-1. Range of HIX and BIX values and the associated OM characterization as determined by Huguet et al., 2009.

HIX Values	**FOM Characterization**
> 16	Humic, terrestrial-like
6-10	Mainly humic, terrestrial-like with some very weak autochthonous influence
4-6	Little humic, terrestrial-like influence with greater autochthonous influence
< 4	Autochthonous, biological sources
BIX Values	**FOM Characterization**
> 1	Autochthonous, biological sources
0.8-1	Relatively large, autochthonous contribution
0.7-0.8	Small autochthonous contribution
0.6-0.7	Very low autochthonous contribution

Table 3-2. Previously identified and characterized fluorescence peaks from the literature used in the peak-picking method. Excitation and emission wavelengths and peak characterization were designated by Coble 2007, Fellman et al., 2010 and Huguet et al., 2009 (and references within).

Peak identification	**Excitation/Emission Wavelength (nm)**	**Peak Characterization**
A	260/400-460	Terrestrial, humic-like, allochthonous
C	320-360/420-460	Terrestrial, humic-like, anthropogenic
T	275/340	Protein, tryptophan-like
B	275/305	Protein, tyrosine-like
M	290-310/370-410	Marine, humic-like, recent production, anthropogenic
N	280/370	Potential indicator of autochthonous material

3.3 Chlorophyll *a* analysis

Phytoplankton biomass was measured as Chl *a* using a modified version of EPA method 445.0 (Arar and Collins, 1997). Briefly, collected filters were extracted overnight in 90% acetone followed by processing in a tissue grinder. Extracts were analyzed un-acidified on a Turner Designs TD-700 fluorometer with a narrow bandpass filter.

3.4 River discharge and meteorological data

Neuse River discharge data was obtained 26 km upstream from the head of the NRE (Station 0) at USGS gaging station #02091814 located at Ft. Barnwell, NC (Figure 3.1). Discharge data was scaled to the area of un-gaged watershed in the NRE (31% un-gauged watershed) (Peierls et al., 2012). Meteorological data (wind speed, gusts, and direction) were obtained from the State Climate Office of NC, CRONOS weather station located at Cherry Point Marine Corps Air Station (station KNKT) in Havelock, NC which is located about mid-estuary (Figure 3.1). I assume meteorological measurements at this location are representative of the entire NRE.

Discharge and wind speed data were averaged over the time period spanning each ModMon sampling date, such that for each ModMon date discharge and wind speed were averaged from the date of the prior ModMon collection date to the ModMon collection date of interest (Appendix 3, Figure A3.1). I assume the conditions in the NRE, as sampled by ModMon, are a reflection of all processes occurring in the estuary in the days and weeks prior to the collected sample. For wind gusts, the maximum wind gust during the averaging period, as described above, were used. The prevailing wind direction for each time point was determined by calculating the mode for each time period (Appendix 3, Figure A3.1).

3.5 Statistical analyses

For statistical analysis, all collected data from the NRE were divided into three separate data matrices: an environmental data matrix that included measurements of temperature, salinity, turbidity, dissolved oxygen, and Chl *a*; a DOM matrix that included all concentration ([DOC], [DON], DOC:DON), absorbance (a_{254}, $SUVA_{254}$), and fluorescence (HIX, BIX, Peaks A, C, T, B, N, M) measurements for the DOM pool; and a POM matrix that included all concentration ([POC], [PN], POC:PN), absorbance (a_{254}, $SUVA_{254}$), and fluorescence (HIX, BIX, Peaks A, C, T, B, N, M) measurements for the POM pool. Multivariate statistical analyses were applied to the three data sets in an effort to retain and use all information from the multiple variables that were collected.

Briefly, principal component analysis (PCA) is a statistical decomposition technique which calculates principal components that represent a linear combination of original variables and which sequentially explain the most to least amount of variation within the data (Paliy and Shankar, 2016). PCA was conducted on each individual data set (Environmental, DOM, and POM data) to help visualize all variables and data for each matrix on a single plot. Redundancy analysis (RDA) is a combination of PCA and multiple linear regression which uses an explanatory data matrix (environmental data) to describe the variability of a response matrix (either DOM or POM data). Like multiple linear regression, forward, stepwise addition can be used to select the explanatory variables (Temp, Sal, Turb, DO, Chl *a*) which explain the most variation in the response data set (Borcard et al., 2018). Co-inertia Analysis (CoIA) is similar to RDA in that it relates two data matrices to each other, but unlike RDA, is a symmetric analysis such that it does not assume an explanatory or response matrix and is a useful tool for directly

relating two data sets without any assumptions (i.e., DOM and POM data sets) (Borcard et al., 2018).

All multivariate statistical analyses were conducted in RStudio. PCA and RDA were conducted using the vegan package for R (https://cran.r-project.org/web/packages/vegan/index.html). CoIA was conducted using the ade4 package (https://cran.r-project.org/web/packages/ade4/index.html). All data corrections, peak-picking methods, and calculation for EEMs and fluorescent indices were conducted in Matlab R2017b.

4 Results and Discussion

4.1 Environmental and organic matter parameters

The study period (July 2015-2016) was characterized by above average discharge from the Neuse River (Hounshell et al., 2019) which resulted in depressed estuarine salinity in the NRE during this period as compared to the longer term median as calculated from historical ModMon data (2000 - 2017) (Figure 3.2a). Chl *a* during the spring (March-May) and summer (June-August) were close to the long term median for the estuary, but the estuary was characterized by above average Chl *a* in fall (September-November) and below average Chl *a* in the winter (December - February) (Figure 3.2b).

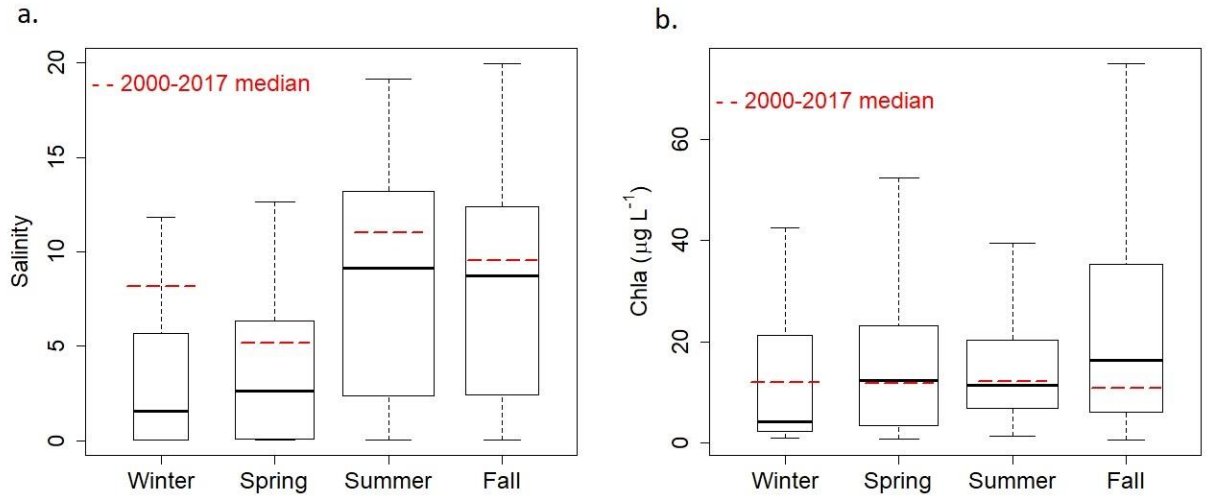

Figure 3-2. Salinity and Chl *a* plotted seasonally (Winter = December – February; Spring = March – May; Summer = June – August; Fall = September - November) for all time points, stations, and depths collected during the sampling period. The long term median (2000-2017) is plotted as the dashed red lines for each season. Outliers were removed for the Chl *a* data.

[DOC] plotted seasonally during the study period appears to be inversely related to salinity in the estuary (Figure 3.3a) with the highest [DOC] in the winter followed by a decrease in concentration during the spring and summer. [POC], however, does not exhibit a seasonal pattern, with little variation in the median concentration through the seasons (Figure 3.3b). Compared to [DOC], [POC] is about an order of magnitude lower for all seasons. As an indicator of the quality of the two OM pools, HIX was plotted seasonally for both DOM and POM (Figure 3.3c-d). HIX > 16 is generally thought of as humic-like, aromatic, allochthonous OM while HIX < 6 is considered fresher, more autochthonous-like material (Huguet et al., 2009) (Table 3.1). Unlike for bulk concentration, both the DOM and POM pools exhibited seasonal variation in HIX with higher HIX values (more humic-like, terrestrial OM) in the winter and progressively lower values (fresher, more autochthonous-like OM) in the spring and summer. Overall, the POM pool had much lower values of HIX, indicative of more autochthonous, fresher OM than

the DOM pool, with the lowest POM HIX values occurred during spring and summer when phytoplankton biomass (Chl *a*) was highest and estuarine salinity was greatest.

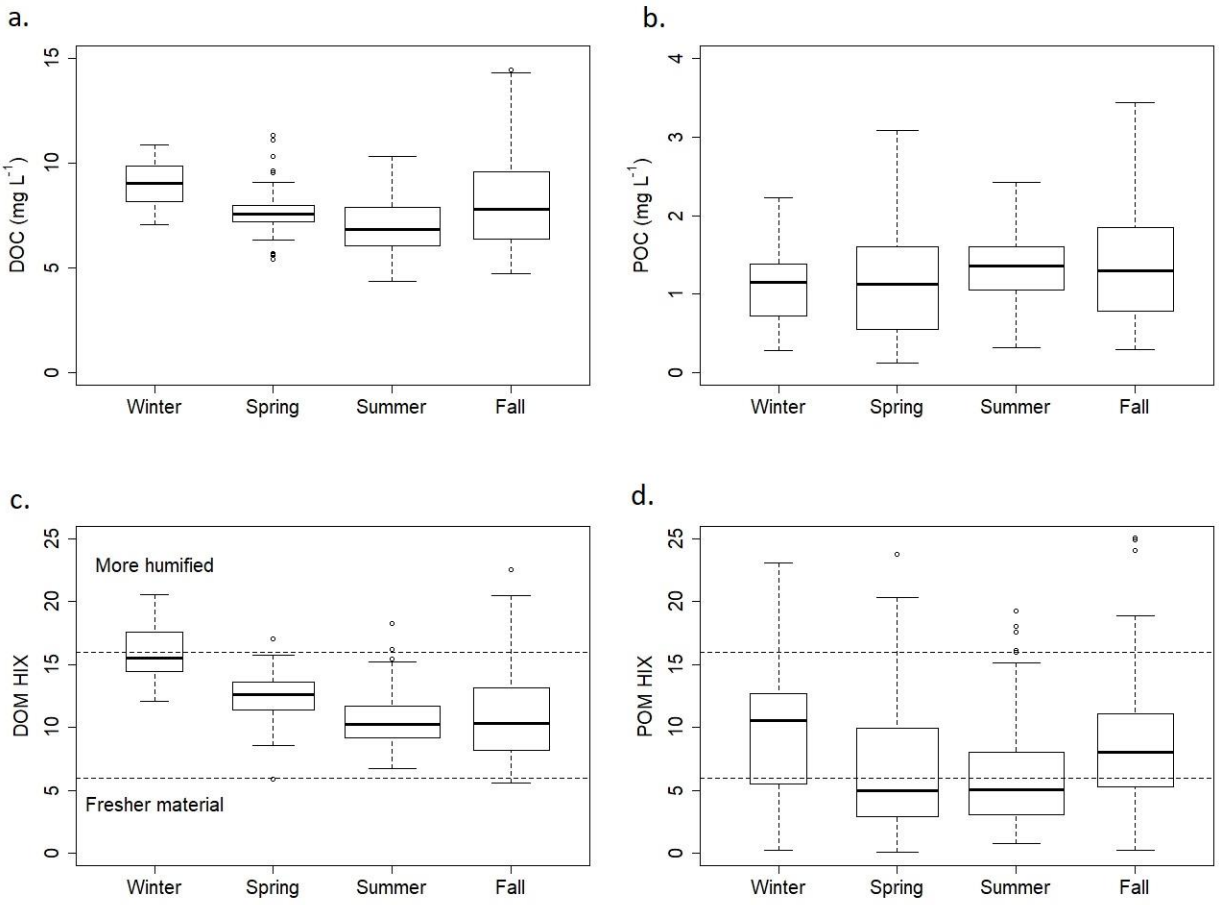

Figure 3-3. a. DOC (mg L^{-1}), b. POC (mg L^{-1}), c. DOM HIX, and d. POM HIX plotted seasonally for all collected time points, stations, and depths. The dashed line indicates the designation between highly humified material (HIX > 16) and fresher material (HIX < 6). Outliers were removed for [POC].

Seasonal patterns in the DOM pool were compared to Dixon et al., 2014 who conducted a seasonal study of DOM concentration, absorbance, and fluorescence indices (HIX and BIX) from March 2010 to February 2011 (Figure 3.4). During the late spring and summer months of 2016, the salinity in the NRE was comparable to the 2010-2011 study period and the current study period (2015-2016), however, as discussed previously, fall, winter, and spring 2015-2016 were characterized by above average discharge. This was reflected in the salinity data compared

to 2010-2011; starting from October – March, the average estuarine salinity was much lower for 2015-2016 compared to the 2010-2011 period (Figure 3.4a). The additional freshwater in the estuary led to elevated [DOC] and more terrestrial-like HIX values; however, there was little change in $SUVA_{254}$ between these two time periods (Figure 3.4b-d). By comparing results from Dixon et al., 2014 to this study, the influence of riverine discharge on the DOM pool in the NRE was clear; additional freshwater during fall, winter and spring 2015-2016 lead to increased [DOC] in the estuary, which had a more terrestrial, humic-like composition than following the reduced riverine discharge conditions during 2010-2011.

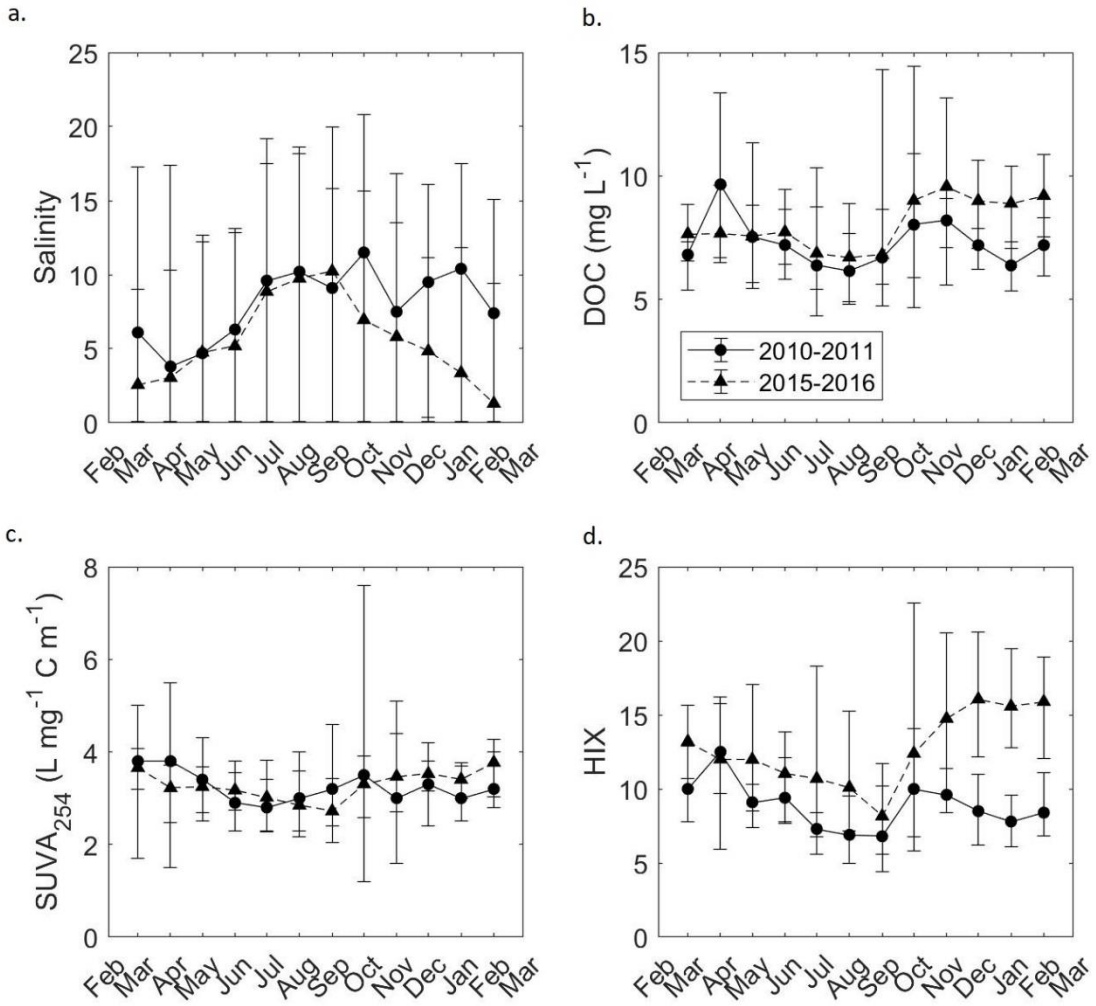

Figure 3-4. Comparison between salinity and DOM parameters averaged monthly from 2010-2011 (Dixon et al., 2014) compared to 2015-2016 (this study). a. Salinity, b. DOC (mg L^{-1}), c. $SUVA_{254}$ (L mg^{-1} C m^{-1}), d. HIX. Samples from 2010-2011 were published in Dixon et al., 2014 (plotted circles; solid line). Samples from 2015-2016 were collected as part of this study (plotted triangles; dashed line). Dots represent the mean for each month while the error bars are the minimum and maximum values, respectively.

4.2 Multivariate statistics

Multivariate statistics are useful tools for analyzing large quantities of data that include multiple variables collected over both temporal and spatial gradients. These techniques allow for easier visualization of large data sets and allow for the utilization of all collected data simultaneously. One of the first steps in using multivariate statistical techniques is to visualize

the data to assess the degree to which the data are considered 'normal' and to determine if any data transformations are necessary. A second goal is to reduce the number of variables included in the analyses by removing variables that are considered collinear. A general rule of thumb is to remove any variables that have a Pearson $r^2 > 0.80$ with other, similar variables.

Each data set (environmental, DOM, POM) were assessed individually for both normality and collinearity among variables. For the environmental parameters (Temp, Sal, DO, Turb, Chl *a*) all of the variables were relatively normal and none of the variables were collinear (Appendix 3, Figure A3.2), indicating each variable represents a different physical or biological process in the estuary. Generally, temperature is representative of seasonality; salinity represents the extent and amount of freshwater in the estuary; dissolved oxygen is a combination of seasonality, freshwater discharge, and biological activity; turbidity is an indicator of freshwater influence as well as location in the estuary (higher turbidity upstream; lower turbidity downstream); and Chl *a* is an indicator of phytoplankton biomass. All environmental parameters were retained for subsequent analyses.

For the DOM dataset ([DOC], [DON], DOC:DON, a_{254}, $SUVA_{254}$, HIX, BIX, Peaks B, T, A, C, M, N), several of the parameters were left skewed and considered collinear (Pearson $r^2 > 0.8$) (Appendix 3, Figure A3.3). [DOC] was collinear with the most parameters ([DON], a_{254}, HIX, Peaks A, C, M, N; parameters removed). In addition, many of the fluorescence peaks were collinear with each other (Peaks A, C, M, N; parameters removed) and therefore, only Peaks T and B were retained for subsequent analyses; both of these peaks are characterized as protein-like OM, where peak T is characteristic of tryptophan and peak B is more characteristic of tyrosine (Table 3.2). DOM data were transformed (square root) prior to multivariate analysis.

For the POM parameters ([POC], [PN], POC:PN, a_{254}, $SUVA_{254}$, HIX, BIX, Peaks B, T, A, C, M, N), the data were also left-skewed and required transformation (square root) prior to multivariate analysis. Compared to the DOM pool, fewer POM pool parameters were considered collinear (Pearson $r^2 > 0.80$) (Appendix 3, Figure A3.4), indicating there were more unique concentration, absorbance, and fluorescence parameters for the POM pool than the DOM pool. [POC] and [PN] were considered collinear as well as several of the fluorescence peaks (Peaks B, M, N, C; parameters removed); however, two fluorescence peaks were retained. Peak A which is largely considered an to be an indicator of terrestrial, humic-like OM while Peak T is thought to be representative of protein, tryptophan-like OM and is often used as an indicator of fresh, autochthonous OM production (Coble, 2007). Parameters retained, as environmental, DOM, and POM, for subsequent analyses are listed in Table 3.3.

Table 3-3. Parameters that are not correlative ($r^2 < 0.80$) and were included in subsequent multivariate analyses for each data pool.

Environmental:	**DOM:**	**POM:**
Salinity	DOC	POC
Temperature	DOC:DON	POC:PN
Turbidity	SUVA	a_{254}
Dissolved oxygen	BIX	SUVA
Chlorophyll-a	Peak T	HIX
	Peak B	BIX
		Peak T
		Peak A

To begin to assess the relationships between data parameters, a correlation plot was generated to examine linear relationships between the different data sets (Environmental vs. DOM vs. POM) (Table 3.4; Appendix 3 Figure A3.5). Many of the DOM indicators ([DOC], DOC:DON, SUVA) were negatively correlated with temperature and salinity, reinforcing the notion that [DOC] and terrestrial-like DOM are largely controlled by riverine discharge. Unlike [DOC], [POC] was not negatively correlated with salinity, indicating there were other controls on [POC]

besides just freshwater extent; however, several of the POM quality indicators (a_{254}, SUVA) were negatively correlated with salinity, indicating terrestrial sources of POM were still prevalent in the estuary. [POC] was strongly correlated with Chl *a* along with OM indicators of recent biological activity (Peak T), demonstrating that biological activity (i.e., phytoplankton growth) was an important source of POM to the NRE. The relationships between DOM and POM parameters were much weaker than the linear relationships between the respective OM and environmental parameters. $SUVA_{254}$ DOM and $SUVA_{254}$ POM were positively correlated, indicating these two parameters may have a similar source while $SUVA_{254}$ DOM and BIX POM were negatively correlated and likely had different sources.

Table 3-4. Pearson r^2 for all parameters (environmental, DOM, POM) used for multivariate analyses. n.s. indicates relationships that were not statistically significant ($p > 0.05$). Boxes bin the various data matrices (environmental, DOM, and POM).

	Sal	DO	Turb	Chl *a*	DOC	DOC:DON	SUVA DOM	BIX DOM	B DOM	T DOM	POC	POC:PN	a254 POM	SUVA POM	HIX POM	BIX POM	T POM	A POM
Temp	0.42	-0.64	-0.51	n.s.	-0.46	-0.45	-0.58	0.60	0.18	0.10	0.14	-0.22	-0.44	-0.52	-0.17	0.23	n.s.	-0.37
Sal		-0.46	-0.58	0.14	-0.65	-0.26	-0.73	0.76	-0.18	-0.32	0.41	-0.28	-0.43	-0.71	-0.25	0.32	n.s.	-0.17
DO			0.32	0.25	0.36	0.36	0.45	-0.40	n.s.	n.s.	0.11	0.18	0.48	0.38	n.s.	-0.19	0.28	0.45
Turb				-0.25	0.28	0.14	0.44	-0.57	n.s.	n.s.	-0.28	0.39	0.53	0.70	0.38	-0.24	-0.16	0.31
Chl *a*					n.s.	0.14	n.s.	0.22	n.s.	n.s.	0.81	n.s.	0.41	-0.24	-0.53	0.16	0.72	0.51
DOC						0.57	0.66	-0.62	0.32	0.53	-0.16	0.22	0.41	0.48	0.11	-0.25	n.s.	0.32
DOC:DON							0.39	-0.36	n.s.	n.s.	0.12	n.s.	0.35	0.19	n.s.	-0.10	0.17	0.31
SUVA DOM								-0.74	n.s.	0.19	-0.24	0.19	0.46	0.58	0.10	-0.17	0.10	0.30
BIX DOM									n.s.	n.s.	0.37	-0.26	-0.43	-0.67	-0.23	0.28	n.s.	-0.20
B DOM										0.76	n.s.	n.s.	n.s.	n.s.	n.s.	n.s.	n.s.	n.s.
T DOM											n.s.	0.11	n.s.	0.11	n.s.	-0.17	n.s.	n.s.
POC												n.s.	0.32	-0.47	-0.59	0.26	0.67	0.49
POC :PN													0.30	0.25	0.16	-0.13	n.s.	0.21
a254 POM														0.66	-0.20	-0.13	0.49	0.76
SUVA POC															0.30	-0.34	n.s.	0.32
HIX POM																-0.42	-0.71	-0.12
BIX POM																	0.31	-0.15
T POM																		0.58

4.3 Principal component analysis

One way to begin assessing how multiple parameters are related to each other is to use PCA which reduces the dimensionality of the data and allows for all variables to be plotted on a single graph for each of the three data matrices (environmental, DOM, and POM) (Figure 3.5). For the environmental data, the data points were distributed along a freshwater to marine gradient with high salinity on one side and high turbidity on the other, distributing samples with greater freshwater influence in the upper right to more marine influence in the bottom left (Figure 3.5a). The samples were also distributed along a seasonal gradient with high temperature in the upper left hand corner to high dissolved oxygen in the bottom right hand corner. Along these two gradients, samples were plotted and distributed seasonally (winter, spring, summer, fall), with samples collected in the summer and fall clustered towards higher temperature, lower DO, with more estuarine influence. Samples collected in the winter and spring were clustered towards lower temperature, high DO and more freshwater influence, indicating the impact of the very wet winter and subsequent spring periods.

DOM samples were distributed along a gradient from more autochthonous DOM to more allochthonous DOM. Indicators of autochthonous DOM were clustered in the bottom left (BIX) and indicators of allochthonous DOM were clustered in the upper right corner (DOC:DON, $SUVA_{254}$) (Figure 3.5b). For the DOM pool, [DOC] was clustered with indicators of terrestrial-like DOM, indicating the main source of DOC to the estuary was largely from terrestrial (i.e., riverine) sources. The two fluorescence peaks, Peaks B and T were clustered together in PCA space and oriented 90 degrees to other indicators of allochthonous (DOC:DON, $SUVA_{254}$) and autochthonous, microbially produced DOM (BIX). Parameters oriented 90 degrees from each other indicate there is no relationship between variables. Peaks B and T are indicators of protein-

like fluorescence, often associated with recent primary production (i.e., Chl *a*) (Fellman et al., 2011). BIX, however, is calculated from the Peak M region of fluorescence and is more characteristic of microbial production of FOM (Huguet et al., 2009). In estuarine environments, BIX has been shown to increase with increasing salinity (Huguet et al., 2009). The orientation of peaks B and T relative to indicators of allochthonous and autochthonous DOM indicate there was no relationship between autochthonous FDOM produced microbially versus indicators of protein-like FDOM, as produced via recent primary production, indicating there may be two sources of autochthonous (phytoplankton vs. microbially produced) FDOM in the estuary.

Like the environmental parameters, samples from the DOM pool were also distributed seasonally with samples in the winter and spring clustered with indicators of allochthonous DOM and higher [DOC] and samples collected in the summer and fall clustered with indicators of autochthonous DOM. The seasonal distribution is likely a reflection of the high riverine discharge associated with the winter-spring period as well as an increase in primary production in the summer and fall. However, these two seasonal clusters do overlap and were therefore not completely distinct in terms of OM composition.

Similar to the DOM pool, the POM pool was also distributed along a gradient from more allochthonous POM associated with negative loadings of PC2 (HIX, $SUVA_{254}$, POC:PN, a_{254}, Peak A) to more autochthonous POM associated with positive loadings of PC2 (BIX, Peak T) (Figure 3.5c). Unlike the DOM pool, [POC] was clustered with indicators of autochthonous POM, indicating the main source of POC to the estuary was from phytoplankton and microbial sources. Additionally, fluorescence peak T was more closely related to BIX in the POM versus the DOM pools, indicating the production of POM from microbial sources was related to the production of POM from primary production. This is most likely a reflection of the close

association between primary production (i.e., phytoplankton biomass) and bacterial productivity in the POM pool, including in the NRE (Peierls and Paerl, 2011). The POM pool did not exhibit any strong seasonal distribution along these identified gradients.

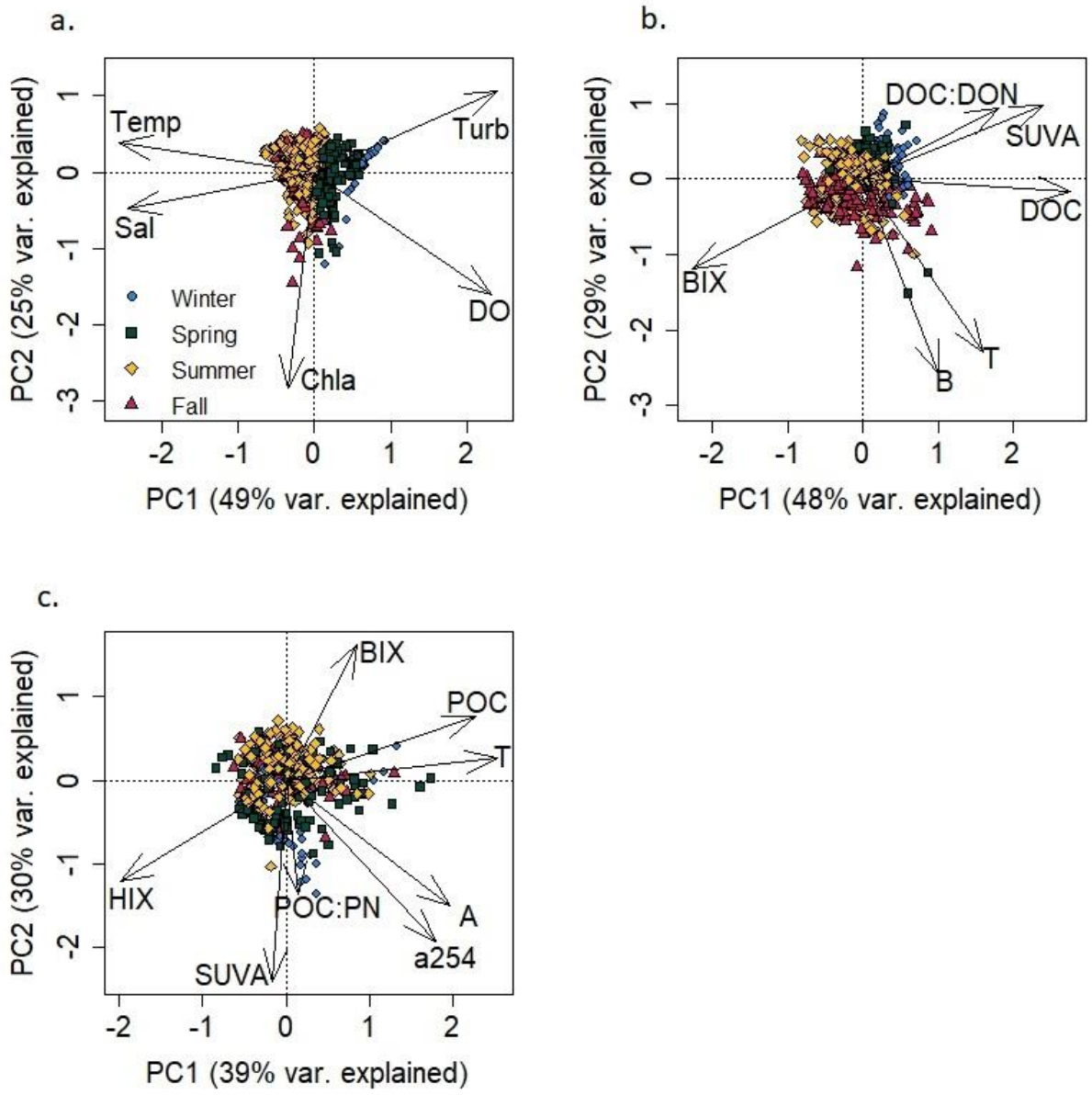

Figure 3-5. PCA results for the a. Environmental, b. DOM, and c. POM data sets. Data points are plotted by season.

In addition to plotting by season, samples were also plotted in PCA space by depth (surface vs. bottom) and by location in the estuary (upper, mid, and lower) (Appendix 3, Figure A3.6,

Figure A3.7). Briefly, for environmental parameters, surface samples were largely clustered towards high DO and high Chl *a*, while bottom samples were clustered towards lower DO and Chl *a*. For POM parameters, samples collected from the upper estuary were clustered more towards allochthonous like OM while samples collected from the mid- and lower-estuary were clustered towards autochthonous like OM, indicating there was a shift in POM source down the estuary from more allochthonous in the upper estuary to more autochthonous in the mid- to lower-estuary.

To assure the data matrices fulfill the assumptions of PCA and metric analyses (i.e., normality, linear relationships between variables, no significant outliers), PCA results from the three data matrices were compared to non-metric multidimensional scaling (nMDS) which is a non-metric statistical analysis with more relaxed data assumptions (Appendix 3.5). Results from PCA compared to nMDS, via Procrustes analysis, were similar, indicating the assumptions of PCA (and metric analyses) were valid for these three data sets. Therefore, for the remaining analyses, metric statistical analyses were used.

In addition to riverine discharge, another physical factor that has been shown to be important in controlling the DOM pool in the NRE, is wind speed and direction (Dixon et al., 2014). In their year-long environmental assessment, Dixon et al., 2014 observed increases in degraded, planktonic DOM following suspected resuspension events, concluding that under low discharge conditions, wind events (i.e., increasing wind speed; shifting wind direction) can play an important role in controlling the quality of DOM in the NRE. Due to these previous findings, we incorporated wind speed and direction data into our analyses. For my analyses, I assumed the wind speed and direction were constant over the NRE as measured at the CRONOS weather station, KNKT and therefore, resulted in a single averaged wind speed, maximum wind gust, and

prevailing wind direction for all stations and depths at each ModMon sampling time point. As such, to incorporate wind direction and discharge data into PCA results, I averaged each of the collected environmental, DOM, and POM parameters, respectively, over both depths (surface and bottom) and across all stations (Station 0-180) for each ModMon time point.

Prior to conducting PCA, linear relationships were assessed between all environmental, DOM, and POM parameters, respectively, to test for collinearity ($r^2 > 0.80$) among variables (Appendix 3, Figure A3.8, Figure A3.9, Figure A3.10). For environmental parameters DO and temperature were excluded. For DOM parameters DOC:DON, a_{254}, HIX, and Peaks A, C, M, N, and B were removed. For POM parameters PN, a_{254}, and Peaks C, B, M, N were removed prior to analysis. When comparing the environmental, DOM, and POM data sets for linear relationships, several indicators of terrestrial OM ([DOC], SUVA_DOM, SUVA_POM, A_POM) were negatively related to salinity further highlighting the role riverine discharge, played on controlling OM dynamics in the NRE (Appendix 3, Figure A.311, Table A3.1).

For PCA, wind direction can either be included as a numerical value (i.e., degrees) or as a categorical variable (i.e., cardinal wind direction). For PCA, wind direction was classified as a categorical variable and samples plotted by predominant wind direction (Figure 3.6). Results indicate wind direction had little influence on the distribution of samples in PCA space. Maximum wind speed was clustered with turbidity, indicating that as wind speed increased, turbidity also increased. This relationship was validated with the linear regression results (Appendix 3, Table A3.1). Maximum wind speed was also clustered with SUVA_P which is used as an indicator of terrestrial, humic-like POM. It was possible resuspension events resulted in resuspended sedimentary material that was more characteristic of previously deposited terrestrial, humic-like POM in the upper to mid-estuary.

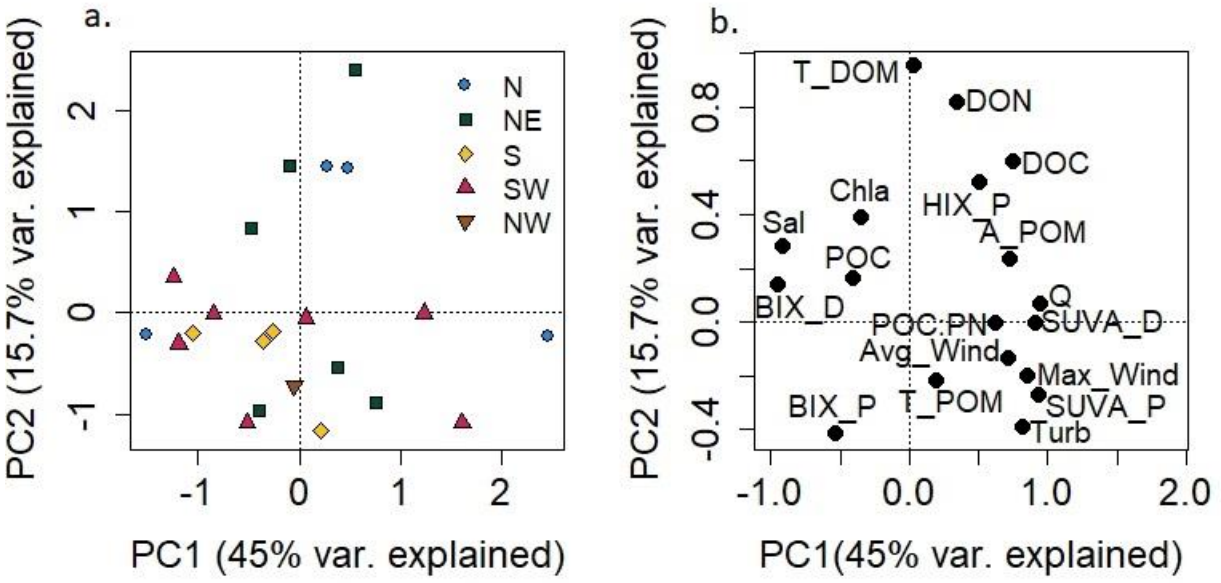

Figure 3-6. PCA results including wind direction and speed data. a. Sample loadings plotted by prevailing wind direction and b. Variable loadings. Variables are indicated on the graph.

Wind direction was also included as a numerical variable and plotted in PCA space with samples plotted by season (Appendix 3, Figure A3.12). Results indicated season was a much stronger determinant for the distribution of samples in PCA space. Samples collected in winter and spring were indicative of higher maximum and average wind speeds as well as higher turbidity and SUVA_POM. Samples collected in the summer and fall were more characteristic of lower maximum and averaged wind speed with more autochthonous like characterization. I hypothesize that a clear response of OM quality to wind speed and direction was masked by both seasonal effects (windier winter and spring) as well as the above average riverine discharge measured during the study period (2015-2016) (Hounshell et al., 2019) which likely dominated the estuarine OM pool with terrestrial, riverine OM.

4.4 Redundancy analysis

RDA is a combination of PCA and multiple linear regression such that an explanatory data set (environmental parameters) is used to explain the variation in a response data matrix (i.e., DOM

or POM, respectively). Like multiple linear regression, explanatory variables are added stepwise to determine the least amount of environmental parameters that can be used to best explain the variation in the respective response data matrix (Table 3.4) (Borcard et al., 2018). For the DOM parameters, salinity explained the most variation ($r^2 = 0.29$) followed by temperature (cumulative $r^2 = 0.37$). These results indicate freshwater inputs strongly influence DOM quality and quantity in the NRE. This was validated visually by plotting RDA results in triplot space, such that [DOC] and indicators of terrestrial-like DOM ($SUVA_{254}$), were clustered opposite of salinity (i.e., low salinity) and at low temperatures (i.e., winter) when freshwater discharge and extent of freshwater in the estuary was greatest (Figure 3.7a). RDA results validate PCA results and demonstrate that peaks B and T, which were oriented 90 degrees to the main allochthonous to autochthonous OM gradient, are largely associated with recent primary production (i.e., Chl *a*), while the BIX pool is most likely derived from bacterial production, which is tightly coupled with temperature.

For the POM pool, Chl *a* explained the most variability in the POM quality and quantity data ($r^2 = 0.25$) followed by turbidity (cumulative $r^2 = 0.42$). Unlike with the DOM pool, biological activity (as Chl *a*) was an important source of POM to the estuary and was potentially balanced by POM flushed into the system from the terrestrial end-member, as represented by the relatively high r^2 for turbidity. Plotted in triplot space, [POC] and indicators of autochthonous POM (BIX, Peak T) were clustered with Chl *a*, again, indicating that phytoplankton production was an important source of POM in the NRE (Figure 3.7b). Unlike the DOM pool, there was no clear distinction between microbially produced POM and POM produced via phytoplankton production. It should be noted that the RDA results only explain about 50% of the total variability within the DOM and POM pools, respectively, indicating that there was a significant

portion of other controls (~50%) that cannot be explained by the environmental parameters collected during this study.

Table 3-5. RDA results for DOM and POM data. Variables were selected for inclusion based on forward selection.

DOM			**POM**		
Env. Variable	**Cumulative Adj. r^2**	**p value**	**Env. Variable**	**Cumulative Adj. r^2**	**p value**
Sal	0.29	0.001	Chl *a*	0.25	0.001
Temp	0.37	0.001	Turb	0.42	0.001
Turb	0.39	0.001	Sal	0.45	0.001
Chl *a*	0.40	0.001	Temp	0.47	0.001

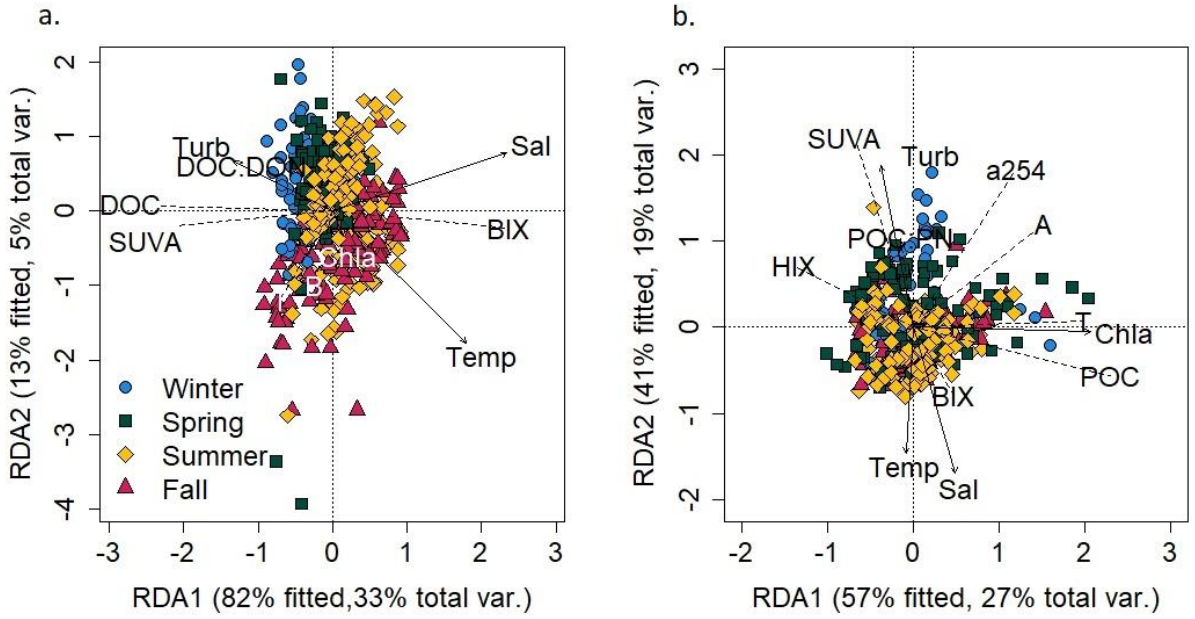

Figure 3-7. RDA results plotted for a. DOM and b. POM. Data points are plotted by season. OM variables (loadings) are displayed as dashed lines. Environmental variables (loadings) are plotted as solid arrows.

4.5 Co-inertia analysis

The ultimate goal of the study was to assess the direct relationships between the respective DOM and POM data matrices to determine the degree to which these two pools were related. Unlike RDA which assumes an explanatory (i.e., environmental data) and a response data matrix (either the DOM or POM data matrices), CoIA is a symmetric analysis that makes no

assumptions about the relationship between the data matrices. In the case of the OM data matrices, this allowed us to relate the two without explicitly assuming one was an explanatory or response matrix (Borcard et al., 2018). In order to assess the applicability of this type of analysis to relate two data matrices, CoIA was first conducted by comparing the environmental data matrix to each DOM and POM data matrix respectively (Appendix 3.6). Results obtained by CoIA were similar to those obtained by RDA.

The first step when conducting CoIA was to use an ordination method (i.e., PCA) to transform the data and determine the two axes that explain the most variation in each respective data set. It was then possible to compute the co-inertia between the two data sets by crossing the two ordination data matrices and computing the covariance matrix. The total computed co-inertia is the sum of squared co-variances. The data points and two sets of variables can then be plotted in the common co-inertia space (Figure 3.8, Appendix 3, Figure A3.18). Figure 3.8a-b is the projection of the unconstrained axes (i.e., after PCA but prior to CoIA) as projected into CoIA space. Figure 3.8c-d is the projection of the two sets of variables (i.e., loadings) in the same CoIA space. Appendix 3, Figure A3.18 is the representation of the data points plotted in CoIA space as the x-coordinates (DOM; solid black circles) with arrows pointing towards the y-coordinates (POM; open, white circles).

CoIA on the DOM and POM data matrices only resulted in a correlation coefficient of 0.22 (RV = 0.22) (Appendix 3, Figure A3.18), which was low, especially when compared to the correlation coefficients between the environmental data and the DOM and POM data matrices (RV = 0.43 and 0.53, respectively). The relationships between the two pools can be assessed by examining the DOM and POM loadings, as determined by CoIA (Figure 3.8c-d). Interpretations of these relationships, are up to the investigator, but for the DOM and POM pools, it appears the

variables were largely related by their source within the estuary. BIX_DOM was clustered with both [POC] and BIX_POM, in the upper right hand corner of the biplot. As discussed previously, an important source of [POC] and autochthonous-like POM was from phytoplankton production in the mid- to lower-estuary. Like BIX produced in the POM pool, BIX in the DOM pool was also thought to largely be derived from production within the estuary; therefore, the clustering of BIX_DOM, BIX_POM, and [POC] in the CoIA biplot space, indicates all three of these indicators of OM quantity and quality were derived from the same source (i.e., phytoplankton production).

Similarly, [DOC] and indicators of terrestrial-like OM (SUVA_DOM, SUVA_POM, a_{254}_POM) were clustered together towards the left-hand side of the biplot, indicating [DOC] and indicators of terrestrial OM quality from both the DOM and POM pools were derived from the same source (i.e., terrestrial, humic-like OM from the riverine endmember). While these results don't exclusively indicate whether or how the POM pool may be transformed into the DOM pool (or vice versa), they do demonstrate that certain indicators of OM quantity and quality can be used across OM pools to assess the relative source of both DOM and POM in estuarine environments.

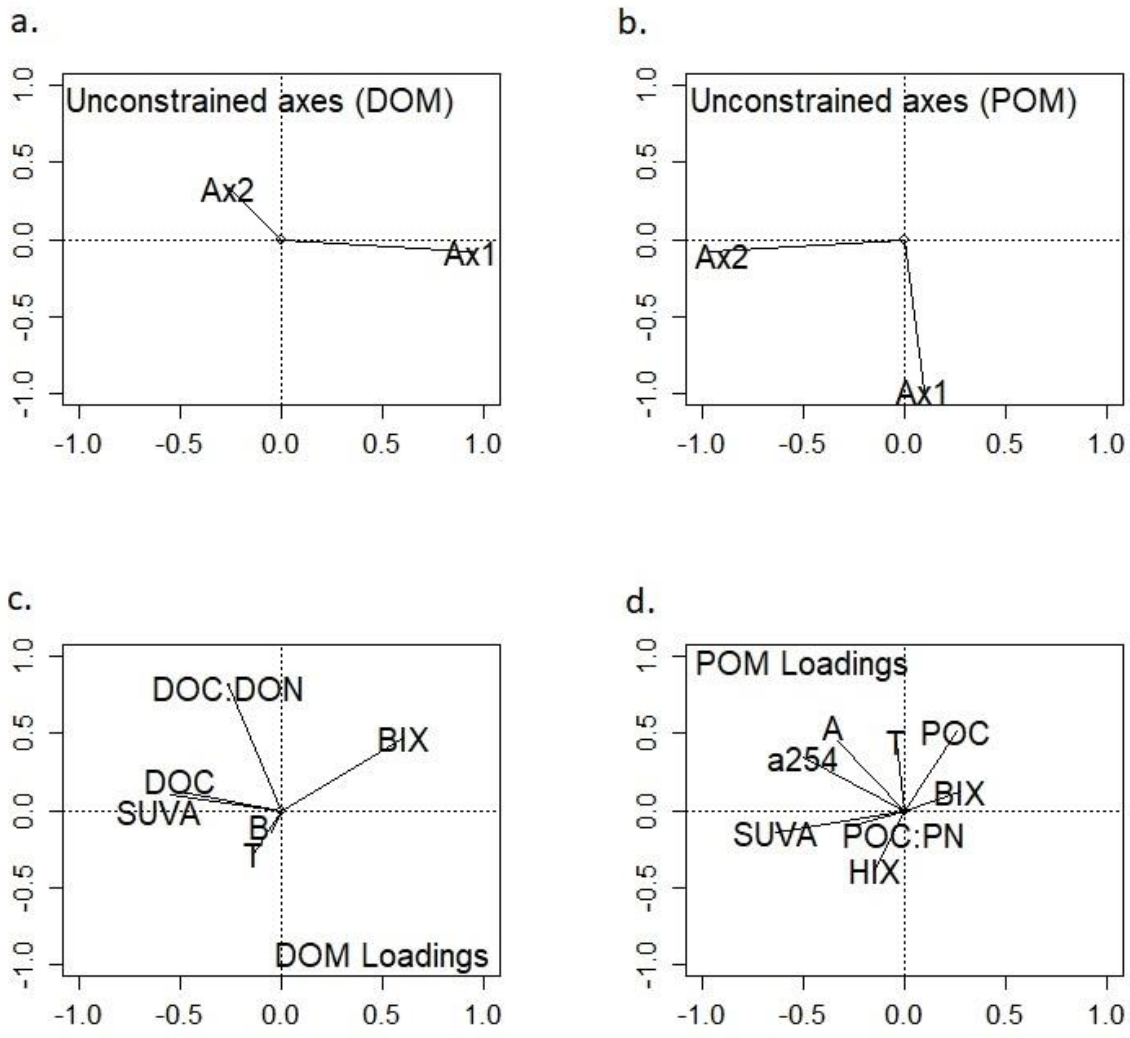

Figure 3-8. CoIA results for DOM vs. POM parameters. a. projection of DOM parameter axes on the CoIA axes. b. projection of POM parameter axes on the CoIA axes. c. projection of DOM parameters in CoIA space. d. Projection of POM variables in CoIA space.

5 Conclusions: Implications for organic matter dynamics in estuarine environments

Results from this study indicate the quality and quantity of OM in the NRE were largely controlled by two main factors: terrestrial, humic-like OM loaded into the estuary via riverine discharge, and biological production of autochthonous OM by phytoplankton. Specifically, the DOM pool is almost completely dominated by the influence of terrestrial OM contained in freshwater discharge, influencing both the quantity and quality of this pool in the NRE over the

observed study period. Results from this study could be skewed due to the overwhelming influence of the very wet fall, winter, and spring period observed during the study. The influence of freshwater discharge on the DOM pool could be obscuring the influence of wind direction and speed on the DOM pool in the NRE, as observed by Dixon et al., 2014. Compared to Dixon et al., 2014, the above average discharge period from 2015-2016 resulted in higher [DOC] and more humic-like terrestrial DOM in the estuary than in the 2010-2011 period, further highlighting the strong control riverine discharge plays on the quantity and quality of the DOM pool in this estuary. Any seasonal influence on the DOM pool may also be obscured by the above average fall, winter, and spring riverine discharge period. Unlike the DOM pool, however, the quantity and quality of the POM pool was driven by freshwater discharge in the upper estuary and by autochthonous POM production by phytoplankton in the mid- to lower-NRE, indicating a shift in not only the dominant source of POM through the estuary but also a shift in the quality of the POM pool.

While CoIA results were unable to resolve potential transformations between the DOM and POM pools, results did indicate how the quality of OM in the two respective pools may be related. When comparing the DOM and POM pools, results indicate there were similar sources of both DOM and POM quantity and quality in the estuary; such that while phytoplankton production largely influences the POM pool, there were indicators of DOM quality that were also correlated with phytoplankton biomass (i.e., BIX_DOM). Similarly, indicators of terrestrial-like OM quality, for both the DOM and POM pools were related to freshwater extent in the estuary and therefore riverine discharge. Therefore, while there were differences in the relative sources, quantity and composition of the DOM and POM pools in estuarine environments, it was still possible to use similar indices of OM quality to assess both these pools, simultaneously.

Overall, results from this study indicate that multivariate statistics, commonly applied to ecological data (Borcard et al., 2018; Paliy and Shankar, 2016; Zurr et al., 2007), can also be used by OM biogeochemists to understand the complex relationships of OM in natural environments. These statistical techniques allow users to simultaneously assess multiple 'pools' of data that include multiple variables measured along both temporal and spatial gradients. Using multivariate statistics allows for the incorporation of multiple parameters measured and leads to a more robust understanding of the relationships of the OM pool.

REFERENCES

Arar, E.J., Collins, G.B., 1997. In Vitro Determination of Chlorophyll a and Pheophytin a in Marine and Freshwater Algae by Fluorescence. EPA Method 445.0. Technical report for USA-EPA, Cincinnati, Ohio, September 1997.

Asmala, E., Haraguchi, L., Markager, S., Massicotte, P., Riemann, B., Staehr, P.A., Carstensen, J., 2018. Eutrophication Leads to Accumulation of Recalcitrant Autochthonous Organic Matter in Coastal Environment. Global Biogeochemical Cycles 32, 1673–1687. https://doi.org/10.1029/2017GB005848

Bhattacharya, R., Osburn, C.L., 2017. Multivariate Analyses of Phytoplankton Pigment Fluorescence from a Freshwater River Network. Environmental Science & Technology 51(12), 6683-6690. https://doi.org/10.1021/acs.est.6b05880

Bianchi, T.S., 2007. Organic matter cycling, in: Biogeochemistry of Estuaries. Oxford University Press, New York, pp. 177–223.

Borcard, D., Gillet, F., Legendre, P., 2018. Numerical Ecology with R, 2nd ed. Spring International Publisher, Cham, Switzerland.

Brym, A., Paerl, H.W., Montgomery, M.T., Handsel, L.T., Ziervogel, K., Osburn, C.L., 2014. Optical and chemical characterization of base-extracted particulate organic matter in coastal marine environments. Marine Chemistry 162, 96–113. https://doi.org/10.1016/j.marchem.2014.03.006

Carlson, C.A., Hansell, D.A., 2014. DOM Sources, Sinks, Reactivity, and Budgets, in: Biogeochemistry of Marine Dissolved Organic Matter: Second Edition. Elesvier, pp 66-109. https://doi.org/10.1016/B978-0-12-405940-5.00003-0

Christian, R.R., Boyer, J.N., Stanley, D.W., 1991. Multiyear Distribution Patterns of Nutrients within the Neuse River Estuary, North Carolina. Marine Ecology Progress Series 71, 259–274. https://doi.org/Doi 10.3354/Meps071259

Coble, P.G., 2007. Marine optical biogeochemistry: The chemistry of ocean color. Chemical Reviews 107, 402–418. https://doi.org/10.1021/cr050350

Dixon, J.L., Osburn, C.L., Paerl, H.W., Peierls, B.L., 2014. Seasonal changes in estuarine dissolved organic matter due to variable flushing time and wind-driven mixing events. Estuarine, Coastal and Shelf Science 151, 210–220. https://doi.org/10.1016/j.ecss.2014.10.013

Fellman, J.B., Hood, E., Spencer, R.G.M., 2010. Fluorescence spectroscopy opens new windows into dissolved organic matter dynamics in freshwater ecosystems: A review. Limnology and Oceanography 55, 2452–2462. https://doi.org/10.4319/lo.2010.55.6.2452

Fellman, J.B., Petrone, K.C., Grierson, P.F., 2011. Source, biogeochemical cycling, and fluorescence characteristics of dissolved organic matter in an agro-urban estuary. Limnology and Oceanography 56(1), 243-256. https://doi.org/10.4319/lo.2011.56.1.0243

Hall, N.S., Paerl, H.W., Peierls, B.L., Whipple, A.C., Rossignol, K.L., 2013. Effects of climatic variability on phytoplankton community structure and bloom development in the eutrophic, microtidal, New River Estuary, North Carolina, USA. Estuarine, Coastal and Shelf Science 117, 70–82. https://doi.org/10.1016/j.ecss.2012.10.004

Hounshell, A.G., Rudolph, J.C., Van Dam, B.R., Hall, N.S., Osburn, C.L., Paerl, H.W. 2019. Extreme weather events modulate processing and export of dissolved organic carbon in the Neuse River Estuary, NC. Estuarine, Coastal, and Shelf Science. 219, 189-200. https://doi.org/10.1016/j.ecss.2019.01.020

Huguet, A., Vacher, L., Relexans, S., Saubusse, S., Froidefond, J.M., Parlanti, E., 2009. Properties of fluorescent dissolved organic matter in the Gironde Estuary. Organic Geochemistry 40, 706–719. https://doi.org/10.1016/j.orggeochem.2009.03.002

Luettich, R.A., McNinch, J.E., Paerl, H.W., Peterson, C.H., Wells, J.T., Alperin, M.J., Martens, C.S., Pinckney, J.L., 2000. Neuse River Estuary Modeling and Monitoring Project Stage 1: Hydrography and Circulation, Water column nutrients, and Productivity, Sedimentary processes, and Benthic-Pelagic coupling, and Benthic ecology. Report submitted to NC WRRI. Report no. 325B. Raleigh, NC.

Markager, S., Stedmon, C.A., Søndergaard, M., 2011. Seasonal dynamics and conservative mixing of dissolved organic matter in the temperate eutrophic estuary Horsens Fjord. Estuarine, Coastal and Shelf Science 92, 376–388. https://doi.org/10.1016/j.ecss.2011.01.014

McCallister, S.L., Bauer, J.E., Ducklow, H.W., Canuel, E.A., 2006. Sources of estuarine dissolved and particulate organic matter : A multi-tracer approach. Organic Geochemistry 37, 454–468. https://doi.org/10.1016/j.orggeochem.2005.12.005

Murphy, K.R., Stedmon, C.A., Graeber, D., Bro, R., 2013. Decomposition routines for Excitation Emission Matrices. Analytical Methods 5(23), 1–29. https://doi.org/10.1039/c3ay41160e.drEEM

Osburn, C.L., Handsel, L.T., Mikan, M.P., Paerl, H.W., Montgomery, M.T., 2012. Fluorescence tracking of dissolved and particulate organic matter quality in a river-dominated estuary. Environmental Science & Technology 46, 8628–8636. https://doi.org/10.1021/es3007723

Osburn, C.L., Handsel, L.T., Peierls, B.L., Paerl, H.W., 2016. Predicting Sources of Dissolved Organic Nitrogen to an Estuary from an Agro-Urban Coastal Watershed. Environmental Science & Technology 50, 8473–8484. https://doi.org/10.1021/acs.est.6b00053

Paerl, H.W., Crosswell, J.R., Dam, B. Van, Hall, N.S., Rossignol, K.L., Osburn, C.L., Hounshell, A.G., Sloup, R.S., Harding, L.W., 2018. Two decades of tropical cyclone impacts on North Carolina's estuarine carbon, nutrient and phytoplankton dynamics: implications for biogeochemical cycling and water quality in a stormier world. Biogeochemistry 141(3), 307-332. https://doi.org/10.1007/s10533-018-0438-x

Paerl, H.W., Mallin, M.A., Donahue, C.A., Go, M., Peierls, B.L., 1995. Nitrogen loading sources and eutrophication of the Neuse River Estuary, North Carolina: Direct and indirect roles of atmospheric deposition. Report submitted to NC Sea Grant. Report no. 291. Raleigh, NC.

Paerl, H.W., Pinckney, J.L., Fear, J.M., Peierls, B.L., 1998. Ecosystem responses to internal and watershed organic matter loading: consequences for hypoxia in the eutrophying Neuse River Estuary, North Carolina, USA. Marine Ecological Progress Series 166, 17–25.

Paerl, H.W., Valdes, L.M., Joyner, A.R., Piehler, M.F., Lebo, M.E., 2004. Solving problems resulting from solutions: Evolution of a dual nutrient management strategy for the eutrophying Neuse River Estuary, North Carolina. Environmental Science & Technology 38, 3068–3073. https://doi.org/10.1021/es0352350

Paliy, O., Shankar, V., 2016. Application of multivariate statistical techniques in microbial ecology. Molecular Ecology 25, 1032–1057. https://doi.org/10.1111/mec.13536

Peierls, B.L., Christian, R.R., Paerl, H.W., 2003. Water Quality and Phytoplankton as Indicators of Hurricane Impacts on a Large Estuarine Ecosystem. Estuaries 26, 1329–1343. https://doi.org/10.1007/BF02803635

Peierls, B.L, Paerl, H.W., 2011. Longitudinal and depth variation of bacterioplankton productivity and related factors in a temperate estuary. Estuarine, Coastal, and Shelf Science 96, 207-215. https://doi.org/10.1016/j.ecss.2011.08.033

Peierls, B.L., Hall, N.S., Paerl, H.W., 2012. Non-monotonic Responses of Phytoplankton Biomass Accumulation to Hydrologic Variability: A Comparison of Two Coastal Plain North Carolina Estuaries. Estuaries and Coasts 1–17. https://doi.org/10.1007/s12237-012-9547-2

Pellerin, B.A., Kaushal, S.S., McDowell, W.H., 2006. Does Anthropogenic Nitrogen Enrichment Increase Organic Nitrogen Concentrations in Runoff from Forested and Human-dominated Watersheds? Ecosystems 9, 852–864. https://doi.org/10.1007/s10021-006-0076-3

Raymond, P.A., Bauer, J.E., 2001. Use of ^{14}C and ^{13}C natural abundances for evaluating riverine, estuarine, and coastal DOC and POC sources and cycling: A review and synthesis. Organic Geochemistry 32, 469–485. https://doi.org/10.1016/S0146-6380(00)00190-X

Rothenberger, M.B., Burkholder, J.M., Brownie, C., 2009. Long-Term Effects of Changing Land Use Practices on Surface Water Quality in a Coastal River and Lagoonal Estuary. Environmental Management 44, 505–523. https://doi.org/10.1007/s00267-009-9330-8

Rudek, J., Paerl, H.W., Mallin, M.A., Bates, P.W., 1991. Seasonal and hydrological control of phytoplankton nutrient limitation in the lower Neuse River Estuary, North Carolina. Marine Ecological Progress Series 75, 133–142. https://doi.org/10.3354/meps075133

Spencer, R.G.M., Aiken, G.R., Dornblaser, M.M., Butler, K.D., Holmes, R.M., Fiske, G., Mann, P.J., Stubbins, A., 2013. Chromophoric dissolved organic matter export from U.S. rivers. Geophysical Research Letters 40, 1575–1579. https://doi.org/10.1002/grl.50357

Stedmon, C., Markager, S., Søndergaard, M., 2006. Dissolved organic matter (DOM) export to a temperate estuary: seasonal variations and implications of land use. Estuaries and Coasts 29, 388–400.

Stow, C., Borsuk, M.E., Stanley, D.W., 2001. Long-term Changes in Watershed Nutrient inputs and Riverine Exports in the Neuse River, North Carolina. Water Research 35, 1489–1499.

Vlahos, P., Whitney, M.M., 2017. Organic carbon patterns and budgets in the Long Island Sound estuary. Limnology and Oceanography 62, S46–S57. https://doi.org/10.1002/lno.10638

Weishaar, J.L., Fram, M.S., Fujii, R., Mopper, K., 2003. Evaluation of Specific Ultraviolet Absorbance as an Indicator of the Chemical Composition and Reactivity of Dissolved Organic Carbon. Environmental Science & Technology 4702–4708. https://doi.org/10.1021/es030360x

Zurr, A.F., Ieno, E.N., Smith, G.M., 2007. Analysing Ecological Data, 1st ed. Springer Science, New York, New York.

CHAPTER 4: UNDERSTANDING ORGANIC MATTER SOURCE AND SINK TERMS IN A HYDROLOGICALLY VARIABLE ESTUARY USING A NON-STEADY STATE BOX MODEL APPROACH

1. Summary

As the interface between riverine and coastal systems, estuaries play a key role in receiving, transporting, and processing terrestrial organic carbon prior to export to downstream coastal systems. Estuaries can switch from terrestrial organic carbon reactors under low river flow to pipelines under high flow, but it remains unclear how estuarine terrestrial organic carbon processing responds to the full spectrum of discharge conditions, which are bracketed by these high and low discharge events. The amount of riverine dissolved organic carbon and colored dissolved organic matter imported, processed, and exported was assessed for riverine discharge events spanning from 4^{th} to 99^{th} flow quantiles in the Neuse River Estuary, North Carolina, USA using spatially and temporally (July 2015 – December 2016) resolved measurements. The extent of dissolved organic matter processing in the estuary under various flow conditions was estimated using two non-steady state box models to calculate 1. Flow into and out of the estuary at the marine end member using the conservative tracer, salinity and 2. Estuarine-wide dissolved organic carbon and colored dissolved organic matter source & sink terms. Results from this study indicate the box model approach, as applied to estimating both flow into and out of the marine end member as well as to *in situ* OM dynamics as OM source & sink terms, is unable to accurately resolve processes in the estuary due to highly variable model results. This is likely a result of the coarse spatial and temporal resolution used to constrain salinity and OM in the Neuse River Estuary, particularly under variable riverine discharge and wind conditions. Results

do suggest an extreme riverine discharge event (99^{th} flow quantile) led up to a 400% increase in dissolved organic carbon loading to the coastal end member as compared to baseline conditions. This is especially important in light of predications of increasing extreme precipitation events due to climate change, which will serve to increase annual loads of terrestrial carbon to the coastal end member.

2. Introduction

The past two decades have witnessed an increased focus on the function, transport, cycling, and storage of dissolved organic carbon (DOC) from headwater streams to the coastal ocean (Bauer et al., 2013; Bianchi, 2011). Much of this research has centered on the transport of terrestrial DOC (tDOC) from soils to streams, specifically how the quantity and quality of tDOC in streams change in response to factors like: discharge, antecedent soil wetness, temperature, and seasonality (Dhillon and Inamdar, 2013; Raymond and Saiers, 2010; Sanderman et al., 2009; Yoon and Raymond, 2012). It is well documented that extreme weather events (EWEs) defined here as river flow $\geq 99^{th}$ flow quantile, including tropical storms and hurricanes, magnify precipitation and discharge in streams and rivers, resulting in increased fluxes of tDOC in downstream aquatic systems (Bauer et al., 2013; Raymond et al., 2016; Raymond and Saiers, 2010), including coastal rivers and estuaries (Bianchi et al., 2013; Osburn et al., 2012; Paerl et al., 2018).

During EWEs, there is a 'pulse' of tDOC exported from land to adjacent streams and rivers, as conceptualized by the pulse-shunt concept (PSC) (Raymond et al., 2016). This tDOC pulse is then 'shunted' and transported further downstream than would typically occur under baseflow conditions. The pulse-shunt mechanism results in the upper stream and river systems acting as a pipeline for the transport of tDOC to downstream ecosystems. While the PSC has been applied to

headwater streams and rivers, it has yet to be applied to downstream, estuarine systems. Previous studies examining the impact of tropical cyclone events on estuaries show that under elevated precipitation and riverine discharge conditions conditions, minimal amounts of the riverine DOC received by estuaries is processed, leading to subsequent export of riverine DOC to coastal waters (Bauer et al., 2013; Bianchi et al., 2013).

Under baseflow conditions when flushing times are relatively long, estuaries are thought to be sites of riverine DOC processing prior to export to the coastal ocean (Del Giorgio and Pace, 2008). Processing of riverine DOC includes its conversion to dissolved inorganic C (DIC) via microbial and photochemical degradation, which may push estuaries towards net CO_2 emission (Bauer et al., 2013; Bianchi et al., 2013; Crosswell et al., 2014, 2012; Van Dam et al., 2018). The role estuaries play, as either reactors or conduits for riverine DOC under varying discharge conditions, has important implications for understanding their function as sites of riverine DOC consumption and DIC production prior to export to the coastal ocean. This is especially important in the larger context of climate change, where the frequency and intensity of EWEs are predicted to increase, including along the US east coast (Bender et al., 2009; Janssen et al., 2016).

While several studies have assessed the binary impact of variable river discharge, as either baseflow or extreme-flow, on DOC in estuaries (Bianchi et al., 2013; Dixon et al., 2014; Osburn et al., 2012; Paerl et al., 2006, 2001), few studies have evaluated the full continuum of flow conditions, from baseflow to extreme-flow. Prior studies conducted in the Neuse River Estuary (NRE), North Carolina indicate that, under low-flow conditions, physical factors like river discharge, wind speed and wind direction are dominant controls on estuarine dissolved organic matter (DOM) quantity and quality (Dixon et al., 2014). Following tropical cyclone events,

associated with elevated precipitation and river discharge, studies conducted in this system have demonstrated riverine DOC enrichment from elevated river inputs throughout the estuary and adjacent sound, including after Hurricane Fran in 1996 (Paerl et al., 1998), Hurricanes Dennis, Floyd and Irene in 1999 (Paerl et al., 2001; 2006), and Hurricane Irene in 2011 (Osburn et al. 2012). The 1999 hurricane season resulted in organic matter (OM) inputs which led to long-term internal nutrient loading to the NRE (Paerl et al., 2006), indicating that tropical cyclone events and associated precipitation and river discharge can have long-term impacts on coastal lagoons due to their long flushing times (Peierls et al., 2003).

More recent studies in the NRE assessing the impact of Hurricane Irene in September 2011 also demonstrated an increase in riverine DOC following this event and observed changes in DOM and particulate OM (POM) quality from that produced by phytoplankton to more terrestrial OM sources (Osburn et al., 2012). The large CO_2 efflux out of the NRE observed during and immediately following (~ 1 day) Hurricane Irene, was partially attributed to conversion of re-suspended sedimentary OC to DIC. However, in the ~ 2 weeks following this event, the sustained CO_2 efflux was attributed to increased rates of biological and photochemical riverine DOC processing, loaded into the system during the storm (Crosswell et al., 2014). While riverine DOC processing and air-water CO_2 exchange in estuaries may represent significant fluxes in the global C cycle, quantitative links between these processes have yet to be clarified, especially after EWEs.

The goal of this study was to examine the response of DOC quantity and quality to a range of flow conditions spanning from baseflow (4^{th} flow quantile) to a 99^{th} flow quantile event in a shallow, microtidal estuary, the NRE, by analyzing seven discrete discharge events captured from July 20, 2015 to December 13, 2016. I hypothesized that large-scale changes in DOC

dynamics of the NRE following EWEs indicate the system may be able to move from a simple "pipeline" of riverine DOC export immediately following an event to a reactor in the weeks (~ 2-3 weeks) following these events as the system returns to normal flow conditions.

3. Methods

3.1 Study site and sampling methods

The NRE is a shallow (average depth ~3.5 m), micro-tidal (<4 cm tidal range) estuary located in the coastal plain of NC (Luettich et al., 2002) (Figure 4.1). The NRE watershed extends from the urbanized Raleigh-Durham metropolitan area through rural eastern NC, where land use is mainly characterized as agricultural (row crop; concentrated animal feeding operations), forested, and freshwater wetlands (Rothenberger et al., 2009; Stow et al., 2001). The NRE extends from Streets Ferry Bridge (station 0), north of New Bern, NC to the outlet into Pamlico Sound (PS) (station 180) (Figure 4.1). The NRE-PS is bounded to the east by the Outer Banks barrier islands which limit exchange between NRE-PS and W. Atlantic ocean waters, leading to long flushing times in the NRE (average ~ 5-8 weeks) (Peierls et al., 2012). This allows sufficient time for consumption of inorganic nutrients and degradation of OM in the estuary (Christian et al., 1991; Paerl et al., 1998).

The NRE has been the site of extensive water quality monitoring assessments (1994 - present) conducted by the University of North Carolina – Chapel Hill (UNC-CH), Institute of Marine Sciences (IMS), Neuse River Monitoring and Modeling project (ModMon; http://paerllab.web.unc.edu/projects/modmon/) (Luettich et al., 2000). I used ModMon data for the NRE from July 20, 2015 to December 13, 2016. Water quality assessments including DOC, colored DOM (CDOM), and primary production (PP) were conducted on samples collected from the middle channel of the NRE at 11 stations across the estuary (Appendix 4, Table A4.2), from

the location of maximum salinity intrusion (station 0) to the estuary mouth near PS (station 180) (Figure 4.1). Assessments from July 20, 2015 to October 3, 2016 were conducted twice-monthly from March to October and monthly from November to February. Assessments from October 17, 2016 to December 13, 2016 were conducted weekly as part of a project to assess the impacts of Hurricane Matthew (October 7-8, 2016) on water quality in the NRE following this extreme flood event (Musser et al., 2017).

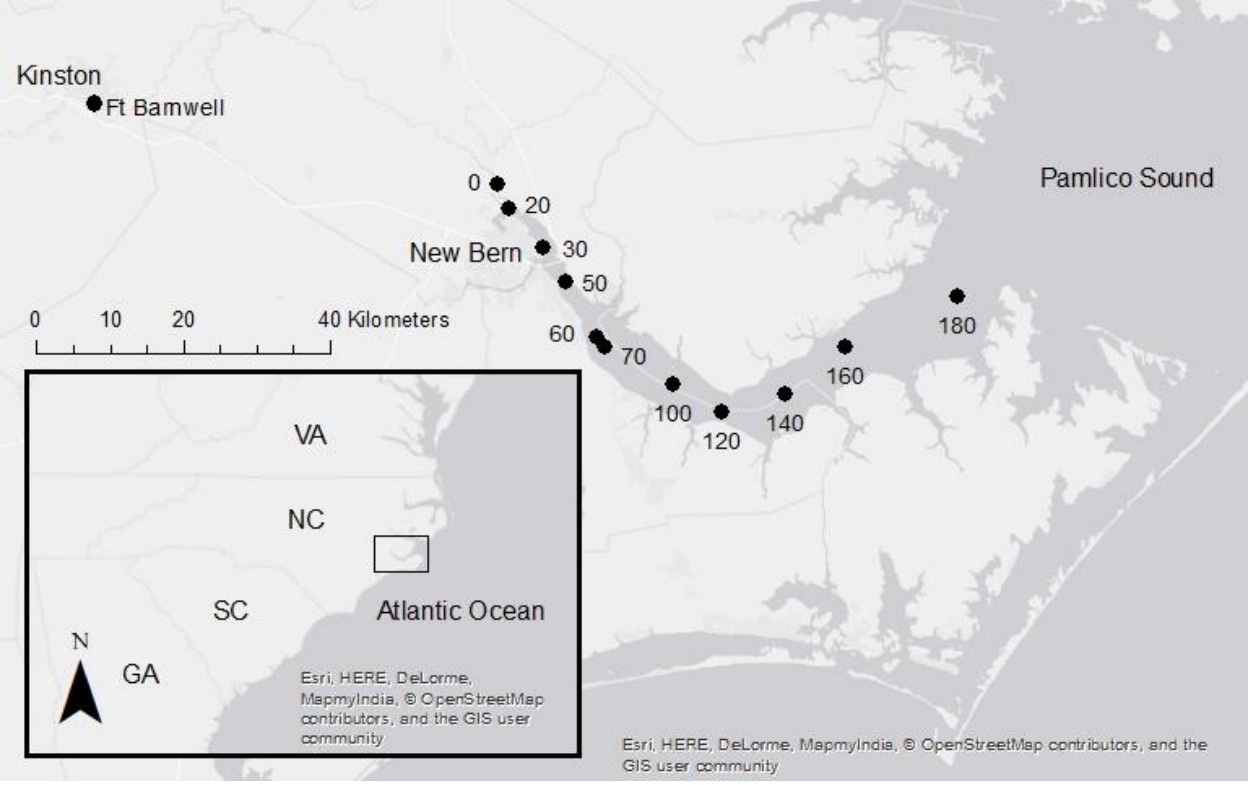

Figure 4-1. Map of the NRE located in Eastern NC. ModMon sampling stations start at Station 0 at the head of the estuary to Station 180 at the mouth of the estuary. Ft. Barnwell is the location of the USGS gaging station used for riverine discharge.

At each sampling station and time point salinity was measured from surface (0.2 m below surface) to bottom (0.5 m above bottom) at 0.5 m intervals using a YSI 6600 multi-parameter, water quality sonde (Hall et al., 2013). Surface (0.2 m below surface) and bottom (0.5 m above bottom) water samples were collected for various chemical analyses at each of the 11 stations. Samples were maintained in the dark at ambient temperature and returned to UNC-CH IMS

located in Morehead City, NC within ~6 hours of collection then filtered through a combusted (450^{o}C, 4 hours) 0.7 µm mesh size, GF/F glass fiber filter. The filtrate was collected and frozen at -20°C in the dark until DOM quantitative and qualitative analyses.

DOC concentration ([DOC]) was determined via high-temperature catalytic oxidation, using a Shimadzu TOC-5000 analyzer (Peierls et al., 2003). CDOM absorbance was measured on samples collected from July 20, 2015 to July 18, 2016 and from October 3, 2016 to December 13, 2016. UNC-CH IMS measured absorbance on samples collected prior to Hurricane Matthew (July 2015 – July 2016; October 3, 2016). Absorbance spectra (200-800 nm) on filtered surface samples were measured on a Shimadzu UV-1700 Pharma-Spec spectrophotometer. For samples following Hurricane Matthew (October 17, 2016 to December 13, 2016), absorbance spectra were determined by the Osburn Laboratory at North Carolina State University (NCSU) on a Varian Cary 300UV spectrophotometer. Absorbance spectra were corrected using a Nanopure (UNC-CH IMS) or Milli-Q (NCSU) water blank collected on the same day as analysis. All samples with > 0.4 raw absorbance units at 240 nm were diluted (Osburn et al., 2012). Absorbance values at 350 nm were converted to Napierian absorbance coefficients (a_{λ}, m^{-1}) (Spencer et al., 2013). A comparison between UNC-CH IMS and NCSU measured absorbance values at 350 nm (a_{350}) is presented in the Appendix 4.1 (n = 6) (Appendix 4, Table A4.1). NCSU values were on average, 11% greater than values measured at UNC-CH IMS.

Neuse River (NR) freshwater discharge data were collected from USGS gauging station #02091814 located at Ft. Barnwell, NC about 26 km upstream of station 0 (Paerl et al., 2014). To account for freshwater inputs downstream of the gauging station, discharge data from Ft. Barnwell was scaled to the area of the un-gaged watershed (31% un-gaged watershed) (Peierls et al., 2012).

3.2 DOM load

To assess changes in DOC quantity and quality related to specific discharge events, the sampling period was divided into seven discrete segments. Each event corresponded to a ~40 day time span (range: 29-44 days; mean = 38 days; median = 41 days) between ModMon sampling dates with each time span starting prior to the defined discharge event and spanning the rising and falling limb of the hydrograph (Figure 4.2; Table 4.1). A baseline period was designated at the beginning of sampling which corresponded to a period of below median discharge (< 67 m^3 s^{-1}). This was followed by an increase in discharge during September-October 2015 associated with bands of Hurricane Joaquin and its associated Nor'easter. Joaquin was followed by a winter period of above average discharge, which was divided into three distinct events termed: Pulse 1, Pulse 2, and Pulse 3. In the spring of 2016, there was a distinct discharge event in the NRE which was designated as Spring Q. Finally, in fall 2016 Hurricane Matthew delivered extreme amounts of rainfall over the study area and its watershed, resulting in record discharge measured at Ft. Barnwell.

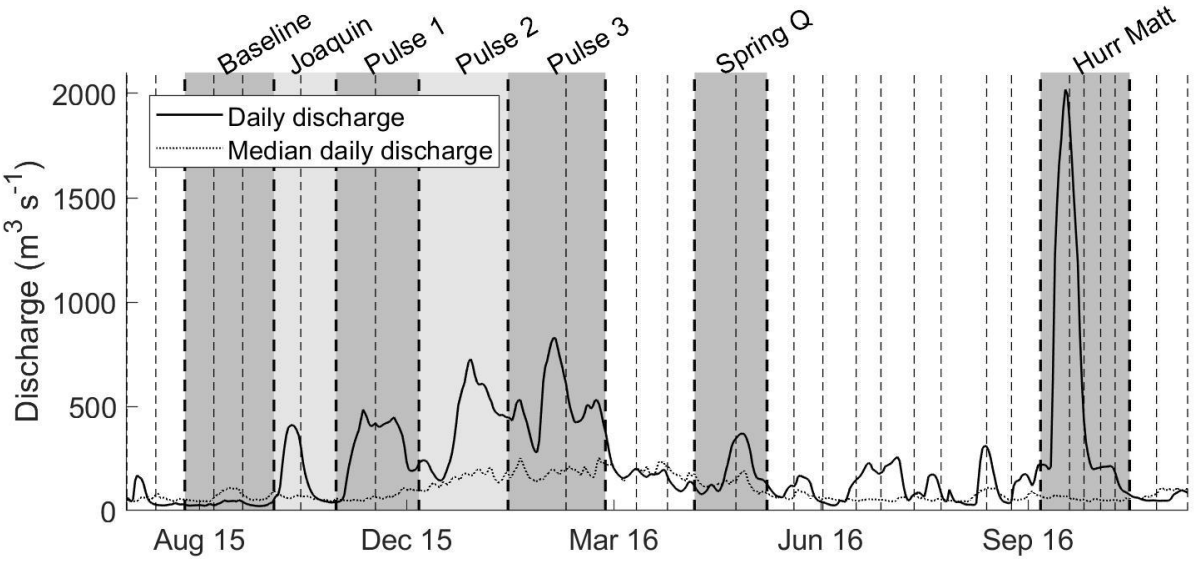

Figure 4-2. Daily discharge (black lines) obtained from Ft. Barnwell USGS gaging station plotted for the study period. The grey dashed line corresponds to the median daily discharge from 1997 – 2017. Dashed vertical lines correspond to ModMon sampling dates. Bolded dashed vertical lines are bounds for each discrete discharge event (1-7) (Table 1).

Table 4-1. Discharge values for the seven discrete discharge events. Historical data were calculated from median discharge values from 1997-2017. Cumulative discharge refers to the averaged daily discharge ($m^3\ s^{-1}$) summed over the corresponding time period.

Time Period	Description	Dates	Number of days	Average Q ($m^3\ s^{-1}$)	Average of historical median Q ($m^3\ s^{-1}$)	Cumulative Q (m^3)	Historical cumulative Q (m^3)
	All	07/20/15 – 12/13/16	513	237	98	120,321	50,046
1	Baseline	08/17/15 – 09/29/15	44	32	67	1,425	2,965
2	Joaquin	09/29/15 – 10/29/15	31	143	63	3,994	1,942
3	Pulse #1	10/29/15 – 12/08/15	41	312	69	12,805	2,812
4	Pulse #2	12/08/15 – 01/20/16	44	411	151	17,661	6,652
5	Pulse #3	01/20/16 – 03/07/16	48	517	188	24,810	9,015
6	Spring Q	04/19/16 – 05/24/16	36	192	129	6,904	4,655
7	Hurricane Matthew	10/03/16 – 11/15/16	44	625	56	27,518	2,486

For each discrete discharge event and the entire sampling period, DOC and a_{350} loads at station 0 were calculated using weighted regressions on time, discharge and season (WRTDS) (Stackpoole et al., 2017). WRTDS fits a relationship between continuous discharge (Q) and discrete measurements of [DOC] and a_{350} to model DOC and a_{350} riverine concentration accounting for variation in discharge, season, and time using the following equation:

$$\ln(c) = \beta_1 + \beta_2(\ln(Q)) + \beta_3(T) + \beta_4 \sin(2\pi T) + \beta_5 \cos(2\pi T) + \varepsilon \quad (4.1)$$

where c is the concentration, Q is the measured discharge, T is time in decimal years, ε is the error, and β_1-β_5 are the coefficients estimated from the sample data. [DOC] and a_{350} were calculated by WRTDS using the EGRET R-package (Hirsch and De Cicco, 2015; https://CRAN.R-project.org/package=EGRET). By coupling continuous discharge (Q) measurements at Ft. Barnwell with measurements of [DOC] and a_{350} collected discretely at Station 0, it was possible to interpolate the total DOC and a_{350} load to the estuary, using the WRTDS concentration estimates, over the entire time period (July 20, 2015 – December 13, 2016) and across each discrete discharge event.

There was some uncertainty associated with these load estimates, particularly as the discharge and [DOC] and a_{350} measurements were collected at two different locations. The greatest uncertainty was associated with the discharge measurements, as these values were measured 26 km upstream from the head of the estuary. However, there are no large tributaries to the NR between Ft. Barnwell and the head of the estuary (Station 0). Additionally, the discharge measured at Ft. Barnwell was scaled to the area of un-gaged watershed to account for any additional tributaries (Peierls et al., 2012). Therefore, while I acknowledge the [DOC] and a_{350} loads were estimates, I feel confident that they accurately captured the variability and dynamics of riverine OC loading from the Neuse River to the NRE.

3.3 Volume weighted DOM concentrations

Volume-weighted averaged salinity, [DOC] and a_{350} were calculated for each sampling date in the NRE from station 20 to 160. Briefly, the mean value for each station (as surface and bottom) was multiplied by the volume of each segment centered on the respective station, as calculated for the box models (Appendix 4, Figure A4.1). The product for each segment was then summed and divided by the total volume of the estuary (Peierls et al., 2012). Volume-weighted averages serve as a representation of the total DOM (as [DOC] or a_{350}) pool contained in the NRE at each ModMon sampling accounting for differences in volume in the upper versus lower estuary.

3.4 DOM source & sink term

A box model approach following Hagy et al., (2000), was used to estimate flow out of the estuary (surface flow) and into the estuary (bottom flow) at station 160 for each ModMon date (Appendix 4.4). Briefly, the estuary was divided into nine boxes with each box centered on a ModMon sampling station (station 20-160). For each sampling date, the head of the estuary was defined as the most upstream site with measurable salinity and vertical stratification. The defined head of the estuary ranged from station 20 during low flow to station 140 following the Pulse 3 event, when discharge was consistently above the historical median. Stations upstream of the designated head of the estuary were treated as 'river boxes'. The head of the estuary was designated as a 'transition box' where the river transitions into the estuary, the first signs of salt were observed, and estuarine circulation began. Downstream of the transition box, each box was divided by the depth of the pycnocline into a surface and bottom layer to represent time-varying stratification. These boxes were designated 'estuarine boxes' and the surface discharge out of each box was calculated along with the bottom salt water influx. I acknowledge that a dV/dt term

should have been included in the box model to account for changes in volume of the surface and bottom boxes through time, however, I assumed this term is negligible and have not included it in the salinity box model. A more detailed description of the salinity box model can be found in Appendix 4.4. The 95% confidence intervals from the 1001 bootstrap model runs were determined for all box model calculations assuming that discharge data varied up to 14% from the measured value (Q ± 14%), [DOC] varied up to 13% ([DOC] ± 13%), and a_{350} varied 17% (a_{350} ± 17%). A discussion of uncertainty values is included in Appendix 4.5.

Once flows into and out of each designated box were determined using the salinity box model, it was possible to calculate a DOC (kg d^{-1}) and a_{350} (m^2 d^{-1}) source & sink term for the entire estuary at each ModMon time point assuming the inputs were constrained to riverine load from the Neuse River, estuarine export from station 160S and import from the PS at station 180B (Appendix 4.4). The respective DOM source & sink term represented any source & sink processes that occurred in the estuary besides conservative mixing. A source indicates internal estuarine production of DOC not accounted for in the box model (i.e., porewater flux; inputs from un-gaged tributaries and wetlands; production by primary and microbial production), while a sink indicates internal estuarine consumption of DOC (i.e., microbial or photochemical oxidation and conversion to DIC; flocculation). A more detailed description of the DOC and a_{350} box model can be found in Appendix 4.4.

3.5 Estimates of biological processes

CO_2 flux out of the estuary and production of DOC by PP were used to constrain the major biological sources and sinks of DOC in the NRE. Determinations of sea-to-air CO_2 flux were obtained from Van Dam et al., (2018) for July 20, 2015 to October 17, 2016. Briefly, Van Dam et al., (2018) measured *in situ*, surface water partial pressure CO_2 (pCO_2) using a shower-head

gas equilibrator paired with an infrared detector (LI-COR, Li-840A) along longitudinal transects from the head of the NRE (Station 30) to the outlet at PS (Station 180). The NRE was divided into upper-, mid-, and lower-estuary sections and CO_2 fluxes were calculated for each section from distance-weighted pCO_2, temperature and salinity, along with gas transfer velocities derived from daily-average wind speed (Jiang et al., 2008). The upper-, mid-, and lower-estuary CO_2 fluxes as reported by Van Dam et al., (2018) were aerially weighted to calculate the total CO_2 flux for the NRE at each time point. It is important to note these CO_2 fluxes represent the net sea-to-air CO_2 flux, and include CO_2 transported in from the river, as well as net biological and photochemical processes in the estuary.

PP was measured using the ^{14}C method on surface water samples under natural irradiance and temperature conditions (Paerl et al., 1998). To estimate total C-production by phytoplankton for each ModMon sampling time point, the surface PP measurements (mg C m^{-3} hr^{-1}) for each station were multiplied by eight to convert the daylight incubation period to 8 hours (approximate length of daylight) and then multiplied by the surface volume (volume above the pycnocline) as defined for the salinity box model at each station and sampling date (Wetzel and Likens, 2000). The PP values as calculated for each station were then summed across the estuary for each ModMon date. Previous studies have estimated DOC production by phytoplankton as about 15-25% (averaged: 19%) of total C-production for coastal, eutrophic systems (Marañón et al., 2004). Therefore, the amount of DOC produced by phytoplankton was estimated as 15-25% of the total PP, with an averaged value of 19%, for the estuary. This represents a maximum amount of [DOC] produced by phytoplankton and does not capture net [DOC] from phytoplankton (i.e., [DOC] production by phytoplankton minus that removed by heterotrophic consumption).

All calculations, linear regression models, and statistical analyses were conducted in Matlab 2017b. Linear regression models were fitted using the Matlab *fitlm* function.

4. Results

4.1 Discrete discharge events

The time period used for this study encompassed a range of freshwater discharge conditions, spanning the 4th to 99th flow quantiles and included two hurricane-associated discharge events (Figure 4.2, Table 4.1). The NRE was impacted by fringing effects from Hurricane Joaquin and an associated Nor'easter in September 2015, which resulted in elevated discharge from the NR and moderate wind conditions (~ 9 m s^{-1} max. wind speed) over the NRE. In October 2016, the NRE and its watershed were directly impacted by Hurricane Matthew, which resulted in a historic 500-year flood event in the NR watershed (Musser et al., 2017). In addition to these two tropical storms, there were also several notable seasonal discharge events, including three sequential events in the winter of 2015-2016 and a spring discharge event in April 2016. All of these events were compared to a low-flow baseline period captured during summer 2015. I acknowledge the location of rainfall within the NR basin is important in altering the quantity and quality of DOC flushed from the watershed into the NRE following various discharge events. A discussion of this variability is included in Appendix 4.6.

4.2 DOM load

At the head of the estuary, [DOC] and a_{350} followed a logarithmic relationship with riverine discharge (Figure 4.3a-b). DOC loads were positively and linearly correlated with a_{350} loads (Figure 4.3c), indicating the DOC loaded into the estuary from the riverine end member was derived from terrestrial sources (Spencer et al., 2013). DOC and a_{350} loads were approximately

twice as high immediately following Hurricane Matthew as for the other discharge events which resulted in the log relationships observed.

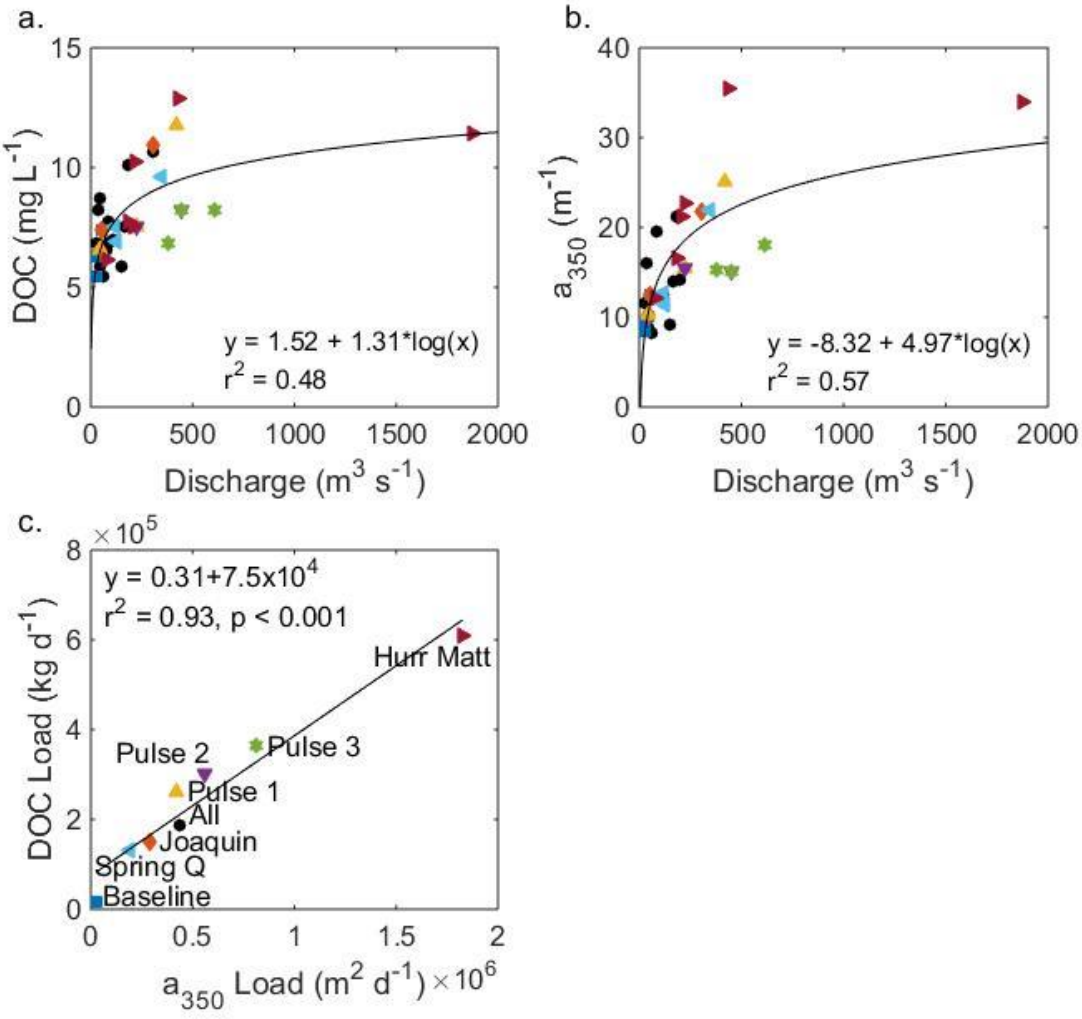

Figure 4-3. a. Head of estuary [DOC] (mg L^{-1}) and b. a_{350} (m^{-1}) plotted against discharge (m^3 s^{-1}). c. DOC load (kg d^{-1}) plotted against a_{350} load (m^2 d^{-1}). Discrete discharge events are identified by colors and symbols as indicated in Fig. 3c. The log relationship for both DOC and a_{350} as a function of discharge is plotted along with the equation and coefficient of determination (r^2).

4.3 Volume weighted DOM concentrations

Volume weighted [DOC] and a_{350} at each sampling time point closely followed the amount of freshwater in the estuary as indicated by its inverse relationship with salinity (Figure 4.4; Appendix 4 Figure A4.13). The impacts of the wet 2015-2016 winter and Hurricane Matthew

were obvious in both volume weighted DOM parameters ([DOC] and a_{350}) and volume-weighted salinity. In terms of volume-weighted salinity, there were similar values following the winter 2016 Pulse 3 event and Hurricane Matthew (~2 PSU), indicating the same volume of freshwater was flushed into the estuary during both of these events. The difference between these two events, however, was their duration: Pulses 1 through 3 occurred over several months while Hurricane Matthew's freshwater loading occurred within a span of days to weeks.

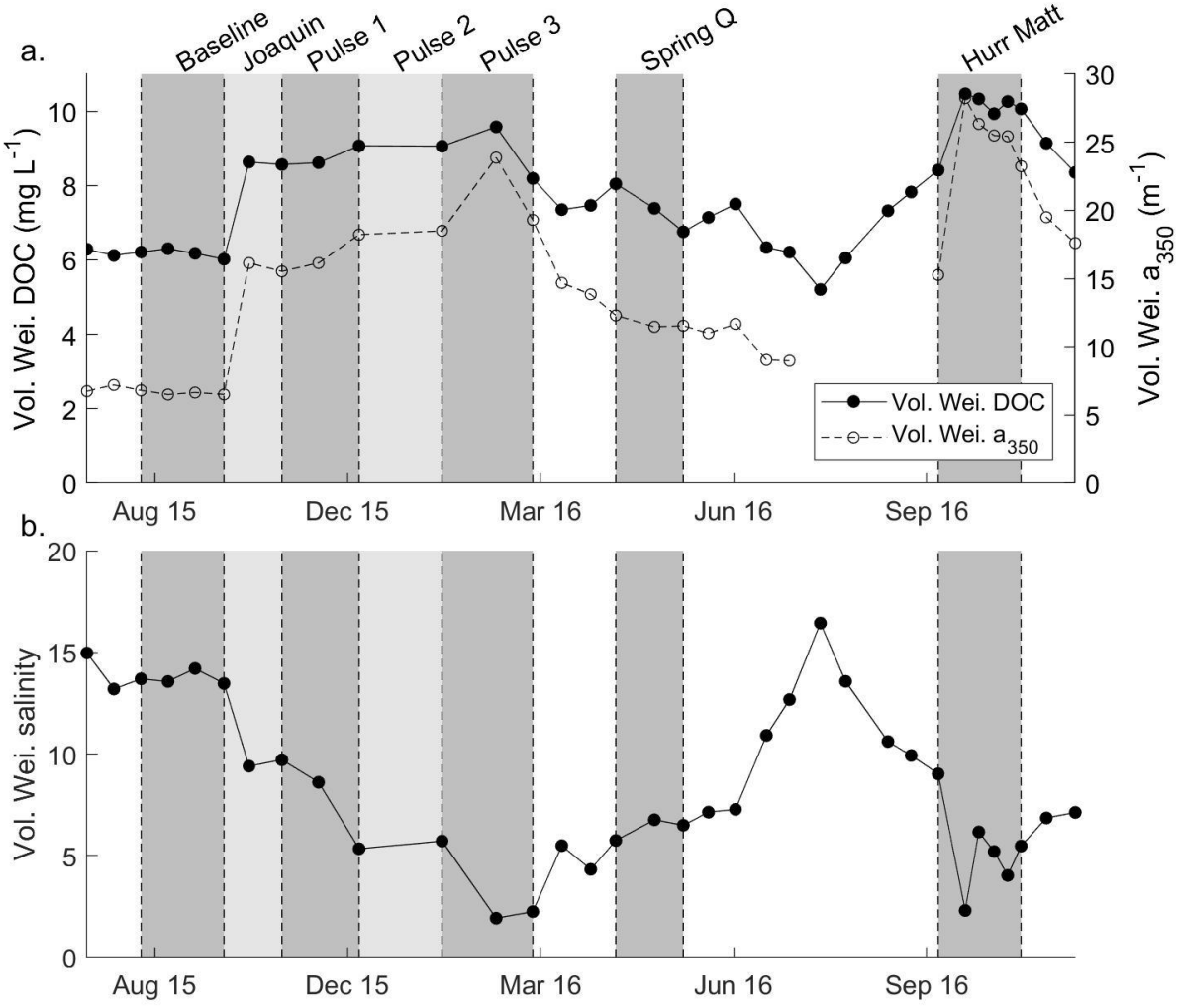

Figure 4-4. a. Volume weighted [DOC] (mg L^{-1}) plotted in the black circles and volume weighted a_{350} (m^{-1}) plotted in white circles. b. Volume weighted salinity. Dashed vertical lines indicate the boundaries of each of the 7 discrete discharge events.

4.4 Estuarine flow

Confidence intervals calculated for estuarine flow, as both surface flow at station 160S and bottom flow at station 160B, often span zero, indicating the salinity box model as applied to the NRE, was not capable of accurately capturing flow dynamics at the marine end member. This was particularly common during the baseline period when riverine discharge was low for an extended period of time (i.e., several weeks). Generally, as riverine discharge increased, the ability of the box model to resolve flow at the marine end member, improved. Despite this shortcoming, the flow values calculated from the salinity box model represent the best estimate for flow at station 160. Therefore, I will still discuss and use these values to constrain [DOC] and a_{350} in the NRE with the caveat that the flow values are highly variable as estimated with this method.

For estuarine flow at station 160, surface flow was generally out of the estuary with bottom estuarine flow into the estuary, following normal estuarine circulation (Geyer and MacCready, 2014) (Figure 4.5c). Surface outflow at station 160 generally tracked riverine flow as measured at Ft. Barnwell, and DOC export was often driven by river flow (Figures 4.3 and 4.5). Following highly elevated riverine discharge periods (i.e., Joaquin, Hurricane Matthew) the estuary acted like a river, such that flow at 160S and 160B were both out of the estuary.

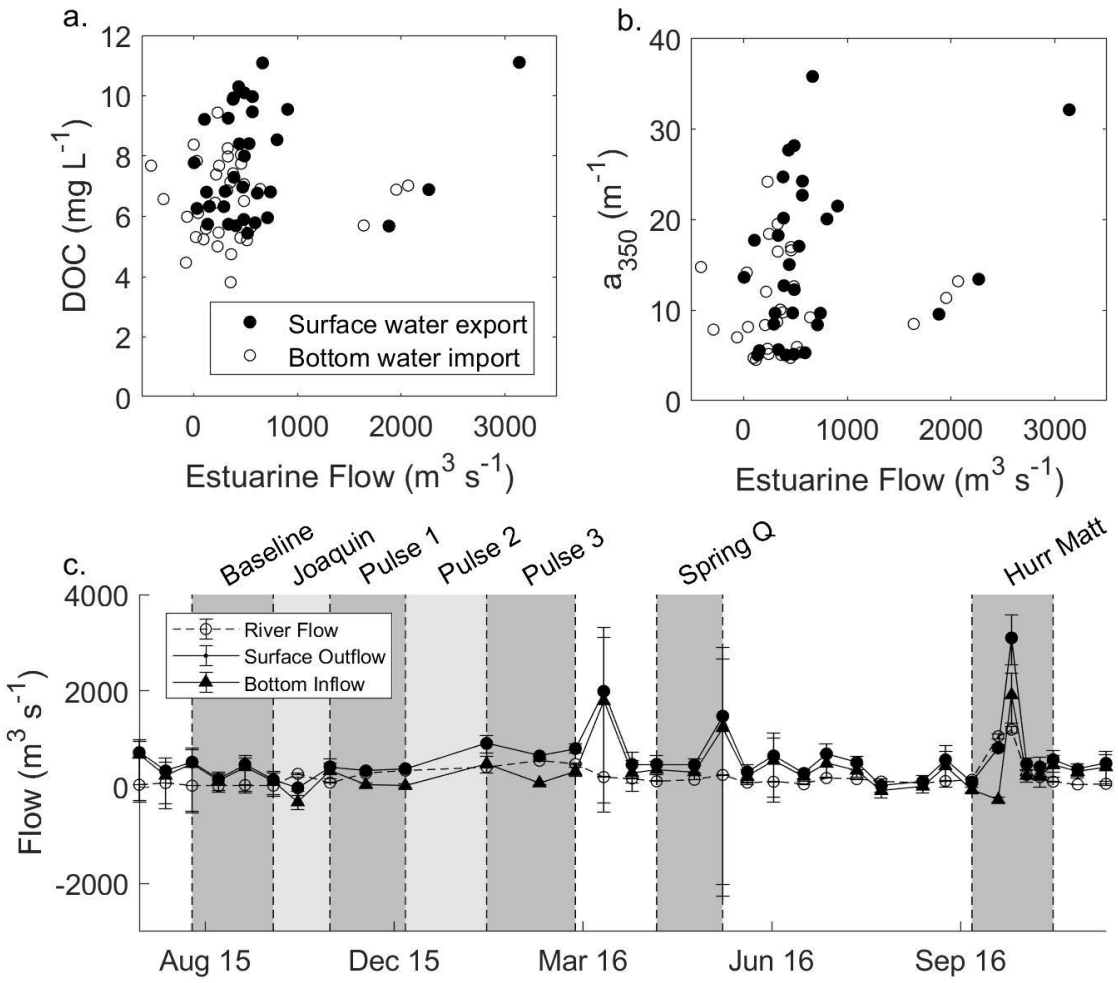

Figure 4-5. a. [DOC] (mg L^{-1}) and b. a_{350} (m^{-1}) plotted for station 160 versus estuarine flow. Black circles represent surface water at 160S and white circles represent bottom water at 180B. c. Estuarine flow (m^3 s^{-1}) as calculated for station 160. Surface outflow is plotted in the black circles, bottom inflow in the black triangles, and river flow as the white circles. Linear relationships were not statistically significant ($p > 0.1$).

4.5 Estimates of biological processes

Estimates of a_{350} and DOC source & sink terms had a high amount of variability, indicating the box model was not able to accurately resolve DOC dynamics, as DOC sources or sinks, *in situ*. Generally, the NRE was a source for both a_{350} and DOC (Figure 4.6a-b), with the highest source terms (and associated variability) in the weeks following tropical cyclone events (i.e., Joaquin, Matthew). The estuary was a source of CO_2 to the atmosphere immediately following

these events (~1 week) (Figure 4.6c). PP was a significant source of total C, as both particulate OC (POC) and DOC, produced in the estuary and was nearly twice the magnitude of the DOC source and sink term (Figure 4.6d) (Paerl et al., 1998). Assuming DOC production by phytoplankton is only 15-25% of the total estuarine PP (Marañón et al., 2004), phytoplankton DOC production was on the same order of magnitude as the DOC source & sink term calculated for the NRE (Figure 4.6d).

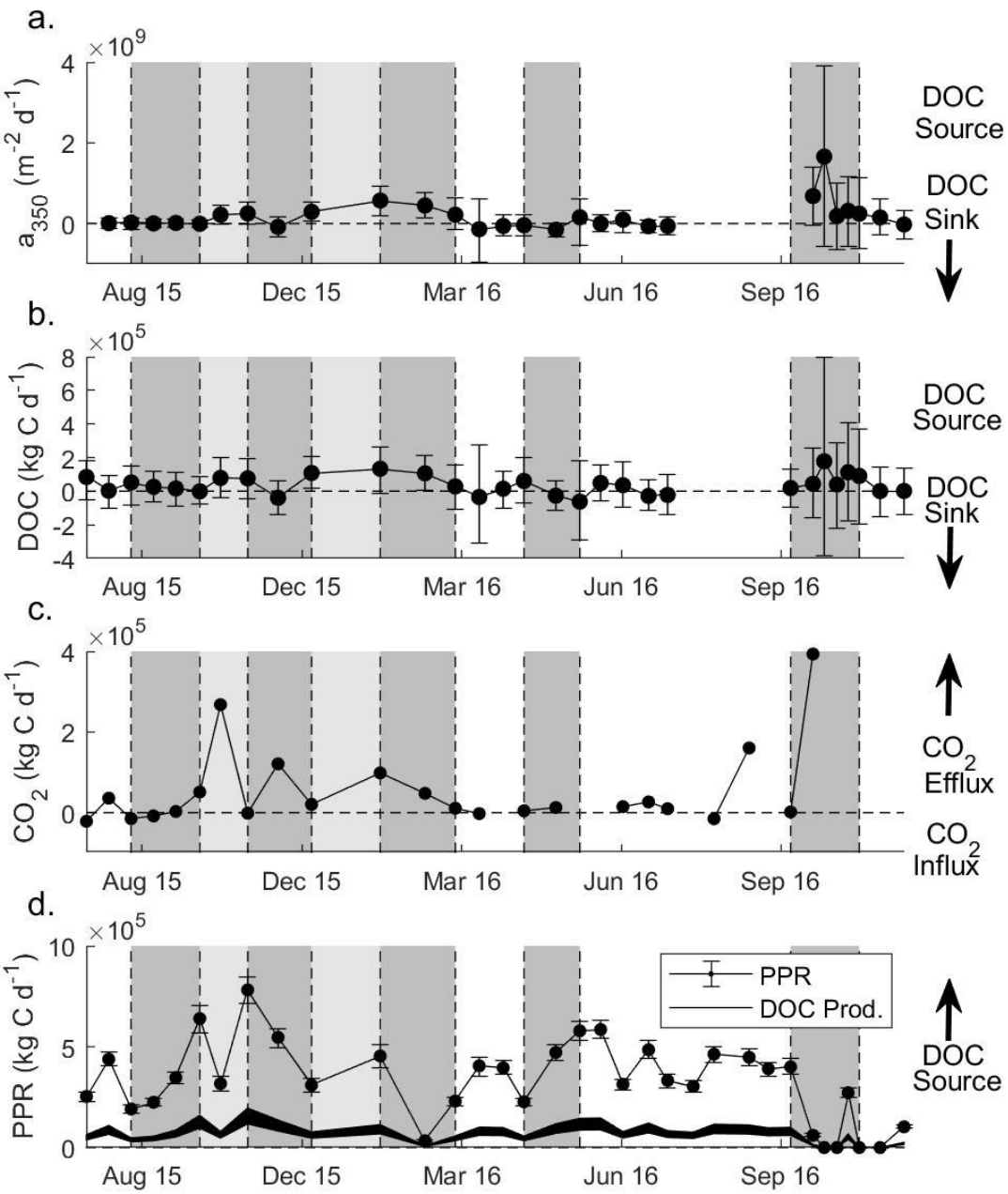

Figure 4-6. Box model results showing a. a_{350} (m^2 d^{-1}) and b. DOC (kg C d^{-1}) source & sink terms for each ModMon sampling date. Values represent internal estuarine a_{350} and DOC processing, respectively in excess of fluxes in and out of the system. c. water-air CO_2 flux (kg C d^{-1}). d. PPR (primary productivity, kg C d^{-1}) measured for the NRE plotted as black circles. DOC production by PP (estimated as 15-25% of total PP) is plotted in the shaded black. In all graphs, the vertical dashed lines indicate bounds of the 7 discrete discharge events. The horizontal dashed line indicates 0.

5. Discussion

It is well established that a modest increase in freshwater discharge leads to an increase in riverine [DOC] and an increase in [DOC] downstream, a paradigm that has previously been shown to apply in the NRE under low to mid-range discharge conditions (Dixon et al., 2014; Osburn et al., 2012; Paerl et al., 1998). Often lacking, though, are estimates of fluxes for individual estuaries based on observed properties of DOM and not inferred from modeled net ecosystem rates for large geographical regions (e.g., Herrmann et al., 2014; Najjar et al., 2018). Results from this study show that this paradigm applies when assessed for a single estuary, especially pertaining to DOC and a_{350} loading from the riverine end-member, where increasing riverine discharge resulted in a log relationship between discharge and [DOC] and a_{350} (Figure 4.3a-b). These relationships led to increased DOM loads at the head of the estuary under modest flow conditions (Figure 4.3c). Following Hurricane Matthew, there were indications of the 'dilution effect', where anomalously high discharge led to a decrease in [DOC] compared to what would be predicted by a positive, linear relationship between [DOC] and discharge under more normal flows ($Q < 750$ m^3 s^{-1}), which resulted in the log relationship observed.

The statistically significant, positive, linear relationship between DOC and a_{350} riverine loads indicate the DOC flushed into the estuary following these events is derived from terrestrial material stored in the NRE's watershed (Spencer et al., 2013). In the NRE, these terrestrial sources likely include flushing of terrestrial soils and freshwater wetlands, the latter of which are abundant between Ft. Barnwell and head of tides at station 0 (Rudolph, 2018). The extreme discharge following Hurricane Matthew, resulted in DOM loads that were as much as double those from any other discrete discharge event during this study (Figure 4.3). The DOC and a_{350} loads computed following Hurricane Matthew demonstrated that the primary control on the

NRE's C-cycle is likely caused by hydrologic connectivity of wetlands to the main river channel following EWEs, as was observed in the nearby Yadkin-PeeDee River basin (Majidzadeh et al., 2017).

Table 4-2. Summary of C fluxes as averaged over each discrete discharge event including river DOC load as calculated for each ModMon sampling date, estuarine DOC export as calculated for station 160, the DOC source & sink term, PP production of DOC (assuming 19% of PP is produced as DOC), and CO_2 flux as reported in Van Dam et al., (2018). Confidence intervals are reported.

	River DOC load (kg C d^{-1})*	**Estuarine DOC export (kg C d^{-1})***	**PS DOC import (kg C d^{-1})***	**DOC source & sink term (kg C d^{-1})***	**PP DOC production (kg C d^{-1})****	**CO_2 flux (kg C d^{-1})*****
All	$1.81x10^5$ ($1.61x10^5$, $2.01x10^5$)	$4.20x10^5$ ($1.43x10^5$, $5.92x10^5$)	$2.26x10^5$ ($-3.10x10^4$, $3.72x10^5$)	$3.81x10^4$ ($-1.20x10^5$, $1.97x10^5$)	$6.97x10^4$ ($6.31x10^4$, $7.61x10^4$)	$5.29 \times 10^4 \pm 1.00 \times 10^5$
Baseline	$1.74x10^4$ ($1.55x10^4$, $1.92x10^4$)	$1.65x10^5$ ($-1.04x10^5$. $2.68x10^5$)	$1.23x10^5$ ($-9.74x10^4$, $2.08x10^5$)	$2.31x10^4$ ($-7.88x10^4$, $1.16x10^5$)	$6.66x10^4$ ($6.00x10^4$, $7.33x10^4$)	$7.77 \times 10^3 \pm 2.98 \times 10^4$
Joaquin	$1.11x10^5$ ($9.85x10^4$, $1.23x10^5$)	$1.24x10^5$ ($-2.42x10^4$, $2.44x10^5$)	$2.13x10^4$ ($-9.23x10^4$, $1.15x10^5$)	$5.13x10^4$ ($-5.38x10^4$, $1.60x10^5$)	$1.10x10^5$ ($9.91x10^4$, $1.21x10^5$)	$1.06 \times 10^5 \pm 1.42 \times 10^5$
Pulse #1	$1.88x10^5$ ($1.68x10^5$, $2.08x10^5$)	$3.02x10^5$ ($2.02x10^5$, $3.79x10^5$)	$7.17x10^4$ ($1.22x10^4$, $1.16x10^5$)	$4.85x10^4$ ($-5.57x01^4$, $1.55x10^5$)	$1.04x10^5$ ($9.41x10^4$, $1.13x10^5$)	$4.67 \times 10^4 \pm 6.52 \times 10^4$
Pulse #2	$2.58x10^5$ ($2.31x10^5$, $2.85x10^5$)	$5.39x10^5$ ($4.10x10^5$, $6.46x10^5$)	$1.70x10^5$ ($8.75x10^4$, $2.36x10^5$)	$1.21x10^5$ ($1.88x10^3$, $2.36x10^5$)	$7.25x10^4$ ($6.36x10^4$, $8.15x10^4$)	$5.95 \times 10^4 \pm 5.52 \times 10^4$
Pulse #3	$3.21x10^5$ ($2.89x10^5$, $3.56x10^5$)	$6.23x10^5$ ($4.94x10^5$, $7.37x10^5$)	$1.95x10^5$ ($1.17x10^5$, $2.61x10^5$)	$8.94x10^4$ ($-3.73x10^4$, $2.12x10^5$)	$4.55x10^4$ ($4.01x10^4$, $5.06x10^4$)	$5.24 \times 10^4 \pm 4.40 \times 10^4$
Spring Q	$1.18x10^5$ ($1.05x10^5$, $1.31x10^5$)	$4.43x10^5$ ($-1.95x10^5$, $7.51x10^5$)	$3.25x10^5$ ($-3.04x10^5$, $6.19x10^5$)	$-9.44x10^3$ ($-1.60x10^5$, $1.47x10^5$)	$8.09x10^4$ ($7.41x10^4$, $8.75x10^4$)	$8.58 \times 10^3 \pm 5.80 \times 10^3$
Hurr Matt	$4.79x10^5$ ($4.24x10^5$, $5.32x10^5$)	$8.53x10^5$ ($6.08x10^5$, $1.07x10^6$)	$3.16x10^5$ ($1.43x10^5$, $4.57x10^5$)	$8.06x10^4$ ($-2.04x10^5$, $3.75x10^5$)	$4.64x10^4$ ($4.20x10^4$, $5.11x10^4$)	n.d.

* 95% confidence intervals calculated for each ModMon date using 1001 model runs, then averaged over the time period of interest.

** 95% confidence intervals calculated assuming PP ± 14% (SI, Appendix 2) then averaged over the time period of interest.

5.1 DOM processes in the NRE

The goal of the project was to assess how the NRE responds to different discrete discharge events and establish under what discharge conditions the estuary might act as a sink for riverine DOC versus as a pipeline for export of un-altered riverine DOC to the downstream PS. To accomplish this, a DOC and a_{350} source & sink term was calculated for each ModMon date (Figure 4.6a-b; Table 4.2). Variability of the source & sink terms were high and often spanned zero, indicating the model was not able to accurately constrain when the estuary was acting as either a source or sink of DOC. Estimating DOC export and processing in estuarine environments is difficult given the spatial and temporal sampling resolution of estuarine monitoring programs. This is especially important when capturing variable discharge events, as during this study. Net ecosystem metabolism, often used as a proxy for DOC transformation and consumption processes in estuaries, has been shown to be highly variable due to annual discharge (Vlahos and Whitney, 2017; Crosswell et al., 2017).

In the present study, the box model occasionally indicated the NRE was a source of DOC and a_{350}, primarily following the wet winter of 2015-2016 (Pulse 1 - 3). This indicated that either DOM was produced internally or that secondary and tertiary sources of DOM were not accounted for with the box model (i.e., sedimentary and porewater resuspension, inputs from un-gaged tributaries and wetlands). Times when the NRE was a source of DOC generally followed elevated precipitation events when river discharge was elevated and PP was depressed (Figure 4.6). Therefore, while DOC production from PP as estimated for the NRE was on the same order of magnitude as the DOC source & sink term, it was not a significant source of PP following these elevated precipitation events. This was confirmed when plotting the estimated DOC source & sink term versus DOC production by PP (Figure 4.7a). There was no statistical relationship

between DOC and DOC production by PP, indicating PP was not a significant source of internal DOC to the NRE during this time period.

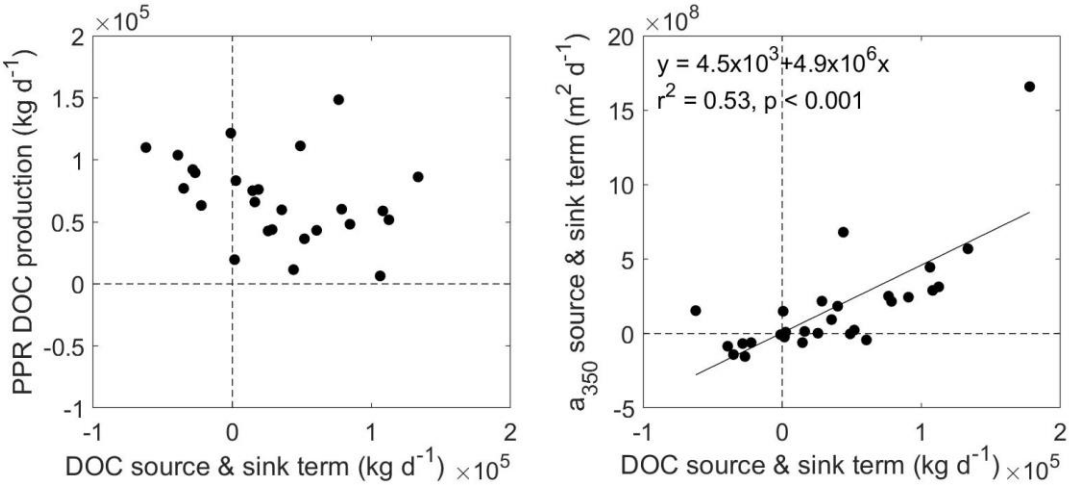

Figure 4-7. a. DOC source & sink term (kg d^{-1}) plotted against estimates of DOC production by PP (kg d^{-1}). There was no statistically significant linear relationship. b. DOC source & sink term (kg d^{-1}) plotted against a_{350} source & sink term. There was a statistically significant, positive, linear relationship. The linear relationship, r^r, and p-value are displayed.

While it was beyond the scope of this study to specifically identify other sources of DOM to the estuary, we can speculate on potential mechanisms modulating DOM dynamics. Due to the strong linear relationship between the DOC and a_{350} source & sink terms, it is likely the source of DOC to the NRE is from terrestrial or terrestrial-like sources (Figure 4.7b). The NRE is a relatively shallow estuary (average depth ~3.5 m) where resuspension events are common and well documented (Corbett, 2010). It was possible these resuspension events resulted in release of previously deposited and stored C back to the water column (Crosswell et al., 2014; Luettich et al., 2000). Evidence from bottom water observations of DOM concentrations and properties from the NRE in 2010 – 2011 suggested higher [DOC] and more terrestrial-like DOM in bottom waters following wind-driven mixing events (Dixon et al. 2014). I approximated the DOC pool in sedimentary porewater to be about 1.66 x 10^5 kg C in the top 2.2 cm of sediment (Appendix 4.8) which represents an additional source of DOC to the NRE, especially when riverine DOC

loading is low and wind speeds are elevated. Preliminary experiments conducted during the summer of 2018 in the NRE indicate little [DOC] diffuses from the sediment porewater to the water column under calm conditions (Clerkin et al., unpublished).

Another source of DOC not accounted for in the calculated DOM source & sink term were un-gaged and un-characterized streams and tributaries lining the NRE. For example, the Trent River intersects the NRE between station 30 and 50 and contains dark, humic-rich water that has [DOC] and a_{350} about the same as the upper NRE, and which may represent an additional DOM source (Vähätalo et al., 2005). Additionally, there are several other smaller tributaries, pocosins, and wetlands along the NRE that could contribute to this un-accounted source of DOC. Generally, the NRE was a source of DOC following elevated precipitation events when contributions from these un-gaged tributaries and wetlands may be contributing an unrealized amount of terrestrial-OM to the NRE

5.2 Pulse-Shunt concept in estuarine ecosystems

The PSC suggests that under high river flow events (99^{th} flow quantile), DOC pulsed from watersheds is shunted downstream (Raymond et al. 2016). Indeed, we observed the NRE acting as a river following EWEs (Joaquin, Matthew), such that flow at both station 160S and 160B was out of the estuary (Figure 4.5c). This indicates there was likely direct export of un-altered riverine DOC to the PS following these elevated riverine discharge events. However, due to the resolution of the DOC box model, I am unable to conclude under what discharge conditions the estuary may act as a source or sink of riverine DOC.

Rainfall associated with Hurricane Matthew largely fell in the upper- and mid-NR watershed, meaning it took several weeks (> 2 weeks) for the NRE to receive the entire river pulse associated with Matthew (Appendix 4.6). This resulted in elevated river DOC loading to the

NRE even two weeks post-storm, which suggests that the 'pulse' from the NRE's watershed was gradual. Extensive flooding of riparian wetlands after Matthew's passage was observed and likely represented an important source of the riverine DOC contained in the "pulse" (Rudolph, 2018). However, after this two-week period, the salinity of the estuary started to increase (Figure 4.4b), indicating a return to normal estuarine circulation. I suspect that under these conditions, elevated DOC loading from the NR was combined with import of previously exported, un-degraded riverine DOC from PS in the bottom water.

Table 4-3. Estuarine C export (as DOC and TOC) estimated across systems located along the US east coast. Confidence intervals are reported when available.

Study system	Watershed area (km^2)*	C fraction**	Estuarine C export ($kg\ C\ d^{-1}$)	Estuarine C export scaled to watershed ($kg\ C\ d^{-1}\ km^{-2}$)	Reference
NRE	14,066				
All		DOC	$4.20x10^5$ ($1.43x10^5$, $5.92x10^5$)	29.9 (10.2, 42.0)	This study
Baseline		DOC	$1.65x10^5$ ($-1.04x10^5$. $2.68x10^5$)	11.7 (-7.4, 19.0)	This study
Joaquin		DOC	$1.24x10^5$ ($-2.42x10^4$, $2.44x10^5$)	8.8 (-1.7, 17.3)	This study
Pulse #1		DOC	$3.02x10^5$ ($2.02x10^5$, $3.79x10^5$)	12.5 (14.4, 27.0)	This study
Pulse #2		DOC	$5.39x10^5$ ($4.10x10^5$, $6.46x10^5$)	38.3 (29.2, 48.0)	This study
Pulse #3		DOC	$6.23x10^5$ ($4.94x10^5$, $7.37x10^5$)	44.3 (35.1, 52.4)	This study
Spring Q		DOC	$4.43x10^5$ ($-1.95x10^5$, $7.51x10^5$)	31.5 (-13.9, 53.4)	This study
Hurr Matt		DOC	$8.53x10^5$ ($6.08x10^5$, $1.07x10^6$)	60.7 (43.2, 76.1)	This study
South Atlantic Bight Estuaries	330,944	TOC	$5.48 \times 10^6 \pm 2.47 \times 10^6$	16.6±7.5	Herrmann et al., 2014
East Coast Estuaries	714,289	TOC	$9.32 \times 10^6 \pm 3.84 \times 10^6$	13.0±5.4	Herrmann et al., 2014
Long Island Sound, NY	42,373	DOC	$1.53 \times 10^5 \pm 1.75 \times 10^5$	3.6±4.1	Vlahos and Whitney, 2017
Chesapeake Bay, VA	166,793	TOC	7.70×10^5	4.6	Kemp et al., 1997
New River Estuary, NC	1,177	TOC	$1.29\ x10^4$	11.0	Crosswell et al., 2017

* Data obtained from Bricker et al., 2008

** Indicates the fraction of C for which export values were calculated. DOC = dissolved organic carbon; TOC = total organic carbon (particulate OC (POC) + DOC).

Estuarine OC export, scaled to estuarine watershed area estimated for this study, was comparable to export values reported for other coastal ecosystems (Table 4.3). The NRE baseline, watershed normalized DOC export was in good agreement with watershed normalized TOC export calculated for other US East Coast estuaries as well as export values calculated for the South Atlantic Bight and US East Coast. The NRE baseline value was remarkably similar to the normalized TOC export calculated for the nearby New River Estuary (Crosswell et al., 2017). DOC is only a fraction of the TOC, which represents both DOC and POC and therefore, we would expect estimates of OC export from the NRE to increase if POC data were also included. Evidence in the NRE, however, suggests POC is only about 10% of the total TOC pool (Hounshell et al., Chapter 3). Unlike under baseline conditions, the NRE watershed normalized DOC export which includes elevated discharge events, was much greater than the baseline value and any of the other reported estuarine OC exports. This further indicates the large impact elevated discharge events have on altering the amount of OC exported from estuarine systems. Hurricane Matthew alone, exported up to 5 times more DOC than the TOC value estimated for all US East Coast estuaries (Herrmann et al., 2014). The paucity of EWE-related C export measurements likely means that regional C export from estuaries is under-estimated.

6. Conclusion

This study attempted to estimate OM source & sink terms, as DOC and a_{350} to constrain how the NRE receives, processes and exports terrestrial OM under a range of discharge conditions, including a 99^{th} quantile flood event. The box model approach utilized during this study, however, was unable to consistently resolve estuarine flow, as surface and bottom flow, at the marine end member. This is likely a function of the poor temporal and spatial resolution at which the estuary is routinely sampled, which makes it difficult to resolve how the estuary changes in

response to variable river discharge and wind conditions. This difficulty was exacerbated in the DOC and a_{350} box models, such that the method was unable to resolve when or if the estuary was acting as an OM source or sink on daily or annual time scales. Results do indicate riverine discharge was an order of magnitude greater than any calculated source or sink term, indicating river discharge is likely the dominate control on OM dynamics in the NRE. This likely makes it difficult to resolve relatively small changes in OM dynamics *in situ*.

Results from this study did indicate the estuary may act as a river following extreme discharge events, supporting the application of the PSC to estuarine systems (Raymond et al., 2016). Specifically, following EWE's (Joaquin, Matthew) flow at both station 160S and 160B was out of the estuary, indicating direct export of riverine water and riverine OM to the PS. Comparisons with other estimates of DOC export from estuarine systems, suggest EWE's will have a large impact on the annual export of DOC to the coastal ocean and represent more than a 400% increase in export of DOC from estuaries following a 99^{th} flow quantile event compared to baseline conditions. The additional export of C following EWE's should be incorporated into our understanding of how C-cycling will change in the future especially under predictions of increasing frequency and intensity of EWEs as predicted by climate change models (Bender et al., 2009; Janssen et al., 2016).

REFERENCES

Alber, M., Sheldon, J.E., 1999. Use of a Date-specific Method to Examine Variability in the Flushing Times of Georgia Estuaries. Estuarine, Coastal, and Shelf Science 49, 469–482.

Bauer, J.E., Cai, W., Raymond, P.A., Bianchi, T.S., Hopkinson, C.S., Regnier, P.A.G., 2013. The changing carbon cycle of the coastal ocean. Nature 504, 61–70. https://doi.org/10.1038/nature12857

Bender, M.A., Knutson, T.R., Tuleya, R.E., Sirutis, J.J., Vecchi, G.A., Garner, S.T., Held, I.M., 2009. Modeled Impact of Anthropogenic Atlantic Hurricanes. Science 327, 454-458.

Bianchi, T.S., 2011. The role of terrestrially derived organic carbon in the coastal ocean: A changing paradigm and the priming effect. Proceedings of the National Academy of Science 108, 19473–19481. https://doi.org/10.1073/pnas.1017982108

Bianchi, T.S., Garcia-Tigreros, F., Yvon-Lewis, S.A., Shields, M., Mills, H.J., Butman, D., Osburn, C., Raymond, P., Shank, G.C., Dimarco, S.F., Walker, N., Reese, B.K., Mullins-Perry, R., Quigg, A., Aiken, G.R., Grossman, E.L., 2013. Enhanced transfer of terrestrially derived carbon to the atmosphere in a flooding event. Geophysical Research Letters 40, 116–122. https://doi.org/10.1029/2012GL054145

Bricker, S.B., Longstaff, B., Dennison, W., Jones, A., Boicourt, K., Wicks, C., Woerner, J., 2008. Effects of nutrient enrichment in the nation's estuaries: A decade of change. Harmful Algae 8, 21-32.

Christian, R.R., Boyer, J.N., Stanley, D.W., 1991. Multiyear Distribution Patterns of Nutrients within the Neuse River Estuary, North Carolina. Marine Ecology Progress Series 71(3), 259–274. https://doi.org/Doi 10.3354/Meps071259

Corbett, D.R., 2010. Resuspension and estuarine nutrient cycling: Insights from the Neuse River Estuary. Biogeosciences 7, 3289–3300. https://doi.org/10.5194/bg-7-3289-2010

Crosswell, J.R., Anderson, I.C., Stanhope, J.W., Van Dam, B.R., Brush, M.J., Ensign, S., Piehler, M.F., Mckee, B., Bost, M., Paerl, H.W., 2017. Carbon budget of a shallow, lagoonal estuary: Transformations and source-sink dynamics along the river-estuary-ocean continuum. Limnology and Oceanography 62, S29–S45. https://doi.org/10.1002/lno.10631

Crosswell, J.R., Wetz, M.S., Hales, B., Paerl, H.W., 2014. Extensive CO_2 emissions from shallow coastal waters during passage of Hurricane Irene (August 2011) over the Mid-Atlantic coast of the U.S.A. Limnology and Oceanography 59(5), 1651–1665. https://doi.org/10.4319/lo.2014.59.5.1651

Crosswell, J.R., Wetz, M.S., Hales, B., Paerl, H.W., 2012. Air-water CO_2 fluxes in the microtidal Neuse River Estuary, North Carolina. Journal of Geophysical Research 117, 1–12. https://doi.org/10.1029/2012JC007925

Del Giorgio, P.A., Pace, M.L., 2008. Relative independence of dissolved organic carbon transport and processing in a large temperate river: The Hudson River as both pipe and reactor. Limnology and Oceanography 53(1), 185–197.

Dhillon, G.S., Inamdar, S., 2013. Extreme storms and changes in particulate and dissolved organic carbon in runoff: Entering uncharted waters? Geophysical Research Letters 40, 1322–1327. https://doi.org/10.1002/grl.50306

Dixon, J.L., Osburn, C.L., Paerl, H.W., Peierls, B.L., 2014. Seasonal changes in estuarine dissolved organic matter due to variable flushing time and wind-driven mixing events. Estuarine, Coastal, and Shelf Science 151, 210–220. https://doi.org/10.1016/j.ecss.2014.10.013

Evans, W., Hales, B., Strutton, P.G., 2013. pCO_2 distributions and air-water CO_2 fluxes in the Columbia River Estuary. Estuarine, Coastal and Shelf Science 117, 260–272. https://doi.org/10.1016/j.ecss.2012.12.003

Geyer, W.R., MacCready, P., 2014. The Estuarine Circulation. Annual Review of Fluid Mechanics 46, 175–197. https://doi.org/10.1146/annurev-fluid-010313-141302

Hagy, J.D., Boynton, W.R., Sanford, L.P., 2000. Estimation of net physical transport and hydraulic residence times for a coastal plain estuary using box models. Estuaries 23(3), 328-340. https:/doi.org/10.2307/1353325

Hall, N.S., Paerl, H.W., Peierls, B.L., Whipple, A.C., Rossignol, K.L., 2013. Effects of climatic variability on phytoplankton community structure and bloom development in the eutrophic, microtidal, New River Estuary, North Carolina, USA. Estuarine, Coastal, and Shelf Science 117, 70–82. https://doi.org/10.1016/j.ecss.2012.10.004

Herrmann, M., Najjar, R.G., Kemp, W.M., Alexander, R.B., Boyer, E.W., Cai, W., Griffith, P.C., Kroeger, K.D., McCallister, S.L., Smith, R.A., 2014. Net ecosystem production and organic carbon balance of U.S. East Coast estuaries: A synthesis approach. Global Biogeochemical Cycles 29, 96–111. https://doi.org/10.1002/2013GB004736

Hirsch, R.M., De Cicco, L., 2015. User guide to Exploration and Graphics for River Trends (EGRET) and data retrieval: R packages for hydrologic data (Version 2.0, February 2015). U.S. Geological Survey Techniques and Methods book 4, chap A10, 93 p. https://doi.org/http://dx.doi.org/10.3133/tm4A10

Hunt, C.W., Salisbury, J.E., Vandemark, D., McGillis, W., 2011. Contrasting Carbon Dioxide Inputs and Exchange in Three Adjacent New England Estuaries. Estuaries and Coasts 34, 68–77. https://doi.org/10.1007/s12237-010-9299-9

Janssen, E., Sriver, R.L., Wuebbles, D.J., Kunkel, K.E., 2016. Seasonal and regional variations in extreme precipitation event frequency using CMIP5. Geophysical Research Letters 43, 5385–5393. https://doi.org/10.1002/2016GL069151

Jiang, L., Cai, W., Wang, Y., 2008. A comparative study of carbon dioxide degassing in river- and marine-dominated estuaries. Limnology and Oceanography 53(6), 2603-2615.

Kemp, W.M., Smith, E.M., Marvin-DiPasquale, M., Boynton, W.R., 1997. Organic carbon balance and net ecosystem metabolism in Chesapeake Bay. Marine Ecology Progress Series 150, 229-248.

Luettich, R.A., Carr, S.D., Reynolds-Fleming, J. V, Fulcher, C.W., McNinch, J.E., 2002. Semi-diurnal seiching in a shallow, micro-tidal lagoonal estuary. Continental Shelf Research 22, 1669–1681.

Luettich, R.A., McNinch, J.E., Paerl, H.W., Peterson, C.H., Wells, J.T., Alperin, M.J., Martens, C.S., Pinckney, J.L., 2000. Neuse River Estuary modeling and monitoring project stage 1: hydrography and circulation, water column nutrients and productivity, sedimentary processes and benthic-pelagic coupling, and benthic ecology. Technical Report No. 2000-325B. NC Water Research and Resources Institute, Raleigh, NC, Unpublished.

Majidzadeh, H., Uzun, H., Ruecker, A., Miller, D., Vernon, J., Zhang, H., Bao, S., Tsui, M.T.K., Karanfil, T., Chow, A.T., 2017. Extreme flooding mobilized dissolved organic matter from coastal forested wetlands. Biogeochemistry 136, 293–309. https://doi.org/10.1007/s10533-017-0394-x

Marañón, E., Cermeñ0, P., Fernádez, E., Rodríguez, J., Zabala, L., 2004. Significance and mechanisms of photosynthetic production of dissolved organic carbon in a coastal eutrophic ecosystem. Limnology and Oceanography 49(5), 1652–1666.

Musser, J.W., Watson, K.M., Gotvald, A.M., 2017. Characterization of Peak Streamflows and Flood Inundation at Selected Areas in North Carolina Following Hurricane Matthew, October 2016 (ver 1.1, June 2017). U.S. Geological Survey Open-File Report 2017-1047, p. 23. Unpublished. https://doi.org/10.3133/ofr20171047

Najjar, R.G., Herrmann, M., Alexander, R., Boyer, E.W., Burdige, D.J., Butman, D., Cai, W., Canuel, E.A., Chen, R.F., Friedrichs, M.A.M., Feagin, R.A., Griffith, P.C., Hinson, A.L., Holmquist, J.R., Hu, X., Kemp, W.M., Kroeger, K.D., Mannino, A., Mccallister, S.L., McGillis, W.R., Mulholland, M.R., Pilskaln, C.H., Salisbury, J., Signorini, S.R., St-Laurent, P., Tian, H., Tzortziou, M., Vlahos, P., Wang, Z.A., Zimmerman, R.C., 2018. Carbon budget of tidal wetlands, estuaries, and shelf waters of Eastern North America. Global Biogeochemical Cycles 32, 1-28.

Osburn, C.L., Rudolph, J.C., Paerl, H.W., Hounshell, A.G., Van Dam, B.R., (2019). Lingering carbon cycle effects of Hurricane Matthew in North Carolina's coastal waters. Geophysical Research Letters. https://doi.org/10.1029/2019GL082014

Osburn, C.L., Boyd, T.J., Montgomery, M.T., Bianchi, T.S., Coffin, R.B., Paerl, H.W., 2016. Optical Proxies for Terrestrial Dissolved Organic Matter in Estuaries and Coastal Waters. Frontiers in Marine Science 2(127). https://doi.org/10.3389/fmars.2015.00127

Osburn, C.L., Handsel, L.T., Mikan, M.P., Paerl, H.W., Montgomery, M.T., 2012. Fluorescence tracking of dissolved and particulate organic matter quality in a river-dominated estuary. Environmental Science and Technology 46, 8628–8636. https://doi.org/10.1021/es3007723

Paerl, H., Pinckney, J., Fear, J., Peierls, B., 1998. Ecosystem responses to internal and watershed organic matter loading: consequences for hypoxia in the eutrophying Neuse River Estuary, North Carolina, USA. Marine Ecology Progress Series 166, 17–25. https://doi.org/10.3354/meps166017

Paerl, H.W., Bales, J.D., Ausley, L.W., Buzzelli, C.P., Crowder, L.B., Eby, L.A., Fear, J.M., Go, M., Peierls, B.L., Richardson, T.L., Ramus, J.S., 2001. Ecosystem impacts of three sequential hurricanes (Dennis, Floyd, and Irene) on the United States' largest lagoonal estuary, Pamlico Sound, NC. Proceedings of the National Academy of Science 98, 5655–5660. https://doi.org/10.1073/pnas.101097398

Paerl, H.W., Crosswell, J.R., Dam, B. Van, Hall, N.S., Rossignol, K.L., Osburn, C.L., Hounshell, A.G., Sloup, R.S., Harding, L.W., 2018. Two decades of tropical cyclone impacts on North Carolina's estuarine carbon, nutrient and phytoplankton dynamics: implications for biogeochemical cycling and water quality in a stormier world. Biogeochemistry 141,307–332. https://doi.org/10.1007/s10533-018-0438-x

Paerl, H.W., Hall, N.S., Peierls, B.L., Rossignol, K.L., 2014. Evolving Paradigms and Challenges in Estuarine and Coastal Eutrophication Dynamics in a Culturally and Climatically Stressed World. Estuaries and Coasts 37, 243–258. https://doi.org/10.1007/s12237-014-9773-x

Paerl, H.W., Valdes, L.M., Joyner, A.R., Peierls, B.L., Piehler, M.F., Riggs, S.R., Christian, R.R., Eby, L.A., Crowder, L.B., Ramus, J.S., Clesceri, E.J., Buzzelli, C.P., Luettich, R.A., 2006. Ecological Response to Hurricane Events in the Pamlico Sound System, North Carolina, and Implications for Assessment and Management in a Regime of Increased Frequency. Estuaries and Coasts 29, 1033–1045.

Peierls, B.L., Christian, R.R., Paerl, H.W., 2003. Water Quality and Phytoplankton as Indicators of Hurricane Impacts on a Large Estuarine Ecosystem. Estuaries 26(5), 1329–1343. https://doi.org/10.1007/BF02803635

Peierls, B.L., Hall, N.S., Paerl, H.W., 2012. Non-monotonic Responses of Phytoplankton Biomass Accumulation to Hydrologic Variability: A Comparison of Two Coastal Plain North Carolina Estuaries. Estuaries and Coasts 35(6), 1–17. https://doi.org/10.1007/s12237-012-9547-2

Raymond, P.A., Saiers, J.E., 2010. Event controlled DOC export from forested watersheds. Biogeochemistry 100, 197–209. https://doi.org/10.1007/sl0533-010-9416-7

Raymond, P.A., Saiers, J.E., Sobczak, W.V, 2016. Hydrological and biogeochemical controls on watershed dissolved organic matter transport: pulse-shunt concept. Ecology 97(1), 5–16.

Rothenberger, M.B., Burkholder, J.M., Brownie, C., 2009. Long-Term Effects of Changing Land Use Practices on Surface Water Quality in a Coastal River and Lagoonal Estuary. Environmental Management. 44, 505–523. https://doi.org/10.1007/s00267-009-9330-8

Rudolph, J.C., 2018. Hurricane Matthew's effect on wetland organic matter sources to the North Carolina coastal waters. Unpublished Thesis, North Carolina State University.

Sanderman, J., Lohse, K.A., Baldock, J.A., Amundson, R., 2009. Linking soils and streams: Sources and chemistry of dissolved organic matter in a small coastal watershed. Water Resources Research 45, 1–13. https://doi.org/10.1029/2008WR006977

Spencer, R.G.M., Aiken, G.R., Dornblaser, M.M., Butler, K.D., Holmes, R.M., Fiske, G., Mann, P.J., Stubbins, A., 2013. Chromophoric dissolved organic matter export from U.S. Rivers. Geophysical Research Letters 40, 1575–1579. https://doi.org/10.1002/grl.50357

Stackpoole, S.M., Stets, E.G., Clow, D.W., Burns, D.A., Aiken, G.R., Aulenbach, B.T., Creed, I.F., Hirsch, R.M., Laudon, H., Pellerin, B.A., Striegl, R.G., 2017. Spatial and temporal patterns of dissolved organic matter quantity and quality in the Mississippi River Basin, 1997–2013. Hydrological Processes 31, 902–915. https://doi.org/10.1002/hyp.11072

Stow, C., Borsuk, M.E., Stanley, D.W., 2001. Long-term Changes in Watershed Nutrient inputs and Riverine Exports in the Neuse River, North Carolina. Water Research 35(6), 1489–1499.

Vähätalo, A.V., Wetzel, R.G., Paerl, H.W., 2005. Light absorption by phytoplankton and chromophoric dissolved organic matter in the drainage basin and estuary of the Neuse River, North Carolina (U.S.A.). Freshwater Biology 50, 477–493. https://doi.org/10.1111/j.1365-2427.2004.01335.x

Van Dam, B.R., Crosswell, J.R., Anderson, I.C., Paerl, H.W., 2018. Watershed-scale drivers of air-water CO2 exchanges in two lagoonal North Carolina (USA) estuaries. Journal of Geophysical Research: Biogeosciences 123, 271-287.

Vlahos, P., Whitney, M.M., 2017. Organic carbon patterns and budgets in the Long Island Sound estuary. Limnology and Oceanography 62, S46-S57. https://doi.org/10.1002/lno.10638

Wetzel, R.G., Likens, G.E., 2000. Primary productivity of phytoplankton, in: Limnological Analyses. Springer, New York, pp. 219–240.

Yoon, B., Raymond, P.A., 2012. Dissolved organic matter export from a forested watershed during Hurricane Irene. Geophysical Research Letters 39, 1–6. https://doi.org/10.1029/2012GL052785

CHAPTER 5: STIMULATION OF PHYTOPLANKTON PRODUCTION BY ANTHROPOGENIC DISSOLVED ORGANIC NITROGEN IN A COASTAL PLAIN ESTUARY[1]

1. Summary

There is increased focus on nitrogen (N)-containing dissolved organic matter (DOM) as a nutrient source supporting eutrophication in N-sensitive estuarine ecosystems. This is particularly relevant in watersheds undergoing urban and agricultural development, leading to increased dissolved organic N (DON) loading. To understand how this shift in N-loading influences estuarine phytoplankton production, nutrient addition bioassays were conducted in the N-limited Neuse River Estuary, North Carolina from 2014-2015. Additions included N-rich DOM sources characteristic of urban and agricultural development, including chicken and turkey litter leachate, wastewater treatment facility effluent, and concentrated river DOM (used as a reference). Each DOM addition was coupled with an inorganic nutrient treatment to account for inorganic nutrient concentrations ($NO_{2/3}$, NH_4, PO_4) in each respective DOM addition. Repeated measures analysis of variance (RM-ANOVA) showed that chicken litter leachate stimulated phytoplankton growth greater than its coupled inorganic nutrient treatment. Wastewater treatment facility effluent, turkey litter leachate, and concentrated river DOM did not stimulate phytoplankton growth greater than their respective inorganic nutrient controls. DOM fluorescence (EEM-PARAFAC) indicated the chicken litter contained a biologically reactive

[1] This Chapter previously appeared as an article in the journal Environmental Science & Technology. The original citation is as follows:
Hounshell, A.G., Peierls, B.L., Osburn, C.L., Paerl, H.W. (2017). Stimulation of phytoplankton production by anthropogenic dissolved organic nitrogen in a coastal plain estuary. *Environmental Science & Technology* 51, 13104-1311. https://doi.10.1021/acs.est.7b03538

fluorescent DOM component, identified as the non-humic, biologically labile, 'N-peak' which may be responsible for stimulating the observed phytoplankton growth in the chicken litter leachate treatments. Overall, results from this study suggest, broadly, that the majority of DON watershed sources are not responsible for continued observations of excess phytoplankton growth in the Neuse River Estuary; however, results do indicate source specific watershed management plans may be important to limit potentially bio-reactive (i.e., chicken litter leachate) forms of DON from reaching estuarine waters.

2. Introduction

Globally, coastal systems are experiencing increasing pressures on ecosystem function and health as a result of rapidly expanding urban, industrial, and agricultural activities in their water- and airsheds (Howarth, 2008; Pellerin et al., 2006; Stow et al., 2001). These changes in land-uses and activities have resulted in changes in the form of nutrient loading, specifically as nitrogen (N) to downstream coastal systems, as a shift from a combination of inorganic and organic N (ON) to a larger proportion of ON loading (Lebo et al., 2012; Pellerin et al., 2006). Since the mid-1990's, efforts have been enacted to reduce total N loading to N-sensitive, eutrophying systems, e.g., the introduction of total maximum daily loads (TMDLs) that mandated reductions in total N-loading to these systems (Linker et al., 2013; Paerl et al., 2004). While efforts to reduce sources of inorganic N to many impaired estuaries have been successful, there has been a simultaneous increase in dissolved organic N (DON) loading, resulting in a shift in the proportion of inorganic N to DON loading (Howarth, 2008; Lebo et al., 2012; Pellerin et al., 2006). Primary production in most receiving coastal systems and estuaries is N-limited (Conley et al., 2009; Nixon et al., 1986; Paerl and Piehler, 2008) and N loads continue to exacerbate

eutrophication and its associated negative impacts (i.e., nuisance and harmful algal blooms, hypoxia/anoxia, fish kills), despite management efforts (Lebo et al., 2012; Paerl et al., 2010).

It has been hypothesized that changing watershed land uses and resultant changes in N-loading to estuarine systems play a key role in the continued eutrophication of these N-limited ecosystems (Pellerin et al., 2006; Rothenberger et al., 2009). I tested this hypothesis by conducting a series of dissolved organic matter (DOM) nutrient addition bioassays on natural phytoplankton and microbial communities from 2014-2015 in the eutrophic Neuse River Estuary (NRE), located in eastern North Carolina, USA. Treatments included various N-containing DOM additions that reflected watershed urban and agricultural activities as well as "natural" watershed sources such as forests and wetlands. Using this approach, the study addressed the following research question: Does DOM found in specific watershed sources (chicken litter, turkey litter, wastewater treatment facility effluent, river DOM) stimulate phytoplankton standing stock and primary production in excess of growth stimulated by the dissolved inorganic nutrients also contained in these DOM sources?

Results from this study have important implications for focusing on specific anthropogenic OM and ON sources (i.e., chicken litter) that may require additional management in order to protect N-impaired systems experiencing continued eutrophication despite ongoing efforts to reduce inorganic N inputs.

3. Materials and Methods

3.1 Site description

The NRE is a river-dominated, micro-tidal estuary located in the coastal plain of North Carolina, USA (Appendix 5, Figure A5.1). The Neuse River flows through the increasingly urbanized Raleigh-Durham area and several growing, downstream municipalities (Goldsboro,

Kinston, and New Bern, NC) before entering the estuary where land use is characterized by agriculture (concentrated animal feeding, mainly as poultry; row crop operations), wetlands, and forested watersheds (Rothenberger et al., 2009; Stow et al., 2001). Due to the mixed land use in the watershed, a variety of nutrient and DOM sources exist in both the river and estuary (Pellerin et al., 2006; Rothenberger et al., 2009; Stedmon et al., 2006). The estuary drains into the Albemarle-Pamlico Sound, a semi-lagoonal system which has restricted exchange with the Atlantic Ocean, leading to a freshwater flushing time of about five to eight weeks in the NRE (Christian et al., 1991; Peierls et al., 2012). This provides ample time for phytoplankton and associated microbial assemblages to utilize both inorganic and organic nutrients flushed into the system (Christian et al., 1991; Paerl et al., 2013). The NRE is mainly N-limited and can exhibit large phytoplankton blooms in the summer and fall months, which exacerbate bottom water hypoxia and fish kills (Paerl et al., 2004).

3.2 Experimental Design

Five nutrient addition bioassays were conducted using natural phytoplankton and bacterial communities collected from the NRE (June 2014, October 2014, July 2015) where phytoplankton blooms are common (Appendix 5, Figure A5.1) (Rudek et al., 1991) . Bioassays received different DOM additions representative of N-rich, DOM sources to the NRE, including; chicken litter leachate, wastewater treatment facility effluent (effluent), turkey litter leachate, and concentrated river DOM. The volume of DOM source additions were added such that the total DON concentration in each DOM addition equaled 140 µg DON L^{-1}, which is representative of DON concentrations measured in the lower NRE (Hounshell and Paerl, 2017; Osburn et al., 2012). Each DOM addition was paired with an inorganic nutrient addition treatment made up of nitrate/nitrite, ammonium, and phosphate (NO_x^-, NH_4^+, PO_4^{3-}) added to concentrations matching

those measured in each respective DOM addition (Table 5.1). By coupling each DOM addition treatment with an inorganic nutrient addition, the impact of DOM specific sources to phytoplankton productivity could be isolated. For this study, I assume growth responses to dissolved inorganic N and DON are additive, and additional growth stimulated in the DOM treatments compared to the coupled inorganic nutrient treatment is due to the DOM pool contained in the respective DOM source addition. Previous research in the NRE showed that P-limitation is not commonly observed (Paerl et al., 1995; Rudek et al., 1991), but to ensure that P-limitation did not occur during the bioassay, phosphate was added to each treatment. The coupled nutrient control for the concentrated river DOM treatment did not contain added inorganic nutrients, since none were detectable in the addition. Iron and trace metal levels in the NRE are sufficient for supporting macronutrient (N and P)-stimulated growth (Paerl et al., 1995), and were not added to the bioassays.

Table 5.1. Nutrient additions (DOM and inorganic nutrients) for June 2014, October 2014, and July 2015 bioassays. Nutrient concentrations for the DOM additions reflect the concentrations inherent to the respective DOM source.

Date	**Treatments**			
June 2014	Chicken litter addition	Coupled inorganic nutrient addition (Chicken litter)	Effluent addition	Coupled inorganic nutrient addition (Effluent)
	2.8 μg L^{-1} NO_X 10.5 μg L^{-1} NH_4 31.6 μg L^{-1} PO_4 140.1 μg L^{-1} DON	2.8 μg L^{-1} NO_X 10.5 μg L^{-1} NH_4 31.6 μg L^{-1} PO_4	93.8 μg L^{-1} NO_X 13.6 μg L^{-1} NH_4 425.6 μg L^{-1} PO_4 140.1 μg L^{-1} DON	93.8 μg L^{-1} NO_X 13.6 μg L^{-1} NH_4 425.6 μg L^{-1} PO_4
October 2014	Chicken litter addition	Coupled inorganic nutrient addition (Chicken litter)	Turkey litter addition	Coupled inorganic nutrient addition (Turkey litter)
	44.8 μg L^{-1} NO_X 154.5 μg L^{-1} NH_4 89.2 μg L^{-1} PO_4 140.1 μg L^{-1} DON	44.8 μg L^{-1} NO_X 154.5 μg L^{-1} NH_4 89.2 μg L^{-1} PO_4	3.8 μg L^{-1} NO_X 171.3 μg L^{-1} NH_4 92.8 μg L^{-1} PO_4 140.1 μg L^{-1} DON	3.8 μg L^{-1} NO_X 171.3 μg L^{-1} NH_4 92.8 μg L^{-1} PO_4
July 2015	River DOM addition		River DOM control	
	31.0 μg L^{-1} PO_4 140.1 μg L^{-1} DON		No addition	

Incubation water, which contained natural phytoplankton and bacterial assemblages, was collected 0.5 m below the surface and pumped through 202 μm mesh into pre-cleaned, acid-rinsed polyethylene carboys. Initial characteristics of the incubation water were measured (Appendix 5, Table A5.1). Temperature and salinity were measured *in-situ* using a YSI 6600 multi-parameter water quality sonde (Hall et al., 2013). Riverine discharge was measured at the USGS gauging station #02091814 located on the Neuse River near Fort Barnwell, NC approximately 26 km from the head of the NRE (Paerl et al., 2013). Nutrient and chlorophyll *a* (Chl *a*) concentrations were measured as described below. Incubation water was transported (< 4 hours) to the University of North Carolina-Chapel Hill, Institute of Marine Sciences in Morehead City, NC and distributed into pre-aged 4-L transparent polyethylene Cubitainers® for nutrient

additions and incubation. Pre-aging of Cubitainers® reduces possible leaching of optically active compounds (Osburn et al., 2001). Cubitainers® have been shown to transmit ~ 95% of light in the 400-700 nm (PAR) range (Rudek et al., 1991) and ~ 20-35% of light in the 300-400 nm range (Peierls, unpublished results). Treatments were incubated for at least 6 days under ambient light and temperature conditions. Quadruplicate (June 2014; October 2014) or triplicate (July 2015) treatments were subsampled for nutrient, OM, and biological analyses on day 0, 1, 2, 3, and 6 of the bioassay incubations.

DOM source additions were obtained from watershed sources that are nutrient rich and high in DON. DOM source additions used during June 2014 were selected to reflect both urban (effluent) and agricultural (chicken litter) DOM sources in the NRE watershed. In October 2014, DOM source additions were selected to examine the difference between poultry operations (chicken vs. turkey litter). River DOM was used in July 2015 as a contrast to anthropogenic sources of DOM and to reflect more natural DOM sources.

Litter treatments were derived from water-soluble extracts of turkey and broiler chicken litter from poultry operations in the NRE watershed (24 hour extraction at room temperature, followed by filtration) which were obtained from the NC Department of Agriculture laboratory (Osburn et al., 2016). The chicken litter additions were collected from two different farms and may represent variability in nutrient and DOM concentrations between chicken operations (Bolan et al., 2010; Edwards and Dainel, 1992). The June 2014 chicken litter was dried and homogenized prior to extraction. The October 2014 litter samples (chicken and turkey) were not manipulated prior to extraction. Effluent was obtained from a wastewater treatment facility located in Raleigh, NC and is representative of effluent discharged into the Neuse River and NRE (Paerl and Peierls, 2014). Concentrated river DOM originated from Contentnea Creek, an agriculturally

dominated tributary of the NRE (Bhattacharya and Osburn, 2017) (Appendix 5, Figure A5.1), and was concentrated via tangential flow filtration using a cellulose filter with 1 kDa cut-off (Paerl and Peierls, 2014). DOM source additions and volumes are listed in Appendix 5, Table A5.2.

3.3 Optical analyses

Samples for optical analyses were filtered through a combusted (450^{o}C; 4 hours) 0.7 µm porosity, GF/F glass fiber filter and the filtrate measured for absorbance (colored DOM = CDOM) and fluorescence (fluorescent DOM = FDOM). Absorbance spectra of CDOM filtrate were collected from 800 nm to 200 nm on a Shimadzu UV-1700 Pharma-Spec spectrophotometer and corrected using a Nanopure water blank measured on the same day as analysis. Fluorescence spectra were measured on a Varian Cary Eclipse spectrofluorometer. Excitation wavelengths were measured from 240 nm to 450 nm every 5 nm. Emission wavelengths were measured from 300 to 600 nm at 2 nm intervals. Instrument excitation and emission corrections were applied to each sample in addition to corrections for inner-filtering effects, calibrated against the Raman signal of Nanopure water, and standardized to quinine sulfate units (Q.S.U.) (Osburn et al., 2012; Stedmon and Bro, 2008). Emission scans for each sample were concatenated into 151 x 43 excitation-emission matrices (EEMs).

Parallel Factor Analysis (PARAFAC) is a multi-way, statistical decomposition technique that can be applied to a collection of EEMs to identify and track broad classes of FDOM, represented as linearly independent components having excitation and emission properties common to organic fluorophores (Murphy, 2013). Similar to principal components analysis (PCA), but without the constraint of orthogonality, PARAFAC identifies a set of components that explains the underlying fluorescent variability of collected EEMs. Unlike traditional PCA, PARAFAC

can be applied to three-way data arrays (i.e., multiple three-dimensional EEMs) by developing a trilinear model (Bro, 1997). A PARAFAC model was fitted to a total of 225 EEMs collected from all bioassays using the DOMFluor toolbox in Matlab (Stedmon and Bro, 2008). EEMs were normalized to their total fluorescence prior to PARAFAC modeling (Osburn et al., 2012). A 5-component PARAFAC model was fitted to the DOM bioassay samples. The model was split-half validated and all 5 components matched (> 95% similarity) with previously identified PARAFAC components on the online database, OpenFluor (Murphy et al., 2014) (Appendix 5, Figure A5.2; Table A5.3).

Fluorescence was also measured on the DOM source additions (chicken and turkey litter, effluent, river DOM). The sources were not included in the PARAFAC modeling; however, the PARAFAC model generated using the bioassay samples was applied to the five DOM sources. Additionally, a previously developed PARAFAC-based mixing model, FluorMod, was applied to the five DOM sources and the starting NRE incubation water. FluorMod is based on sources of FDOM to the Neuse River watershed (Osburn et al., 2016). By applying FluorMod to the source and incubation water used during the bioassay, the proportion of watershed FDOM sources in the initial bioassay samples could be assessed.

A second PARAFAC model was developed on residuals (as the difference between raw EEMs and PARAFAC modeled EEMs) for samples collected from the two chicken litter DOM treatments (n = 50) (June 2014; October 2014). By analyzing and modeling the residuals, a better understanding of the FDOM composition of the chicken litter treatment could be inferred (Bhattacharya and Osburn, 2017; Fellman et al., 2009).

3.4 Phytoplankton biomass, primary productivity, and bacterial productivity

Phytoplankton biomass was measured as Chl *a* according to the modified version of EPA method 445.0 (Arar and Collins, 1997). Briefly, 50 mL of sample was gently filtered through 25 mm GF/F glass fiber filters. Filters were collected and stored at -20^{o}C until analysis. Filters were extracted overnight in 90% acetone following processing in a tissue grinder. Extract was analyzed un-acidified on a Turner Designs TD-700 fluorometer with narrow bandpass filters. Primary productivity in samples was measured using the ^{14}C method (Paerl et al., 1998). Bacterial productivity was measured using the tritiated (^{3}H) leucine uptake method (Peierls and Paerl, 2010).

3.5 Nutrient analysis

Total dissolved N (TDN), nitrate + nitrite (NO_3^- + NO_2^-, reported as NO_x), ammonium (NH_4^+), and phosphate (PO_4^{-3}) were determined colorimetrically (Peierls et al., 2003). DON was calculated by subtracting dissolved inorganic N species (NO_x^- + NH_4^+) from TDN. DOC was measured on a Shimadzu TOC-5000 analyzer via high temperature catalytic oxidation (Peierls et al., 2003).

3.6 Statistical analysis

Phytoplankton growth responses (Chl *a*, primary productivity) to nutrient additions, EEM-PARAFAC FDOM components, and bulk DOC and DON measurements were compared between each coupled treatment (i.e., inorganic nutrient addition compared to the respective DOM addition) with repeated measures analysis of variance (RM-ANOVA) using the statistical program, JASP 0.8.0.0 (Altman and Paerl, 2012). Spearman's correlation coefficients (ρ) were calculated for correlations between DON and the bioassay PARAFAC components and residual model component in Matlab R2016b.

4. Results and Discussion

4.1 Phytoplankton growth response

Phytoplankton growth response, measured as both phytoplankton standing stock (Chl *a*) and primary production, was stimulated by the two chicken litter treatments (June 2014; October 2014) above their respective coupled inorganic nutrient treatments based on RM-ANOVA results (Figure 5.1; Table 5.2). This indicated there was a specific stimulant in the chicken litter, either as a DOM component or other stimulatory compound, which allowed for greater phytoplankton growth and primary production as compared to the addition of inorganic nutrients (NH_4^+, NO_x, PO_4^{-3}) alone. When present, inorganic-N sources (NO_x, NH_4^+) were rapidly depleted between Day 0 and 1, resulting in N-limited conditions by Day 1 (Appendix 5, Figure A5.3). Previous work in the NRE concluded micronutrients were not limiting and would not likely have a stimulatory effect on growth (Paerl et al., 1995), demonstrating the DOM compounds inherent to the chicken litter may be stimulating phytoplankton production greater than the addition of inorganic nutrients alone.

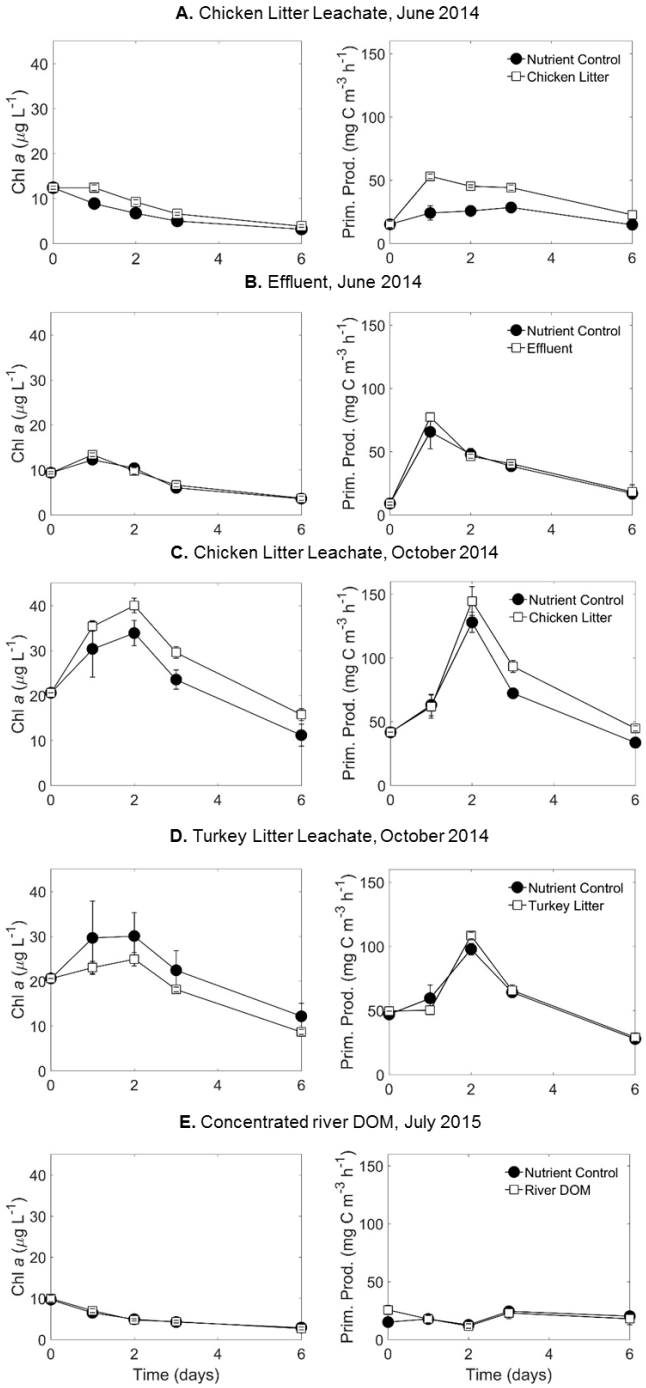

Figure 5.1. Chl *a* (left) and primary productivity (Prim. Prod.) (right) plotted for each coupled DOM addition treatment. Black circles represent the respective inorganic nutrient addition treatments; white squares indicate the coupled DOM addition. RM-ANOVA was used to determine statistically significant differences between the coupled treatments (indicated by p-values for Chl *a* and primary productivity, respectively). A. Chicken litter leachate, June 2014 ($p < 0.001$, $p = 0.001$); B. Effluent, June 2014; C. Chicken litter leachate, October 2014 ($p = 0.02$; $p = 0.022$); D. Turkey litter leachate, October 2014; and E. Concentrated river DOM, July 2015.

Table 5.2. Results from the RM-ANOVA conducted on the coupled DOM addition and inorganic nutrient addition treatments for Chl *a* and primary productivity (Prim. Prod.). Statistically significant p-values ($p < 0.05$) are highlighted in grey. The time column corresponds to differences through time, the treatment column corresponds to differences between the coupled treatments, and the time*treatment column corresponds to differences between the two coupled treatments through time.

	June 2014 Chicken Litter			**June 2014 Effluent**		
	Time	Treatment	Time*Treatment	Time	Treatment	Time*Treatment
Chl *a*	<0.001	<0.001	<0.001	<0.001	0.183	0.024
Prim. Prod.	0.001	0.001	0.031	<0.001	0.695	0.033
	October 2014 Chicken Litter			**October 2014 Turkey Litter**		
	Time	Treatment	Time*Treatment	Time	Treatment	Time*Treatment
Chl *a*	<0.001	0.02	0.759	<0.001	0.107	0.33
Prim. Prod.	<0.001	0.022	0.072	<0.001	0.511	<0.001
	July 2015 River DOM					
	Time	Treatment	Time*Treatment			
Chl *a*	<0.001	0.488	0.333			
Prim. Prod.	<0.001	0.625	<0.001			

For the effluent, turkey litter, and river DOM treatments, the respective DOM addition treatment did not yield greater phytoplankton production compared to the respective inorganic nutrient addition treatments, indicating the DOM pool in these treatments did not lead to greater phytoplankton production. Primary productivity rates measured for the turkey litter leachate treatment were lower than those measured in its coupled inorganic nutrient treatment ($p < 0.001$) despite equal concentrations of inorganic nutrients in both treatments. This indicates there may have been a constituent in the turkey litter that inhibited phytoplankton growth. The exact mechanism of this inhibition is beyond the scope of this study, but could be a result of pharmaceuticals, heavy/trace metal, pathogens, or pesticides contained within the turkey litter that negatively impact phytoplankton productivity (Bolan et al., 2010; Edwards and Dainel, 1992). Further investigation is necessary to determine a specific mechanism.

4.2 DOM characteristics: EEM-PARAFAC FDOM Components, DOC, and DON

All five identified EEM-PARAFAC components were plotted for each coupled treatment (inorganic treatment + DOM addition treatment) through time (Appendix 5, Figure A5.4; Figure A5.5; Table A5.4). All five components exhibited similar patterns during the bioassay, regardless of treatment, which indicates all five components, while identified as mathematically distinct by the PARAFAC model, exhibited similar reactivity irrespective of source. It is assumed the bioassay PARAFAC model is capturing the FDOM pool inherent to the estuarine water used for incubation and is not able to capture FDOM variability in the sources. Because all five components decreased from day 0 to day 6 for all treatments, regardless of DOM source, primary productivity, or bacterial productivity responses (Appendix 5, Figure A5.6), I conclude the decrease in fluorescence intensity for all five components is likely a function of photobleaching and not consumption by phytoplankton. However, I cannot rule out decreases in FDOM intensity due to removal by baseline bacterial degradation, perhaps facilitated by prior photodegradation (Moran et al., 2000). Previous photodegradation studies have demonstrated FDOM components (terrestrial, humic-like; microbial, humic-like; proteins as tyrosine and tryptophan) decrease in fluorescent intensity in response to sunlight exposure, as observed during this study (Osburn et al., 2014, 2011; Del Vecchio and Blough, 2002). The difference in phytoplankton primary production in the two chicken litter treatments is not a function of any of the five identified bioassay PARAFAC modeled FDOM components.

Bulk DOC and DON concentrations were also measured for each bioassay treatment (Appendix 5, Figure A5.7; Table A5.5). DON concentrations were correlated (Spearman's ρ) with each bioassay and residual PARAFAC component (Appendix 5, Table A5.6). All components were positively correlated with DON, indicating components can be considered a

proxy for DON. DOC and DON concentrations were generally higher in the DOM additions compared to the coupled inorganic nutrient treatments. The June 2014 chicken litter was the only treatment statistically different from its coupled inorganic nutrient addition in terms of DON concentration (Appendix, Table A5.5) and which also stimulated phytoplankton production greater than its coupled inorganic nutrient addition. These results indicate the DON portion of the DOM pool in the chicken litter treatment may be stimulating the observed phytoplankton growth. The October 2014 chicken litter treatment also stimulated phytoplankton production, however, the DON concentrations between this DOM addition and its coupled inorganic nutrient treatment were not statistically different, mainly due to the poor replication among quadruplicates. Additional bioassay experiments should be conducted to confirm the linkages between DON, DOM sources, and the stimulation of phytoplankton production to chicken litter, but these preliminary results suggest there is a link. The variability in response to chicken litter (June 2014, October 2014) could either be a function of varying composition and nutrient/DOM quality of different chicken litters (Bolan et al., 2010; Edwards and Dainel, 1992) or could be based on seasonal phytoplankton growth and community composition.

4.3 Source EEMs

DOM source samples (chicken litter, effluent, turkey litter, concentrated river DOM) were under-sampled relative to the DOM treatments in the bioassay experiment, and thus were not included in the bioassay PARAFAC model, as these samples would heavily skew modeling results (Murphy et al., 2014). The bioassay PARAFAC model was applied to the source samples during post-modeling data analysis. The residuals calculated after applying the bioassay PARAFAC model to the source samples were used to identify signals in the source samples that were different from the FDOM pool in the NRE water used for incubations (Fellman et al.,

2009). Results indicated that the poultry litter sources (chicken, turkey) contained fluorescence in the protein-like, biologically labile region of the EEMs that was not captured by the bioassay PARAFAC model (Figure 5.2). This type of fluorescence is considered biologically reactive and has been shown to decrease in fluorescence intensity during laboratory incubation studies, indicating potential uptake by phytoplankton and/or microbial assemblages (Nieto-Cid et al., 2006; Stedmon and Markager, 2005). I argue that the residual fluorescence in the chicken and turkey litter sources is responsible for stimulating primary productivity, but utilization of this DOM component may be inhibited in the turkey litter source due to the presence of contaminants (heavy/trace metals, antibiotics, pesticides, pathogens) which may inhibit phytoplankton growth as explained previously (Bolan et al., 2010; Edwards and Dainel, 1992).

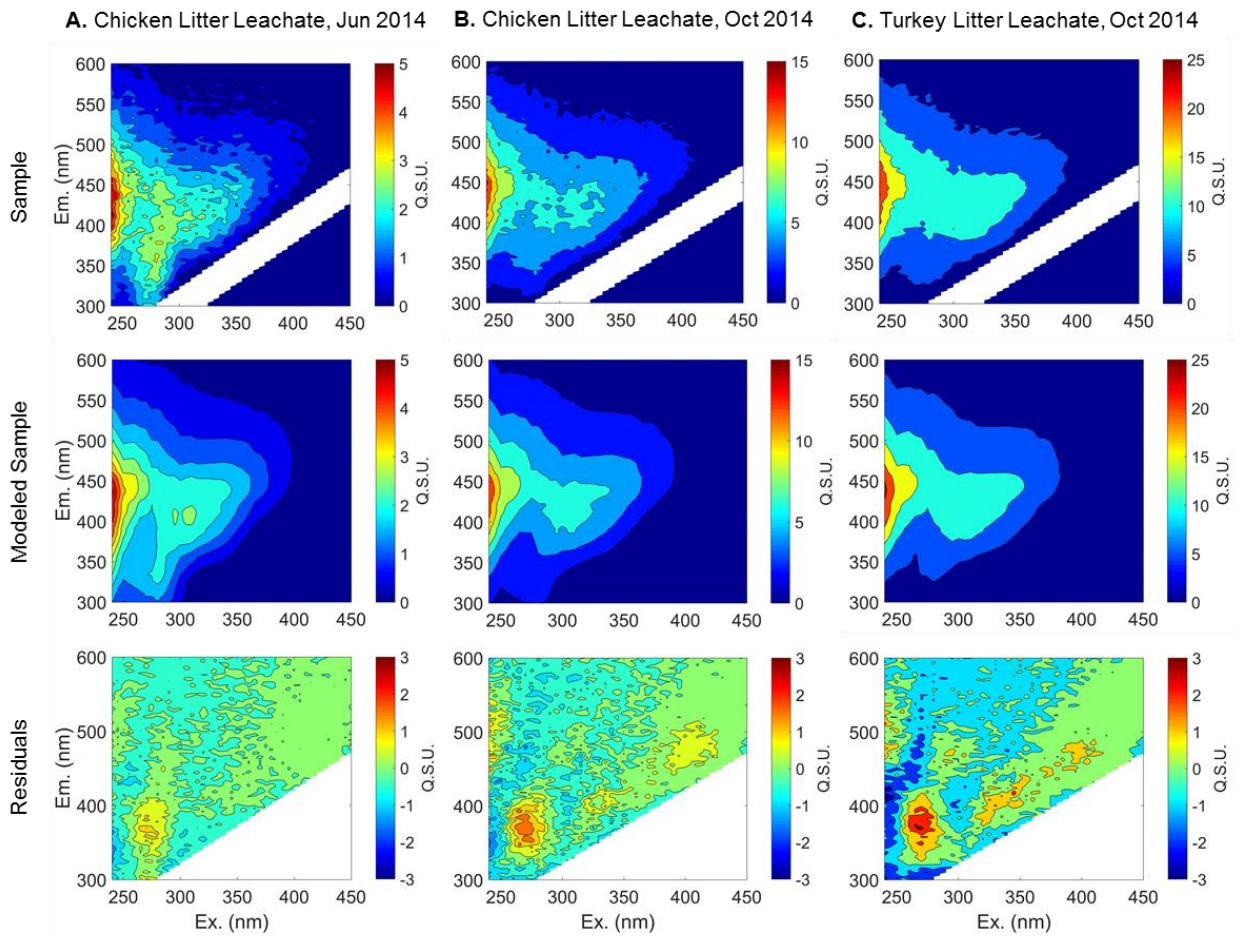

Figure 5.2. Sample EEM (top), PARAFAC modeled EEM (middle), and residual EEM (bottom) for DOM addition sources, A. chicken litter leachate, June 2014; B. chicken litter leachate, October 2014; and C. turkey litter leachate, October 2014. Fluorescence is plotted as Quinine Sulfate Units (Q.S.U.).

The bioassay PARAFAC model was also applied to the effluent and river DOM sources (Appendix 5, Figure A5.8). Residual fluorescence in the effluent sample was similar to the residual signal used in FluorMod to identify effluent FDOM in the Neuse River basin (Osburn et al., 2016), but distinct from the biologically active, protein region of the uncaptured fluorescence in the three litter sources (chicken litter, June 2014, October 2014; turkey litter, October 2014). For the river DOM source, the bioassay PARAFAC model captured virtually all fluorescence variability in the original sample, indicating that the Neuse River FDOM pool dominates the

estuarine water used during the bioassay experiments and confirms the assertion that the bioassay PARAFAC model is dominated by estuarine FDOM signals.

FluorMod was also applied to the five source samples and the initial NRE incubation water (Appendix, Figure A5.9). By applying FluorMod to the source samples, it is possible to calculate the relative proportion of eight previously characterized FDOM sources in the Neuse River basin (reference, effluent, wastewater treatment facility influent, poultry, swine, septic, street, soil) contained within each source and incubation water sample (Hounshell and Paerl, 2017; Osburn et al., 2016). The incubation water used for all three time points was largely dominated by the reference signal, which is characteristic of background stream FDOM, followed by FDOM leached from soil (and possibly from riparian wetlands). Both of these signals are terrestrially derived, high in fluorescent intensity in collected river and estuarine samples, and considered conservative and refractory (Hounshell and Paerl, 2017; Osburn et al., 2016). The incubation water samples also contained a small proportion of poultry litter. All three poultry litter source samples were largely dominated by the reference and poultry signal followed by smaller proportions of the effluent and soil signals. Poultry litter often contains mixtures of soil and bedding material such as wood and straw, which likely explains the presence of other source signals as modeled by FluorMod (Osburn et al., 2016). For the June 2014 chicken litter source, the sample was dominated (>50%) by the poultry litter signal. This source also represented the greatest stimulation of phytoplankton production compared to its coupled inorganic nutrient treatment.

4.4 Residual PARAFAC model

Because the chicken litter leachates were the only DOM sources which promoted phytoplankton growth beyond the coupled inorganic nutrient treatment, a second PARAFAC

model was developed based on the chicken litter treatment residuals (residual model), which were not captured by the bioassay PARAFAC model (Fellman et al., 2010). A single component was identified (Figure 5.3). The component was not split-half validated and did not match with any previously identified components in the OpenFluor database (Murphy et al., 2014); however, this component does appear to represent a separate FDOM class that is inherent to the chicken litter samples and is not accurately captured by the bioassay PARAFAC model. The identified component did match, visually, to the fluorescent N-peak which has been characterized as biologically labile FDOM (Boyd et al., 2010; Coble, 2007), but is not included in the OpenFluor database. Regardless, I have isolated a fluorescence signal specific to poultry litter sources of FDOM in the NRE's watershed.

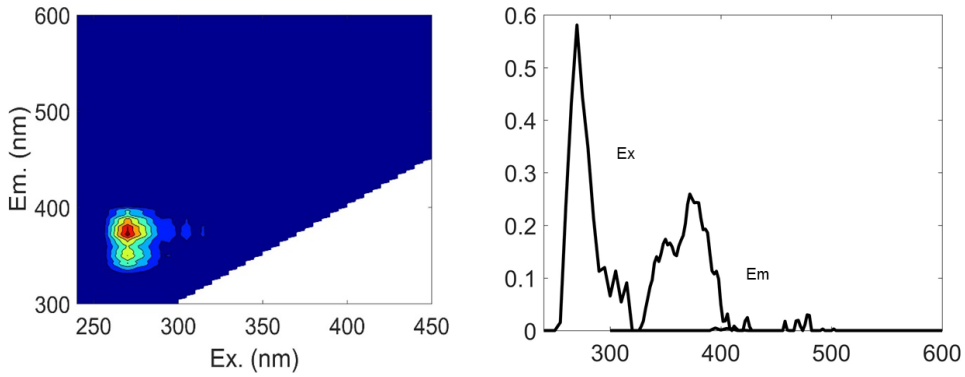

Figure 5.3. PARAFAC component unique to the chicken litter leachate (June 2014, October 2014) treatment samples (left) and the Ex and Em spectra (right). The component was not split-half validated and was identified as the non-humic, biologically labile N-peak (Boyd et al., 2010; Coble, 2007). Excitation maximum at 270 nm; Emission maximum at 372 nm.

The residual PARAFAC model was applied to the sample residuals for all bioassay treatments (chicken litter, effluent, turkey litter, river DOM, and the coupled inorganic nutrient treatments) as a tracer for the behavior of the chicken-specific FDOM during the experiments (Figure 5.4; Appendix 5, Table A5.7). The residual component was present in most inorganic nutrient addition treatments (June 2014; October 2014); I interpret this to indicate the general presence of

biologically labile, poultry-derived FDOM in the NRE, as previously identified by FluorMod. This signal decreased rapidly during the bioassay for both chicken litter treatments (June 2014, October 2014) each of which stimulated greater phytoplankton production than their respective inorganic nutrient treatments. Presence of the residual component in the effluent treatment indicated this signal may not be removed during wastewater treatment. Neither phytoplankton standing stock nor primary productivity were greater in the effluent treatment than its coupled inorganic nutrient treatment, which may be explained by the high inorganic N concentration in the effluent source addition and coupled inorganic nutrient treatment. It is hypothesized these high inorganic-N concentrations stimulated phytoplankton production in both the effluent and its coupled inorganic nutrient treatment greater than potential growth the residual FDOM component could stimulate (Table 5.1; Appendix, Figure A5.3). These results suggest that phytoplankton and microbial assemblages may preferentially use inorganic forms of N, when present, over ON forms for growth (See et al., 2006).

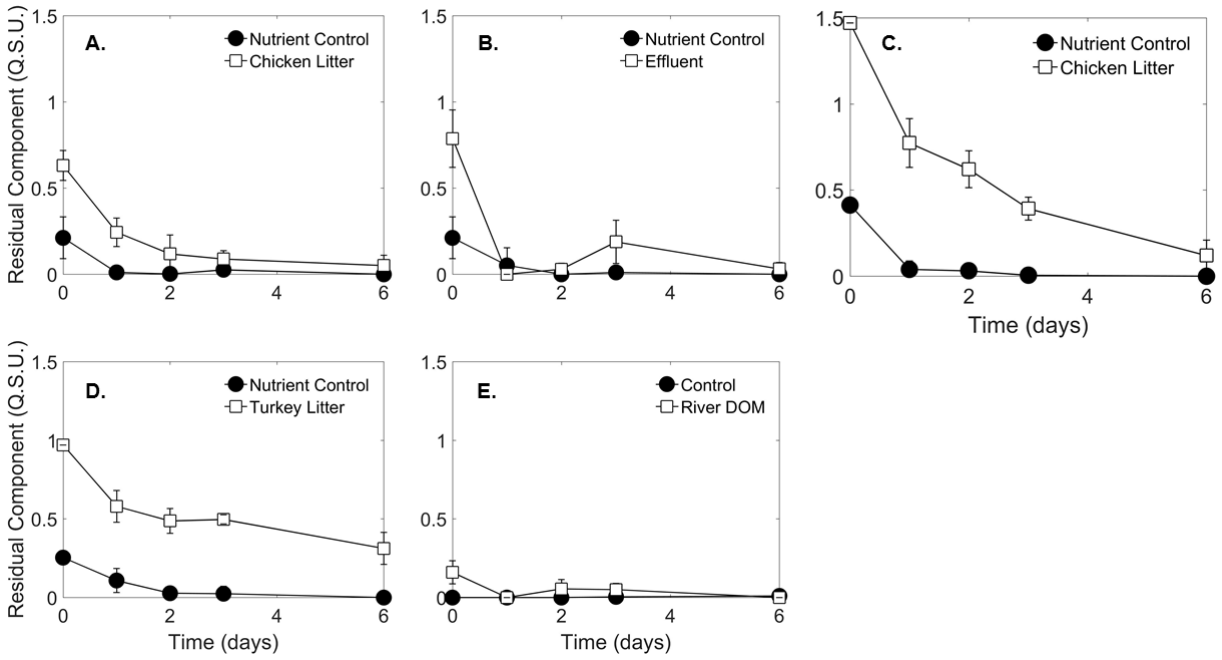

Figure 5.4. Residual PARAFAC component applied to bioassay fluorescence samples for A. chicken litter leachate, June 2014; B. effluent, June 2014; C. chicken litter leachate, October 2014; D. turkey litter leachate, October 2014, and E. concentrated river DOM, July 2015 plotted through the bioassay for both the respective inorganic nutrient addition (black circles) and DOM addition (white squares).

The turkey litter treatment also contained a high initial intensity of this residual fluorescence but was not completely removed during the bioassay incubation as compared to the chicken litter treatments (Figure 5.4). As described previously, phytoplankton growth in the turkey litter treatment appears to be inhibited by an unknown compound allowing this reactive, residual FDOM component to persist during the bioassay. The composition of poultry (chicken, turkey) litter is variable among poultry operations and can contain a range of nutrient, trace metal, pesticide, and pathogen concentrations, making it difficult to predict a consistent impact of different poultry litters on phytoplankton production (Bolan et al., 2010; Edwards and Dainel, 1992). Despite this, the consistent phytoplankton growth responses and FDOM composition observed for two different chicken litters indicates this DOM source can be assumed to stimulate phytoplankton growth in this estuarine environment.

5. Conclusions: Implications for estuarine management

Bioassay results suggest DOM from chicken litter leachates stimulate phytoplankton production and standing stock greater than inorganic N (NO_x^-, NH_4^+) alone. This stimulation of growth attributed to a fluorescent component identified with PARAFAC, shared spectral similarity to the N-peak region of fluorescence that has been previously identified as non-humic and biologically labile (Boyd et al., 2010; Coble, 2007). Chicken litter showed the greatest stimulation; the turkey litter DOM treatment appeared to have an inhibitory effect on primary production, not related to the DOM pool, while the effluent and river DOM treatments had no impact on phytoplankton production compared to their respective inorganic nutrient addition treatments.

Additional chemical analysis is warranted to link specific DOM compounds to the labile peak identified (Stubbins et al., 2014) to understand how and why this specific FDOM component stimulates primary production. The inhibitory effect of the turkey litter treatment also requires further study to understand the mechanism with which this treatment inhibits primary production and whether this inhibitory effect has ramifications for higher trophic levels. These results and future studies are particularly important to coastal ecosystems globally that, like the NRE, are experiencing rapid growth of poultry operations within their watersheds (Mallin et al., 2015; Thorne, 2007). Results from this study demonstrate the need for targeted watershed source nutrient management plans to ensure waste products from poultry operations are properly contained and treated prior to entering a hydrologic system. Untreated waste from animal and other sources that are prevalent in the NRE (Osburn et al., 2016) and other coastal watersheds, are exacerbated during extreme events such as tropical storms (Osburn et al., 2012; Paerl et al., 1998) and have important implications for estuarine water quality. This study points to the need

to account for and manage both inorganic and organic N sources to N-sensitive estuarine and coastal systems in an effort to reduce pervasive eutrophication and its negative impacts.

Furthermore, this study demonstrated that other sources of DON to estuarine systems (i.e., turkey litter, WWTF effluent, concentrated river DOM) were not an important source of N to estuarine phytoplankton and microbial assemblages. These results demonstrate that, more broadly, watershed DON sources are largely not contributing to continued, observed issues associated with eutrophication in estuarine ecosystems. Therefore, more broadly, watershed management of N-sources to estuarine ecosystems should continue to be focused on reducing DIN concentrations from anthropogenic point and non-point sources.

REFERENCES

Altman, J.C., Paerl, H.W., 2012. Composition of inorganic and organic nutrient sources influences phytoplankton community structure in the New River Estuary, North Carolina. Aquatic Ecology 46, 269–282. https://doi.org/10.1007/s10452-012-9398-8

Arar, E.J., Collins, G.B., 1997. In Vitro Determination of Chlorophyll a and Pheophytin a in Marine and Freshwater Algae by Fluorescence. EPA Method 445.0. Technical report for USA-EPA, Cincinnati, Ohio, September 1997.

Bhattacharya, R., Osburn, C.L., 2017. Multivariate Analyses of Phytoplankton Pigment Fluorescence from a Freshwater River Network. Environmental Science & Technology 51, 6683–6690. https://doi.org/10.1021/acs.est.6b05880

Bolan, N.S., Szogi, A.A., Chuasavathi, T., Seshadri, B., Rothrock, M.J., Panneerselvam, P., 2010. Uses and management of poultry litter. Worlds. Poultry Science Journal 66, 673–698. https://doi.org/10.1017/S0043933910000656

Boyd, T.J., Barham, B.P., Hall, G.J., Schumann, B.S., Paerl, R.W., Osburn, C.L., 2010. Variation in ultrafiltered and LMW organic matter fluorescence properties under simulated estuarine mixing transects: 2. Mixing with photoexposure. Journal of Geophysical Research 115, 1–14. https://doi.org/10.1029/2009JG000994

Bro, R., 1997. PARAFAC. Tutorial and applications. Chemometrics and Intelligent Laboratory Systems 38, 149–171. https://doi.org/10.1016/S0169-7439(97)00032-4

Christian, R.R., Boyer, J.N., Stanley, D.W., 1991. Multiyear Distribution Patterns of Nutrients within the Neuse River Estuary, North Carolina. Marine Ecology Progress Series 71, 259–274. https://doi.org/Doi 10.3354/Meps071259

Coble, P.G., 2007. Marine optical biogeochemistry: The chemistry of ocean color. Chemical Reviews 107, 402–418. https://doi.org/10.1021/cr050350

Conley, D.J., Paerl, H.W., Howarth, R.W., Boesch, D.F., Seitzinger, S.P., Havens, K.E., Lancelot, C., Likens, G.E., 2009. Controlling Eutrophication: Nitrogen and Phosphorus. Science 323, 1014–1015. https://doi.org/10.1126/science.1167755

Del Vecchio, R. Del, Blough, N.N. V, 2002. Photobleaching of chromophoric dissolved organic matter in natural waters: kinetics and modeling. Marine Chemistry 78, 231–253. https://doi.org/10.1016/S0304-4203(02)00036-1

Edwards, D.R., Daniel, T.C., 1992. Environmental Impacts of On-Farm Poultry Waste Disposal A Review. Bioresource Technology 41, 9–33.

Fellman, J.B., Hood, E., Spencer, R.G.M., 2010. Fluorescence spectroscopy opens new windows into dissolved organic matter dynamics in freshwater ecosystems: A review. Limnology and Oceanography 55, 2452–2462. https://doi.org/10.4319/lo.2010.55.6.2452

Fellman, J.B., Miller, M.P., Cory, R.M., D'Amore, D. V., White, D., 2009. Characterizing dissolved organic matter using PARAFAC modeling of fluorescence spectroscopy: A comparison of two models. Environmental Science & Technology 43, 6228–6234. https://doi.org/10.1021/es900143g

Hall, N.S., Paerl, H.W., Peierls, B.L., Whipple, A.C., Rossignol, K.L., 2013. Effects of climatic variability on phytoplankton community structure and bloom development in the eutrophic, microtidal, New River Estuary, North Carolina, USA. Estuarine, Coastal and Shelf Science 117, 70–82. https://doi.org/10.1016/j.ecss.2012.10.004

Hounshell, A.G., Paerl, H.W., 2017. Role of organic nitrogen to eutrophication dynamics along the Neuse River Estuary, NC. Report submitted to NC WRRI. Raleigh, NC.

Howarth, R.W., 2008. Coastal nitrogen pollution: A review of sources and trends globally and regionally. Harmful Algae 8, 14–20. https://doi.org/10.1016/j.hal.2008.08.015

Lebo, M.E., Paerl, H.W., Peierls, B.L., 2012. Evaluation of progress in achieving TMDL mandated nitrogen reductions in the Neuse river basin, North Carolina. Environmental Management 49, 253–266. https://doi.org/10.1007/s00267-011-9774-5

Linker, L.C., Batiuk, R.A., Shenk, G.W., Cerco, C.F., 2013. Development of the Chesapeake Bay watershed total maximum daily load allocation. Journal of the American Water Resources Association 49, 986–1006. https://doi.org/10.1111/jawr.12105

Mallin, M.A., McIver, M.R., Robuck, A.R., Dickens, A.K., 2015. Industrial Swine and Poultry Production Causes Chronic Nutrient and Fecal Microbial Stream Pollution. Water, Air, and Soil Pollution 226. https://doi.org/10.1007/s11270-015-2669-y

Moran, M.A., Sheldon, W.M., Zepp, R.G., 2000. Carbon loss and optical property changes during long-term photochemical and biological degradation of estuarine dissolved organic matter. Limnology and Oceanography 45, 1254–1264. https://doi.org/10.4319/lo.2000.45.6.1254

Murphy, K.R., Stedmon, C.A., Graeber, D., Bro, R., 2013. Decomposition routines for Excitation Emission Matrices. Analytical Methods 5(23), 1–29. https://doi.org/10.1039/c3ay41160e.drEEM

Murphy, K.R., Bro, R., Stedmon, C.A., 2014. Chemometric Analysis of Organic Matter Fluorescence Chemometric Analysis of Organic Matter Fluorescence, in: Aquatic Organic Matter Fluorescence. p. 339. https://doi.org/10.13140/2.1.2595.8080

Nieto-Cid, M., Álvarez-Salgado, X. A., Pérez, F.F., 2006. Microbial and photochemical reactivity of fluorescent dissolved organic matter in a coastal upwelling system. Limnology and Oceanography 51, 1391–1400. https://doi.org/10.4319/lo.2006.51.3.1391

Nixon, S.W., Oviatt, C.A., Frithsen, J., Sullivan, B., 1986. Nutrients and the productivity of estuarine and coastal marine ecosystems. Journal of the Limnological Society of South Africa 12, 43–71.

Osburn, C.L., Del Vecchio, R., Boyd, T.J., 2014. Physiochemical effects on dissolved organic matter fluorescence in natural waters, in: Aquatic Organic Matter Fluorescence. pp. 233–277.

Osburn, C.L., Handsel, L.T., Mikan, M.P., Paerl, H.W., Montgomery, M.T., 2012. Fluorescence tracking of dissolved and particulate organic matter quality in a river-dominated estuary. Environmental Science & Technology 46, 8628–8636. https://doi.org/10.1021/es3007723

Osburn, C.L., Handsel, L.T., Peierls, B.L., Paerl, H.W., 2016. Predicting Sources of Dissolved Organic Nitrogen to an Estuary from an Agro-Urban Coastal Watershed. Environmental Science & Technology 50, 8473–8484. https://doi.org/10.1021/acs.est.6b00053

Osburn, C.L., Morris, D.P., Thorn, K.A., Moeller, R.E., 2001. Chemical and optical changes in freshwater dissolved organic matter exposed to solar radiation. Biogeochemistry 54, 251–278. https://doi.org/10.1023/A:1010657428418

Osburn, C.L., Wigdahl, C.R., Fritz, S.C., Saros, J.E., 2011. Dissolved organic matter composition and photoreactivity in prairie lakes of the U.S. Great Plains. Limnology and Oceanography 56, 2371–2390. https://doi.org/10.4319/lo.2011.56.6.2371

Paerl, H., Pinckney, J., Fear, J., Peierls, B., 1998. Ecosystem responses to internal and watershed organic matter loading: consequences for hypoxia in the eutrophying Neuse River Estuary, North Carolina, USA. Marine Ecology Progress Series 166, 17–25. https://doi.org/10.3354/meps166017

Paerl, H.W., Hall, N.S., Peierls, B.L., Rossignol, K.L., Joyner, A.R., 2013. Hydrologic Variability and Its Control of Phytoplankton Community Structure and Function in Two Shallow, Coastal, Lagoonal Ecosystems: The Neuse and New River Estuaries, North Carolina, USA. Estuaries and Coasts 37, 31–45. https://doi.org/10.1007/s12237-013-9686-0

Paerl, H.W., Mallin, M.A., Donahue, C.A., Go, M., Peierls, B.L., 1995. Nitrogen loading sources and eutrophication of the Neuse River Estuary, North Carolina: Direct and indirect roles of atmospheric deposition. Report submitted to NC Sea Grant. Report no. 291. Raleigh, NC.

Paerl, H.W., Peierls, B.L., 2014. Bioavailability and Fate of Organic Nitrogen Loading To Neuse River. Report submitted to NC WRRI. Report no. 440. Raleigh, NC.

Paerl, H.W., Piehler, M.F., 2008. Nitrogen and Marine Eutrophication, in: Nitrogen in the Marine Environment. Elsevier. pp. 521-559. https://doi.org/10.1016/B978-0-12-372522-6.00011-6

Paerl, H.W., Rossignol, K.L., Hall, S.N., Peierls, B.L., Wetz, M.S., 2010. Phytoplankton community indicators of short- and long-term ecological change in the anthropogenically and climatically impacted Neuse River Estuary, North Carolina, USA. Estuaries and Coasts 33, 485–497. https://doi.org/10.1007/s12237-009-9137-0

Paerl, H.W., Valdes, L.M., Joyner, A.R., Piehler, M.F., Lebo, M.E., 2004. Solving problems resulting from solutions: Evolution of a dual nutrient management strategy for the eutrophying Neuse River Estuary, North Carolina. Environmental Science & Technology 38, 3068–3073. https://doi.org/10.1021/es0352350

Peierls, B.L., Christian, R.R., Paerl, H.W., 2003. Water Quality and Phytoplankton as Indicators of Hurricane Impacts on a Large Estuarine Ecosystem. Estuaries 26, 1329–1343. https://doi.org/10.1007/BF02803635

Peierls, B.L., Hall, N.S., Paerl, H.W., 2012. Non-monotonic Responses of Phytoplankton Biomass Accumulation to Hydrologic Variability: A Comparison of Two Coastal Plain North Carolina Estuaries. Estuaries and Coasts 1–17. https://doi.org/10.1007/s12237-012-9547-2

Peierls, B.L., Paerl, H.W., 2010. Temperature, organic matter, and the control of bacterioplankton in the Neuse River and Pamlico Sound estuarine system. Aquatic Microbial Ecology 60, 139–149. https://doi.org/10.3354/ame1415

Pellerin, B.A., Kaushal, S.S., McDowell, W.H., 2006. Does Anthropogenic Nitrogen Enrichment Increase Organic Nitrogen Concentrations in Runoff from Forested and Human-dominated Watersheds? Ecosystems 9, 852–864. https://doi.org/10.1007/s10021-006-0076-3

Rothenberger, M.B., Burkholder, J.M., Brownie, C., 2009. Long-Term Effects of Changing Land Use Practices on Surface Water Quality in a Coastal River and Lagoonal Estuary. Environmental Management 44, 505–523. https://doi.org/10.1007/s00267-009-9330-8

Rudek, J., Paerl, H.W., Mallin, M.A., Bates, P.W., 1991. Seasonal and hydrological control of phytoplankton nutrient limitation in the lower Neuse River Estuary, North Carolina. Marine Ecology Progress Series 75, 133–142. https://doi.org/10.3354/meps075133

See, J.H., Bronk, D. A., Lewitus, A.J., 2006. Uptake of Spartina-derived humic nitrogen by estuarine phytoplankton in nonaxenic and axenic culture. Limnology and Oceanography 51, 2290–2299. https://doi.org/10.4319/lo.2006.51.5.2290

Stedmon, C. A., Bro, R., 2008. Characterizing dissolved organic matter fluorescence with parallel factor analysis: a tutorial. Limnology and Oceanography Methods 6, 572–579. https://doi.org/10.4319/lom.2008.6.572

Stedmon, C. A., Markager, S., 2005. Tracing the production and degradation of autochthonous fractions of dissolved organic matter using fluorescence analysis. Limnology and Oceanography 50, 1415–1426. https://doi.org/10.4319/lo.2005.50.5.1415

Stedmon, C., Markager, S., Søndergaard, M., 2006. Dissolved organic matter (DOM) export to a temperate estuary: seasonal variations and implications of land use. Estuaries and Coasts 29, 388–400.

Stow, C., Borsuk, M.E., Stanley, D.W., 2001. Long-term Changes in Watershed Nutrient inputs and Riverine Exports in the Neuse River, North Carolina. Water Research 35, 1489–1499.

Stubbins, A., Lapierre, J.F., Berggren, M., Prairie, Y.T., Dittmar, T., Del Giorgio, P.A., 2014. What's in an EEM? Molecular signatures associated with dissolved organic fluorescence in boreal Canada. Environmental Science & Technology 48, 10598–10606. https://doi.org/10.1021/es502086e

Thorne, P.S., 2007. Environmental health impacts of concentrated animal feeding operations: anticipating hazards--searching for solutions. Environmental Health Perspectives 115, 296–7. https://doi.org/10.1289/ehp.8831

CHAPTER 6: CONCLUSIONS

Organic matter (OM) in aquatic ecosystems controls several key processes, including light availability (Osburn et al., 2009), the complexation and transport of metals and anthropogenic pollutants (Bergamaschi et al., 2012; Ripszam et al., 2015), as a carbon (C) source to support microbial respiration (Moran et al., 2000), and as a macronutrient source, as either nitrogen (N) or phosphorus (P) to support primary production (Boyer et al., 2006; Bronk et al., 2007). Measuring the quality of OM in aquatic ecosystems receiving both allochthonous and autochthonous OM, each of which contain diverse OM molecules is difficult, time consuming, and often expensive. Techniques to measure the quality of OM either rely on the identification of specific, known OM molecules or are based on bulk techniques which only offer a snapshot of the broader OM pool. Each of these techniques makes assumptions about the type of OM measured and are often biased towards certain types of OM based on the extraction and detection methods used (Minor et al., 2014).

For my dissertation research, I relied on optics to understand the quality of the bulk OM pool, using both absorbance (i.e., colored dissolved OM, CDOM) and fluorescence, measured as excitation emission matrices (EEMs) to identify and track broad classes of OM. These techniques are relatively quick, sensitive, and broad, allowing for a snapshot of the quality of the bulk OM pool in a relatively short amount of time. Because of these characteristics, EEMs are an efficient method for understanding the quality of the OM pool on both temporal and spatial scales necessary to fully constrain the OM pool in seasonally and spatially dynamic ecosystems such as estuaries. While originally developed for the analysis of fluorescent dissolved OM

(FDOM), the EEMs technique has more recently been applied to the particulate OM (POM) pool by analyzing fluorescence signatures from base extracted fluorescent POM (BEFPOM), allowing for the simultaneous analysis of both the fluorescent DOM and POM pools.

The EEM technique, as applied to the FDOM and BEFPOM pools, is capable of capturing signatures of both humic-like, allochthonous fluorescent OM (FOM) and autochthonous FOM, making the technique particularly well-suited for application in estuaries where there are mixed sources of FOM. Results from its application in this study suggest the EEM technique, as applied to BEFPOM samples, is capable of identifying and tracking both allochthonous and autochthonous FOM sources in the NRE. The FDOM pool, however is largely composed of humic-like allochthonous sources of FOM, making it exceedingly difficult to identify autochthonous signals in this pool. This suggests the EEM technique, as applied to estuarine ecosystems, is mainly constrained to understanding the dynamics of the allochthonous FDOM pool and is likely not well-suited for analyzing the autochthonous FDOM pool *in situ*. It is possible, however, to identify autochthonously-produced fluorescent components in the FDOM pool under experimental conditions. Therefore, while autochthonous signatures of FDOM are produced in the estuary under experimental conditions, *in situ* they are not produced in concentrations large enough to identify them above the allochthonous OM pool contained in the estuary.

In Chapter 2, I applied the statistical decomposition technique, parallel factor analysis (PARAFAC), to sets of samples collected from the NRE (i.e., FDOM samples, BEFPOM samples, and FDOM+BEFPOM samples) in order to better characterize the quality of FOM in these two pools. Results from this chapter indicate the FDOM pool is almost entirely dominated by allochthonous FDOM, while the BEFPOM pool is a combination of both humic-like

BEFPOM derived from terrestrial sources as well as protein-like BEFPOM produced *in situ* by phytoplankton and microbial assemblages. When the FDOM and BEFPOM pools were modeled together, PARAFAC was able to identify biologically reactive FOM components in the FDOM pool which, when plotted against salinity, resembled patterns of *in situ* production. These results indicate autochthonous FDOM is produced and can be tracked in the estuary, however, the EEM-PARAFAC technique is not able to resolve these components when only the FDOM pool is modeled.

The second part of chapter 2 used bioassays to isolate an FDOM signal that was produced within the estuary and could be incorporated into an existing Neuse River (NR) source-based, watershed PARAFAC model (FluorMod) (Osburn et al., 2016) to track the sources and fates of watershed FDOM in the estuary. While a unique FDOM signal was identified in the bioassays, this signal was not consistently identifiable in the estuary, except under extreme phytoplankton bloom conditions (Chl *a* > 450 μg L^{-1}). Because autochthonously-produced sources of FDOM were not accurately captured in the NRE, the application of a watershed source based PARAFAC model is not applicable to the NRE.

In chapter 3, I continued to assess the differences between the FDOM and FPOM pools in the NRE by using multivariate statistical analyses to relate FDOM and FPOM dynamics to environmental parameters. Results from Chapter 3 corroborated results from Chapter 2. Specifically, the FDOM pool was almost entirely dominated by terrestrial, humic-like OM that was closely associated with fresh, riverine water. For the FPOM pool, the upper estuary was characterized by more terrestrial, humic-like FPOM associated with the riverine end-member while in the lower estuary, the source of FPOM was mainly autochthonous OM produced by phytoplankton and associated microbial assemblages. Results from this chapter also conclude

that fluorescence indices derived from EEM measurements can be used across the FDOM and FPOM pools to explain allochthonous versus autochthonous FOM.

Chapter 4 focused on how the quantity and quality of the dissolved organic carbon (DOC) pool is affected by riverine discharge, including following an extreme flood event; using a non-steady state box model approach. The hydrodynamic conditions of the estuary, as flow into and out of the estuary at the marine end-member, were no particularly well resolved with this box model approach, indicating the current temporal and spatial resolution of the estuarine monitoring program and the developed non-steady state box model were likely not sufficient at capturing rapidly changing conditions in the estuary (i.e., river discharge, wind conditions). This resulted in high uncertainty in the calculated OM source and sink terms. Results from this chapter indicate extreme discharge events may result in up to a 400% increase in the amount of DOC exported from the NRE following an extreme riverine discharge event (99^{th} flow quantile) as compared to baseline conditions. This has important implications for the role estuaries play as a conduit between the terrestrial and coastal end members following extreme weather events, which is especially important in light of predictions of the increasing frequency of extreme weather events due to climate change (Bender et al., 2009; Janssen et al., 2016).

In the final chapter, I assess the importance of various watershed-based dissolved organic nitrogen (DON) sources on phytoplankton biomass and primary production in the NRE (Hounshell et al., 2017). Broadly, watershed DON sources (i.e., wastewater treatment plant effluent, turkey litter leachate, concentrated river DON) were not considered important sources of N to estuarine phytoplankton and microbial assemblages; at least not during the bioassay period (~7 days). However, results did indicate DON contained in chicken litter leachate was capable of stimulating phytoplankton growth in excess of that stimulated by dissolved inorganic

nutrients (DIN) inherently contained in this source. This suggests that certain watershed DON sources should be managed in order to limit impacts of eutrophicaton in estuarine ecosystems, but that, broadly, watershed DON sources are not an important source of N to estuarine phytoplankton communities, at least not over times frames of days to weeks.

Overall, using bulk OM measurements to measure the quantity of OM as well as absorbance and fluorescence measurements to understand the quality of OM in the NRE suggest this estuary is largely dominated by terrestrial, humic-like FDOM. Specifically, the DOM pool is an order of magnitude greater than the POM pool (Chapter 3), and of the DOM pool, the vast majority of FDOM is considered terrestrial, humic-like DOM (Chapter 2 and 3). Murphy et al., (2018) suggests the EEM-PARAFAC techinque may be reaching a point at which ubiquitous, humic-like fluorescence signatures can be identified in nearly all aquatic environments. If this is the case, the authors suggest it would be possible to subtract these ubiquitous, humic-like signals from measured EEMs, allowing for the identification of potentially underlying, less intense autochthonous fluorescent signals to be more easily identified and tracked *in situ*. This approach could be applicable to the NRE and allow for the identification of more autochthonous signals in the FDOM pool.

While this research has helped expand our knowledge of OM in estuarine environments, there are still many more avenues to explore. As such, I'd like to offer a few future research directions that have resulted from this study. Namely, as discussed above, the identification of a global reference signal for humic-like FDOM in estuaries will greatly improve our ability to identify and capture underlying signals of fluorescent variability, as mediated by biological production, degradation, and transformation, of FDOM *in situ* by subtracting the hypothesized 'global reference' from collected EEMs (Murphy et al., 2018). This will greatly improve the utility of

the EEM-PARAFAC technique to capture potential production and degradation mechanisms of FDOM *in situ*. Additional studies should also focus on linking transformation and degradation processes between the DOM and POM pools. References in the literature are rare (Canuel and Hardison, 2016; McCallister et al., 2006; Raymond and Bauer, 2001) and results from this study suggest it is difficult to assess the dynamics between these two pools with broad fluorescent measurements, suggesting more detailed and focused analyses are needed. Finally, additional research is needed on the role extreme weather events (i.e., extreme riverine discharge events) may play on DOC processing and export in estuarine systems. This includes identifying a riverine discharge threshold at which the estuary switches from a processer of riverine DOC to a pipeline for the direct export of riverine DOC to the coastal end member. Additional bioassays are being conducted using a diverse set of DON watershed sources to further test the availability of watershed DON to phytoplankton and microbial assemblages in the NRE. These additional experiments will help further establish if DON is an important factor in leading to continued Chl *a* exceedances in the NRE and other eutrophic estuaries.

REFERENCES

Bender, M.A., Knutson, T.R., Tuleya, R.E., Sirutis, J.J., Vecchi, G.A., Garner, S.T., Held, I.M., 2009. Modeled Impact of Anthropogenic Atlantic Hurricanes. Science 327, 454–458.

Bergamaschi, B.A., Krabbenhoft, D.P., Aiken, G.R., Patino, E., Rumbold, D.G., Orem, W.H., 2012. Tidally Driven Export of Dissolved Organic Carbon, Total Mercury, and Methylmercury from a Mangrove-Dominated Estuary. Environmental Science & Technology 46, 1371-1378. https://doi.org/10.1021/es2029137

Boyer, J.N., Dailey, S.K., Gibson, P.J., Rogers, M.T., Mir-Gonzalez, D., 2006. The role of dissolved organic matter bioavailability in promoting phytoplankton blooms in Florida Bay. Hydrobiologia 569, 71–85. https://doi.org/10.1007/s10750-006-0123-2

Bronk, D.A., See, J.H., Bradley, P., Killberg, L., 2007. DON as a source of bioavailable nitrogen for phytoplankton. Biogeosciences 4, 283–296.

Canuel, E.A., Hardison, A.K., 2016. Sources, Ages, and Alteration of Organic Matter in Estuaries. Annual Review of Marine Science 8, 409–434. https://doi.org/10.1146/annurev-marine-122414-034058

Hounshell, A.G., Peierls, B.L., Osburn, C.L., Paerl, H.W., 2017. Stimulation of phytoplankton production by anthropogenic dissolved organic nitrogen in a coastal plain estuary. Environmental Science & Technology 51, 13104-13112. https://doi.org/10.1021/acs.est.7b03538

Janssen, E., Sriver, R.L., Wuebbles, D.J., Kunkel, K.E., 2016. Seasonal and regional variations in extreme precipitation event frequency using CMIP5. Geophysical Research Letters 43, 5385–5393. https://doi.org/10.1002/2016GL069151

McCallister, S.L., Bauer, J.E., Ducklow, H.W., Canuel, E.A., 2006. Sources of estuarine dissolved and particulate organic matter: A multi-tracer approach. Organic Geochemistry 37, 454–468. https://doi.org/10.1016/j.orggeochem.2005.12.005

Minor, E.C., Swinson, M.M., Mattson, B.M., Oyler, A.L. 2014. Structural characterization of dissolved organic matter: a review of current techniques for isolation and analysis. Environmental Sciences: Processes & Impacts 9, 2064-2079. https://doi.org/10.1039/C4EM00062E

Moran, M.A., Sheldon, W.M., Zepp, R.G., 2000. Carbon loss and optical property changes during long-term photochemical and biological degradation of estuarine dissolved organic matter. Limnology and Oceanography 45, 1254–1264.

Murphy, K.R., Timko, S.A., Gonsior, M., Powers, L.C., Wünsch, U.J., Stedmon, C.A., 2018. Photochemistry Illuminates Ubiquitous Organic Matter Fluorescence Spectra. Environmental Science & Technology 52, 11243–11250. https://doi.org/10.1021/acs.est.8b02648

Osburn, C.L., Rudolph, J.C., Paerl, H.W., Hounshell, A.G., Van Dam, B.R., 2019. Lingering carbon cycle effects of Hurricane Matthew in North Carolina's coastal waters. Geophysical Research Letters. https://doi.org/10.1029/2019GL082014

Osburn, C.L., Handsel, L.T., Peierls, B.L., Paerl, H.W., 2016. Predicting Sources of Dissolved Organic Nitrogen to an Estuary from an Agro-Urban Coastal Watershed. Environmental Science & Technology 50(16), 8473-8484. https://doi.org/10.1021/acs.est.6b00053

Osburn, C.L., O'Sullivan, D.W., Boyd, T.J., 2009. Increases in the longwave photobleaching of chromophoric dissolved organic matter in coastal waters. Limnology and Oceanography 54, 145–159. https://doi.org/10.4319/lo.2009.54.1.0145

Raymond, P.A., Bauer, J.E., 2001. Use of ^{14}C and ^{13}C natural abundances for evaluating riverine, estuarine, and coastal DOC and POC sources and cycling: A review and synthesis. Organic Geochemistry 32, 469–485. https://doi.org/10.1016/S0146-6380(00)00190-X

Ripszam, M., Paczkowska, J., Veenaas, C., Haglund, P., 2015. Dissolved Organic Carbon Quality and Sorption of Organic Pollutants in the Baltic Sea in Light of Future Climate Change. Environmental Science & Technology 49, 1445-1452. https://doi.org/10.1021/es504437s

APPENDIX 2: CHAPTER 2 SUPPLEMENTARY INFORMATION

Appendix 2.1 Environmental Parameters

In addition to fluorescent dissolved organic matter (FDOM) and base extracted fluorescent particulate organic matter (BEFPOM) analyses, I also conducted analyses for various environmental parameters (dissovled organic carbon, DOC; dissolved organic nitrogen, DON; Chlorophyll-*a*, Chl *a*; particulate organic carbon, POC; particulate nitrogen, PN), as described in Chapter 2. The various environemental parameters were plotted against salininty in order to assess whether the parameters followed conservative or non-conservative mixing in the estuary (Figure A2.1, Table A2.1). Markager et al., (2011) defined conservative mixing as parameters having 1. a statistically significant p-value ($p < 0.05$) and 2. $r^2 > 0.1$.

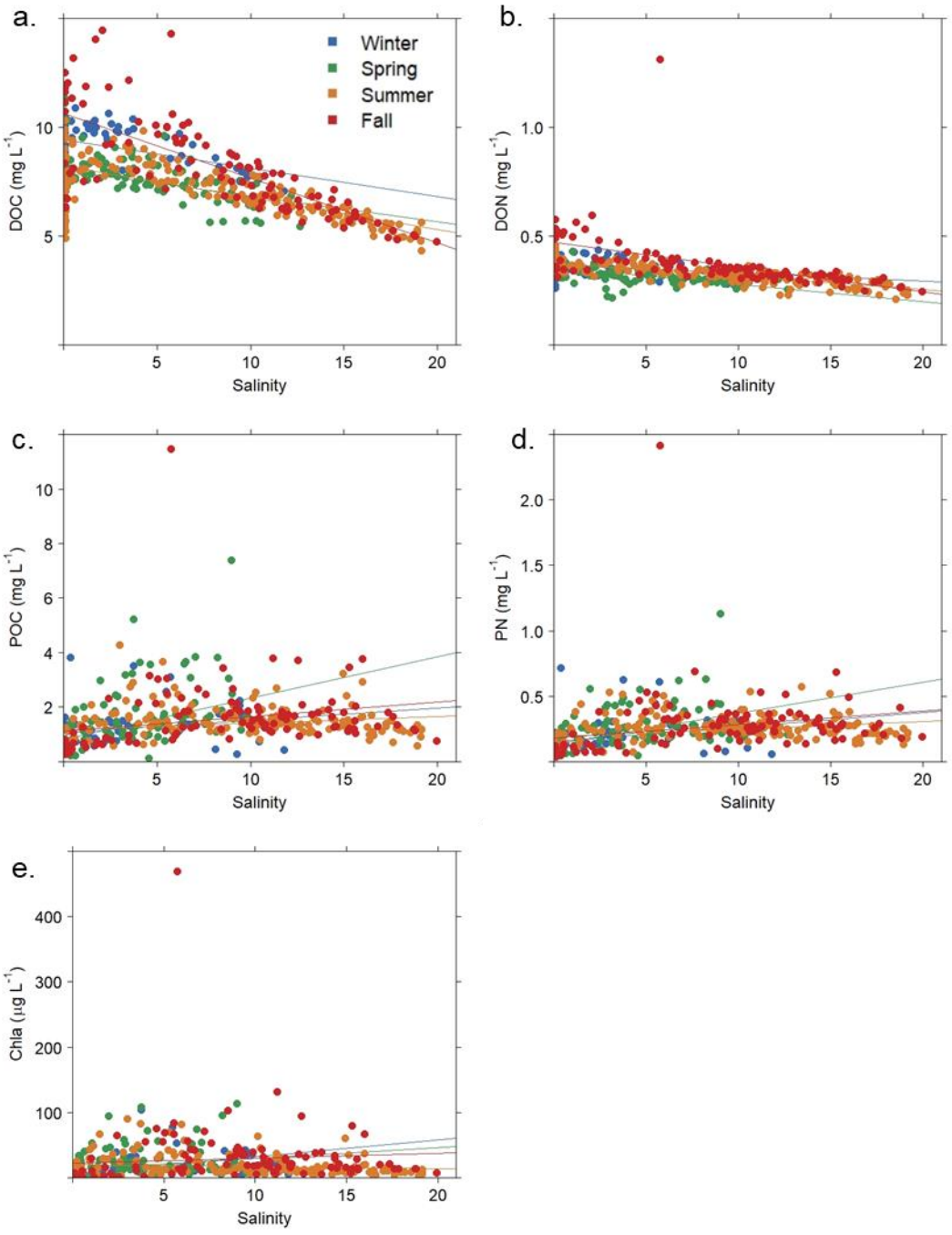

Figure A2.1. Various environmental parameters (DOC, DON, POC, PN, and Chl *a*) plotted versus salinity for each season. Linear regression lines are plotted. Linear regression equations are listed in Table A2.1.

Table A2.1. Linear regression equations, r^2, and p-values for various environmental parameters (DOC, DON, POC, PN, and Chl *a*) versus salinity for each season (winter, spring, summer, fall). Statistically significant relationships ($p < 0.05$) are highlighted in dark grey. Statistically significant relationships with an $r^2 > 0.1$ are highlighted in light grey.

	Linear regression equation	r^2	p-value
DOC			
Winter	y = -0.13x + 9.4	0.23	p < 0.001
Spring	y = -0.12x + 8.0	0.22	p < 0.001
Summer	y = -0.15x + 8.2	0.49	p < 0.001
Fall	y = -0.30x + 10.6	0.55	p < 0.001
DON			
Winter	y = -0.00x + 0.37	0.11	p = 0.05
Spring	y = -0.01x + 0.36	0.38	p < 0.001
Summer	y = -0.01x + 0.38	0.62	p < 0.001
Fall	y = -0.01x + 0.47	0.29	p < 0.001
POC			
Winter	y = 0.05x + 1.1	0.06	p = 0.14
Spring	y = 0.15x + 0.8	0.25	p < 0.001
Summer	y = 0.02x + 1.2	0.05	p = 0.03
Fall	y = 0.05x + 1.1	0.06	p < 0.001
PN			
Winter	y = 0.01x + 0.15	0.09	p = 0.05
Spring	y = 0.02x + 0.13	0.28	p < 0.001
Summer	y = 0.01x + 0.19	0.10	p = 0.004
Fall	y = 0.01x + 0.18	0.06	p < 0.001
Chl-*a*			
Winter	y = 2.6x + 6.6	0.23	p = 0.01
Spring	y = 1.7x + 13.0	0.07	p = 0.02
Summer	y = -0.3x + 19.6	0.01	p = 0.40
Fall	y = 0.7x + 22.4	0.01	p = 0.13

Appendix 2.2. FDOM Model:

A 3-component PARAFAC model was identified from FDOM samples collected as part of this study. Split half validation results for the developed model are plotted (Figure A2.2).

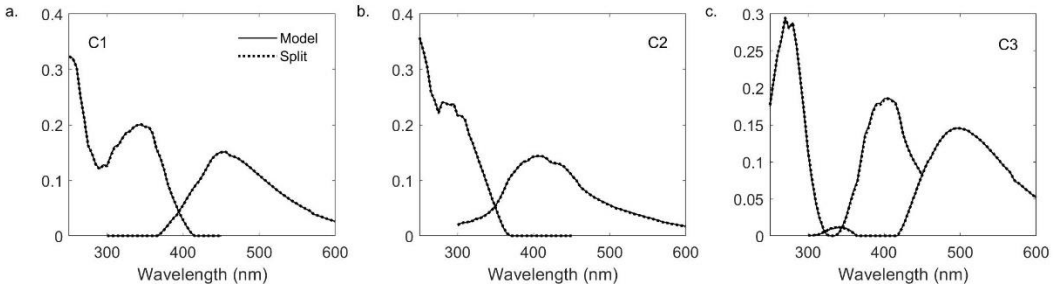

Figure A2.2. Excitation and emission loadings for each of the three identified FDOM components (black line), including split half validation results (dashed line).

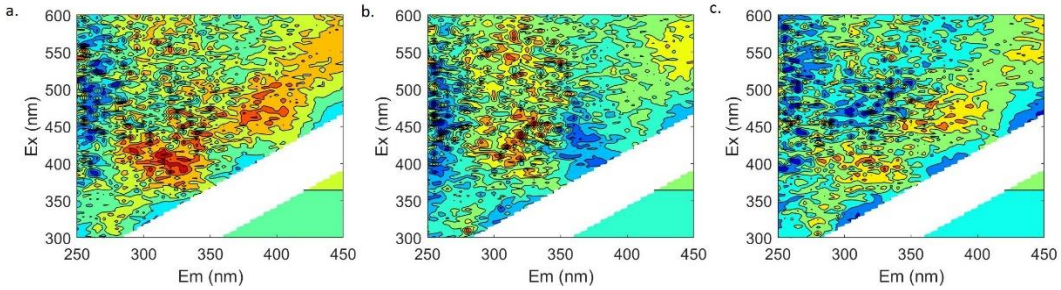

Figure A2.3. Examples of residuals from FDOM samples after application of the 3-component FDOM model.

To verify that all fluorescence variability from the FDOM samples were captured by the 3-component PARAFAC model, the FDOM residual samples were evaluated (Figure A2.3). Sample residuals were low and randomly distributed across all samples, with little evidence of systematic residuals. I attempted to fit a PARAFAC model to the residual samples; however, no model was selected or validated based on the structure of the modeled components. Therefore, I am confident that the original 3-component PARAFAC model developed on the FDOM samples was sufficient at capturing all fluorescence variability in the original FDOM samples.

To assess how the 3 identified components relate to other environmental parameters collected (DOC, DON) each component was plotted against DOC and DON, respectively (Figure A2.4, Table A2.2). The 3 components were also plotted against salinity to assess conservative vs. non-conservative mixing patterns (Figure A2.5, Table A2.3).

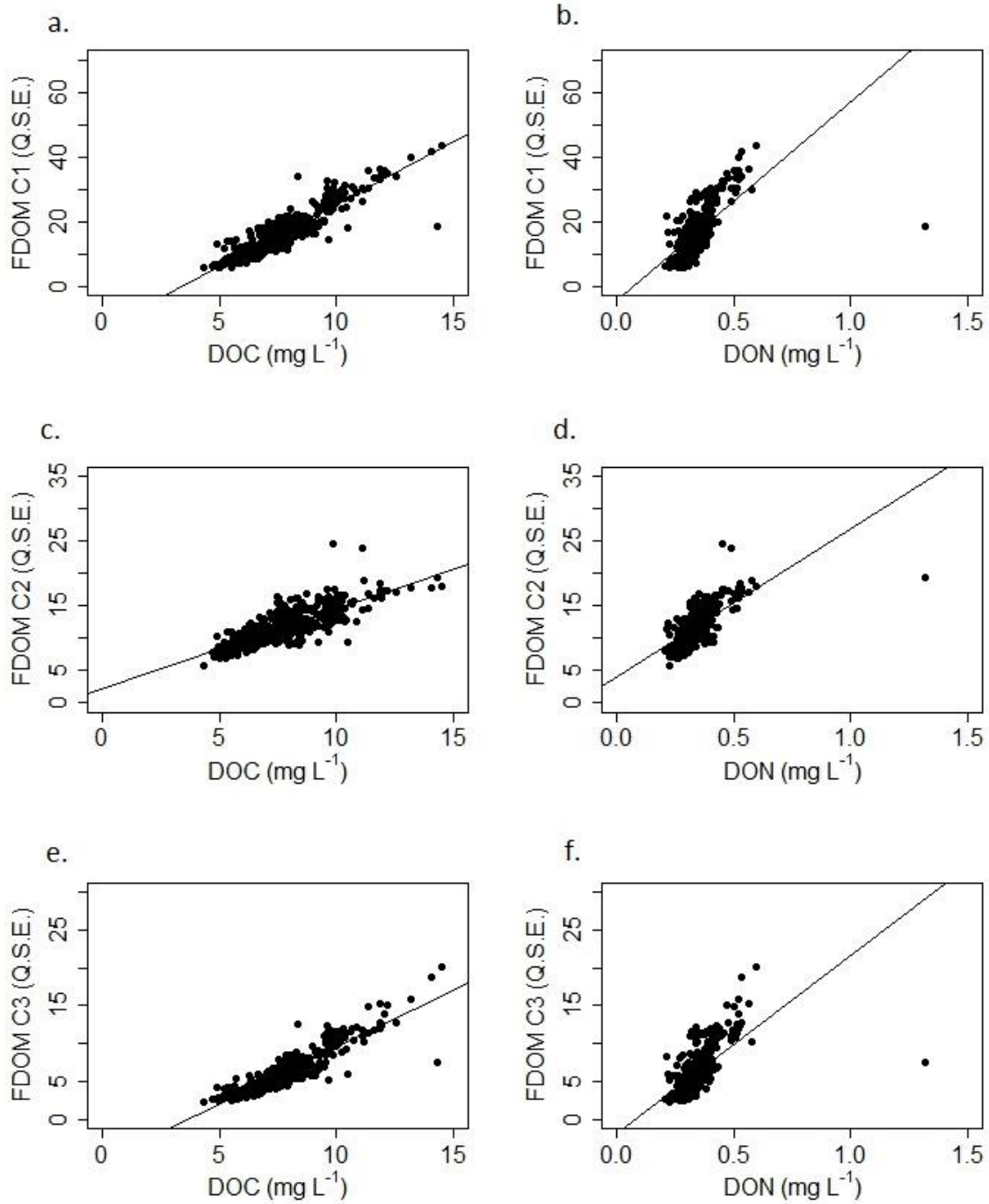

Figure A2.4. Plots of the three components identified in the FDOM model plotted against various environmental parameters. Linear regression lines are plotted. Linear regression equations, r^2, and p-values are listed in Table A2.2.

Table A2.2. Linear regression equations, r^2, and p-values for linear relationships between FDOM components and various environmental parameters (DOC, DON). Statistically significant relationships are highlighted in dark grey.

	Linear regression equation	r^2	p-value
FDOM C1			
DOC	y = 3.9x – 13.2	0.83	p < 0.001
DON	y = 61.5x – 4.3	0.43	p < 0.001
FDOM C2			
DOC	y = 1.2x + 2.3	0.62	p < 0.001
DON	y = 22.9x + 3.9	0.44	p < 0.001
FDOM C3			
DOC	y = 1.5x – 5.5	0.82	p < 0.001
DON	y = 23.6x – 1.9	0.41	p < 0.001

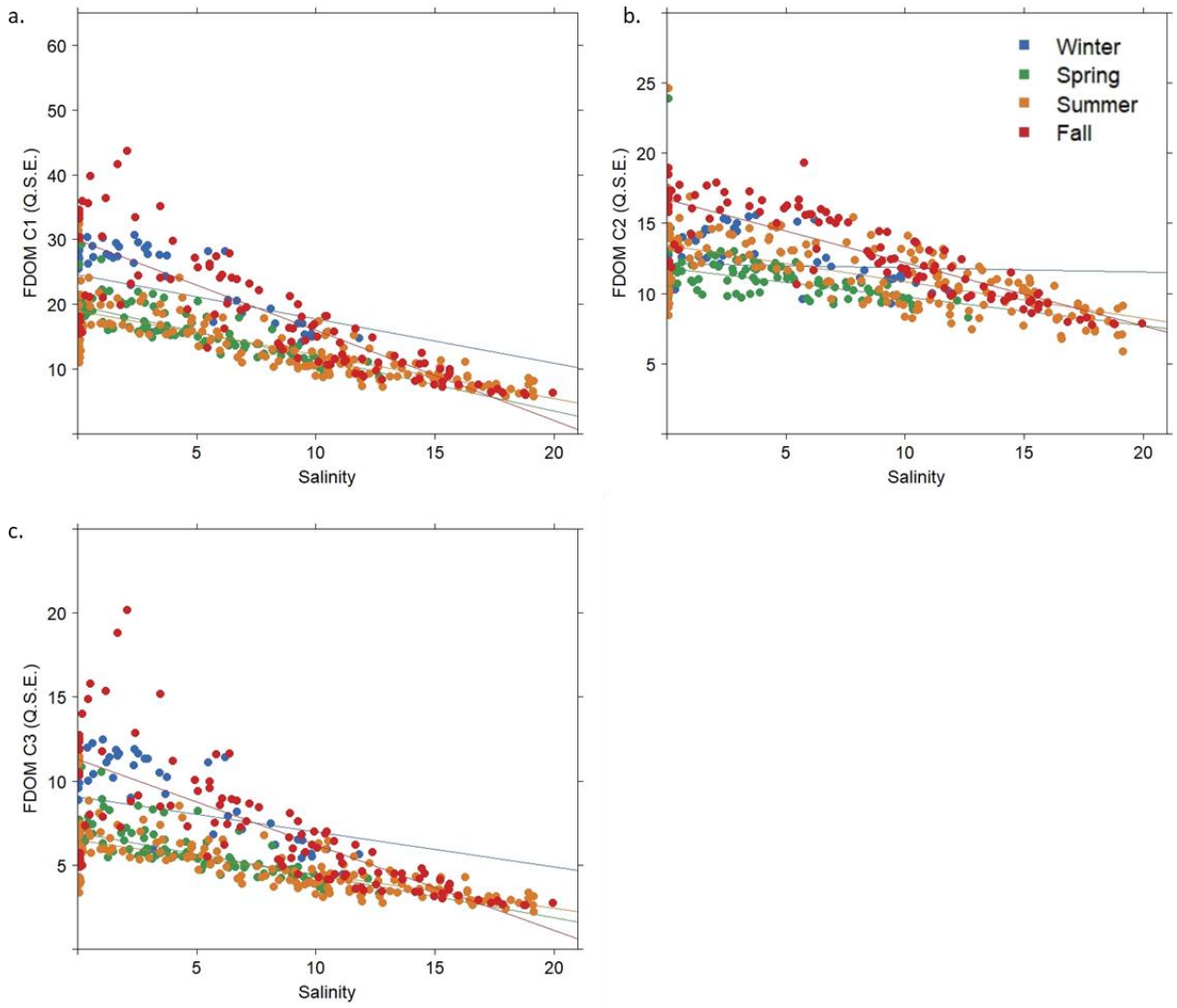

Figure A2.5. Each of the three PARAFAC components identified for the FDOM samples plotted against salinity. Samples are plotted by season with linear regression lines plotted for each season. Table A2.3 contains the associated linear regression equations, r^2, and p-values.

Table A2.3. Linear regression equations, r^2, and p-values for linear relationships calculated between FDOM components C1-C3 and salinity. Equations are displayed for each season. Statistically significant relationships ($p < 0.05$) with $r^2 > 0.1$ are highlighted in dark grey. Statistically significant relationships with $r^2 < 0.1$ are highlighted in light grey.

	Linear regression equation	r^2	p-value
FDOM C1			
Winter	y = -0.68x + 24.5	0.20	p < 0.001
Spring	y = -0.81x + 19.8	0.59	p < 0.001
Summer	y = -0.68x + 19.0	0.63	p < 0.001
Fall	y = -1.40x + 30.0	0.70	p < 0.001
FDOM C2			
Winter	y = 0.03x + 12.1	0.00	p = 0.67
Spring	y = -0.20x + 11.8	0.18	p < 0.001
Summer	y = -0.26x + 13.5	0.38	p < 0.001
Fall	y = -0.45x + 16.7	0.70	p < 0.001
FDOM C3			
Winter	y = -0.21x + 9.1	0.08	p = 0.01
Spring	y = -0.25x + 6.9	0.38	p < 0.001
Summer	y = -0.20x + 6.5	0.51	p < 0.001
Fall	y = -0.51x + 11.3	0.59	p < 0.001

Appendix 2.3. BEFPOM Model:

A 5-component PARAFAC model was identified when applied to the BEFPOM samples collected from the NRE. Split half validation results are plotted below (Figure A2.6).

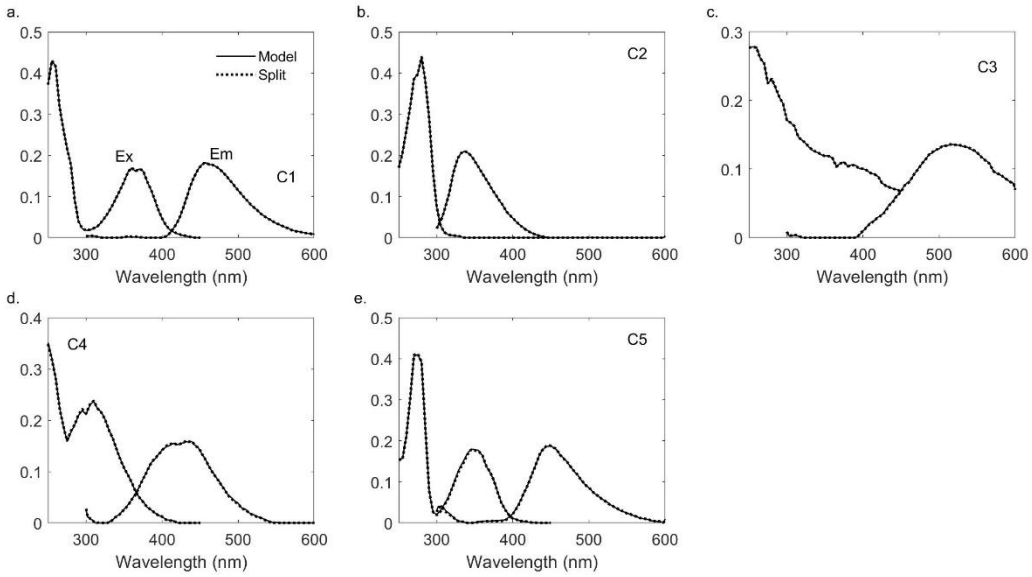

Figure A2.6. Excitation and emission loadings for the 5 components identified by the BEFPOM PARAFAC model (solid line). Split half validation results are also plotted (dashed line).

As described with the FDOM model above, residuals from the BEFPOM samples after the application of the 5-component BEFPOM model were also assessed. The BEFPOM residuals resulted in a 1-component model that appeared to capture some systematic variability in the residual samples at low emission wavelengths (< 300 nm) and excitation wavelengths (250-300 nm) (Figure A2.7). The model was not split half validated, but did match with two previously identified components on OpenFluor (> 0.90) (Table A2.4).

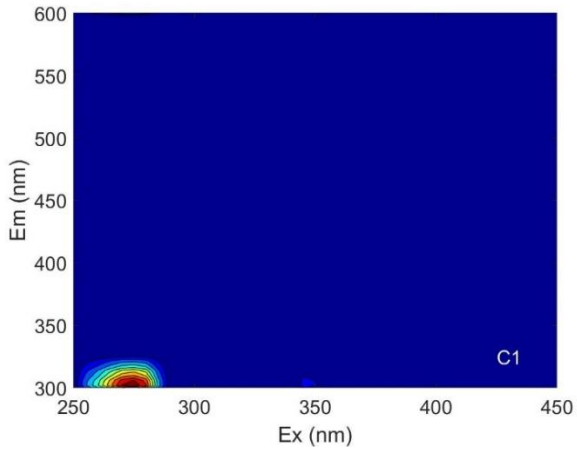

Figure A2.7. 1-component PARAFAC model identified from BEFPOM sample residuals after application of the 5-component BEFPOM model.

Table A2.4. Component identification for the 1-component PARAFAC model fitted to BEFPOM model residuals.

	Ex max. (nm)	**Em max. (nm)**	**OpenFluor Matches**	**Description**	**Reference**
C1	275	302	2	Protein-like, tyrosine	Murphy et al., 2006; Osburn et al., 2016

The 5-components identified in the BEFPOM PARAFAC model were plotted against salinity to assess the conservative vs. non-conservative behavior of these components in the estuary (Figure A2.8, Table A2.5). The 5 BEFPOM components were also plotted against various environmental parameters (Chl *a*, POC, PN) (Figure A2.9, Table A2.6).

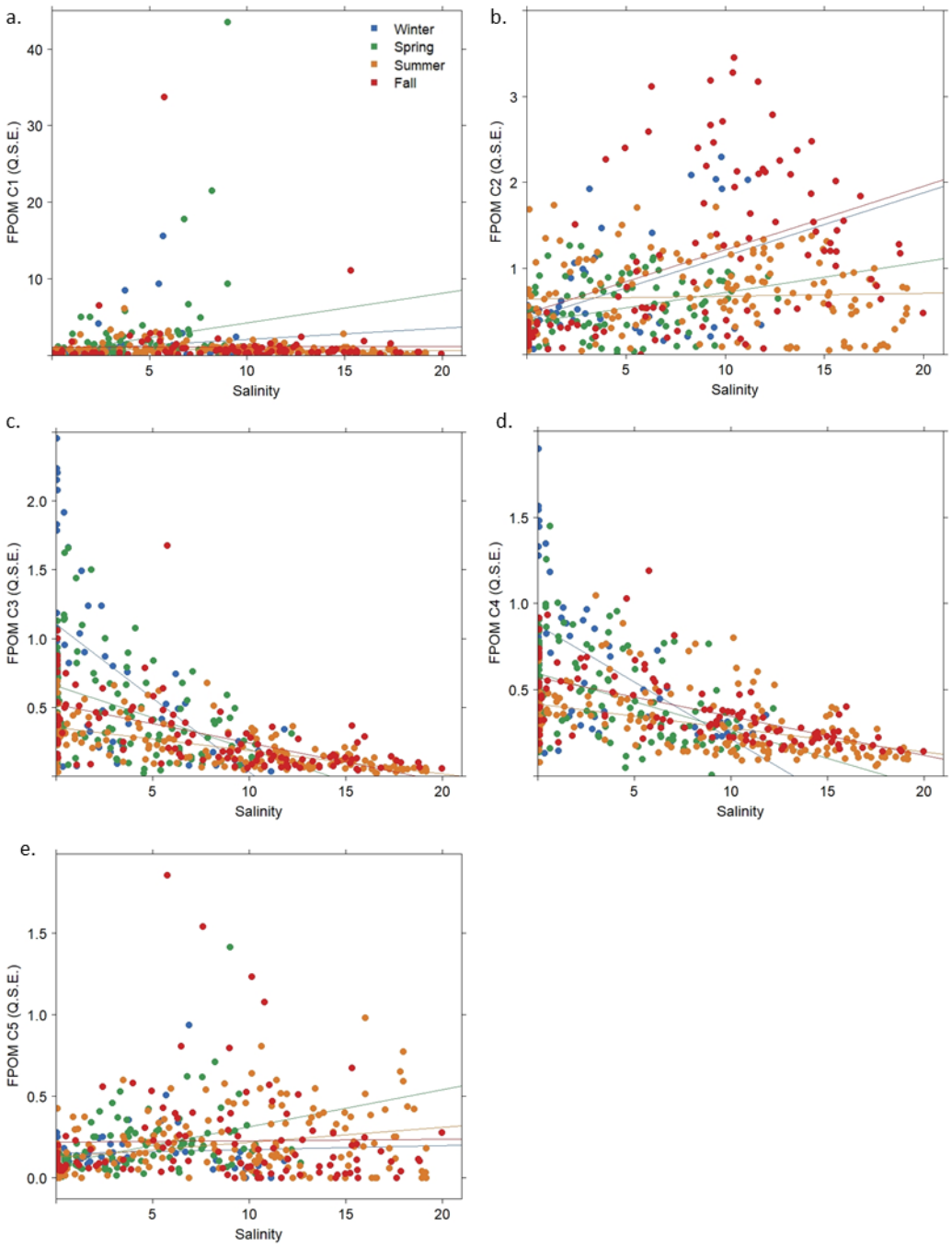

Figure A2.8. BEFPOM components C1-C5 plotted against salinity for all collected samples. Samples are plotted by season. Linear regression lines are plotted. Linear regression equations, r^2, and p-values are listed in Table A2.5.

Table A2.5. Linear regression equation, r^2, and p-values for BEFPOM components versus salinity separated by season. Statistically significant ($p < 0.05$) relationships with $r^2 > 0.1$ are highlighted in dark grey. Statistically significant relationships with $r^2 < 0.1$ are highlighted in light grey.

	Linear regression equation	r^2	p-value
BEFPOM C1			
Winter	y = 0.14x + 0.65	0.03	p = 0.11
Spring	y = 0.39x + 0.36	0.08	p = 0.001
Summer	y = -0.01x + 0.88	0.01	p = 0.16
Fall	y = 0.01x + 1.01	0.00	p = 0.92
BEFPOM C2			
Winter	y = 0.07x + 0.40	0.22	p < 0.001
Spring	y = 0.04x + 0.36	0.15	p = 0.001
Summer	y = 0.00x + 0.64	0.0	p = 0.52
Fall	y = 0.07x + 0.47	0.21	p < 0.001
BEFPOM C3			
Winter	y = -0.11x + 1.1	0.35	p < 0.001
Spring	y = -0.05x + 0.66	0.20	p < 0.001
Summer	y = -0.02x + 0.35	0.43	p < 0.001
Fall	y = -0.03x + 0.52	0.35	p < 0.001
BEFPOM C4			
Winter	y = -0.07x + 0.88	0.33	p < 0.001
Spring	y = -0.03x + 0.59	0.18	p < 0.001
Summer	y = -0.01x + 0.42	0.22	p < 0.001
Fall	y = -0.02x + 0.57	0.37	p < 0.001
BEFPOM C5			
Winter	y = 0.00x + 0.15	0.00	p = 0.63
Spring	y = 0.02x + 0.09	0.19	p < 0.001
Summer	y = 0.01x + 0.12	0.08	p < 0.001
Fall	y = 0.00x + 0.22	0.00	p = 0.86

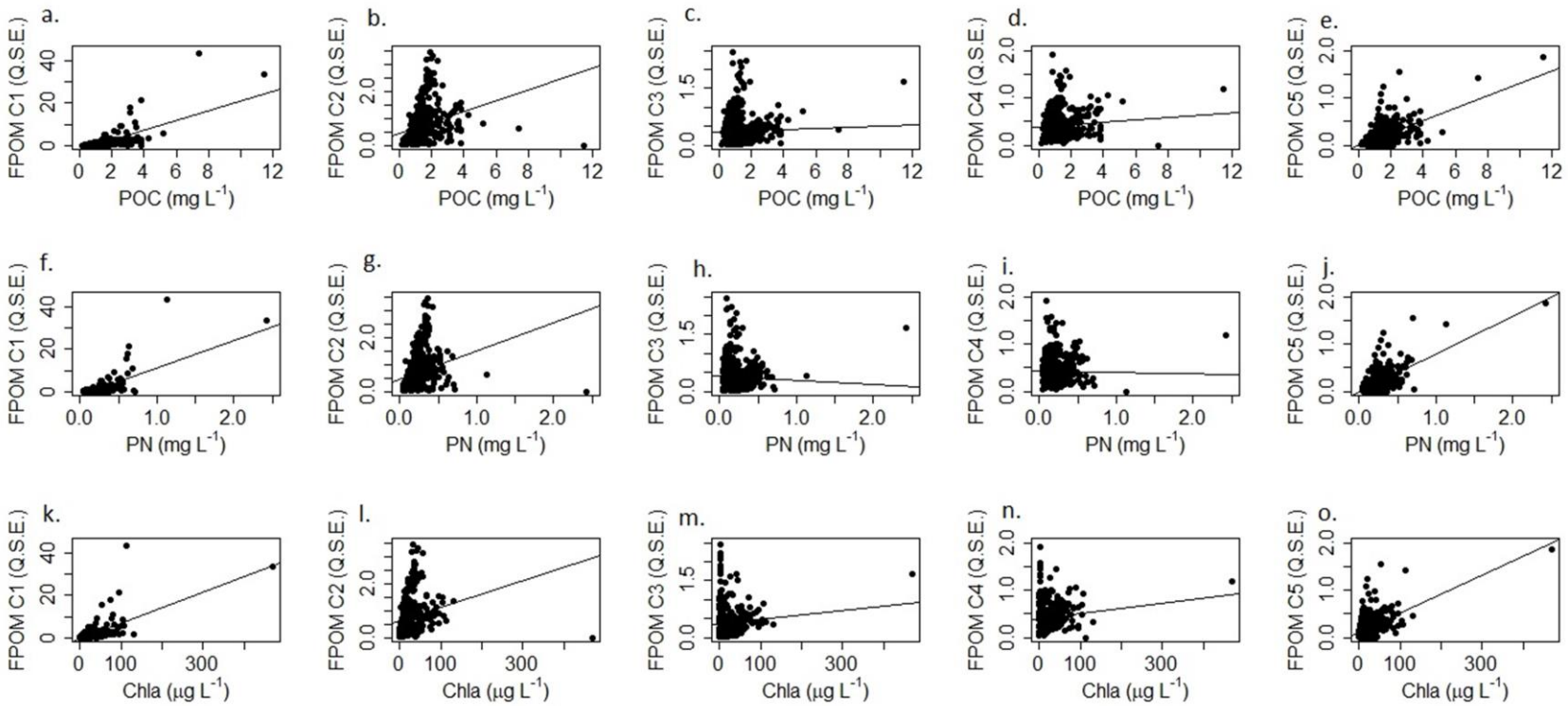

Figure A2.9. BEFPOM components C1-C5 plotted as a function of various environmental parameters (POC, PN, Chl *a*). Linear regression lines are plotted. Linear regression equations, r^2, and p-values are listed in Table A2.6.

Table A2.6. Linear regression equation, r^2, and p-values for linear relationships between BEFPOM components (C1-C5) and various environmental parameters (POC, PN, Chl *a*). Statistically significant relationships ($p < 0.05$) with $r^2 < 0.1$ are highlighted in light grey.

	Linear regression equation	r^2	p-value
BEFPOM C1			
POC	y = 2.3x - 2.0	0.49	p < 0.001
PN	y = 13.1x - 1.9	0.50	p < 0.001
Chl-*a*	y = 0.07x – 0.32	0.47	p < 0.001
BEFPOM C2			
POC	y = 0.20x + 0.43	0.09	p < 0.001
PN	y = 1.0x + 0.47	0.08	p < 0.001
Chl-*a*	y = 0.00x + 0.61	0.05	p < 0.001
BEFPOM C3			
POC	y = 0.01x + 0.37	0.00	p = 0.46
PN	y = -0.11x + 0.41	0.00	p = 0.29
Chl-*a*	y = 0.00x + 0.36	0.01	p = 0.06
BEFPOM C4			
POC	y = 0.02x + 0.37	0.00	p = 0.07
PN	y = -0.03x + 0.43	0.00	p = 0.69
Chl-*a*	y = 0.00x + 0.40	0.01	p = 0.01
BEFPOM C5			
POC	y = 0.13x + 0.01	0.33	p < 0.001
PN	y = 0.80x + 0.01	0.39	p < 0.001
Chl-*a*	y = 0.00x + 0.11	0.30	p < 0.001

Appendix 2.4. FDOM+BEFPOM Model:

A 5 component PARAFAC model was developed on the combined FDOM+BEFPOM samples. The split half validation results are plotted in Figure A2.10. As with the individual models, the components from the combined model (FDOM+BEFPOM) as applied to FDOM and BEFPOM samples, respectively, were plotted against salinity (Figure A2.11, Table A2.7; Figure A2.14, Table A2.9). The components were also plotted down estuary by station as applied to the FDOM and BEFPOM samples, respectively (Figure A2.12; Figure A2.15). The 5-components as applied to the FDOM samples were also plotted against various environmental parameters (Figure A2.13, Table A2.8). Because the BEFPOM model was identical to the

FDOM+BEFPOM model, the results from the FDOM+BEFPOM model as applied to BEFPOM samples were not plotted versus the environmental parameters.

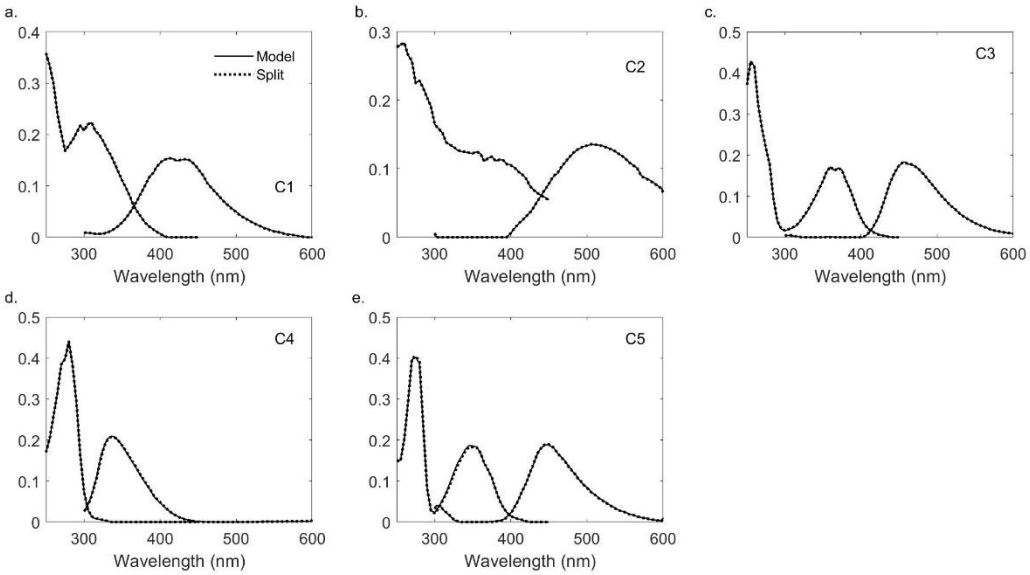

Figure A2.10. Excitation and emission loadings for the FDOM+BEFPOM 5-components identified by PARAFAC (solid line). Split half validation results are also plotted (dashed line).

As described for the FDOM and BEFPOM models, the residuals from the FDOM+BEFPOM model as applied to the FDOM and BEFPOM samples, respectively, were analyzed. For the FDOM samples, no PARAFAC model was fitted to the residuals. For the BEFPOM samples, a residual model was identified and was identical to the 1-component BEFPOM model developed for the individual BEFPOM model.

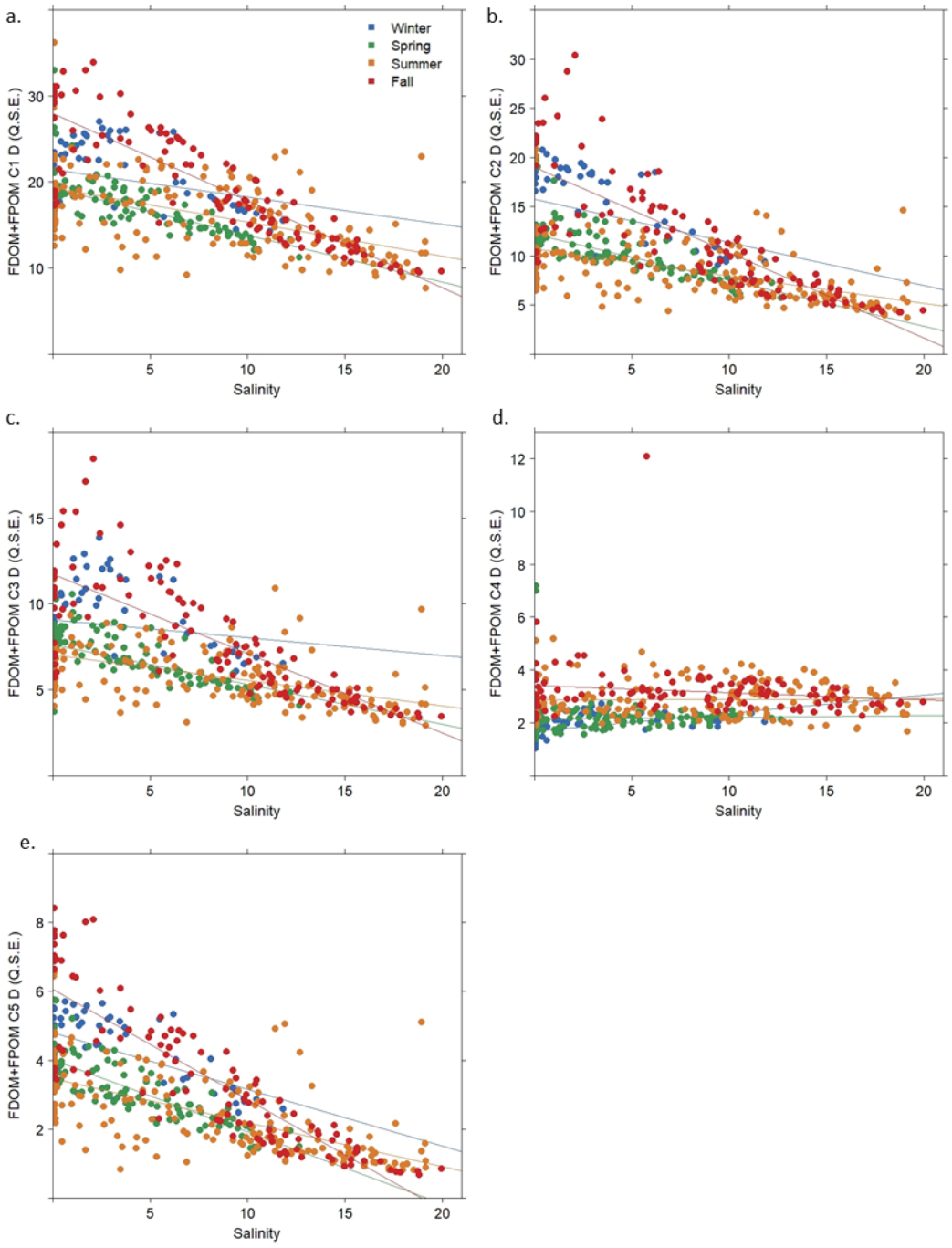

Figure A2.11. The 5 identified components for the combined model (FDOM+BEFPOM) plotted versus salinity for the FDOM samples. Samples are plotted by season. The linear regression for each set of samples is plotted. Linear regression equations, r^2, and p-values are listed in Table A2.7.

Table A2.7. Linear regression equations, r^2, and p-values for linear relationships between FDOM+BEFPOM components applied to FDOM samples and salinity, separated by season. Relationships that are statistically significant ($p < 0.05$) with $r^2 > 0.1$ are shaded in dark grey. Statistically significant relationships with $r^2 < 0.1$ are highlighted in light grey.

	Linear regression equation	r^2	p-value
FDOM+BEFPOM C1 D			
Winter	y = -0.32x + 21.5	0.08	p = 0.02
Spring	y = -0.54x + 19.3	0.46	p < 0.001
Summer	y = -0.40x + 19.4	0.29	p < 0.001
Fall	y = -1.01x + 27.9	0.74	p < 0.001
FDOM+BEFPOM C2 D			
Winter	y = -0.44x + 15.7	0.16	p = 0.001
Spring	y = -0.47x + 12.2	0.47	p < 0.001
Summer	y = -0.28x + 10.7	0.30	p < 0.001
Fall	y = -0.87x + 19.0	0.64	p < 0.001
FDOM+BEFPOM C3 D			
Winter	y = -0.10x + 9.1	0.01	p = 0.20
Spring	y = -0.23x + 7.6	0.38	p < 0.001
Summer	y = -0.15x + 7.0	0.27	p < 0.001
Fall	y = -0.46x + 11.7	0.60	p < 0.001
FDOM+BEFPOM C4 D			
Winter	y = 0.07x + 1.7	0.30	p < 0.001
Spring	y = 0.00x + 2.1	0.00	p = 0.73
Summer	y = 0.00x + 2.9	0.00	p = 0.74
Fall	y = -0.03x + 3.4	0.01	p = 0.11
FDOM+BEFPOM C5 D			
Winter	y = -0.17x + 4.8	0.39	p < 0.001
Spring	y = -0.21x + 4.0	0.64	p < 0.001
Summer	y = -0.13x + 3.5	0.37	p < 0.001
Fall	y = -0.32x + 6.1	0.75	p < 0.001

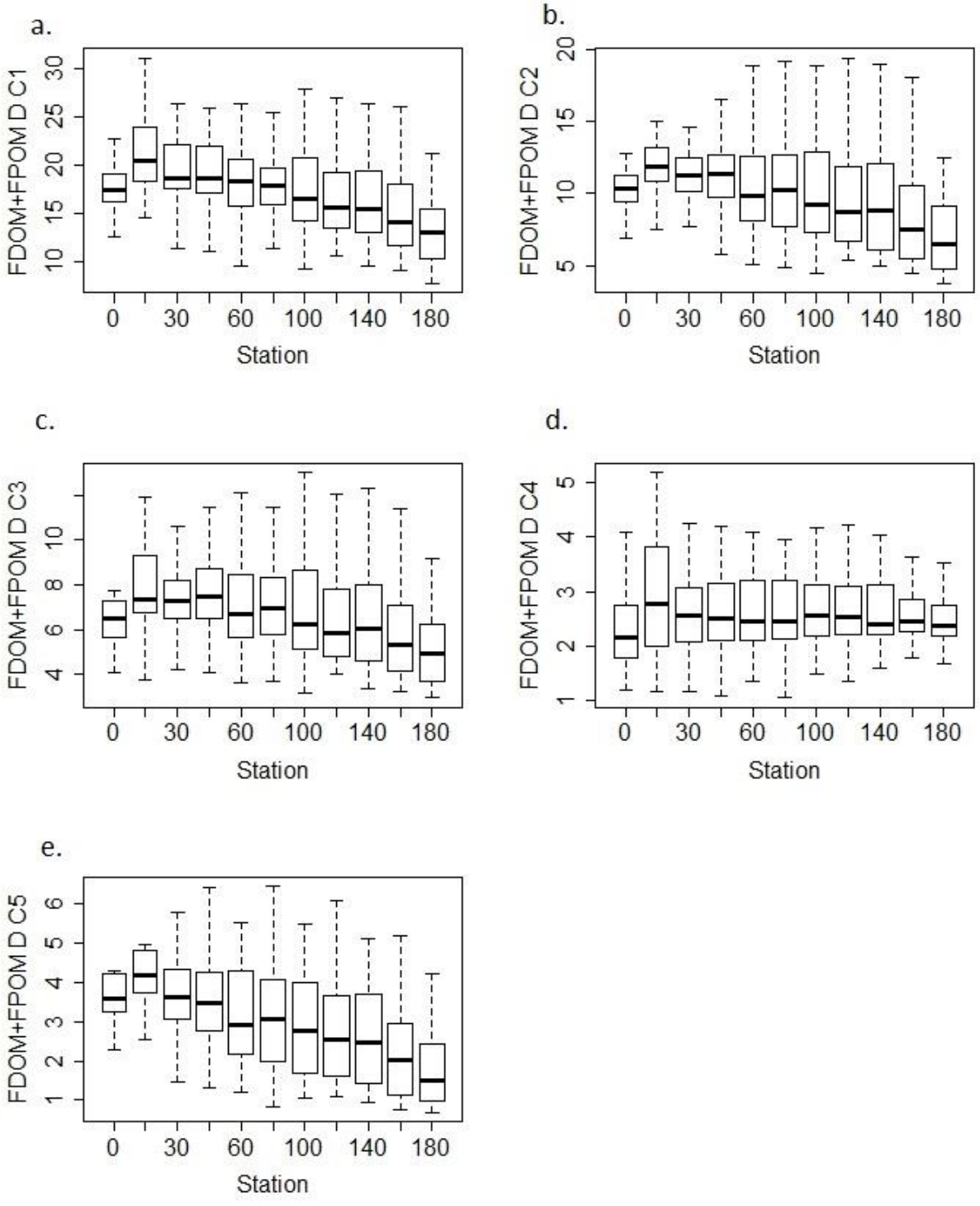

Figure A2.12. Boxplots of the 5 components identified for the combined model (FDOM+BEFPOM) as applied to FDOM samples plotted by station. Each station includes samples from both depths (surface and bottom) and all time points. Outliers were removed for visualization.

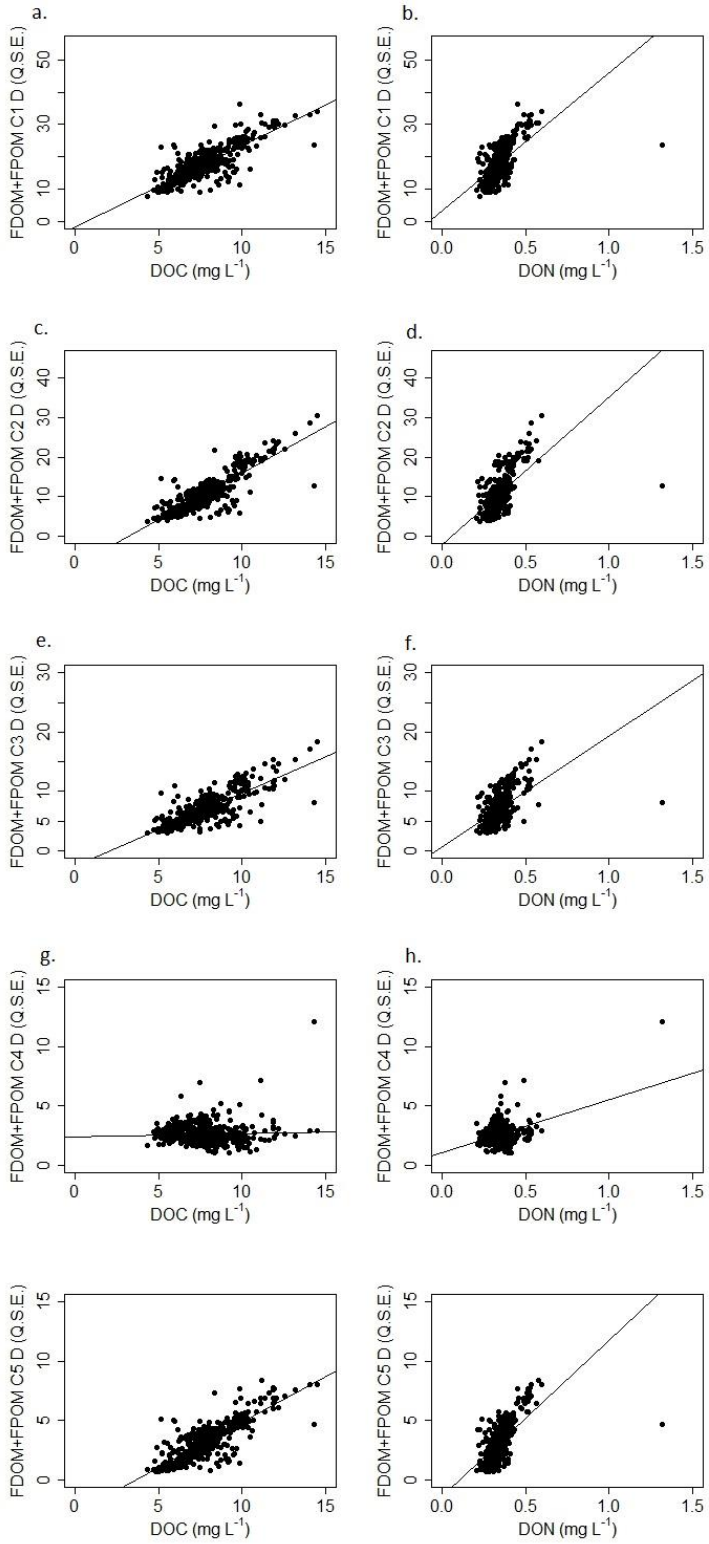

Figure A2.13. Combined model (FDOM+BEFPOM) applied to FDOM samples plotted against various environmental parameters (DON, DOC). Linear regression lines are plotted. Linear regression equations, r^2, and p-values are listed in Table A2.8.

Table A2.8. Linear regression equations, r^2, and p-values for linear relationships between the combined model (FDOM+BEFPOM) as applied to FDOM samples and various environmental parameters. Statistically significant ($p < 0.05$) relationships with $r^2 > 0.1$ are highlighted in dark grey. Statistically significant relationships with $r^2 < 0.1$ are highlighted in light grey.

	Linear regression equation	r^2	p-value
FDOM+BEFPOM C1 D			
DOC	y = 2.5x – 1.64	0.68	p < 0.001
DON	y = 42.9x + 3.1	0.40	p < 0.001
FDOM+BEFPOM C2 D			
DOC	y = 2.4x – 7.5	0.73	p < 0.001
DON	y = 37.3x – 2.2	0.38	p < 0.001
FDOM+BEFPOM C3 D			
DOC	y = 1.2x – 2.5	0.65	p < 0.001
DON	y = 18.8x + 0.54	0.31	p < 0.001
FDOM+BEFPOM C4 D			
DOC	y = 0.03x + 2.4	0.00	p = 0.31
DON	y = 4.4x + 1.1	0.13	p < 0.001
FDOM+BEFPOM C5 D			
DOC	y = 0.77x – 2.8	0.66	p < 0.001
DON	y = 13.2x – 1.4	0.39	p < 0.001

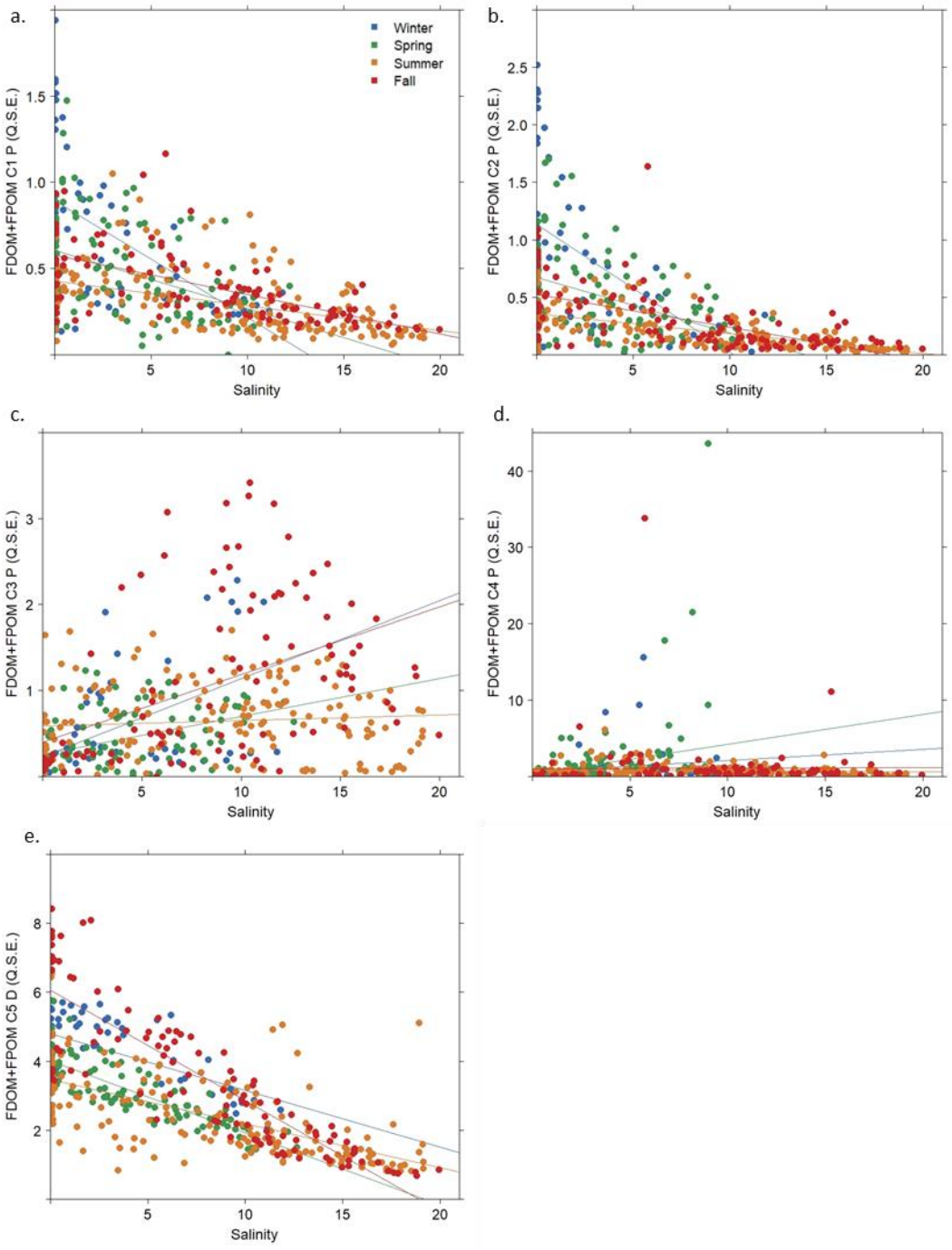

Figure A2.14. Plots of components identified for the combined model (FDOM+BEFPOM) as applied to BEFPOM samples plotted against salinity. Samples are plotted by season. Linear regression lines are plotted for each group of samples. Linear regression equations, r^2, and p-values are listed in Table A2.9.

Table A2.9. Linear regression equation, r^2, and p-values for components identified in the FDOM+BEFPOM model applied to BEFPOM samples as separated by season. Statistically significant ($p < 0.05$) relationships with $r^2 > 0.1$ are highlighted in dark grey. Statistically significant relationships with $r^2 < 0.1$ are highlighted in light grey.

	Linear regression equation	r^2	p-value
FDOM+BEFPOM C1 P			
Winter	y = -0.07x + 0.89	0.33	p < 0.001
Spring	y = -0.03x + 0.61	0.18	p < 0.001
Summer	y = -0.01x + 0.43	0.23	p < 0.001
Fall	y = -0.02x + 0.58	0.37	p < 0.001
FDOM+BEFPOM C2 P			
Winter	y = -0.11x + 1.1	0.35	p < 0.001
Spring	y = -0.05x + 0.67	0.20	p < 0.001
Summer	y = -0.02x + 0.36	0.44	p < 0.001
Fall	y = -0.03x + 0.53	0.36	p < 0.001
FDOM+BEFPOM C3 P			
Winter	y = 0.09x + 0.23	0.29	p < 0.001
Spring	y = 0.04x + 0.26	0.24	p < 0.001
Summer	y = 0.01x + 0.59	0.00	p = 0.23
Fall	y = 0.08x + 0.39	0.23	p < 0.001
FDOM+BEFPOM C4 P			
Winter	y = 0.15x + 0.62	0.03	p = 0.01
Spring	y = 0.40x + 0.34	0.08	p = 0.001
Summer	y = -0.01x + 0.86	0.00	p = 0.18
Fall	y = 0.01x + 1.0	0.00	p = 0.91
FDOM+BEFPOM C5 P			
Winter	y = 0.00x + 0.13	0.00	p = 0.46
Spring	y = 0.02x + 0.08	0.20	p < 0.001
Summer	y = 0.01x + 0.12	0.08	p < 0.001
Fall	y = 0.00x + 0.21	0.00	p = 0.88

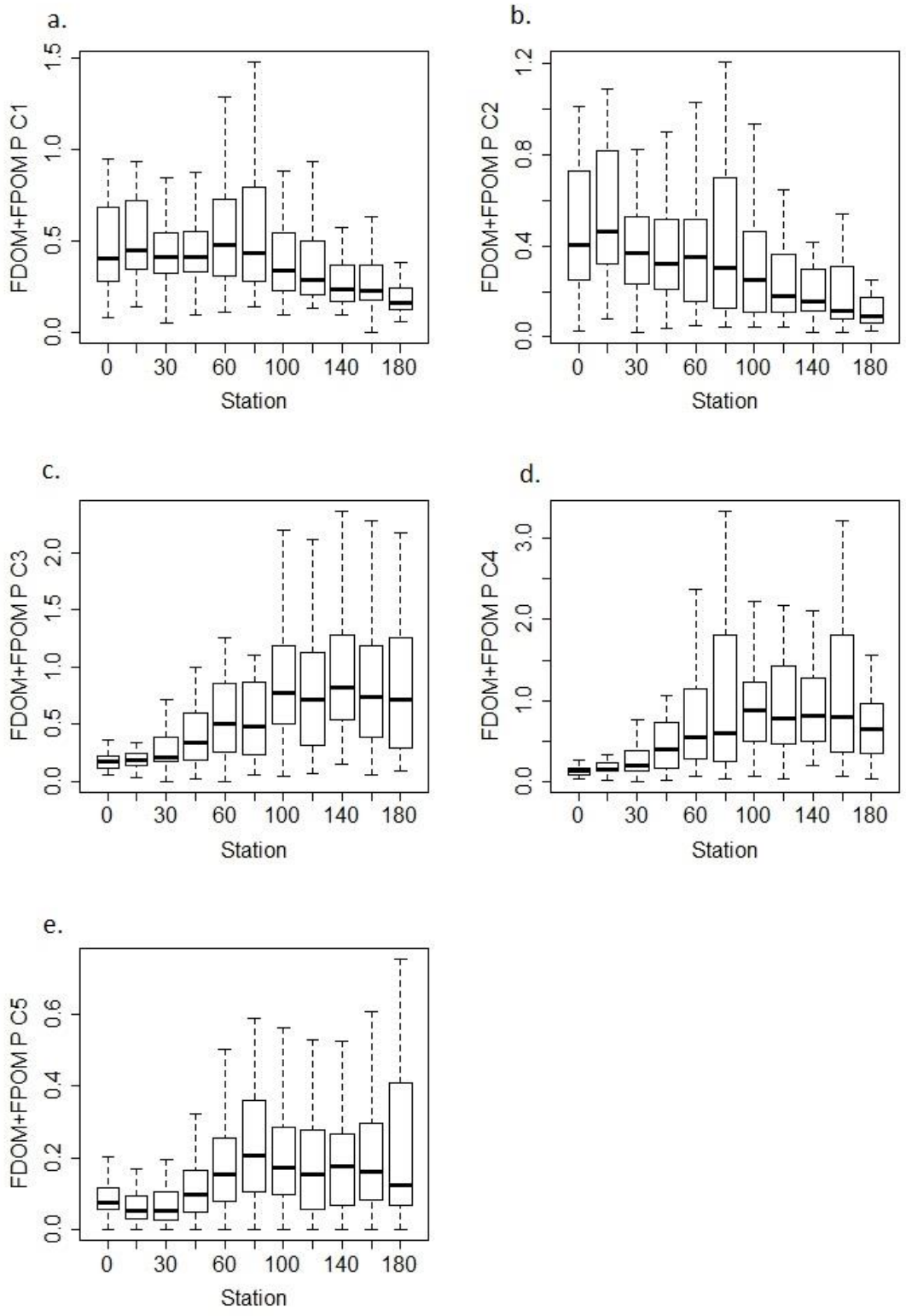

Figure A2.15. Identified components from the combined model (FDOM+BEFPOM) as applied to BEFPOM samples plotted by station. Each station includes both depths (surface and bottom) as well as all time points. Outliers were removed for visualization.

As with the individual models (FDOM, BEFPOM), principal component analysis (PCA) was also applied to the combined model (FDOM+BEFPOM) as applied to FDOM and BEFPOM samples, respectively (Figure A2.16, Figure A2.17). PCA results are discussed in Chapter 2 and are similar to PCA applied to the individual FDOM and BEFPOM models, respectively.

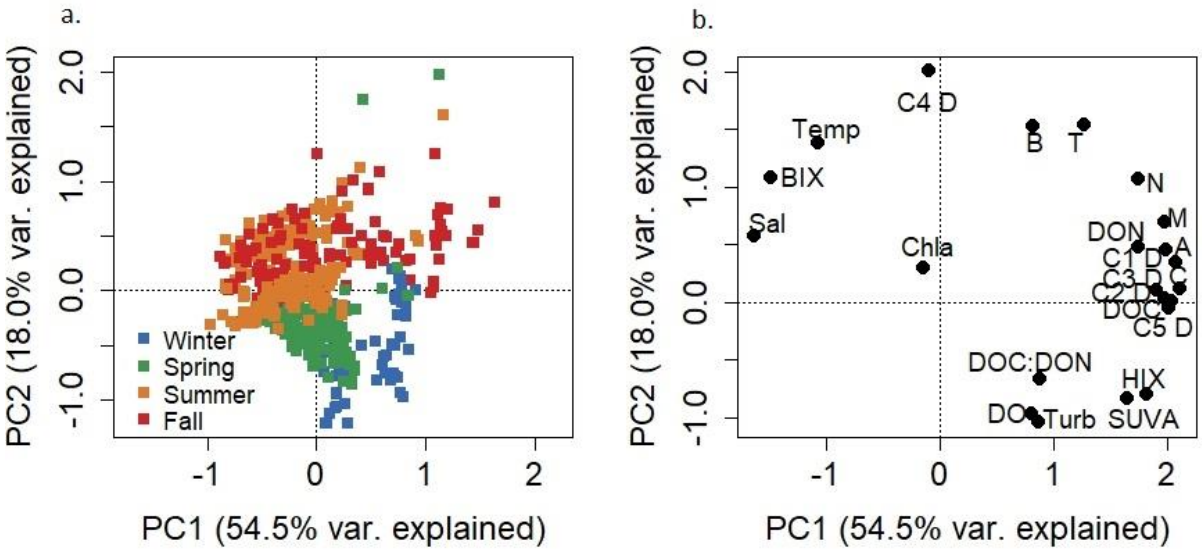

Figure A2.16. PCA results for the FDOM+BEFPOM model applied to FDOM samples. a. Sample loadings plotted by season. b. Variable loadings plotted in PCA space. Variables are identified on the graph.

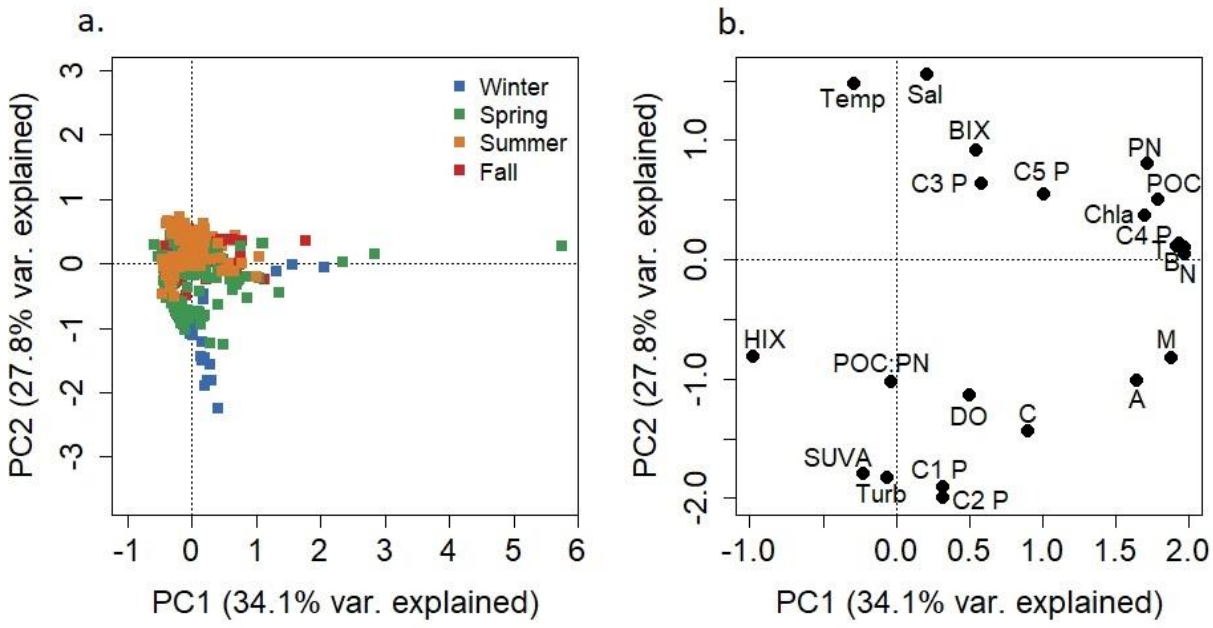

Figure A2.17. PCA results for the FDOM+BEFPOM model applied to FDOM samples. a. Sample loadings plotted by season. b. Variable loadings plotted in PCA space. Variables are identified on the graph.

Appendix 2.5. Estuarine signal:

An estuarine processing signal was identified using seasonal experimental bioassays. Several additional parameters collected during the bioassay were plotted versus time for each of the bioassays (July 2017, October 2017, February 2018, July 2018) including HIX and BIX (Figure A2.18). The 1-component estuarine processing model identified was also applied to raw EEMS and subtracted EEMs from the experimental bioassays and plotted through time for each bioassay (Figure A2.19, Figure A2.20). Results from the application of a 2-component PARAFAC model as applied to raw samples collected from the experimental bioassays, was also conducted (Figure A2.21, Figure A2.22, Table A2.10). The three components (2 component PARAFAC model, 1 component estuarine processing signal) were then applied to the bioassay samples (October 2017, February 2018, April 2018) and plotted through time (Figure A2.23, Figure A2.24, Figure A2.25).

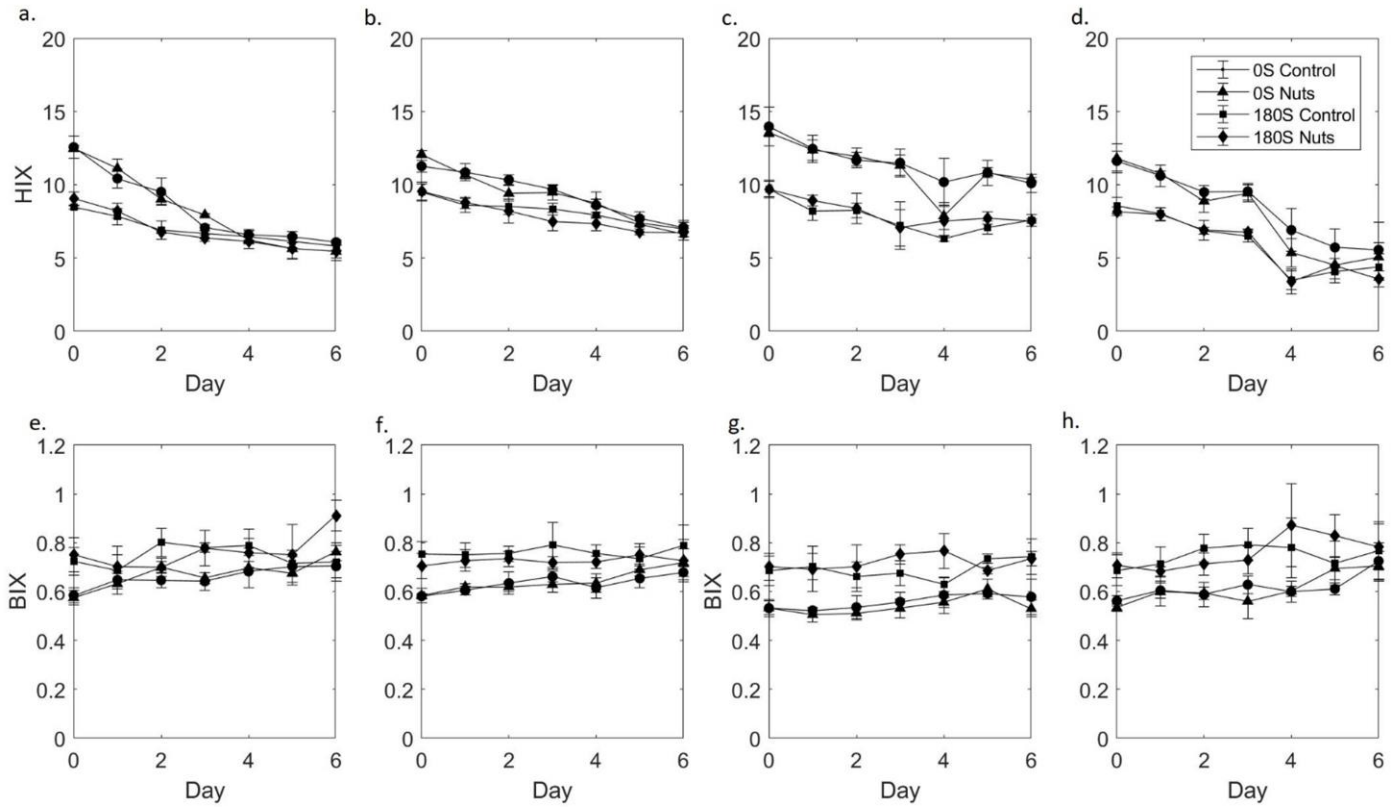

Figure A2.18. HIX (a-d) and BIX (e-h) plotted for each treatment and experimental bioassay (a,e – July 2017; b,f – October 2017; c,g – February 2018; d,h – April 2018).

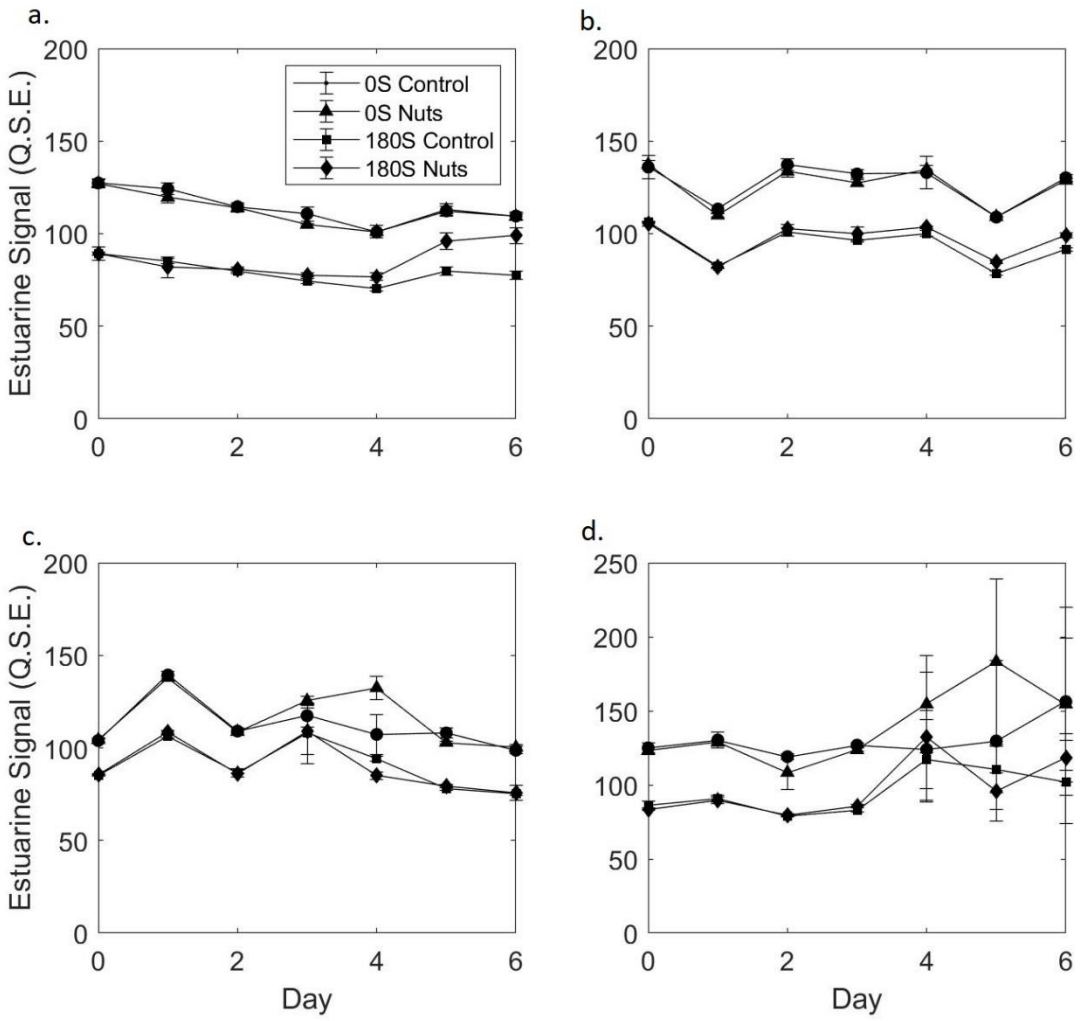

Figure A2.19. 1-component estuarine processing model as applied to raw EEMs collected from each of the experimental bioassays: a. July 2017, b. October 2017, c. February 2018, and d. April 2018. Standard error for each of the quadruplicate treatments are plotted.

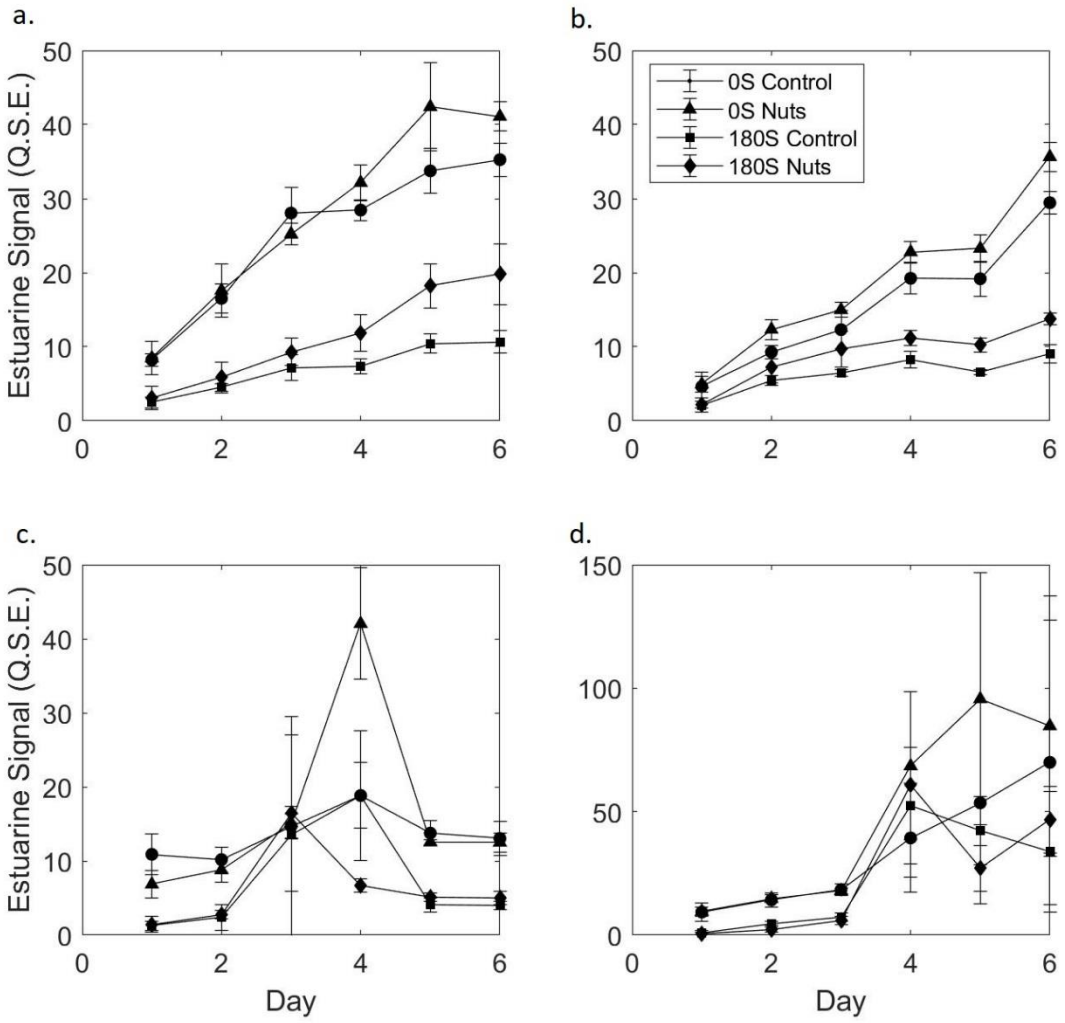

Figure A2.20. Plot of the 1-component estuarine signal applied to subtracted samples used to generate the 1-component PARAFAC model for each bioassay a. July 2017, b. October 2017, c. February 2018, and d. April 2018. Note the change in scale for April 2018 (d). Error bars are included for each set of quadruplicate treatments.

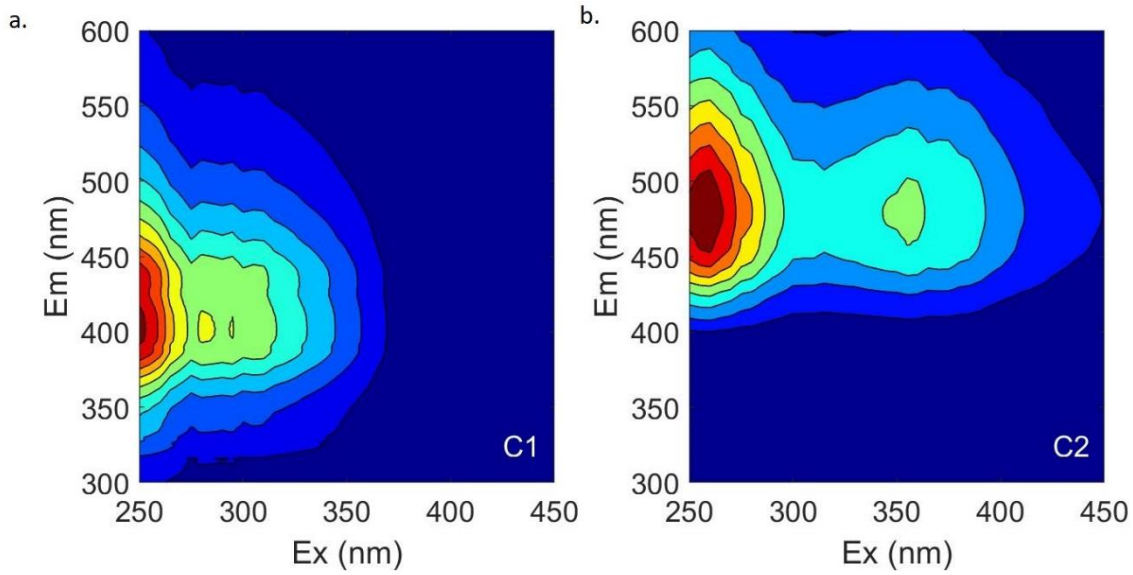

Figure A2.21. 2-component PARAFAC model as developed on raw samples collected from all of the experimental bioassays.

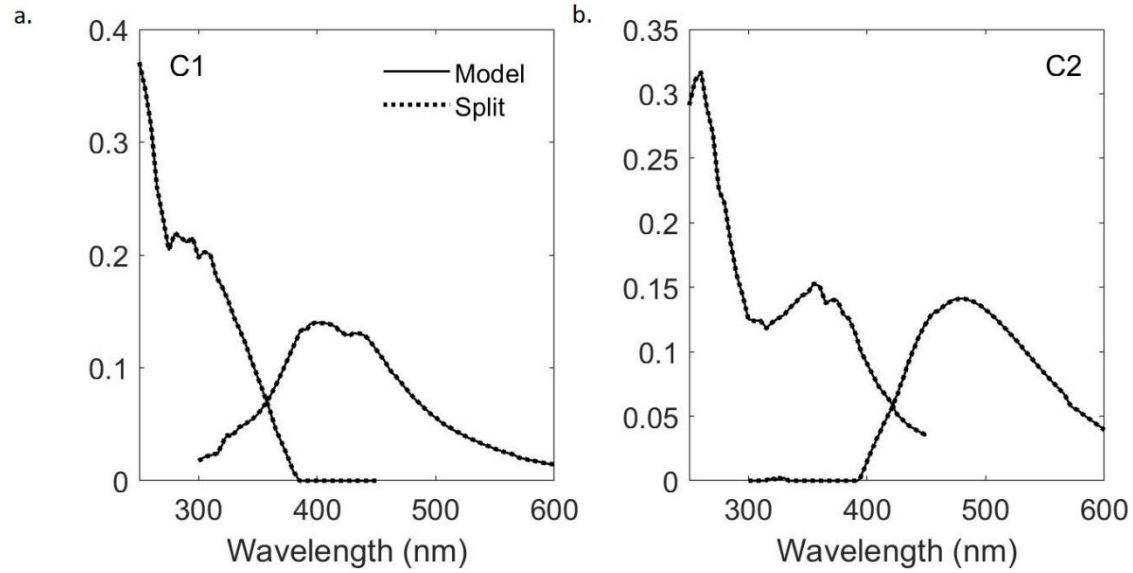

Figure A2.22. Split half validation results for the 2-component PARAFAC model generated on raw samples collected from the experimental bioassays.

Table A2.10. Component identification for the 2-component PARAFAC model fitted to the raw bioassay samples. Included references are only a subsection of the total OpenFluor matches.

	Ex max. (nm)	Em max. (nm)	OpenFluor Matches	Description	Reference
C1	< 250	314	19	Terrestrial, humic-like, possible Peak M	Murphy et al., 2008; Osburn et al., 2012; Yamashita et al., 2013
C2	260, 355	480	41	Terrestrial, humic-like, Peaks A and C	Dainard et al., 2015; Osburn et al., 2016a; Podgorski et al., 2018

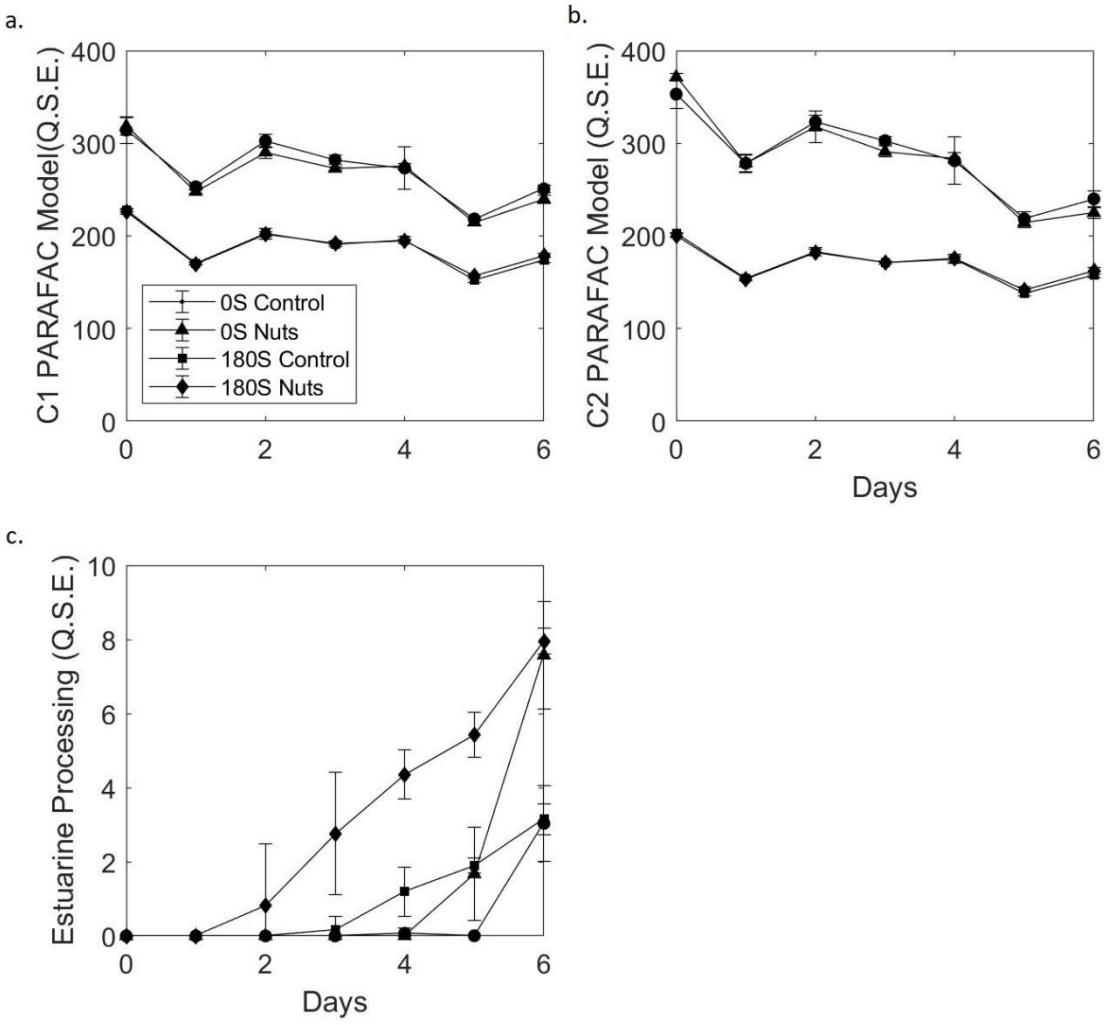

Figure A2.23. Plots of the three experimental bioassay components plotted through time and separated by treatment for the October 2017 experimental bioassay. a. Component 1 of the applied PARAFAC model, b. Component 2 of the applied PARAFAC model, and c. 1 component estuarine processing signal.

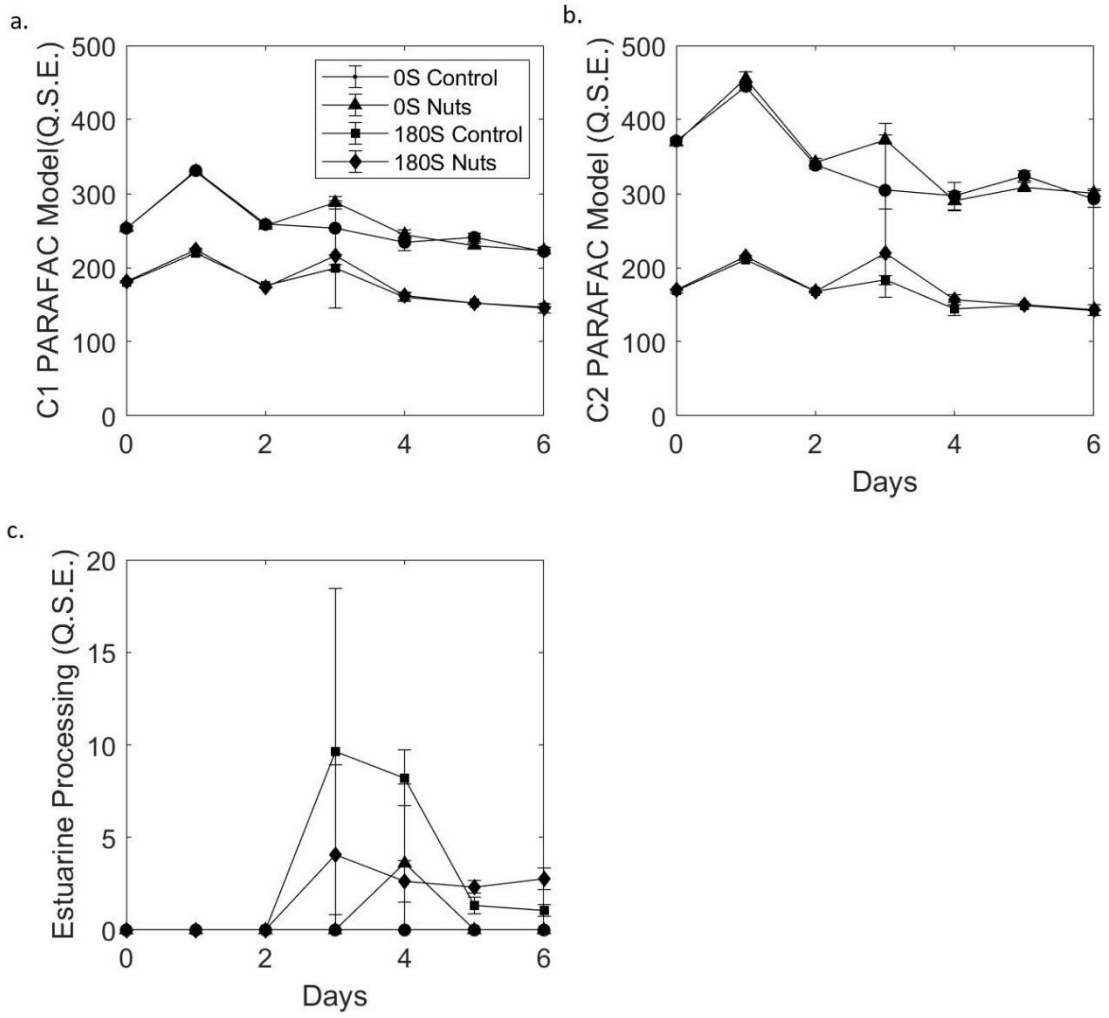

Figure A2.24. Plots of the three experimental bioassay components plotted through time and separated by treatment for the February 2018 experimental bioassay. a. Component 1 of the applied PARAFAC model, b. Component 2 of the applied PARAFAC model, and c. 1 component estuarine processing signal.

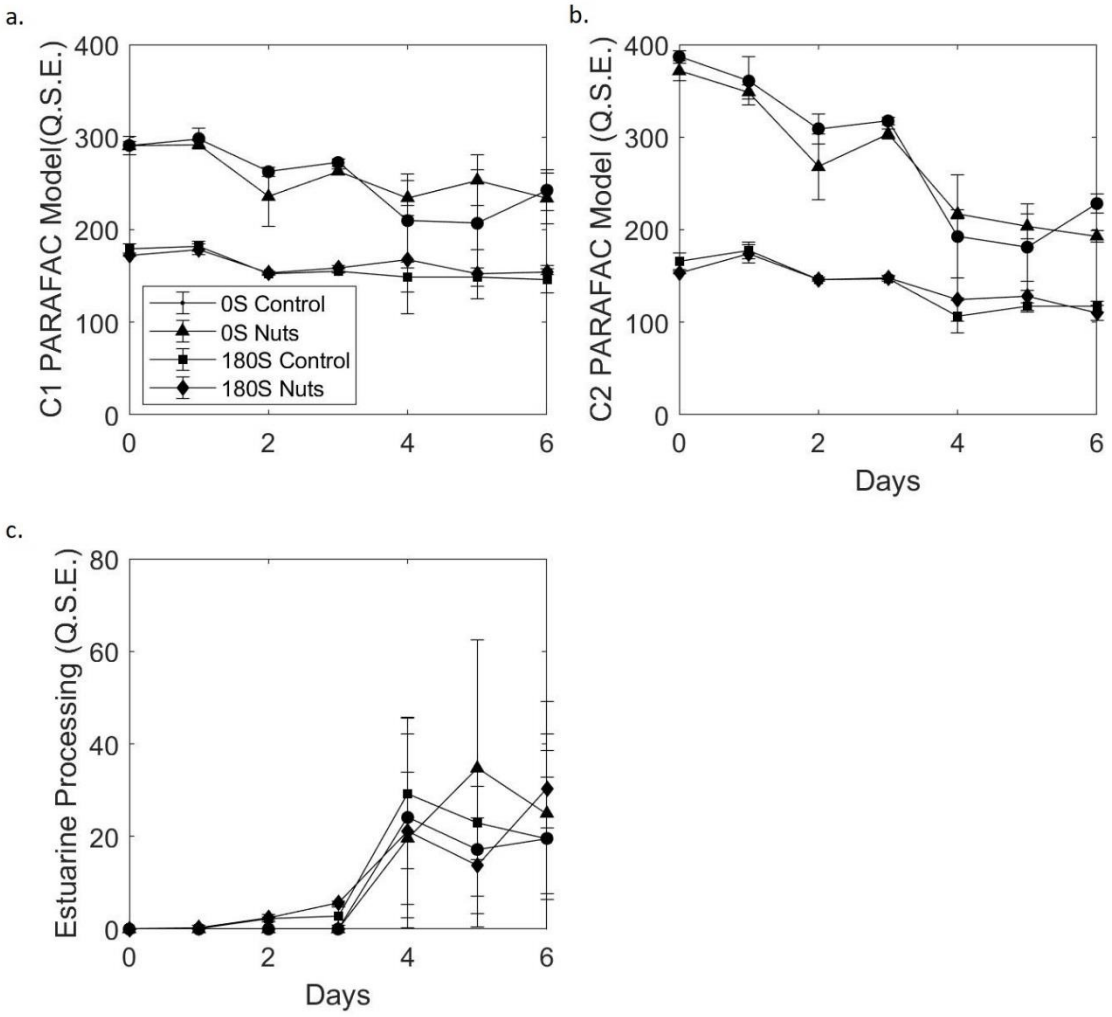

Figure A2.25. Plots of the three experimental bioassay components plotted through time and separated by treatment for the April 2018 experimental bioassay. a. Component 1 of the applied PARAFAC model, b. Component 2 of the applied PARAFAC model, and c. 1 component estuarine processing signal.

Appendix 2.6. Application of FluorMod:

The 9-component PARAFAC model, FluorMod (Osburn et al., 2016), was applied to estuarine samples collected from the NRE. Each of the 8 sources identified in the FluorMod mixing model (reference, effluent, influent, poultry, septic, street, soil, and swine) were plotted for each station as applied to the NRE FDOM samples (Figure A2.26). Each of the 9-

components as applied to the FDOM samples were also plotted versus salinity (Figure A2.27, Table A2.11).

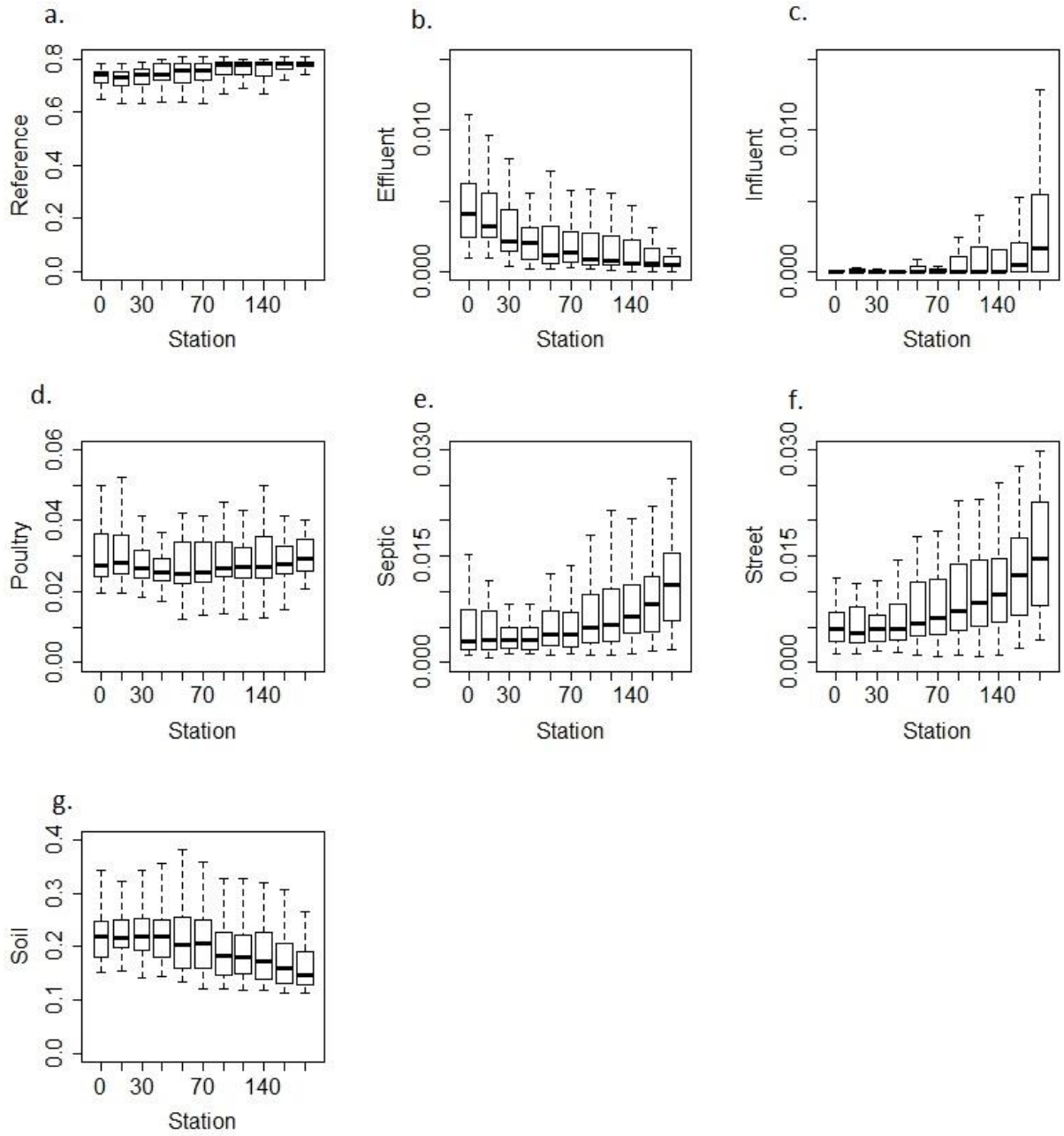

Figure A2.26. Application of the FluorMod mixing model applied to FDOM samples collected from the NRE plotted as the fraction of each source in the sample. The Swine Lagoon source was omitted as all samples had a negligible (< 0.005) fraction of this source.

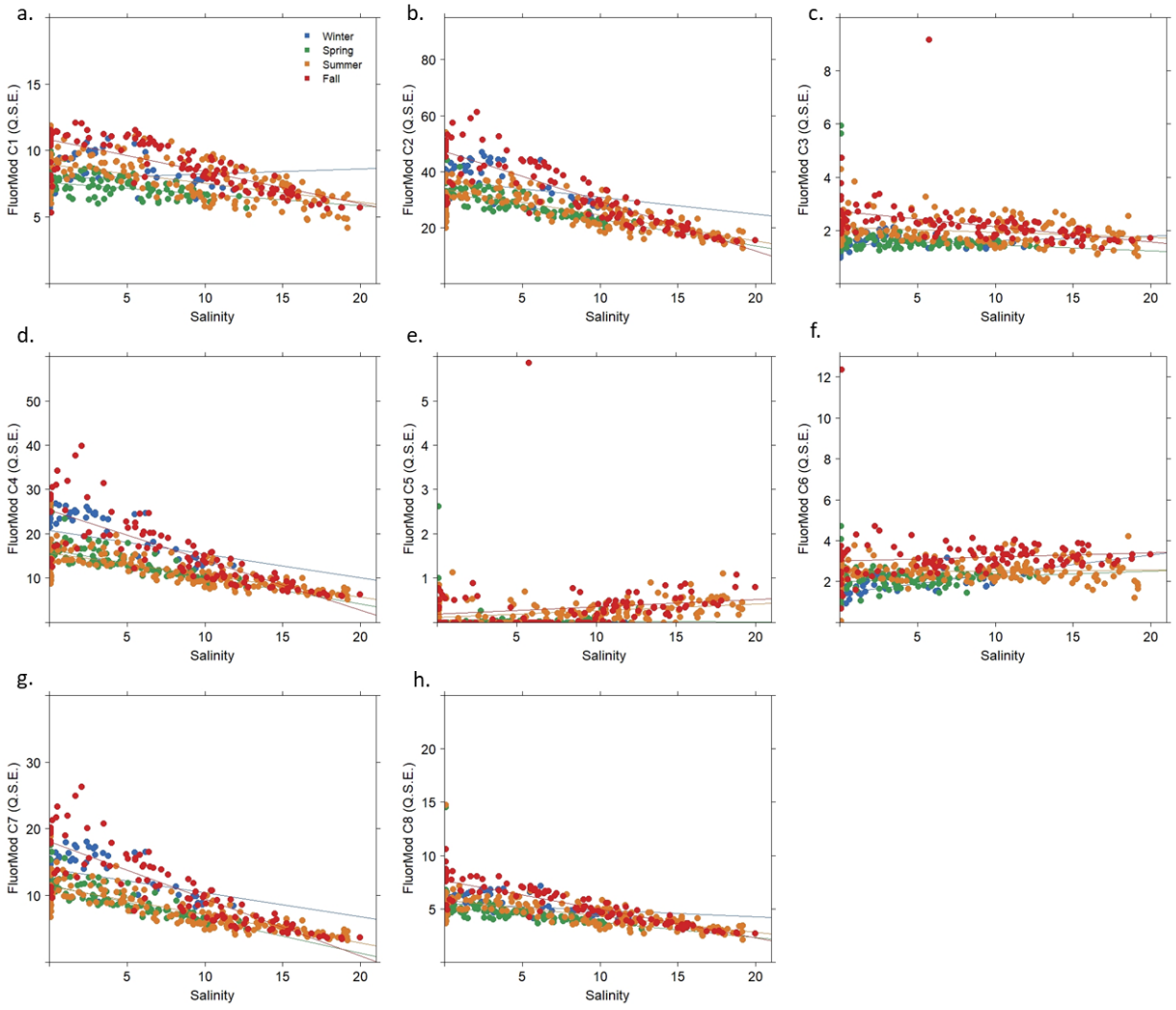

Figure A2.27. Plot of the 9-component FluorMod PARAFAC model applied to FDOM samples collected from the NRE as plotted against salinity. Samples were plotted by season. Component 9 was omitted as all samples had essentially negligible (< 0 Q.S.E.) fluorescence intensity of this component. Linear regression lines were plotted. Linear regression equations, r^2, and p-values are listed in Table A2.10.

Table A2.11. Linear regression equations, r^2, and p-values for relationships between the 9 FluorMod PARAFAC components and salinity as separated by season. Statistically significant relationships ($p < 0.05$) with $r^2 > 0.1$ are highlighted in dark grey. Statistically significant relationships with $r^2 < 0.1$ are highlighted in light grey. For FluorMod component C5, there was no relationship with salinity during winter due to low to non-existent fluorescence intensity for this component and season. Fluorescent intensity for component C9 was essentially zero for all samples and was omitted.

	Linear regression equation	r^2	p-value
FluorMod C1			
Winter	y = 0.04x + 7.9	0.00	p = 0.42
Spring	y = -0.09x + 7.6	0.15	p < 0.001
Summer	y = -0.14x + 9.0	0.31	p < 0.001
Fall	y = -0.24x + 10.8	0.56	p < 0.001
FluorMod C2			
Winter	y = -0.61x + 37.0	0.09	p = 0.01
Spring	y = -0.96x + 32.5	0.52	p < 0.001
Summer	y = -0.93x + 33.7	0.57	p < 0.001
Fall	y = -1.8x + 47.1	0.72	p < 0.001
FluorMod C3			
Winter	y = 0.02x + 1.4	0.04	p = 0.06
Spring	y = -0.02x + 1.7	0.01	p = 0.10
Summer	y = -0.02x + 2.1	0.05	p = 0.002
Fall	y = -0.06x + 2.7	0.15	p < 0.001
FluorMod C4			
Winter	y = -0.53x + 20.8	0.14	p = 0.002
Spring	y = -0.61x + 16.4	0.48	p < 0.001
Summer	y = -0.50x + 15.7	0.56	p < 0.001
Fall	y = -1.1x + 25.3	0.65	p < 0.001
FluorMod C5			
Winter	N/A	N/A	N/A
Spring	y = -0.00x + 0.05	0.00	p = 0.74
Summer	y = 0.02x + 0.11	0.16	p < 0.001
Fall	y = 0.02x + 0.18	0.01	p = 0.11
FluorMod C6			
Winter	y = 0.09x + 1.4	0.40	p < 0.001
Spring	y = 0.03x + 2.0	0.03	p = 0.03
Summer	y =-0.00x + 2.5	0.00	p = 0.54
Fall	y = 0.02x + 3.0	0.00	p = 0.29
FluorMod C7			
Winter	y = -0.36x + 14.0	0.17	p = 0.001
Spring	y = -0.51x + 11.5	0.63	p < 0.001
Summer	y = -0.42x + 11.4	0.66	p < 0.001
Fall	y = -0.86x + 18.0	0.73	p < 0.001
FluorMod C8			
Winter	y = -0.06x + 5.5	0.05	p = 0.05
Spring	y = -0.14x + 5.2	0.20	p < 0.001
Summer	y = -0.15x + 5.8	0.43	p < 0.001
Fall	y = -0.27x + 7.6	0.76	p < 0.001

After application of the 3-component PARAFAC model identified for the FDOM samples, the 1-component estuarine processing model was applied to the respective sample residuals. Results from the application of the estuarine processing model as applied to FDOM sample residuals are plotted against Chl *a* (Figure A2.28).

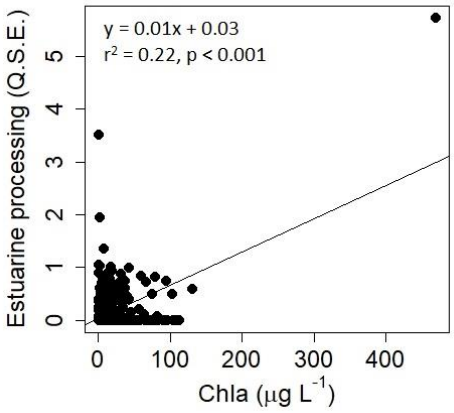

Figure A2.28. Estuarine processing signal, as applied to residual samples after application of the 3-component FDOM model, plotted versus Chl *a*. The linear regression line, linear regression equation, r^2, and p-value are displayed on the plot.

REFERENCES

Dainard, P.G., Guéguen, C., McDonald, N., Williams, W.J., 2015. Photobleaching of fluorescent dissolved organic matter in Beaufort Sea and North Atlantic Subtropical Gyre. Marine Chemistry 177, 630–637. https://doi.org/10.1016/j.marchem.2015.10.004

Markager, S., Stedmon, C.A., Søndergaard, M., 2011. Seasonal dynamics and conservative mixing of dissolved organic matter in the temperate eutrophic estuary Horsens Fjord. Estuarine, Coastal and Shelf Science 92, 376–388. https://doi.org/10.1016/j.ecss.2011.01.014

Murphy, K.R., Ruiz, G.M., Dunsmuir, W.T.M., Waite, T.D., 2006. Optimized parameters for fluorescence-based verification of ballast water exchange by ships. Environmental Science & Technology 40, 2357–2362. https://doi.org/10.1021/es0519381

Murphy, K.R., Stedmon, C. A., Waite, T.D., Ruiz, G.M., 2008. Distinguishing between terrestrial and autochthonous organic matter sources in marine environments using fluorescence spectroscopy. Marine Chemistry 108, 40–58. https://doi.org/10.1016/j.marchem.2007.10.003

Osburn, C.L., Handsel, L.T., Mikan, M.P., Paerl, H.W., Montgomery, M.T., 2012. Fluorescence tracking of dissolved and particulate organic matter quality in a river-dominated estuary. Environmental Science & Technology 46, 8628–8636. https://doi.org/10.1021/es3007723

Osburn, C.L., Handsel, L.T., Peierls, B.L., Paerl, H.W., 2016. Predicting Sources of Dissolved Organic Nitrogen to an Estuary from an Agro-Urban Coastal Watershed. Environmental Science & Technology 50, 8473–8484. https://doi.org/10.1021/acs.est.6b00053

Osburn, C.L., Boyd, T.J., Montgomery, M.T., Bianchi, T.S., Coffin, R.B., Paerl, H.W., 2016a. Optical Proxies for Terrestrial Dissolved Organic Matter in Estuaries and Coastal Waters. Frontiers in Marine Science 2(127). https://doi.org/10.3389/fmars.2015.00127

Podgorski, D.C., Zito, P., McGuire, J.T., Martinovic-Weigelt, D., Cozzarelli, I.M., Bekins, B.A., Spencer, R.G.M., 2018. Examining Natural Attenuation and Acute Toxicity of Petroleum-Derived Dissolved Organic Matter with Optical Spectroscopy. Environmental Science & Technology 52, 6157–6166. https://doi.org/10.1021/acs.est.8b00016

Yamashita, Y., Boyer, J.N., Jaffé, R., 2013. Evaluating the distribution of terrestrial dissolved organic matter in a complex coastal ecosystem using fluorescence spectroscopy. Continental Shelf Research 66, 136–144. https://doi.org/10.1016/j.csr.2013.06.010

APPENDIX 3: CHAPTER 3 SUPPLEMENTARY INFORMATION

Appendix 3.1: Wind speed, gusts, and direction for the Neuse River Estuary

Wind speed, gust, and direction data were obtained from the State Climate Office of North Carolina CRONOS station KNKT located at the Cherry Point Marine Air Station in Havelock, NC. Data used (average wind speed, maximum wind gust, prevailing wind direction) for statistical analyses was averaged between ModMon sampling time points which are represented as red dots and lines on Figure A3.1.

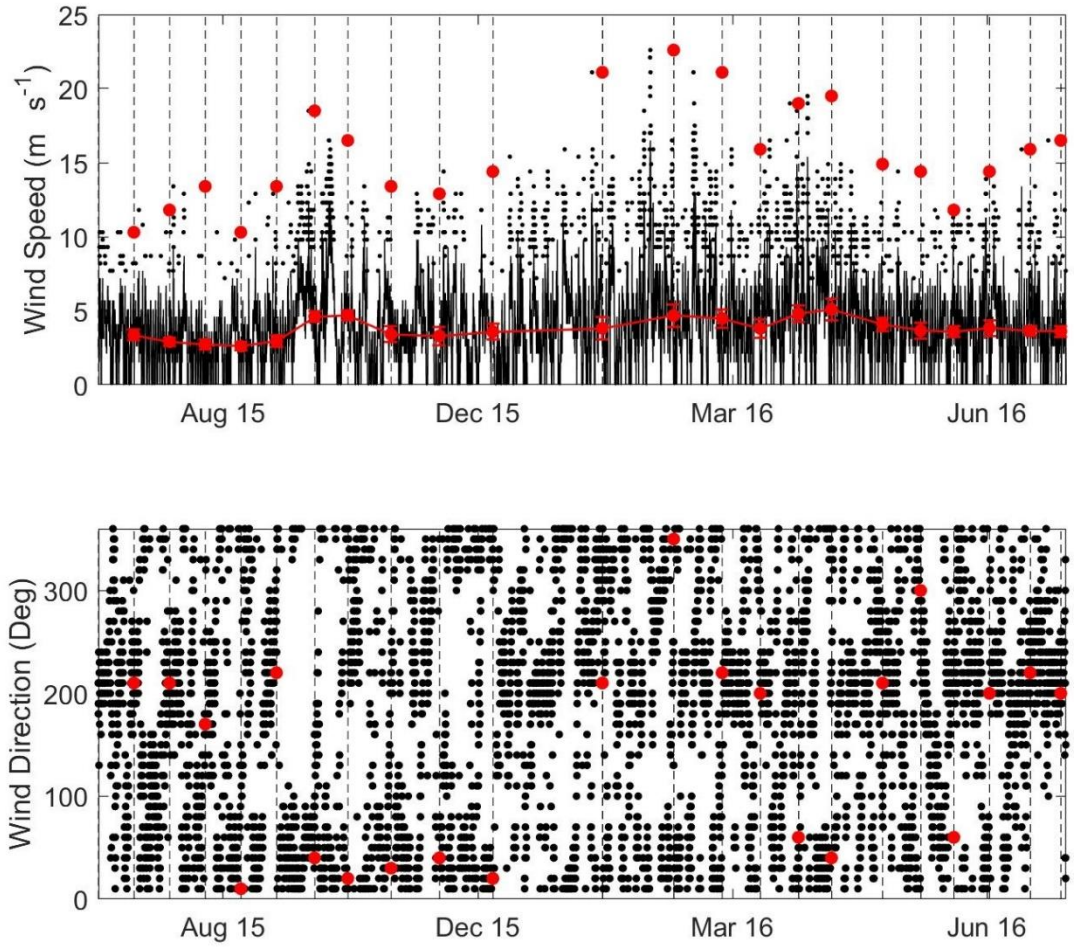

Figure A3.1. a. Wind speed (m s^{-1}). Black lines represent hourly wind speed. Black dots represent maximum hourly wind gusts measured. The red line represents averaged wind speed used in subsequent analyses. Red dots are maximum wind gusts used in subsequent analyses. b. Wind direction (degrees). Red dots represent the most common (prevailing) wind direction for the time period of interest. Dashed, vertical lines correspond to ModMon sampling time points.

Appendix 3.2: Correlations for the Environmental, DOM, and POM data sets

Prior to PCA analysis, linear correlations among respective data sets (environmental, DOM, and POM, individually) were assessed to determine the inclusion of parameters in subsequent multivariate analyses. Parameters with $r^2 > 0.80$ were considered to be collinear and the parameters removed to limit collinearity.

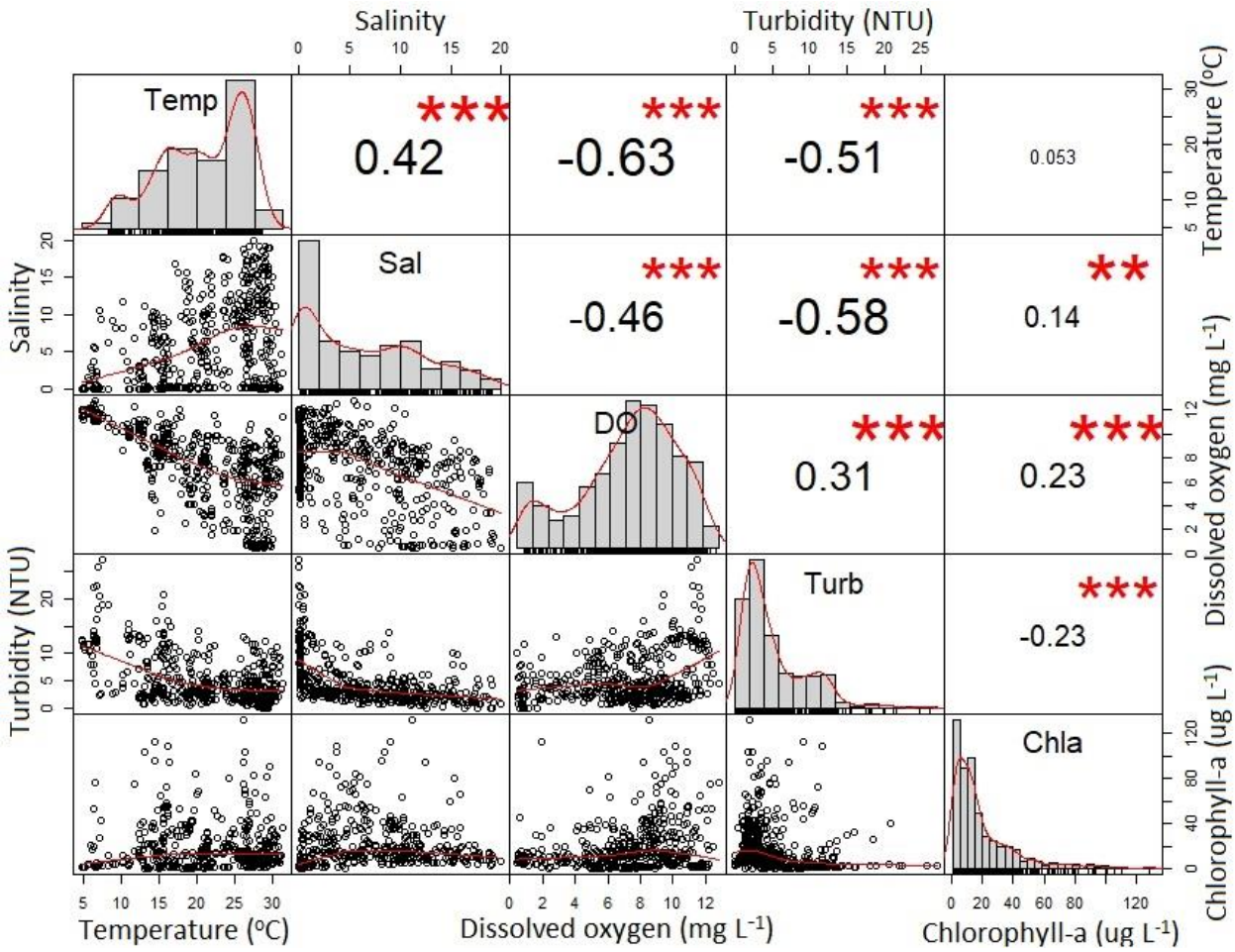

Figure A3.2. Correlation plot (Pearson's r^2) of environmental data collected from the NRE during the study time period. Stars indicate significance. *** p = 0; ** p = 0.001.

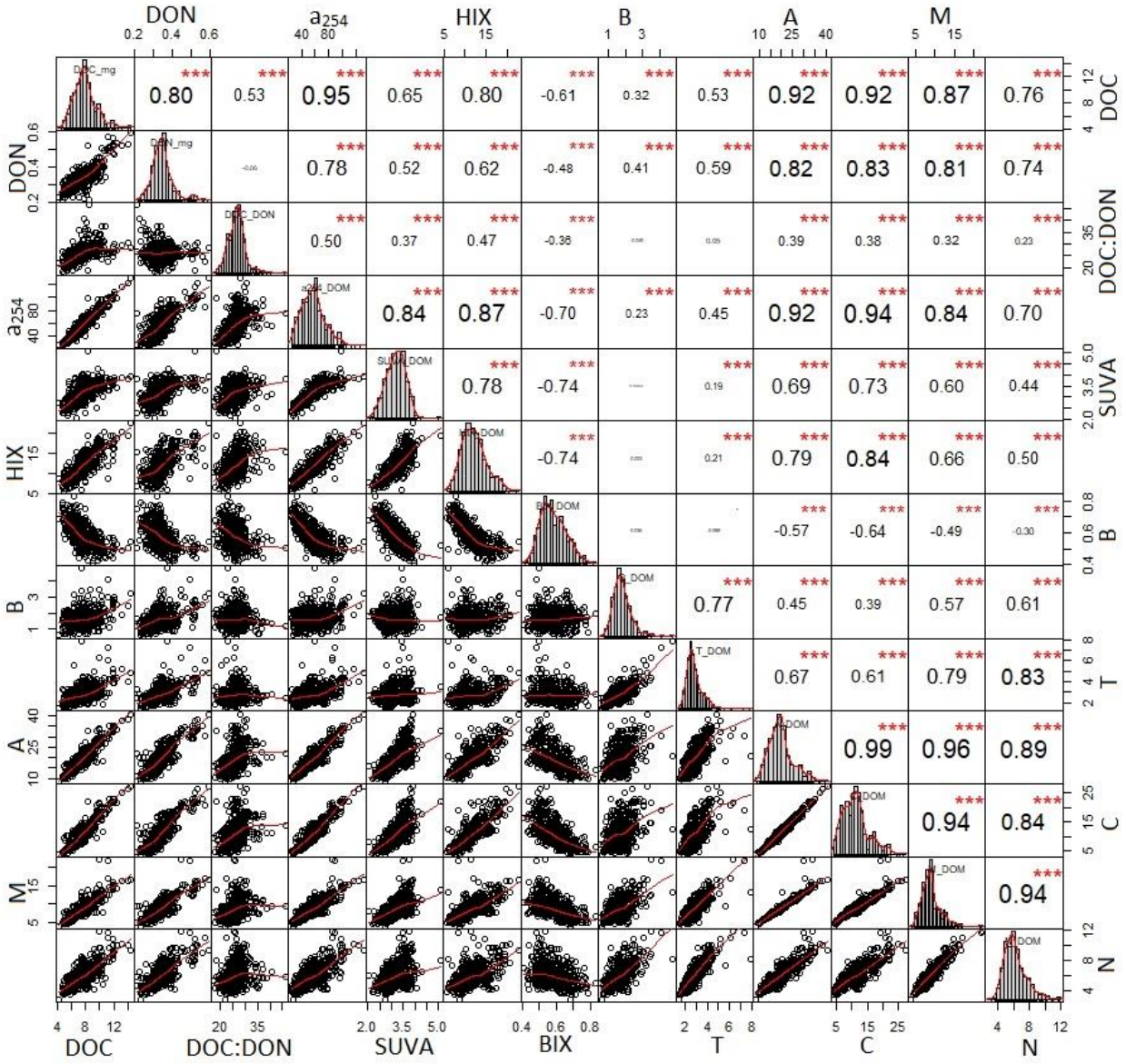

Figure A3.3. Correlation plot (Pearson's r^2) of DOM data collected from the NRE during the study time period. Stars indicate significance. *** p = 0.001.

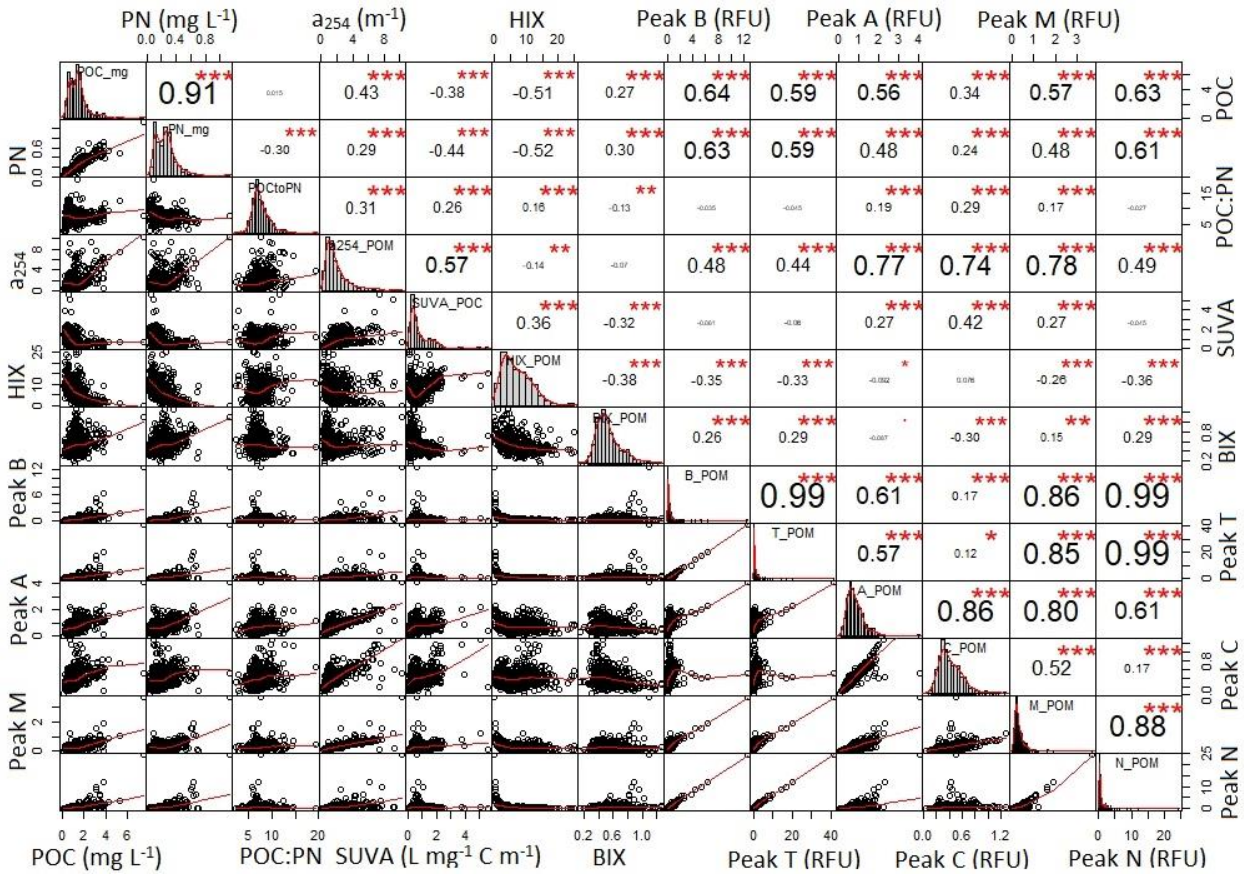

Figure A3.4. Correlation plot (Pearson's r^2) of POM data collected from the NRE during the study time period. Stars indicate significance. *** p = 0; ** p = 0.001; * p = 0.01.

Following removal of collinear parameters and any necessary data transformations, linear relationships between the three data sets were assessed (environmental, DOM, and POM). Results are plotted as a correlation plot in Figure A3.5.

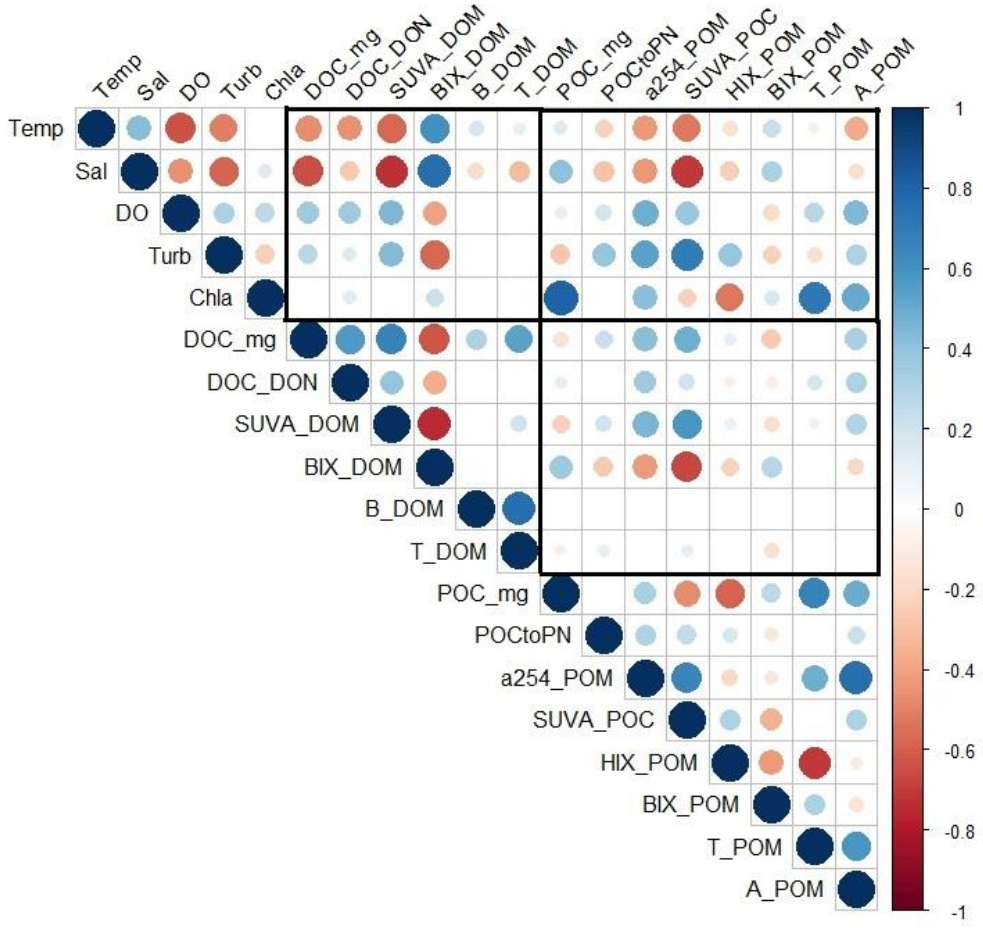

Figure A3.5. Correlation plot (Pearson's r^2) for environmental, DOM (square root transformed), and POM (square root transformed) data that were included in the subsequent multivariate analyses. Boxes divide parameters included into the three data sets (environmental, DOM, and POM).

Appendix 3.3: Principal component analysis results plotted by depth and location

In order to assess the relative importance of different temporal and spatial controls on samples collected from the Neuse River Estuary (NRE), data points plotted in principal component analysis (PCA) space were divided by season (see Chapter 3), depth (surface v. bottom) (Figure A3.6), and location in the estuary (upper, mid, lower) (Figure A3.7). Locations in the estuary

were designated as follows: Station 0 – 50 = upper estuary, Station 60 – 120 = mid-estuary, and Station 140 – 180 = lower estuary. Results are briefly discussed in Chapter 3. For depth, only the environmental parameters (as temperature, salinity, dissolved oxygen, chlorophyll-*a*, turbidity) showed any real difference between surface and bottom samples with surface samples clustered towards the high dissolved oxygen (DO), high chlorophyll-*a* (Chl *a*) region of the biplot, while bottom samples were characterized by low DO, low Chl *a* (Figure A3.6a). Neither the dissolved organic matter (DOM) nor particulate organic matter (POM) samples showed any variation with depth (Figure A3.6b-c).

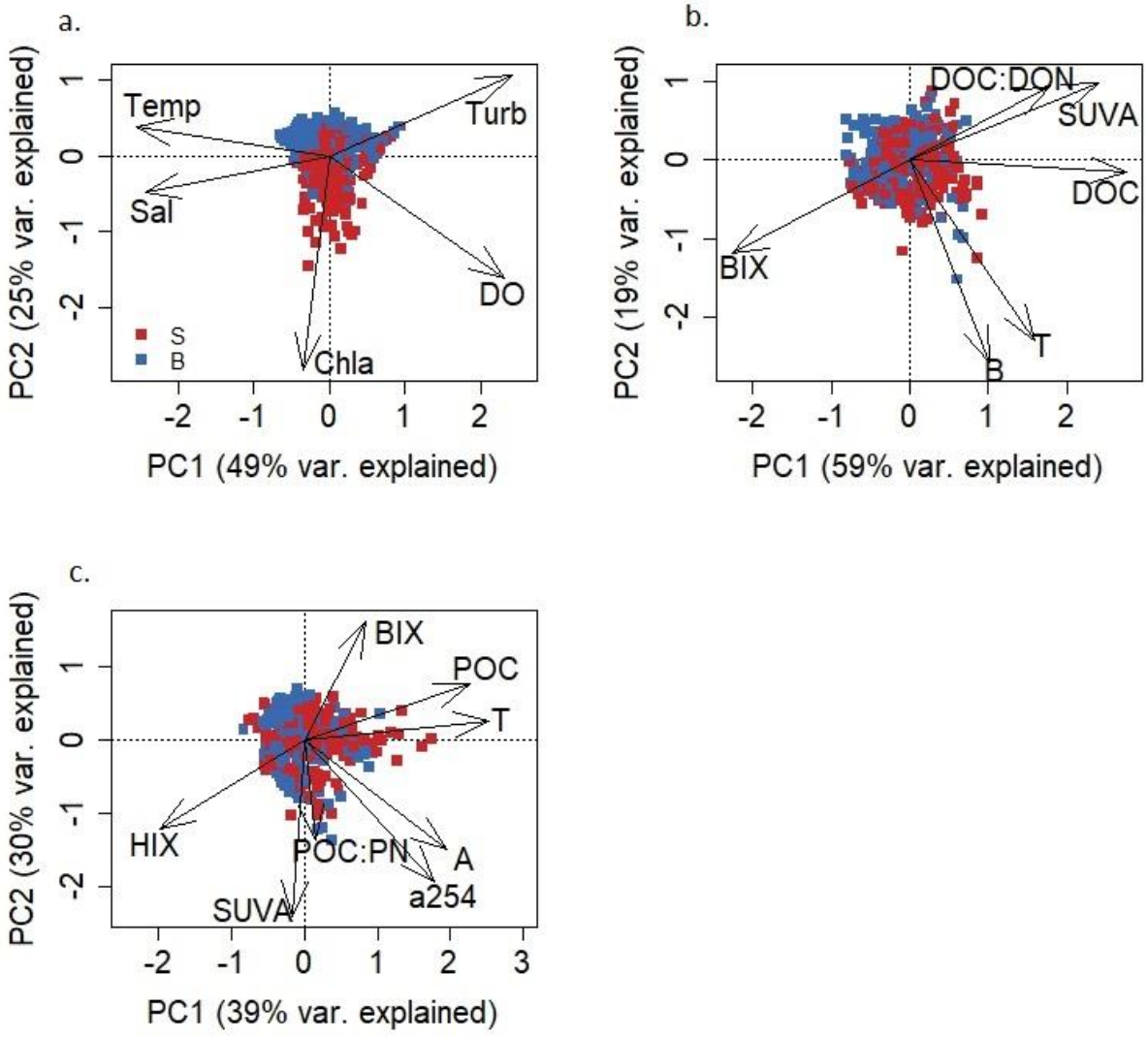

Figure A3.6. PCA results for the a. Environmental, b. DOM, and c. POM data sets. Points are plotted by depth.

For location in the estuary, only POM parameters exhibited any type of variation (Figure A3.7c). Upper estuary samples were clustered towards high terrestrial-like OM (HIX, $SUVA_{254}$) with mid- and lower-estuary samples clustered more towards autochthonous-like indicators of OM (BIX, Peak T). These results indicate a clear progression of POM from the upper estuary (more terrestrial-like, humic OM) to more autochthonous-like POM in the mid- to lower-estuary.

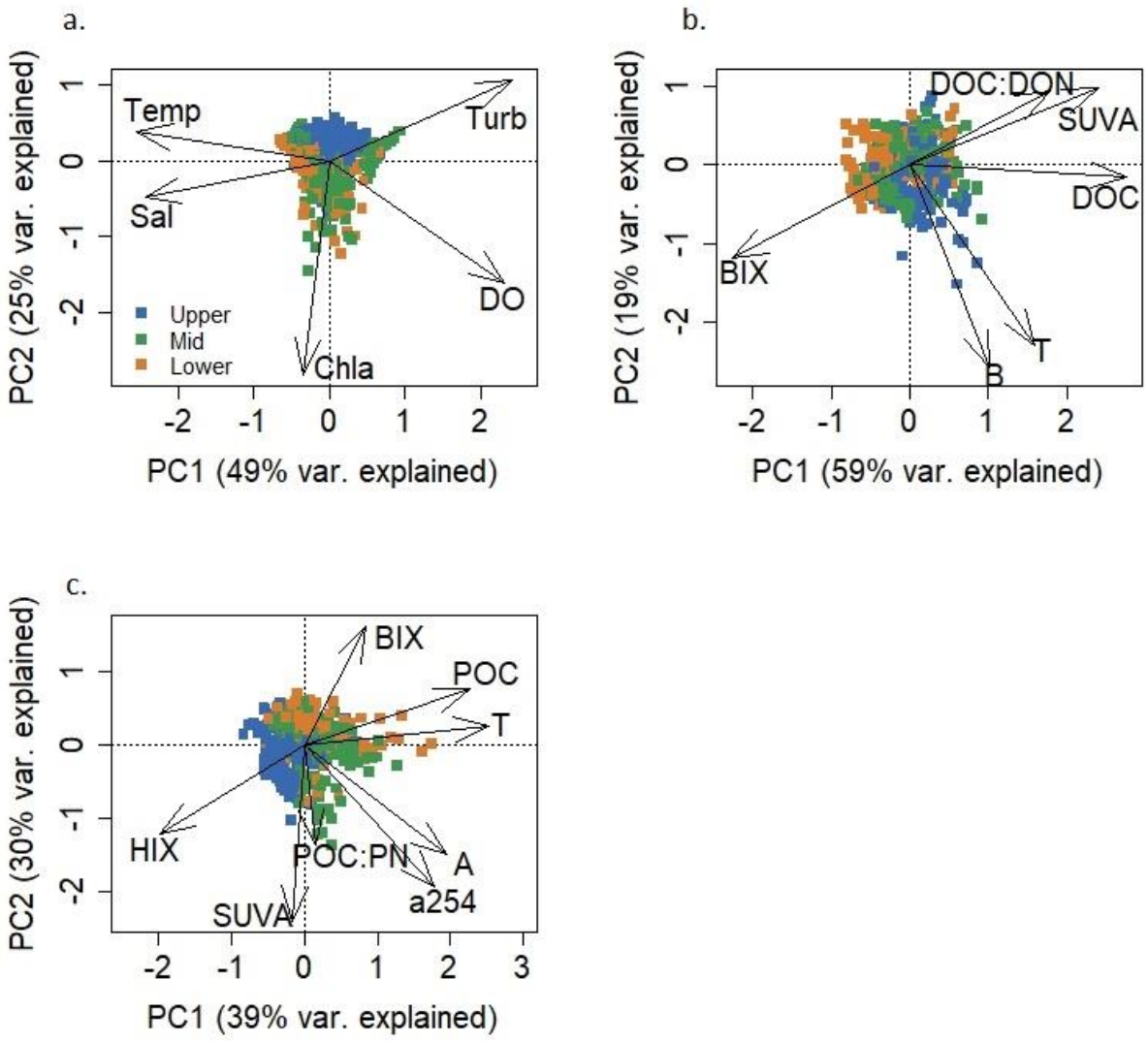

Figure A3.7. PCA results for the a. Environmental, b. DOM, and c. POM data sets. Points are plotted by location down the estuary.

Appendix 3.4: Principal component analysis incorporating wind direction

In order to assess the influence of wind events on OM quantity and quality in the NRE, wind speed, gusts, and direction were included in a subsequent PCA. ModMon parameters, designated as environmental, DOM, and POM were averaged over all depths (surface and bottom) and all stations (Station 0-180) for each ModMon time point. As with the previous PCA analysis, parameters were assessed for collinearity among each respective data set (environmental, DOM,

and POM). Parameters that were considered collinear ($r^2 > 0.80$) were removed prior to subsequent analyses.

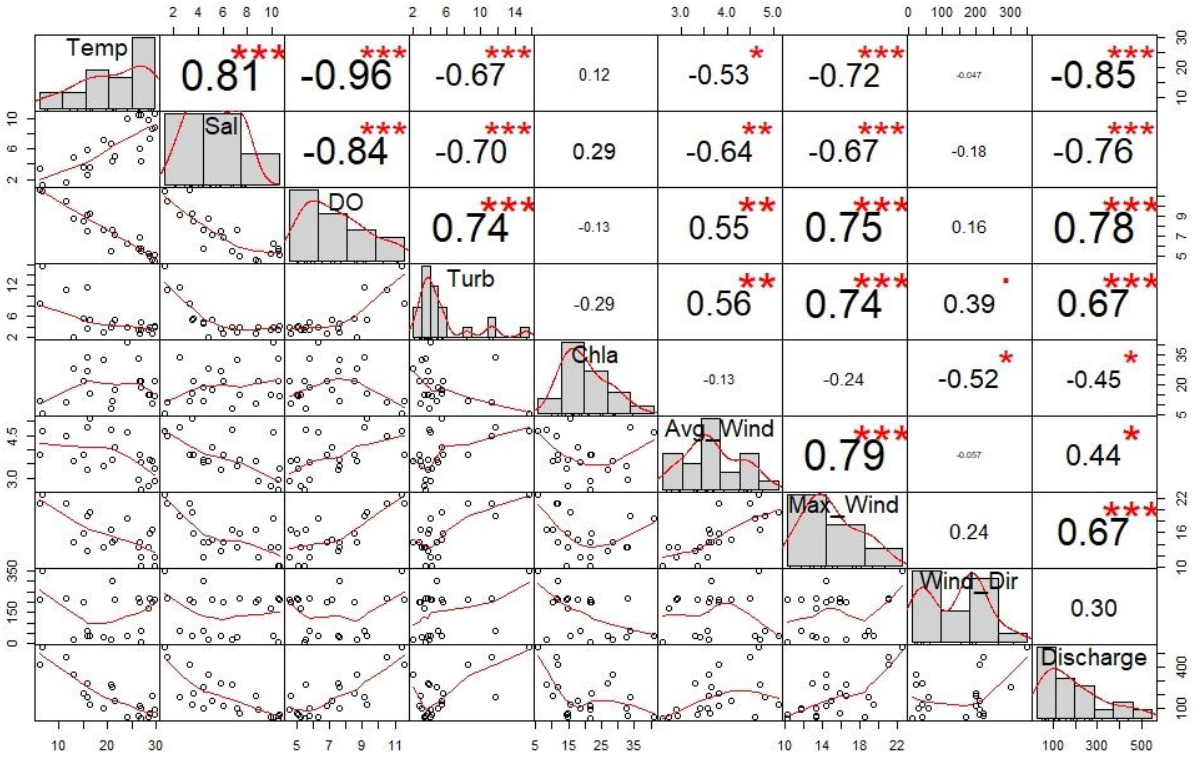

Figure A3.8. Correlation plot (Pearson's r^2) of environmental data collected from the NRE as averaged for each ModMon time point. Stars indicate significance. *** p = 0; ** p = 0.001; *** p < 0.001.

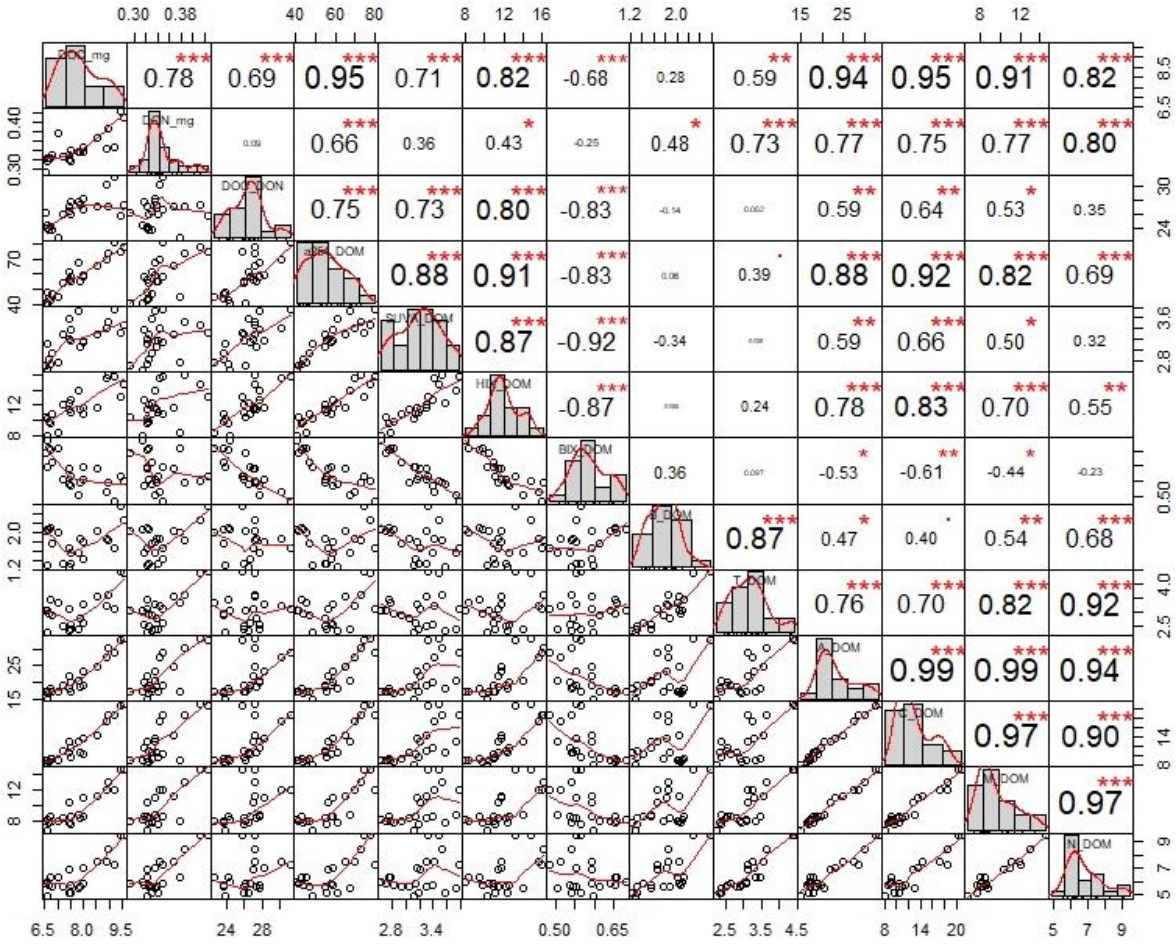

Figure A3.9. Correlation plot (Pearson's r^2) of DOM parameters collected from the NRE as averaged for each ModMon time point. Stars indicate significance. *** p = 0; ** p = 0.001; *** p < 0.001.

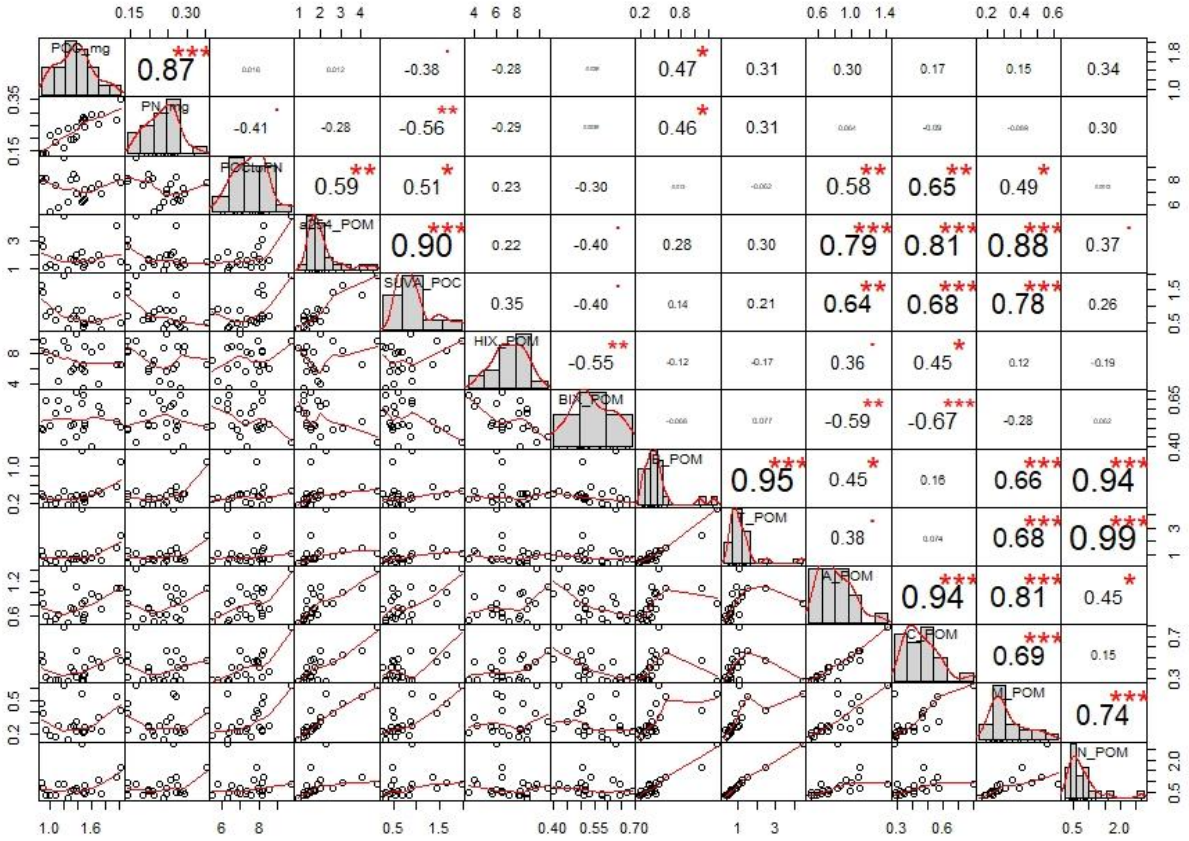

Figure A3.10. Correlation plot (Pearson's r^2) of POM parameters collected from the NRE as averaged for each ModMon time point. Stars indicate significance. *** p = 0; ** p = 0.001; *** p < 0.001.

After assessing individual data sets for collinearity, linear relationships between parameters associated with the three different data sets were assessed. Results are plotted in Figure A3.11 and included in Table A3.1. Results are discussed in Chapter 3.

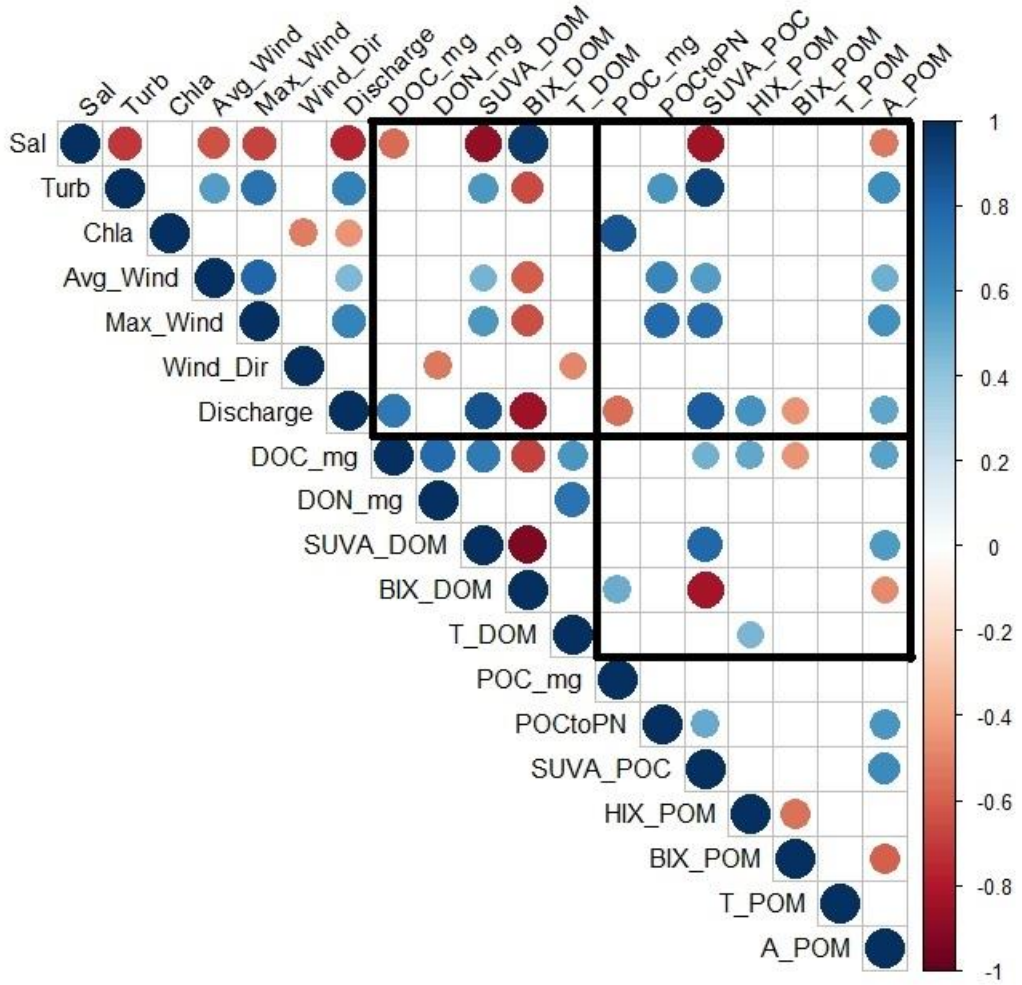

Figure A3.11. Correlation plot (Pearson's r^2) for environmental, DOM, and POM data that were included in the subsequent multivariate analyses. Boxes divide parameters included into the three data sets (environmental, DOM, and POM).

Table A3.1. Linear correlations (Pearson r^2) between all averaged ModMon variables included in subsequent PCA analysis. n.s. indicates a relationship that was not significant ($p > 0.05$).

	Turb	Chl *a*	Avg Wind	Max Wind	Wind Dir	Q	DOC	DON	SUVA D	BIX D	T DOM	POC	POC: PN	SUVA P	HIX P	BIX P	T POM	A POM
Sal	-0.70	n.s.	-0.64	-0.67	n.s.	-0.76	-0.57	n.s.	-0.87	0.96	n.s.	n.s.	n.s.	-0.84	n.s.	n.s.	n.s.	-0.52
Turb		n.s.	0.56	0.74	n.s.	0.67	n.s.	n.s.	0.57	-0.66	n.s.	n.s.	0.58	0.92	n.s.	n.s.	n.s.	0.62
Chl *a*			n.s.	n.s.	-0.52	-0.45	n.s.	n.s.	n.s.	n.s.	n.s.	0.86	n.s.	n.s.	n.s.	n.s.	n.s.	n.s.
Avg Wind				0.79	n.s.	0.44	n.s.	n.s.	0.47	-0.60	n.s.	n.s.	0.65	0.55	n.s.	n.s.	n.s.	0.48
Max Wind					n.s.	0.67	n.s.	n.s.	0.58	-0.65	n.s.	n.s.	0.77	0.76	n.s.	n.s.	n.s.	0.60
Wind Dir						n.s.	n.s.	-0.52	n.s.	n.s.	-0.48	n.s.	n.s.	n.s.	n.s.	n.s.	n.s.	n.s.
Q							0.71	n.s.	0.87	-0.85	n.s.	-0.55	n.s.	0.82	0.60	-0.44	n.s.	0.53
DOC								0.78	0.71	-0.68	0.59	n.s.	n.s.	0.47	0.52	-0.44	n.s.	0.53
DON									n.s.	n.s.	0.73	n.s.	n.s.	n.s.	n.s.	n.s.	n.s.	n.s.
SUVA D										-0.92	n.s.	n.s.	n.s.	0.78	n.s.	n.s.	n.s.	0.56
BIX D											n.s.	0.49	n.s.	-0.82	n.s.	n.s.	n.s.	-0.47
T DOM												n.s.	n.s.	n.s.	0.45	n.s.	n.s.	n.s.
POC													n.s.	n.s.	n.s.	n.s.	n.s.	n.s.
POC: PN														0.51	n.s.	n.s.	n.s.	0.58
SUVA P															n.s.	n.s.	n.s.	0.64
HIX P																-0.55	n.s.	n.s.
BIX P																	n.s.	-0.59
T POM																		n.s.

For PCA, wind direction data was used as both a numerical and categorical variable. PCA resluts when wind direction was included as a numerical variable are plotted below (Figure A3.12). Samples are plotted in PCA space by season. A discussion of results is included in Chapter 3.

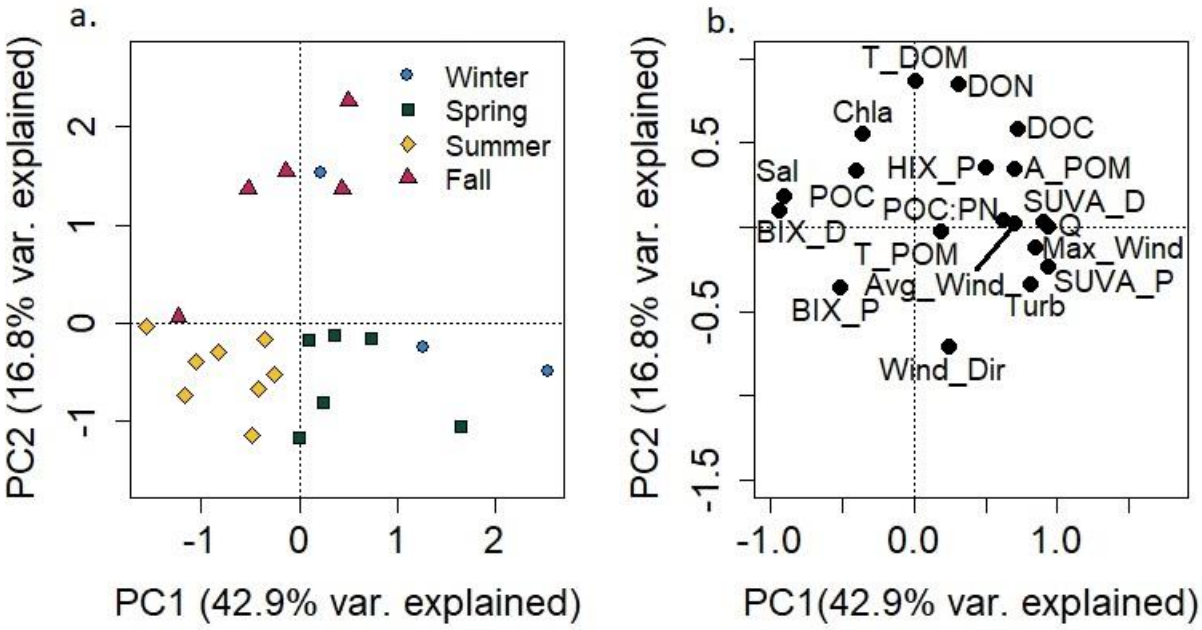

Figure A3.12. PCA results including wind direction and speed data. a. Sample loadings plotted by season and b. Variable loadings. Variables are indicated on the graph.

Appendix 3.5: Comparison between principal component analysis and non-metric multidimensional scaling results

In order to check data assumptions inherent to PCA (i.e., data normality, linear relationships between variables, no significant outliers), non-metric multidimensional scaling (nMDS) was conducted and the results of PCA and nMDS for each data matrix (environmental, DOM, POM) were compared using Procrustes analysis. Procrustes analysis rotates and transforms data to assess how similar the relative shapes of the two data sets are, in this case, how similar the shape is between PCA and nMDS results. For all data matrices, correlations between each of the PCA

and nMDS analyses, as calculated using Procrustes Analysis, were greater than 0.92 indicating the assumptions of PCA are appropriate for these data matrices (Environmental, DOM, POM).

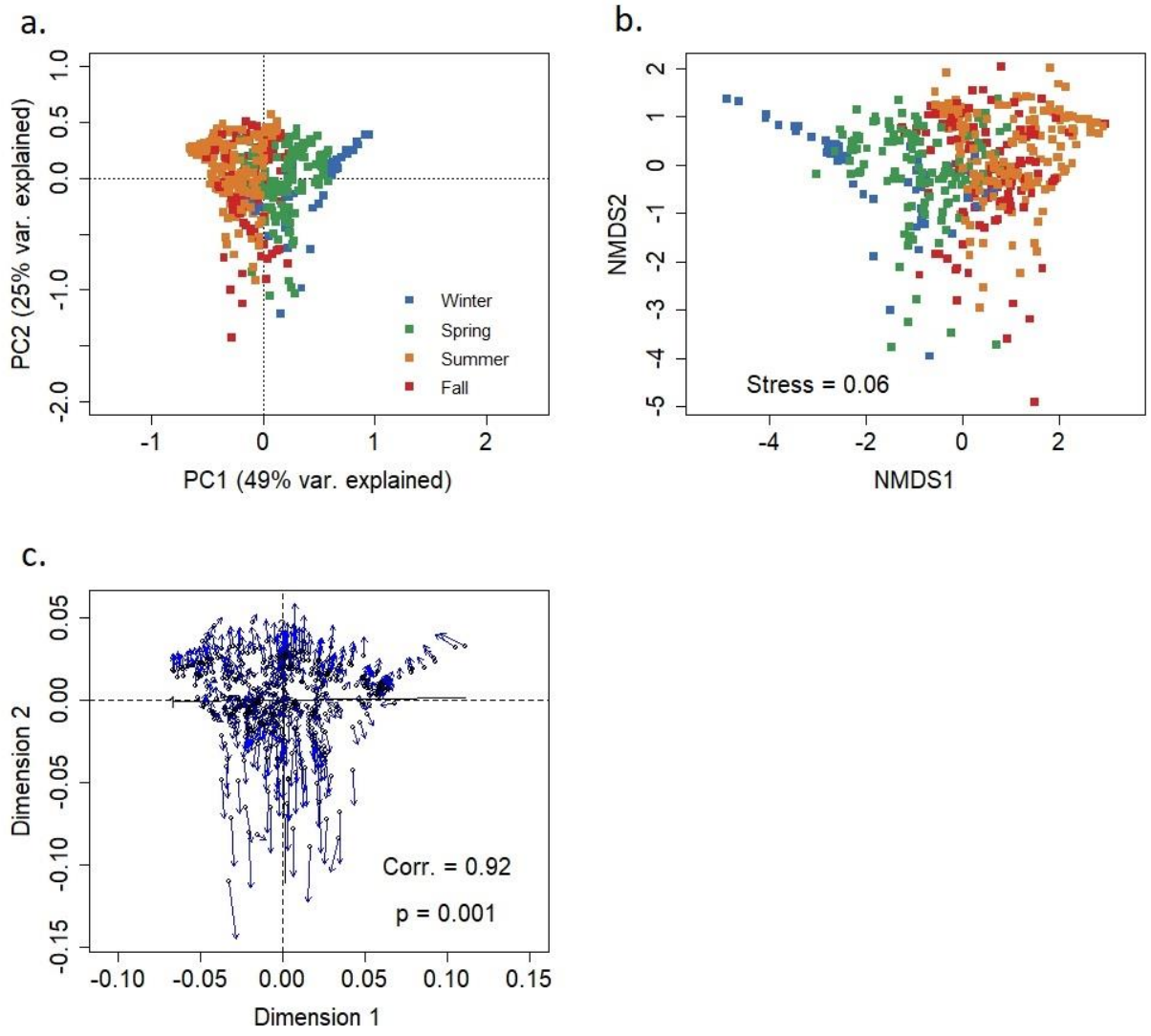

Figure A3.13. a. PCA of environmental data, b. nMDS results of environmental data and the nMDS stress (0.06), and c. Procrustes analysis comparing PCA and nMDS results for the environmental data along with the correlation coefficient (0.92) and the p-value (0.001). Samples are separated by season.

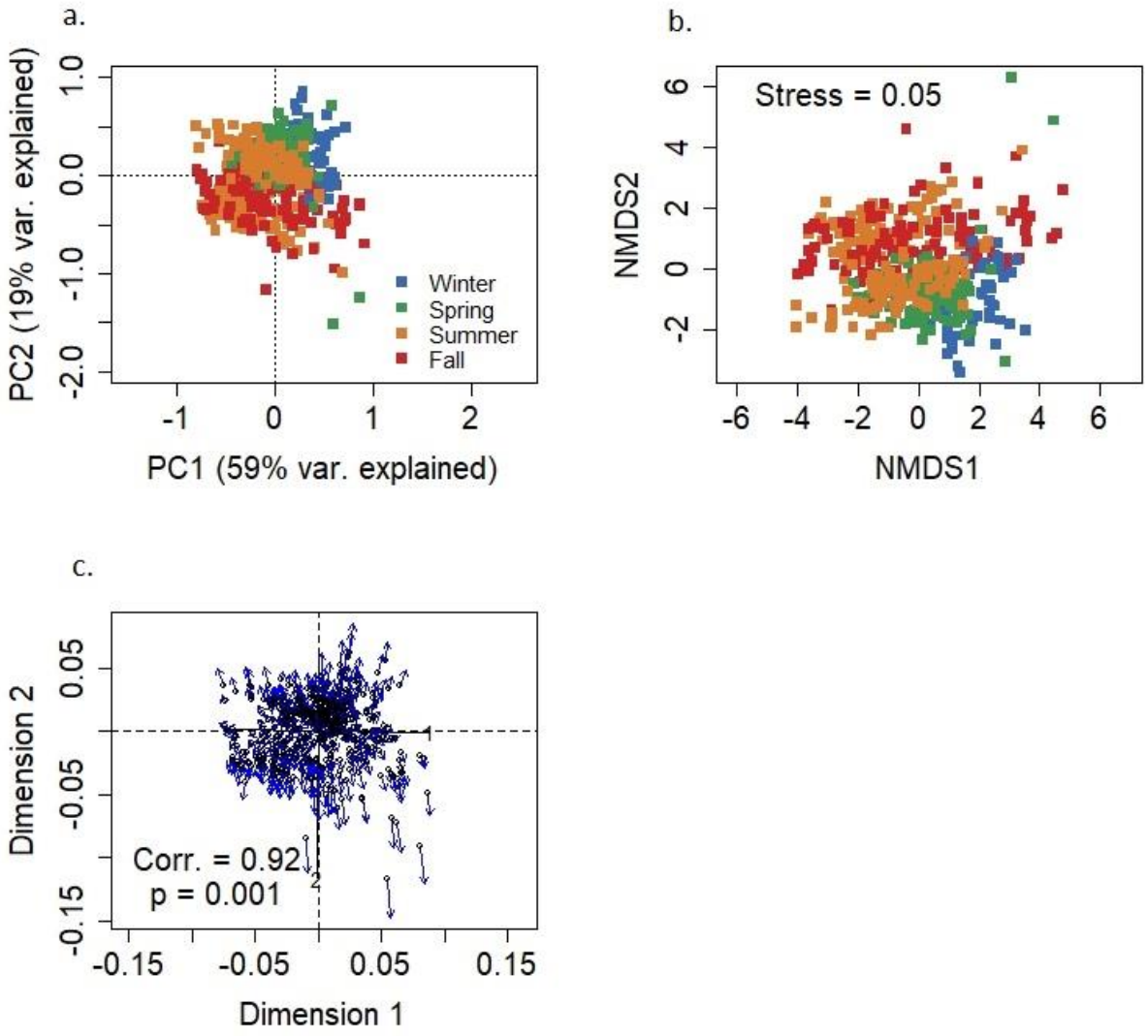

Figure A3.14. a. PCA of DOM data, b. nMDS results of DOM data and the nMDS stress (0.05), and c. Procrustes analysis comparing PCA and nMDS results for the DOM data along with the correlation coefficient (0.92) and the p-value (0.001). Samples are separated by season.

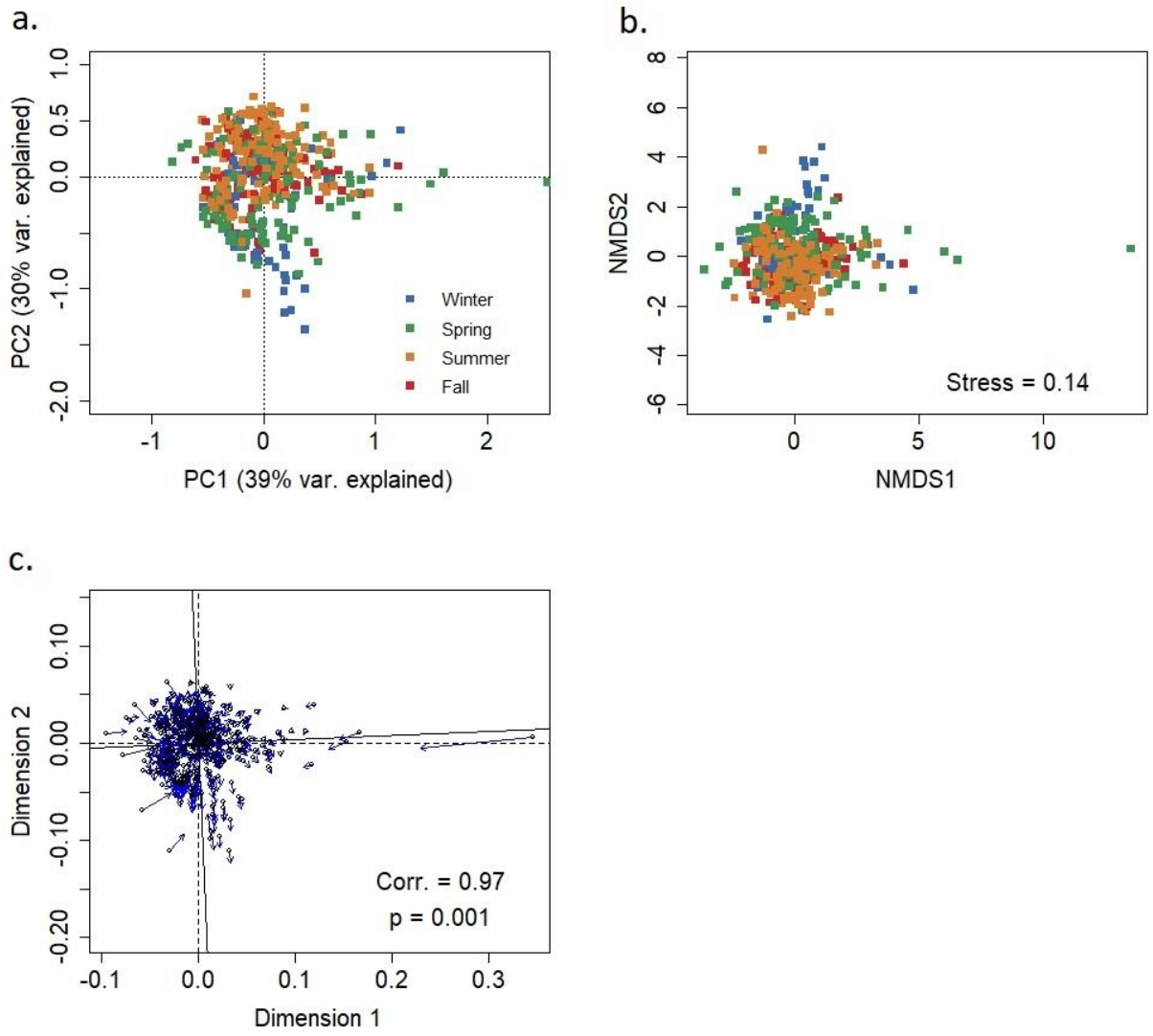

Figure A3.15. a. PCA of POM data, b. nMDS results of POM data and the nMDS stress (0.14), and c. Procrustes analysis comparing PCA and nMDS results for the POM data along with the correlation coefficient (0.97) and the p-value (0.001). Samples are separated by season.

Appendix 3.6: Co-inertia Analysis results for Environmental data vs. DOM and POM data matrices

In order to verify whether co-inertia analysis (CoIA) was an appropriate technique to compare data matrices and to provide a baseline for subsequent analyses, CoIA was conducted on both the environmental and DOM matrices and environmental and POM data matrices, respectively prior to the use of CoIA to compare the DOM and POM data matrices. The CoIA results for the environmental and the DOM and POM data matrices, respectively, were then compared to the

RDA results. See Chapter 3 for a description of CoIA and the plotted results. For both the DOM and POM data matrices, the correlation between the respective OM matrix and the environmental matrix was ~0.50, similar to the results obtained by RDA (Figure A3.16, A3.17). Therefore, it was assumed that CoIA was appropriate for relating two data matrices.

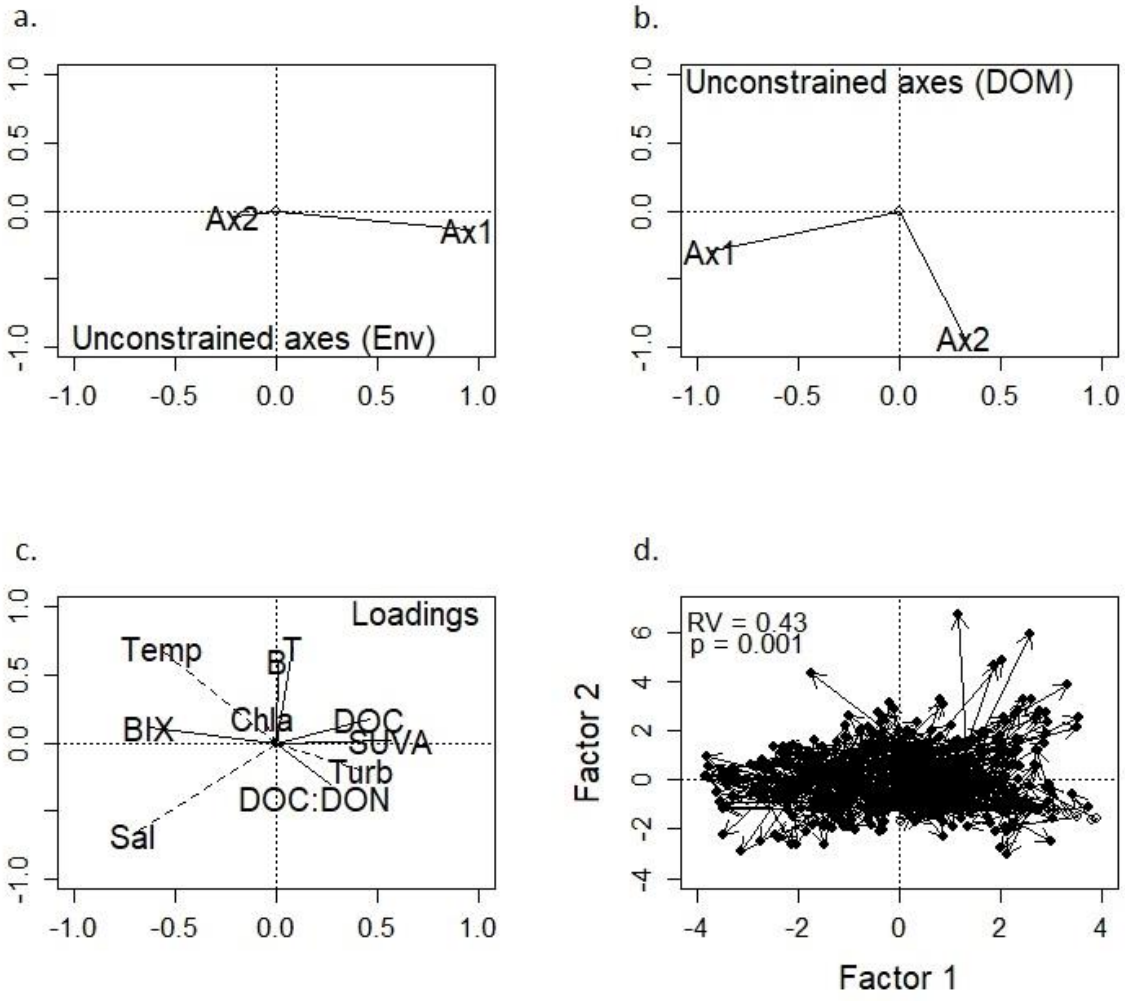

Figure A3.16. CoIA results for Environmental vs. DOM parameters. a. projection of Environmental parameter axes on the CoIA axes. b. projection of DOM parameter axes on the CoIA axes. c. projection of Environment (dashed lines) and DOM (solid lines) parameters in CoIA space. d. Projection of environmental parameters (open circles) with arrows indicating the direction and final location of the DOM parameters (closed circles) in CoIA space for each data point. The correlation (RV) between the two data sets is 0.46 and p = 0.001 as evaluated by permutation test.

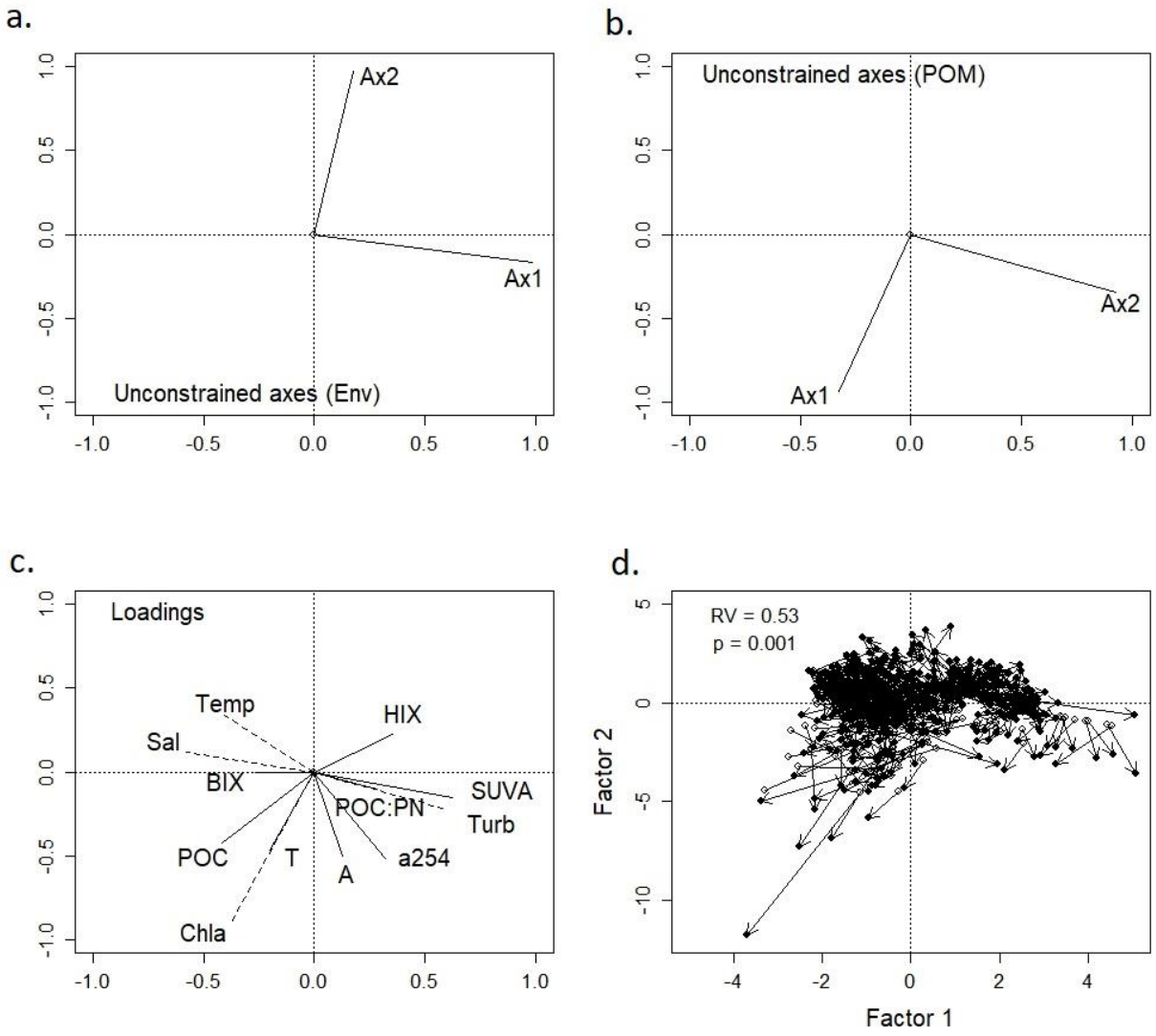

Figure A3.17. CoIA results for Environmental vs. POM parameters. a. projection of Environmental parameter axes on the CoIA axes. b. projection of POM parameter axes on the CoIA axes. c. projection of Environment (dashed lines) and POM (solid lines) parameters in CoIA space. d. Projection of environmental parameters (open circles) with arrows indicating the direction and final location of the POM parameters (closed circles) in CoIA space for each data point. The correlation (RV) between the two data sets is 0.53 and p = 0.001 as evaluated by permutation test.

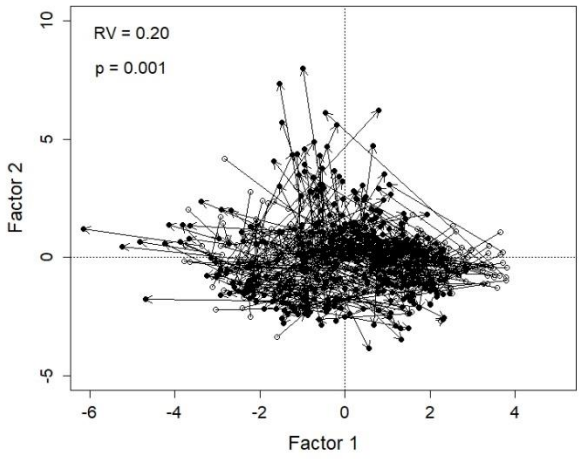

Figure A3.18. Projection of DOM parameters (open circles) with arrows indicating the direction and final location of the POM parameters (closed circles) in CoIA space for each data point. The correlation (RV) between the two data sets is 0.22 and p = 0.001 as evaluated by permutation test.

APPENDIX 4: CHAPTER 4 SUPPLEMENTARY INFORMATION

Appendix 4.1. Absorbance measurements

Table A4.0-1. Comparison between a_{350} as measured at UNC-CH IMS versus NCSU for selected samples Post-Matthew. Percent difference is calculated as the difference between NCSU and IMS samples divided by the average. NCSU samples were consistently higher than IMS samples with an average 11.33% difference.

Sample date	Station	IMS a_{350} (m^{-1})	NCSU a_{350} (m^{-1})	Percent difference
10-17-16	30S	24.9	30.1	19.0
10-17-16	180S	26.4	29.0	9.1
10-24-16	0S	33.9	34.5	2.0
11-01-16	100S	31.8	36.5	13.7
11-01-16	160S	22.8	28.2	21.2
11-08-16	120S	29.6	30.5	3.0

Appendix 4.2: ModMon sampling dates and C-parameters collected

Table A4.2. Dates of ModMon sampling dates and associated C-parameters collected. Stations at which parameters where collected are indicated in the brackets.

Date	C-parameters collected (stations)
7/20/2015	DOC (0-180); a_{350} (0-180); CO_2 (30-180)
8/3/2015	DOC (0-180); a_{350} (0-180); CO_2 (30-180)
8/17/2015	DOC (0-180); a_{350} (0-180); CO_2 (30-180)
8/31/2015	DOC (0-180); a_{350} (0-180); CO_2 (30-180)
9/14/2015	DOC (0-180); a_{350} (0-180); CO_2 (30-180)
9/29/2015	DOC (0-180); a_{350} (0-180); CO_2 (30-180)
10/12/2015	DOC (0-180); a_{350} (0-180); CO_2 (30-180)
10/29/2015	DOC (0-180); a_{350} (0-180); CO_2 (30-180)
11/17/2015	DOC (0-180); a_{350} (0-180); CO_2 (30-180)
12/8/2015	DOC (30-180); a_{350} (30-180); CO_2 (30-180)
1/20/2016	DOC (0-180); a_{350} (0-180); CO_2 (30-180)
2/17/2016	DOC (0-180); a_{350} (0-180); CO_2 (30-180)
3/7/2016	DOC (0-180); a_{350} (0-180); CO_2 (30-180)
3/22/2016	DOC (0-180); a_{350} (0-180); CO_2 (30-180)
4/6/2016	DOC (0-180); a_{350} (0-180)
4/19/2016	DOC (0-180); a_{350} (0-180); CO_2 (30-180)
5/9/2016	DOC (30-180); a_{350} (30-180); CO_2 (30-180)
5/24/2016	DOC (0-180); a_{350} (0-180)
6/6/2016	DOC (0-180); a_{350} (0-180)
6/20/2016	DOC (30-180); a_{350} (30-180); CO_2 (30-180)
7/6/2016	DOC (0-180); a_{350} (0-180); CO_2 (30-180)
7/18/2016	DOC (0-180); a_{350} (0-180); CO_2 (30-180)
8/3/2016	DOC (0, 30, 70, 100, 120, 160)
8/16/2016	DOC (0, 30, 70, 100, 120, 160); CO_2 (30-180)
9/7/2016	DOC (0, 30, 70, 100, 120, 160); CO_2 (30-180)
9/19/2016	DOC (0, 30, 70, 100, 120, 160)
10/3/2016	DOC (0-180); a_{350} (0, 30, 70-180); CO_2 (30-180)
10/17/2016	DOC (0-180); a_{350} (0-180); CO_2 (30-180)
10/24/2016	DOC (0-180); a_{350} (0-180)
11/1/2016	DOC (0-180); a_{350} (0-180)
11/8/2016	DOC (30-180); a_{350} (30-180)
11/15/2016	DOC (0-180); a_{350} (0-180)
11/28/2016	DOC (0-180); a_{350} (0-180)
12/13/2016	DOC (0-180); a_{350} (0-180)

Appendix 4.3. NRE Volumes and surface area

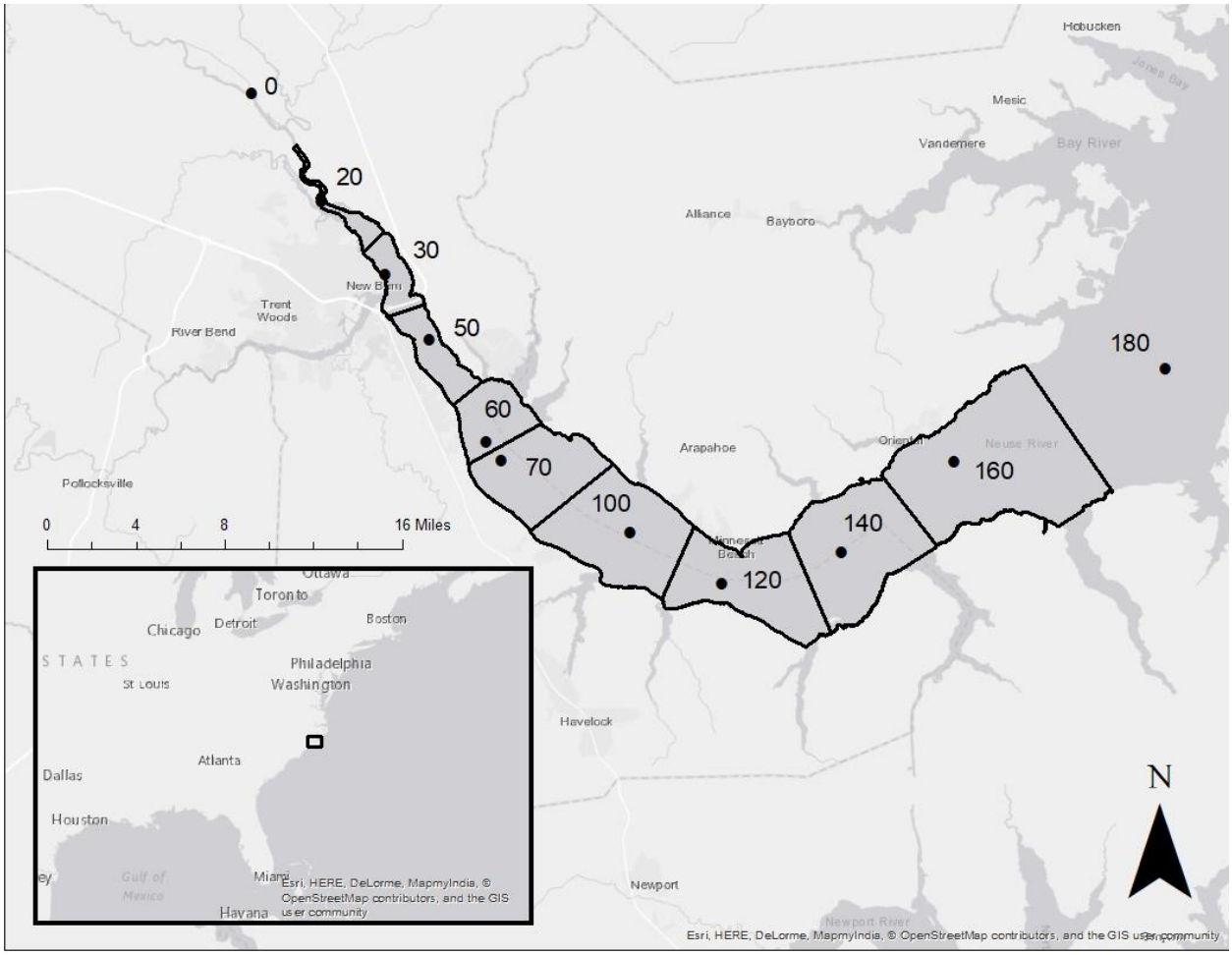

Figure A4.1. Designated NRE surface area and volumes used for volume weighted calculations and box modeling. Each box is centered at a ModMon station. Estuary surface area was calculated using data from the NC Division of Coastal Management, 2015 Estuarine Shoreline Mapping Project and estuary volumes were calculated using data from the NOAA bathymetry data.

Table A4.3. Surface area (m^2) and volume (m^3) of each designated NRE station used for associated calculations.

Station	Surface area (m^2)	Volume (m^3)
20	4.49×10^6	5.95×10^6
30	8.12×10^6	1.80×10^7
50	1.14×10^7	2.98×10^7
60	1.51×10^7	3.94×10^7
70	2.96×10^7	8.04×10^7
100	4.16×10^7	1.38×10^8
120	3.83×10^7	1.40×10^8
140	4.52×10^7	1.73×10^8
160	7.80×10^7	3.30×10^8
Total	2.72×10^8	9.55×10^8

Appendix 4.4: Salinity, DOC, and a_{350} box models:

4.4.1: Salinity box model:

A box model approach was used following Hagy et al., (2000) to calculate non-tidal estuarine flow (surface outflow; bottom inflow) in the NRE using freshwater inflow (i.e., Neuse River discharge) and salinity distributions (surface and bottom) as measured for each ModMon date (Figure S1). This box modeling approach allows for non-steady state assumptions of salinity in the estuary, which is an important qualification for the NRE where the estuary is not at steady state on short time scales (temporal scale of ModMon sampling dates, i.e., weeks) due to the high variability of river inflow. Therefore, it was advantageous to use an approach that accounts for this variability in salinity on short time scales.

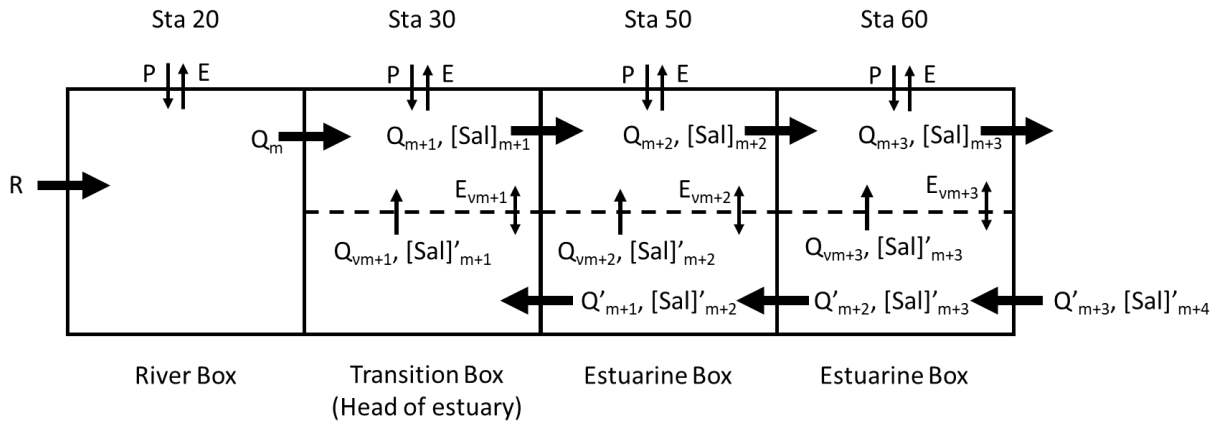

Figure A4.2 Generalized schematic of the box model approach used to calculate surface outflow and bottom water inflow for each river, transition and estuarine box in the NRE during each ModMon sampling date. R = river inflow (m^3 s^{-1}), P = precipitation (m), E = evaporation (m), Q_m = surface outflow, $[Sal]_m$ = surface salinity, Q_{vm} = upward advective flux, E_{vm} = non-advective flux, $[Sal]'_m$ = bottom salinity, Q'_m = bottom inflow.

For each ModMon sampling date, the estuary was divided into 9 boxes centered on stations 20-160. Non-steady state conditions were estimated by including a $\frac{\mathrm{d[Salinity]}}{\mathrm{dt}}$ term for each box to account for changing salinity between ModMon sampling points at each station. This term was multiplied by the volume of the respective box in order to convert units to m^3 s^{-1}. The head of the estuary was defined as the station where salinity and stratification were first detected. Specifically, the head of the estuary was defined as the station where surface or bottom water salinity was > 0.5 (i.e., salt was detected in the estuary) and where the difference between surface and bottom salinity was > 0.5 (i.e., the estuary showed signs of stratification). If the difference between surface and bottom salinity was < 0.5, then both surface and bottom salinity had to be > 0.5 for the station to be considered the head of the estuary. Stations above this defined point were designated as riverine stations such that there was no salt balance and therefore no estuarine circulation. The river discharge used as freshwater input for the box model was obtained from discharge measured at Ft. Barnwell, normalized to the amount of un-gaged watershed (0.31)

(Peierls et al., 2012), and averaged over the time period between the time of sampling and the previous ModMon sampling time point.

For the river box, inputs from the river were assumed to have a salinity of 0 (verified by Station 0 salinity measurements). Surface flow out of the river box was assumed to equal the river inflow plus precipitation and minus evaporation:

$$Q_m = R + P_m - E_m \quad (1)$$

where R is river inflow, P_m is precipitation, Q_m is surface flow out of the box, and E_m is evaporation. While we acknowledge the volume of each box changes with flow, this was not considered in the box model but is included in the variability used for volume (Appendix 5).

Evaporation and precipitation were obtained from the KEWN weather station at the New Bern, NC airport from the State Climate Office of NC located closest to Station 50. It was assumed evaporation and precipitation values obtained at this station were representative of the entire NRE. Each precipitation and evaporation value was multiplied by the area of each defined segment in the NRE as determined using ArcGIS polygon shapefiles obtained from the North Carolina Division of Coastal Management estuarine shoreline mapping project (NC Division of Coastal Management, 2015). The sizes of these areas were fixed and did not change as a function of river flow. As with the discharge data, the evaporation and precipitation data were summed over the time period between ModMon sampling dates.

The transition box represents the first box where salinity was detected in the estuary for each ModMon sampling date. In this box, the estuary is stratified with each station divided into a surface and bottom box. The following equation was used to calculate flow out of the surface transition box:

$$Q_{m+1} = Q_m + P - E$$

$$+ \frac{V'_{m+1} * \frac{d'_{s_{m+1}}}{dt} + V_{m+1} * \frac{d_{s_{m+1}}}{dt} + [Sal]_{m+1}(Q_m + P - E)}{[Sal]_{m+1} - [Sal]'_{m+2}} \quad (2)$$

where V_m is the volume of the surface box as calculated using NOAA bathymetry data in ArcMap 10.4, V_m' is the volume of the bottom box, dS_m is the change in salinity between ModMon runs for the surface box, dS_m' is the change in salinity between ModMon runs for the bottom box, dt is the time between ModMon runs, $[Sal]'_{m+1}$ is the bottom water salinity, and $[Sal]_{m+1}$ is the surface water salinity. Flow into the bottom transition box was calculated according to:

$$Q'_{m+1} = Q_{vm+1} \quad (3)$$

where Q_{vm+1} is the non-advective flux and is calculated as follows:

$$Q_{vm+1} = \frac{V'_{m+1} * \frac{d'_{s_{m+1}}}{dt} + V_{m+1} * \frac{d_{s_{m+1}}}{dt} + [Sal]_{m+1}(Q_m + P - E)}{[Sal]_{m+1} - [Sal]'_{m+2}} \quad (4)$$

The remaining boxes were designated as estuarine boxes and divided into surface and bottom boxes to account for estuarine stratification and two-layer flow. Surface flow out of each box was calculated according to:

$$Q_{m+2} = Q_{m+1} + P - E + (V_{m+2} * \frac{d_{s_{m+2}}}{dt} + V'_{m+2} * \frac{d'_{s_{m+2}}}{dt}$$

$$+ Q'_{m+1}([Sal]'_{m+2} - [Sal]'_{m+3}) + Q_{m+1}([Sal]_{m+2} - [Sal]_{m+1}) \quad (5)$$

$$+ \big((P - E) * [Sal]_{m+2}\big))/([Sal]'_{m+3} - [Sal]_{m+2})$$

Bottom flow into each box was calculated using:

$$Q'_{m+2} = Q_{m+1} + (V_{m+2} * \frac{d_{s_{m+2}}}{dt} + V'_{m+2} * \frac{d'_{s_{m+2}}}{dt} + Q'_{m+1}([Sal]'_{m+2} - [Sal]'_{m+3}) + Q_{m+1}([Sal]_{m+2} - [Sal]_{m+1}) + \big((P - E) * [Sal]_{m+2}\big))/([Sal]'_{m+3} - [Sal]_{m+2}) \quad (6)$$

95% confidence intervals were calculated by using randomly generated discharge, salinity, and volume percent variation (see Appendix 5) and initializing the model 1001 times.

4.4.2 DOC and a_{350} box model:

For DOC and a_{350} the estuary was treated as a single box spanning from the head of the estuary (Station 20) to the bottom of the estuary (Station 160) (Figure A4.3). As with the salinity box model, it was assumed the estuary was at non-steady state. The source & sink term for DOC and a_{350} was calculated as follows (OC represents either DOC or a_{350}):d[DOC]/dt was calculated as the change in volume weighted [DOC] concentration as measured in the NRE.

$$V_{estuary} * \frac{d[DOC]}{dt} = (R * [DOC]_R) + \big(Q'_{160B} * [DOC]'_{160B}\big) - (Q_{160S} * [DOC]_{160S}) + \text{Source \& Sink} \quad (7)$$

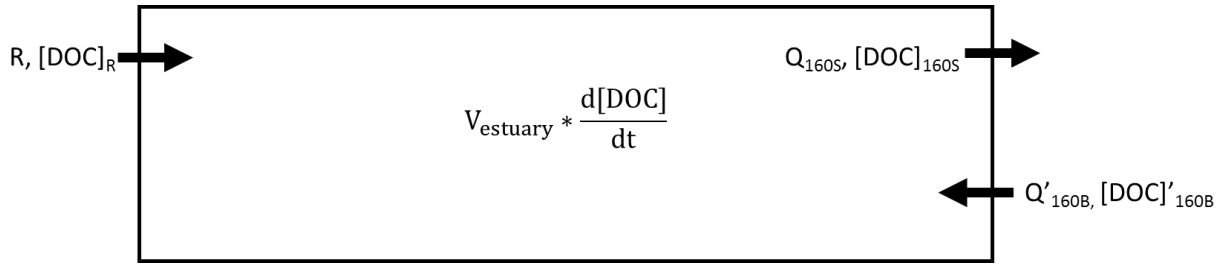

Figure A4.3. Representation of the one-box, non-steady state model used to estimate the OC source & sink term calculated for the NRE.

Appendix 4.5. Estimating the 95% confidence intervals

The 95% confidence intervals were determined for all calculations (salinity box model, DOC and a_{350} box model, and PP). Uncertainty was estimated for each measurement used during the respective calculations as described in Table A4.4. For spatial measurements collected in the estuary (Salinity, [DOC], a_{350}, PP), it was assumed the spatial variability from the single point measurement was within 13% of the true mean of that estuarine box as estimated for the nearby New River Estuary, NC (Paerl et al., 2012). A random number generator was used to calculate 1001 different, modeled measurements based on the measured value plus or minus the percent uncertainty estimated for each parameter. Each respective calculation was then conducted using the 1 measured and 1001 modeled parameters. Pivot confidence intervals (95%) were calculated to constrain the lower and upper bounds of uncertainty for the 1001 bootstrap values.

Table A4.4 Uncertainty as estimated for each parameter.

Measurement	Percent uncertainty	Calculated from
Discharge ($m^3 s^{-1}$)	± 14%	Estimated from Harmel et al., 2009
DOC (mg L^{-1})	± 13%	Combination of analytical uncertainty, estimated by averaging the percent relative standard deviation as calculated for 6 sets of triplicate samples (3%) as well as spatial uncertainty estimated by using a single [DOC] value to represent an entire estuarine box (13%).
a_{350} (m^{-1})	± 17%	Combination of analytical uncertainty, conservatively estimated from the average variability calculated between a_{350} measurements made at UNC-CH IMS vs. NCSU (11%) as well as spatial uncertainty estimated by using a single a_{350} value to represent the entire estuarine box (13%).
Estuarine volume (m^3)	± 10%	Estimated by assuming the water level in the NRE varies by 0.25 m around the mean (Luettich et al., 2000) multiplied by the surface area of the NRE. This was compared to the total volume of the estuary. The ±10% is an over-estimation to incorporate uncertainty in the NOAA bathymetry data.
Salinity (PSU)	± 13%	Estimated as spatial variability of using a single point measurement to estimate the entire estuarine box as estimated for the New River Estuary, NC (Paerl et al., 2012). This uncertainty was also used to constrain spatial uncertainty for DOC, a_{350}, and PP measurements.
Primary productivity (mg C m^3 hr^{-1})	± 14%	Combination of analytical uncertainty estimated from 321 triplicate samples as collected for primary productivity measurements during the study period (2015-2016) in the NRE (6%) as well as spatial uncertainty estimated by using a single PPR value to represent the entire estuarine box (13%).

Appendix 4.6. Location of rainfall in the Neuse River watershed

The Neuse River watershed covers an area of 14,066 km^2 representing a large area within central and eastern NC. Data for the total cumulative rainfall (mm) in the Neuse River watershed was obtained from NASA's Goddard Earth Sciences Data and Information Services Center (GES DISC) to visually assess the amount and location of precipitation accumulated in the watershed

over each discrete discharge event. Data were downloaded from NASA GES DISC via the Giovanni Visualization tool (NLDAS_FORA0125_H for accumulated precipitation in mm) (https://giovanni.gsfc.nasa.gov/giovanni/) and visualized in ArcMap 10.4. The figures were used to qualitatively describe where precipitation largely fell among the seven discrete discharge events and how this variability may contribute to the observed differences in DOC dynamics between these different designated discharge events.

Briefly, within the watershed, cumulative rainfall during the Baseline period in the upper NR basin was low (<130 mm), despite high rainfall totals (~ 400 mm) in the coastal region and over the NRE, most likely due to summer thunderstorm events. Joaquin was associated with elevated cumulative rainfall in the lower watershed (~ 200 mm) with low rainfall totals in the upper and mid-watershed (~ 130 mm). Pulse 1 was characterized by elevated rainfall in the mid to lower watershed (~ 200 mm) with maximum cumulative rainfall around Kinston, NC (~ 300 mm). Pulse 2 had lower cumulative rainfall amounts in the watershed (~ 130 mm) as compared to Pulse 1 and was followed by Pulse 3 which had elevated cumulative rainfall in the mid to lower NR watershed (~ 300 mm). This was followed by the Spring Q event which had lower cumulative rainfall amounts (~ 130 mm). Finally, Hurricane Matthew resulted in high cumulative rainfall totals in the mid watershed (~ 320 mm) with lower cumulative rainfall totals in the upper and lower watershed (~ 150 mm).

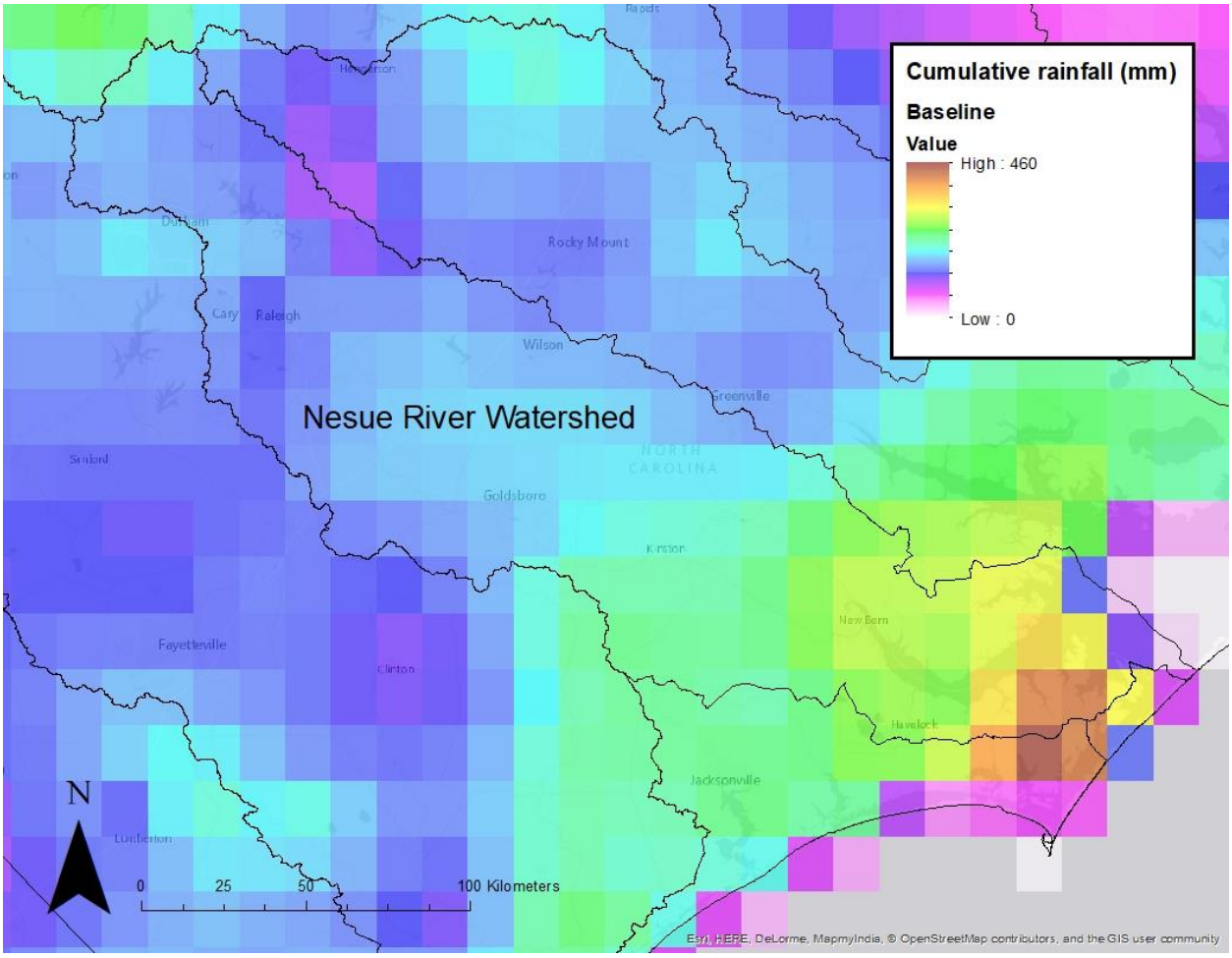

Figure A4.4. Total cumulative rainfall (mm) for the defined Baseline period (8/17/15 – 9/29/15). Watersheds are delineated by the black outlines. High cumulative rainfall is plotted in the warm colors; low cumulative rainfall is plotted in the cooler colors.

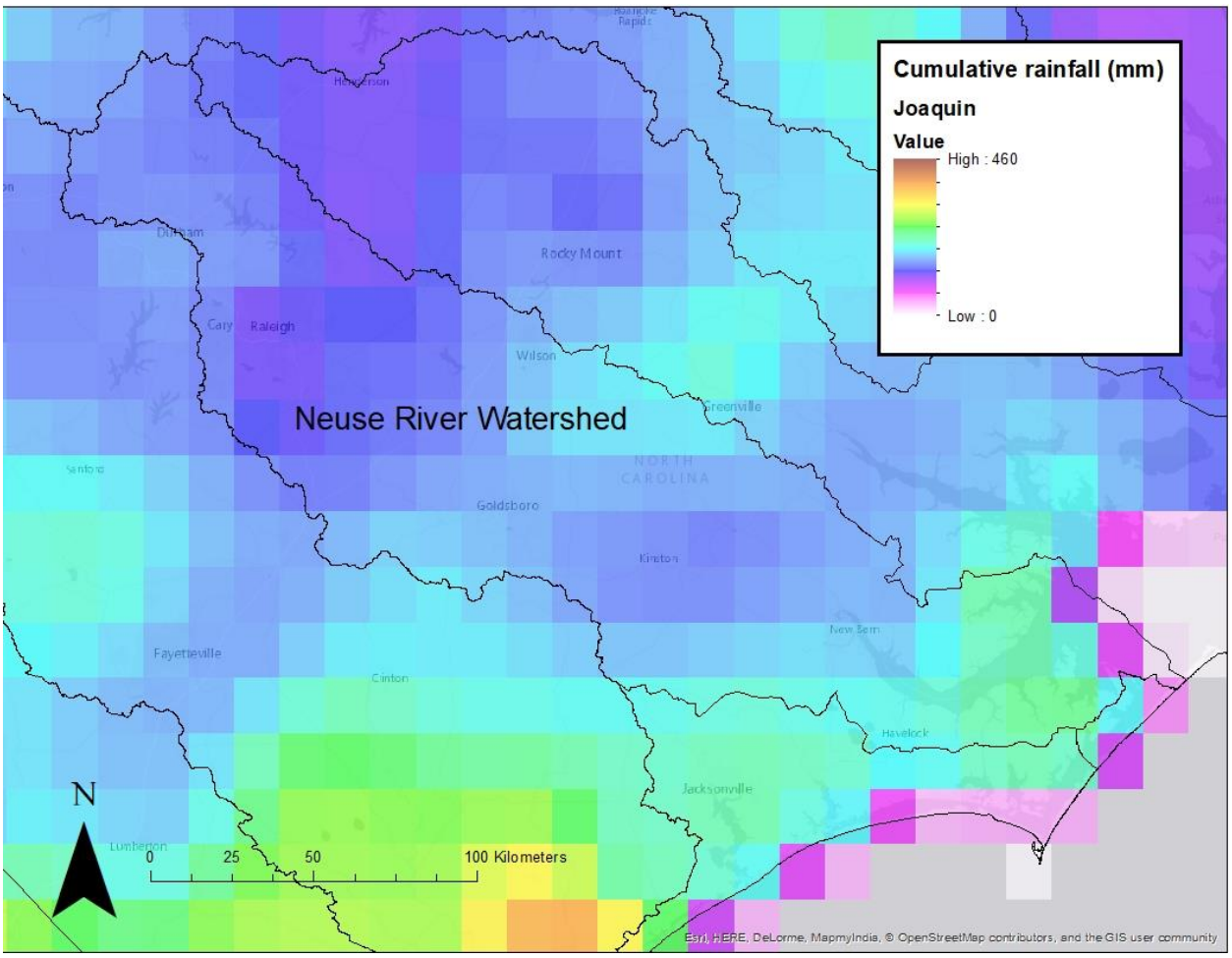

Figure A4.5. Total cumulative rainfall (mm) for Joaquin (9/29/15 – 10/29/15). Watersheds are delineated by the black outlines. High cumulative rainfall is plotted in the warm colors; low cumulative rainfall is plotted in the cooler colors.

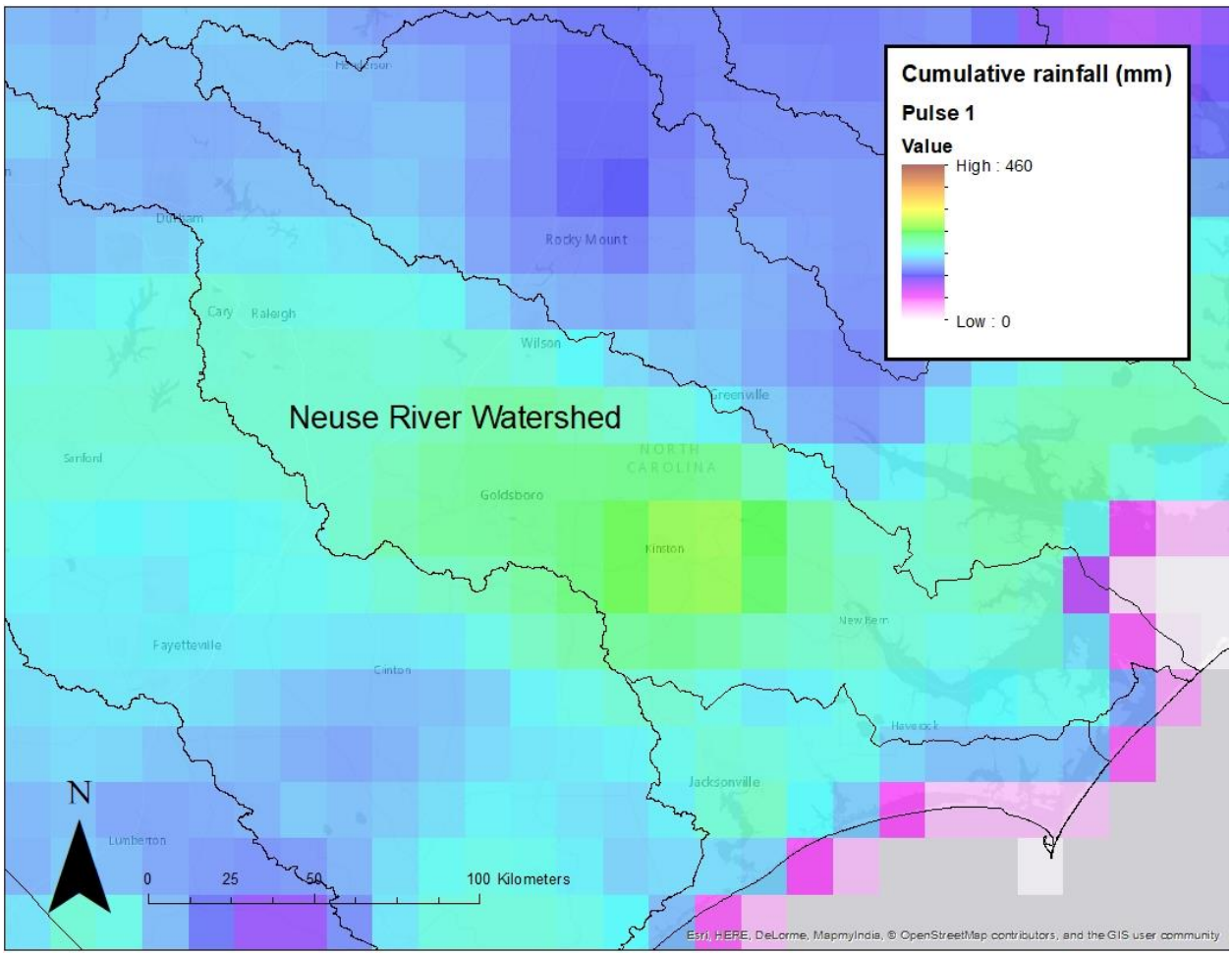

Figure A4.6. Total cumulative rainfall (mm) for Pulse 1 (10/29/15 – 12/08/15). Watersheds are delineated by the black outlines. High cumulative rainfall is plotted in the warm colors; low cumulative rainfall is plotted in the cooler colors.

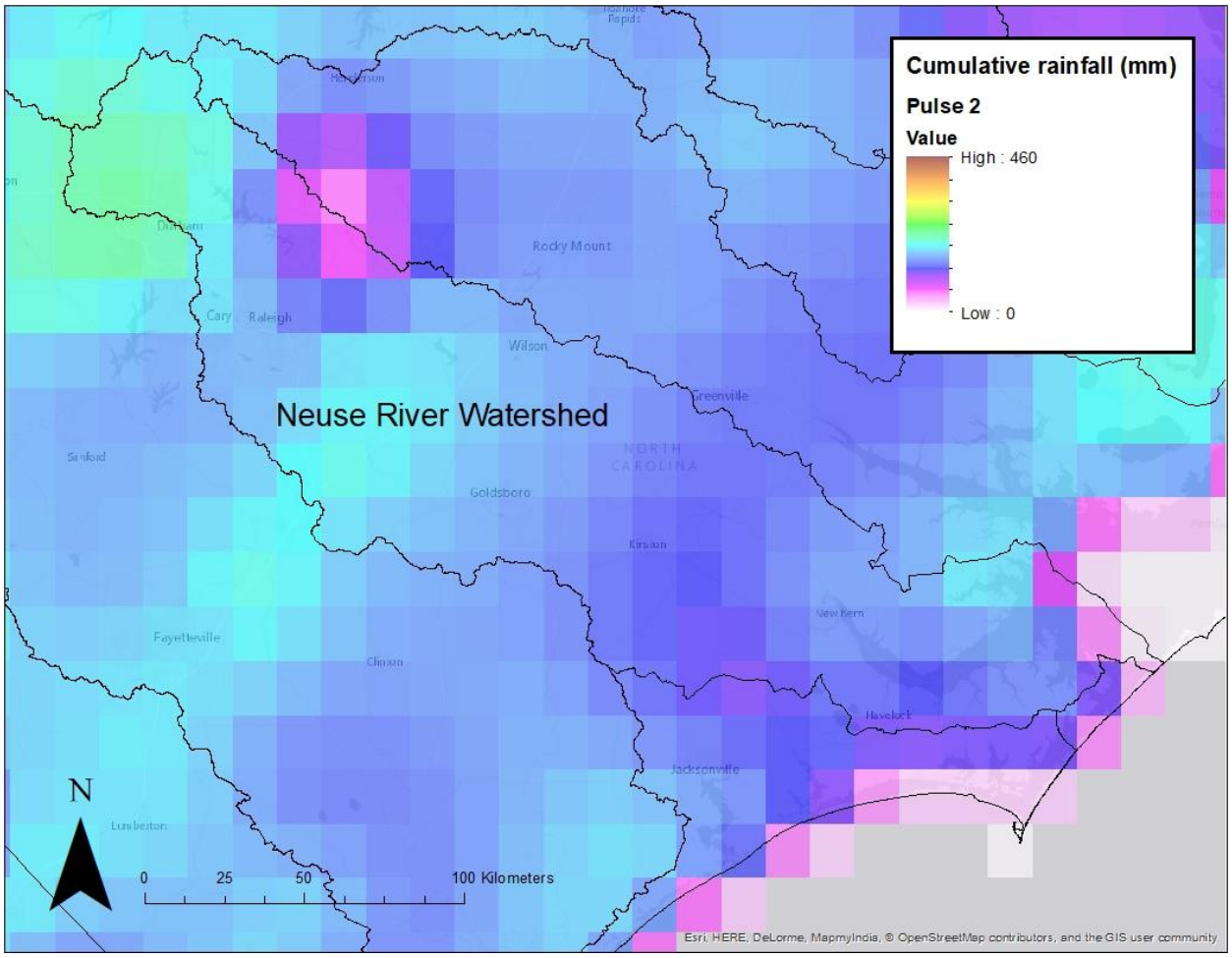

Figure A4.7. Total cumulative rainfall (mm) for Pulse 2 (12/08/15 – 01/20/16). Watersheds are delineated by the black outlines. High cumulative rainfall is plotted in the warm colors; low cumulative rainfall is plotted in the cooler colors.

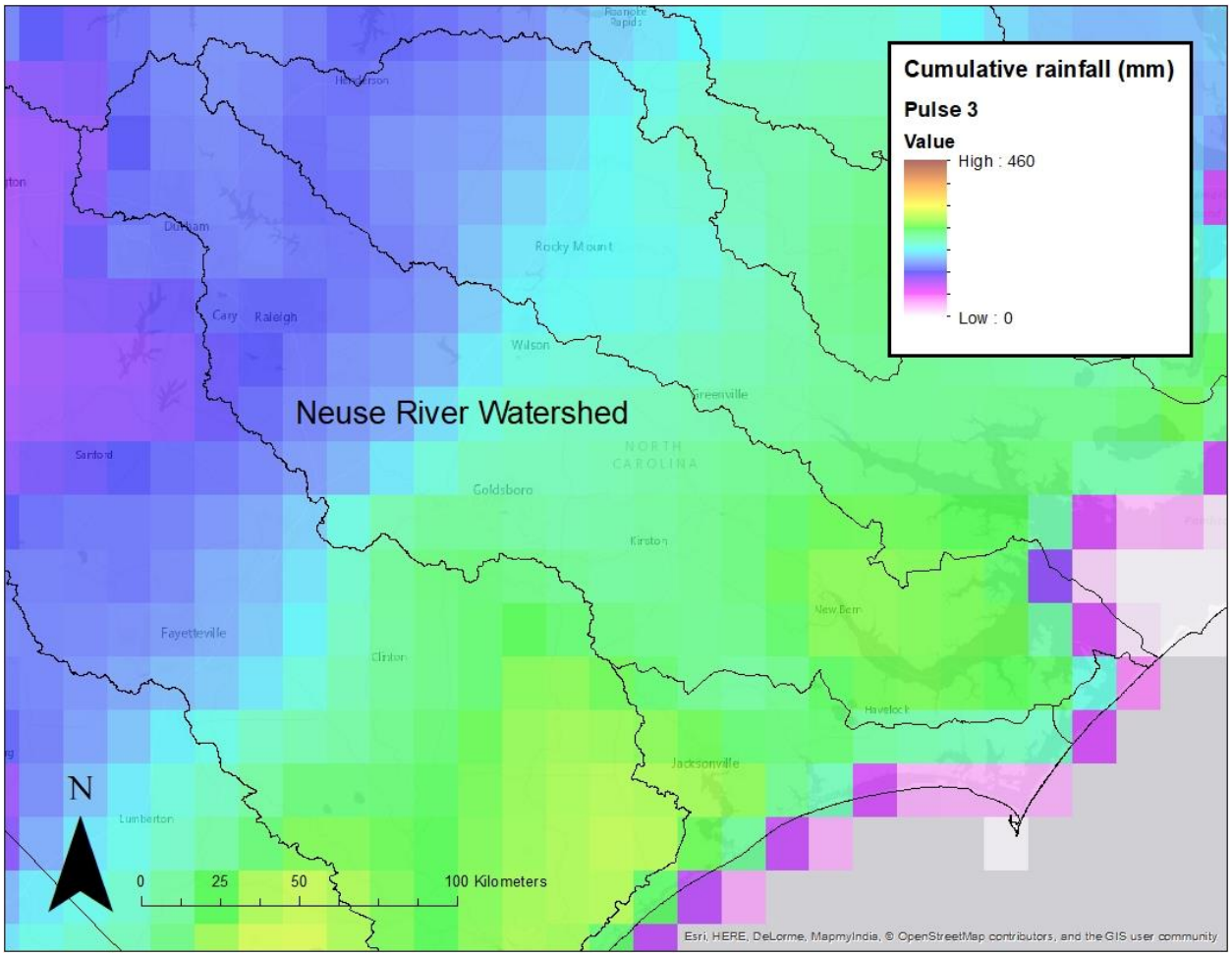

Figure A4.8. Total cumulative rainfall (mm) for Pulse 3 (01/20/16 – 03/07/16). Watersheds are delineated by the black outlines. High cumulative rainfall is plotted in the warm colors; low cumulative rainfall is plotted in the cooler colors.

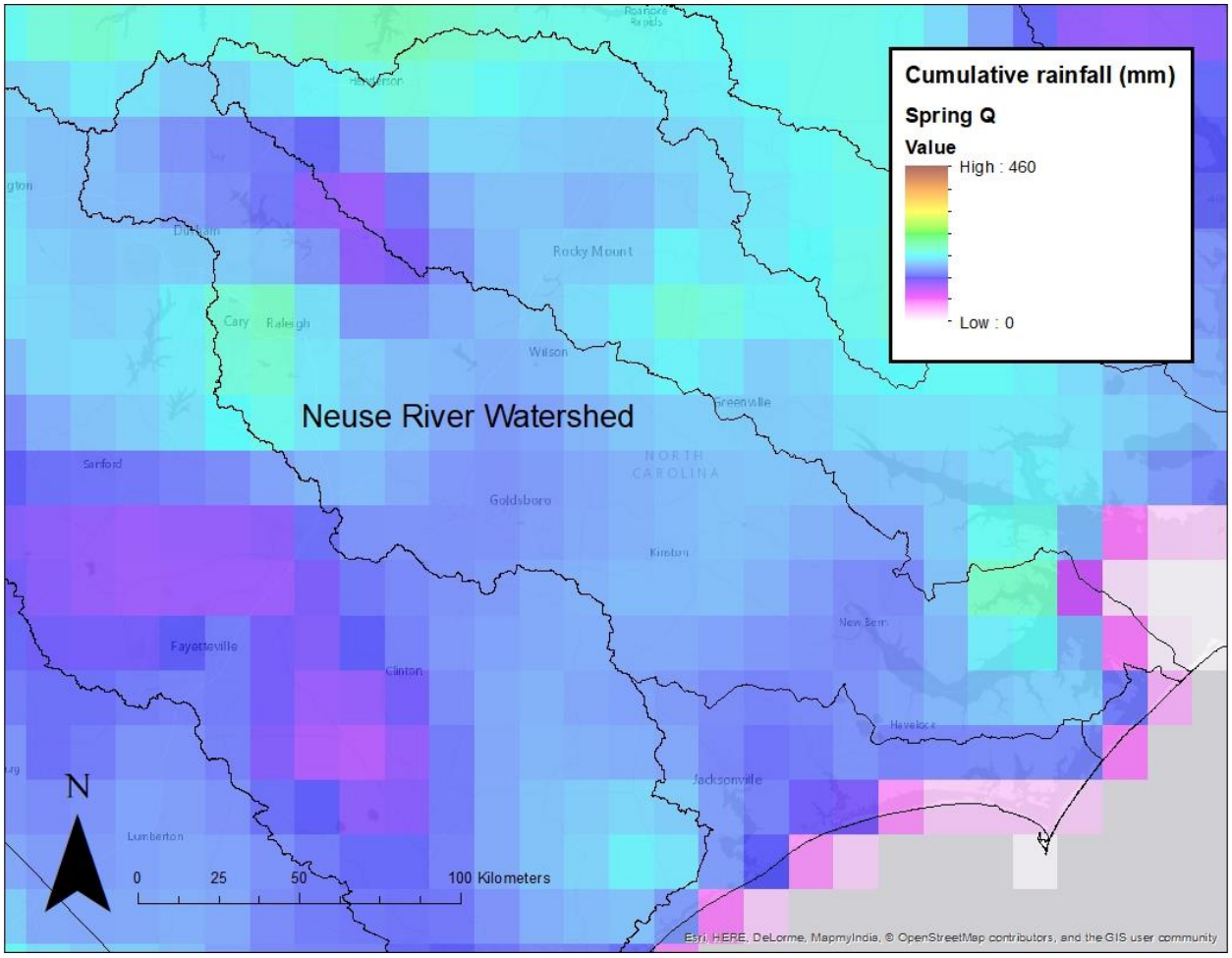

Figure A4.9. Total cumulative rainfall (mm) for Spring Q (04/19/16 – 05/24/16). Watersheds are delineated by the black outlines. High cumulative rainfall is plotted in the warm colors; low cumulative rainfall is plotted in the cooler colors.

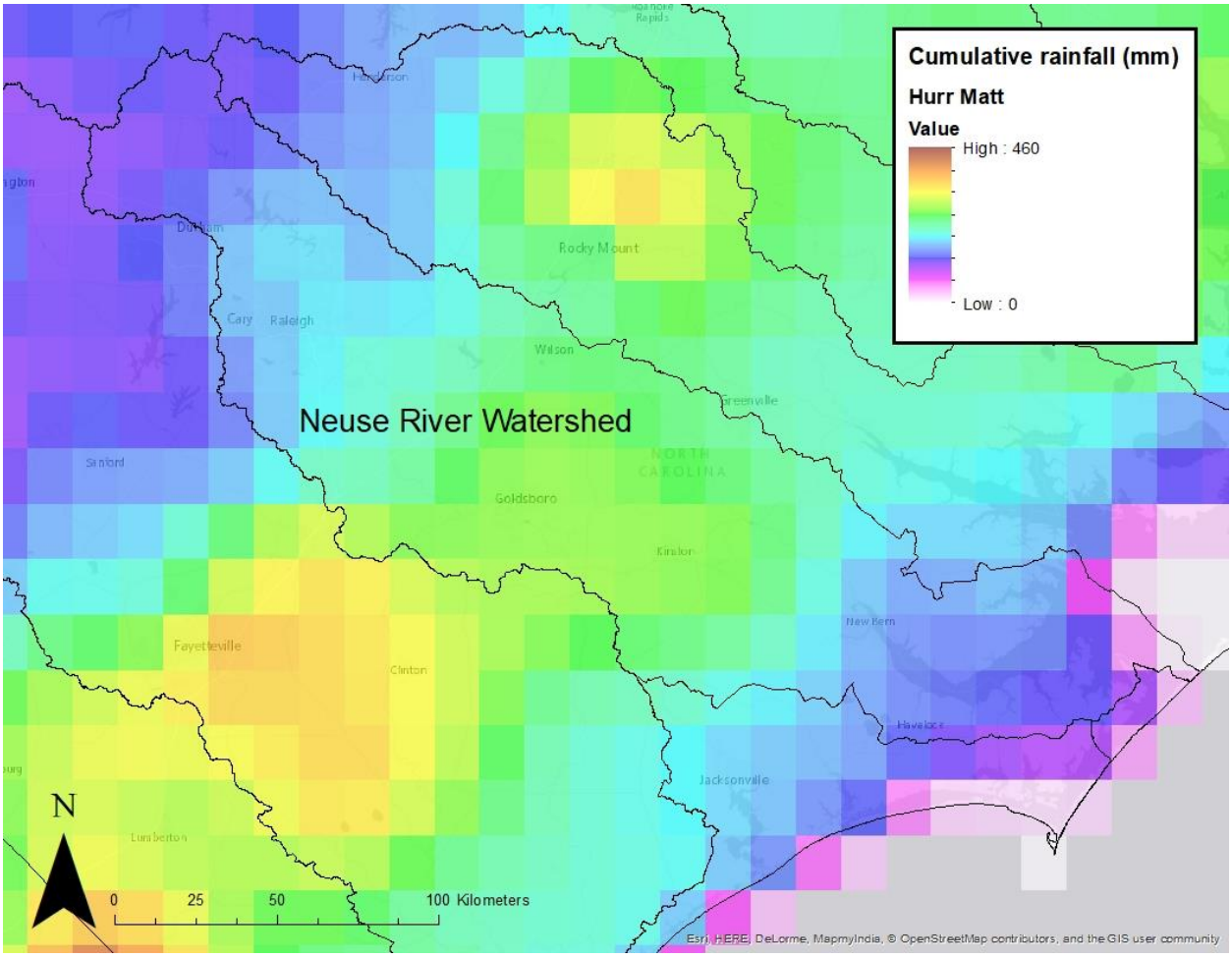

Figure A4.10. Total cumulative rainfall (mm) for Hurricane Matthew (10/03/16 – 11/15/16). Watersheds are delineated by the black outlines. High cumulative rainfall is plotted in the warm colors; low cumulative rainfall is plotted in the cooler colors.

Appendix 4.7. Estimate of pore water DOC stock in the NRE

The total amount of pore water DOC (kg) was estimated for the entire NRE using known sediment characteristics of the NRE (porosity, sediment area, depth of resuspension) and estimates for pore water [DOC] as measured in nearby US East Coast Estuaries (i.e., Chesapeake Bay). This provides a rough estimate for the relative role DOC stored in pore water may play as a source of DOC to the NRE, particularly under conditions when riverine DOC loading is low and wind speeds are elevated. The table below describes the values used, the sources of these values, and justification. By using these values we roughly estimate the pore water DOC stock in the NRE is about 1.66×10^5 kg.

Table A4.5. Parameters used to estimate the DOC stock in pore waters in the NRE.

Parameter	Value	Source	Justification
Porosity	0.8	Luettich et al., 2000	Porosity in the NRE ranges from 0.35-0.97 with 50% of sediments having a porosity > 0.8 and is characteristic of the silt/muds common in the NRE.
Sediment area	393×10^6 m^2	Luettich et al., 2000	Sediment area used for previous calculations in the NRE.
Sediment depth	0.022 m	Corbett, 2010	Conservative estimate for the depth of resuspension. Corbett, 2010 estimated 2.2 cm of sediment was re-suspended during a single event.
[DOC] in pore water	2 mM	Burdige et al., 2004	Measured pore water [DOC] in Chesapeake Bay sediments. This was used as a representative estimate for the [DOC] in NRE sediments.

Appendix 4.8. Volume weighted parameters

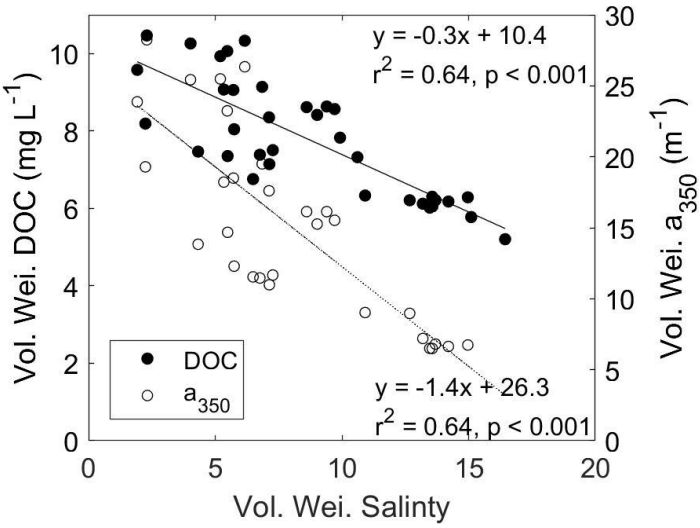

Figure A4.11. Volume weighted DOC (black circles; black line) and a_{350} (white circles; dotted line) plotted against volume weighted salinity. Linear regression equations, r^2, and p-values are displayed. Both volume weighted DOC and volume weighted a_{350} were negatively correlated with volume weighted salinity ($p < 0.001$).

Appendix 4.9. NRE wind conditions

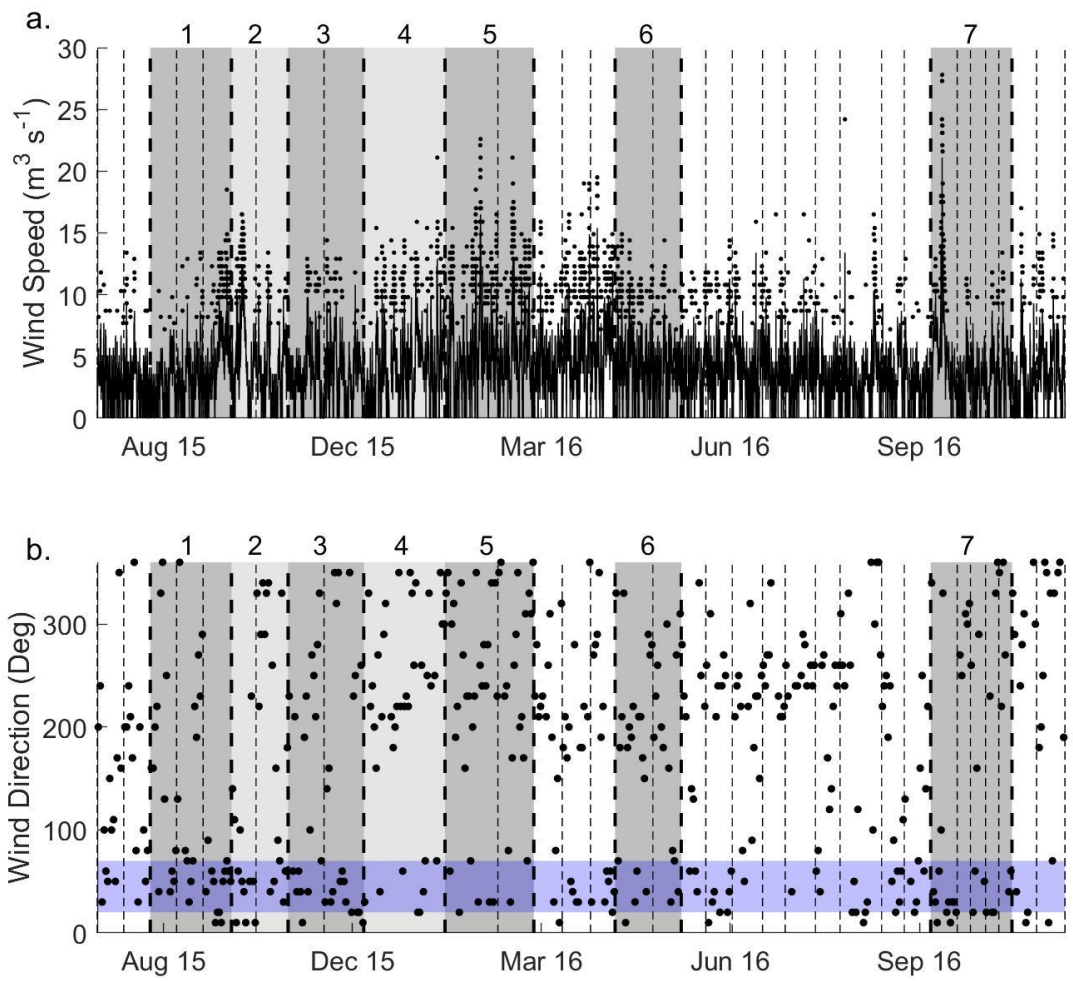

Figure A4.12. a. Wind speed (m^3 s^{-1}) and b. direction (deg) obtained from Havelock, NC (KNKT) for the study time period. Wind speed is plotted as the black line with wind gusts plotted as black circles. Vertical dashed lines indicate ModMon sampling dates while bolded dashed lines indicate the bounds of the 7 discrete discharge events. For wind direction, the blue shaded area represents NE winds (20-70º). Data used was obtained from the NC Climate Office.

REFERENCES

Burdige, D.J., Kline, S.W., Chen, W., 2004. Fluorescent dissolved organic matter in marine sediment pore waters. Marine Chemistry 89, 289–311. https://doi.org/10.1016/j.marchem.2004.02.015

Corbett, D.R., 2010. Resuspension and estuarine nutrient cycling: Insights from the Neuse River Estuary. Biogeosciences 7, 3289–3300. https://doi.org/10.5194/bg-7-3289-2010

Luettich, R.A., McNinch, J.E., Paerl, H.W., Peterson, C.H., Wells, J.T., Alperin, M.J., Martens, C.S., Pinckney, J.L., 2000. Neuse River Estuary modeling and monitoring project stage 1: hydrography and circulation, water column nutrients and productivity, sedimentary processes and benthic-pelagic coupling, and benthic ecology. Technical Report No. 2000-325B. NC Water Research and Resources Institute, Raleigh, NC, Unpublished.

NC Division of Coastal Management, 2015. Estuarine Shoreline Mapping Project [WWW Document]. URL https://deq.nc.gov/about/divisions/coastal-management/coastal-management-estuarine-shorelines/stabilization/estuarine-shoreline-mapping-project (accessed 1.14.18).

Paerl, H.W., Hall, N.S., Peierls, B.L., Rossignol, K.L., Joyner, A.R., Otten, T., Reckhow, K.H., Nojavan, F., 2012. Chapter 3: Develop and deploy microalgal indicators as measures of water quality, harmful algal bloom dynamics, and ecosystem condition. SERDP Project Report Number: RC-1413, Aquatic/Estuarine Module, Research Project AE-1.

Peierls, B.L., Hall, N.S., Paerl, H.W., 2012. Non-monotonic Responses of Phytoplankton Biomass Accumulation to Hydrologic Variability: A Comparison of Two Coastal Plain North Carolina Estuaries. Estuaries and Coasts 1–17. https://doi.org/10.1007/s12237-012-9547-2

APPENDIX 5: CHAPTER 5 SUPPLEMENTARY INFORMATION

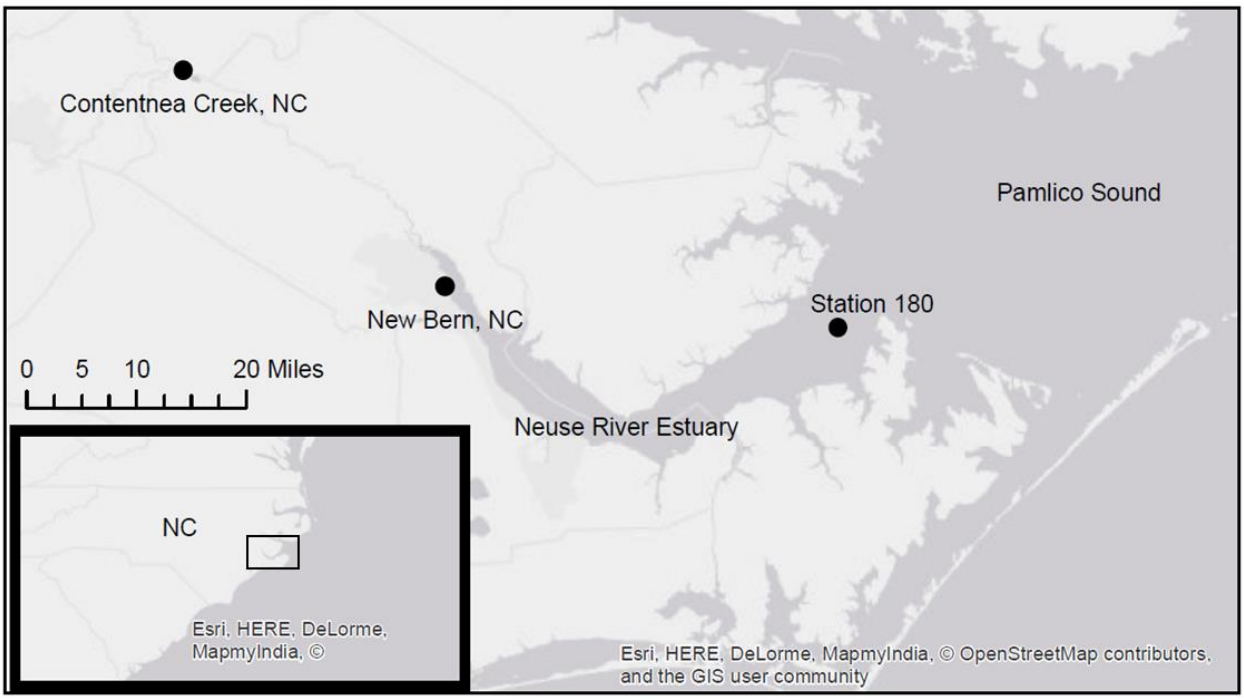

Figure A5.1. Map of the Neuse River Estuary (NRE) and the Pamlico Sound located in eastern North Carolina, USA. Station 180 indicates the location where water was collected for all three bioassays. For the July 2015 bioassay, river DOM was collected from Contentnea Creek and concentrated prior to addition. New Bern, NC is labeled for reference.

Table A5.1. Initial conditions of incubation water used for each bioassay: June 2014, October 2014, and July 2015. Nitrate + nitrite (NO_x) was below detection for all sampling dates.

Date Collected	June 16, 2014	October 13, 2014	July 20, 2015
Temperature (C°)	27.19	22.72	29.05
Salinity (PSU)	11.89	12.74	17.02
Chlorophyll *a* (µg L^{-1})	21.94	20.68	10.07
NH_4 (µg N L^{-1})	13.2	5.4	9.6
DON (µg N L^{-1})	261	313	244
PO_4 (µg P L^{-1})	7.2	12.5	23.5
Discharge (ft^3 s^{-1})	2,240	2,530	982

Table A5.2. DOM additions for each bioassay, mL of each DOM addition added, and the % of total volume the addition constituted. The effluent treatment resulted in significant dilution of the NRE incubation water. The coupled effluent, inorganic nutrient treatment contained a dilution treatment to account for this.

DOM treatment	mL added	% of total volume (4L)
June 2014, Chicken Litter (1:100 Dilution)	20	0.5%
June 2014, Effluent	740	18.5%
October 2014, Chicken Litter (1:100 Dilution)	10	0.25%
October 2014, Turkey Litter (1:100 Dilution)	6	0.15%
July 2015, River DOM	65	1.625%

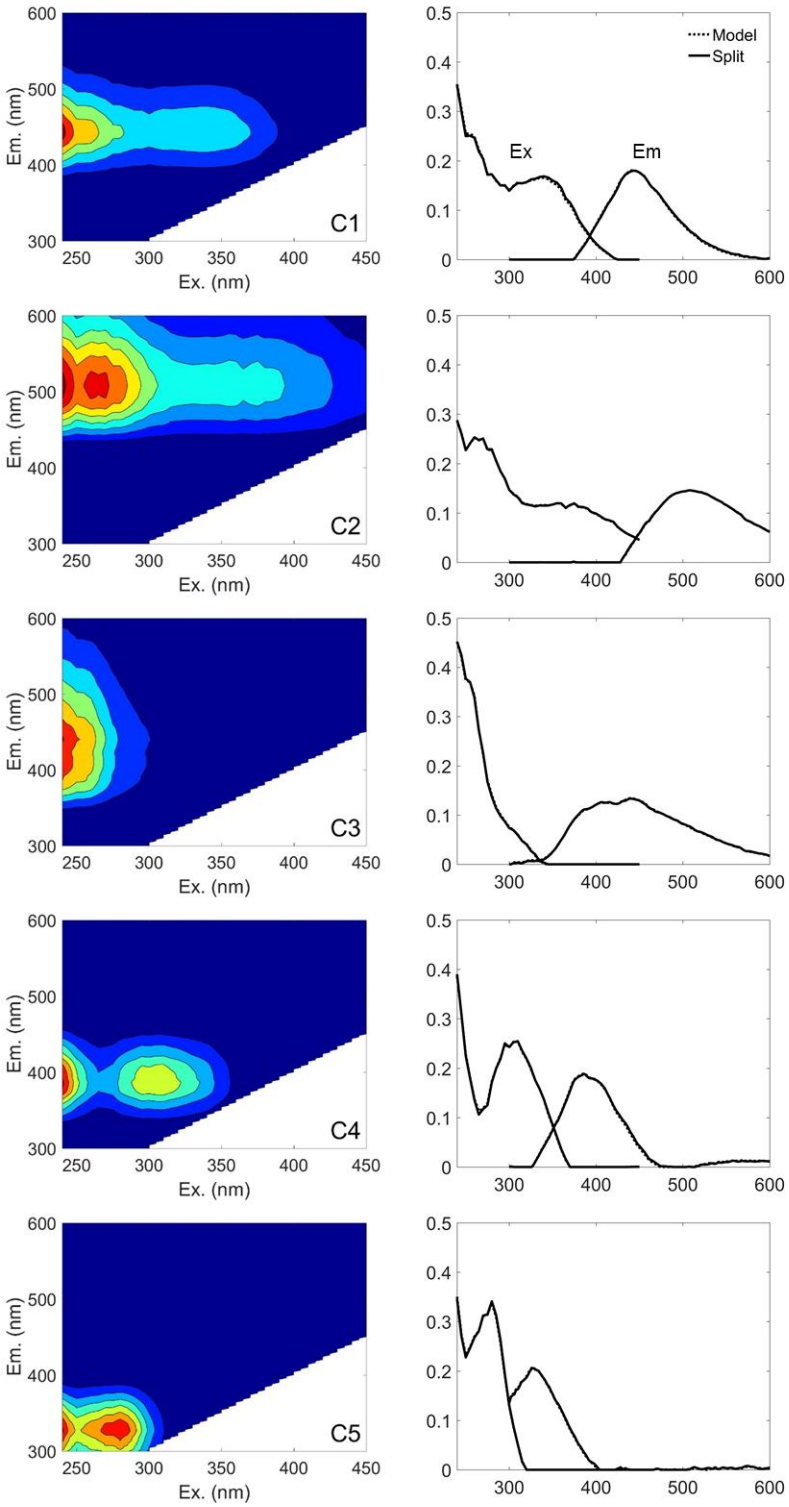

Figure A5.2. The five components identified (left) in the bioassay PARAFAC model developed on all DOM EEM bioassay samples. All five components were split half-validated; right hand panels show the excitation (Ex) and emission (Em) spectra for each component. Each EEM was normalized to its total fluorescence prior to modeling.

Table A5.3. Peak maxima and component designations (>95% match in OpenFluor) for all five identified PARAFAC components for the DOM EEM samples for all bioassay treatments.

	λex (nm)	**λem (nm)**	**Component Description**
C1	< 240	442	Terrestrial, humic-like. Associated with break-down of lignin and high OM loading (Guéguen et al., 2014; Lambert et al., 2016; Murphy et al., 2014; Stedmon et al., 2007).
C2	< 240, 275	508	Humic-acid, fulvic-like, terrestrial. Derived from soil leachate (Brym et al., 2014; Cawley et al., 2012; Graeber et al., 2012; Lambert et al., 2016; Murphy et al., 2014; Osburn et al., 2016, 2012; Stedmon and Markager, 2005; Stedmon et al., 2007; Yamashita et al., 2010b, 2010a).
C3	< 240	440	Humic-like. High molecular weight. Intermediate formed during degradation of terrestrial DOM (Kothawala et al., 2012; Osburn and Stedmon, 2011; Walker et al., 2009).
C4	< 240, 310	386	Microbial, humic-like. Microbially transformed, autochthonous DOM (Murphy et al., 2014; Osburn et al., 2011).
C5	< 240, 280	328	Protein peak. Combination of tryptophan and tyrosine (Cawley et al., 2012; Guéguen et al., 2014; Kowalczuk et al., 2010; Stedmon et al., 2007).

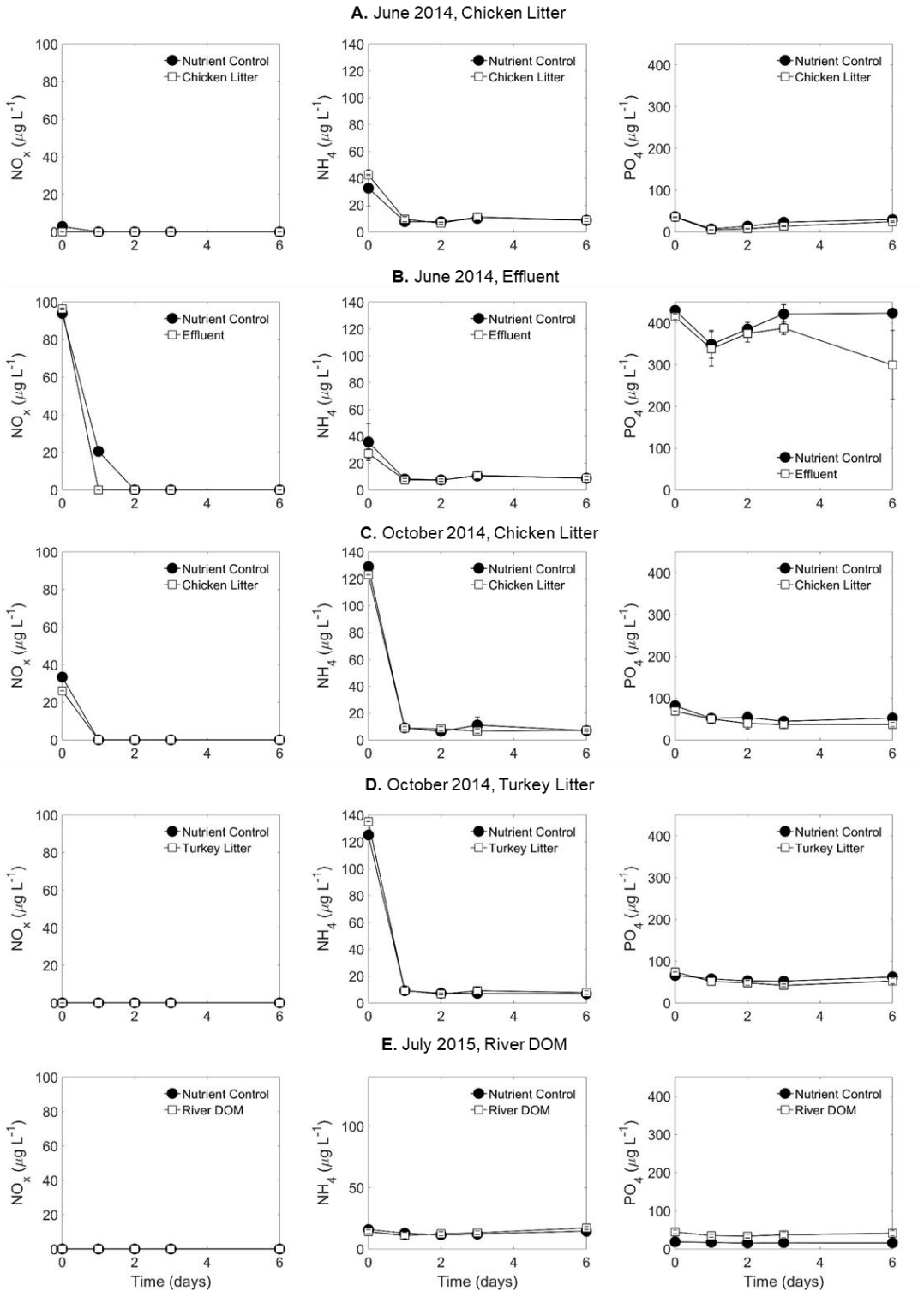

Figure A5.3. Inorganic nutrient concentrations as NO_x (µg L^{-1}), NH_4 (µg L^{-1}), and PO_4 (µg L^{-1}) plotted for each coupled DOM treatment for A. June 2014, chicken litter; B. June 2014, effluent, C. October 2014, chicken litter, D. October 2014, turkey litter, and E. July 2015, river DOM treatments. Black circles represent the inorganic nutrient addition. The white squares represent the coupled DOM addition treatment.

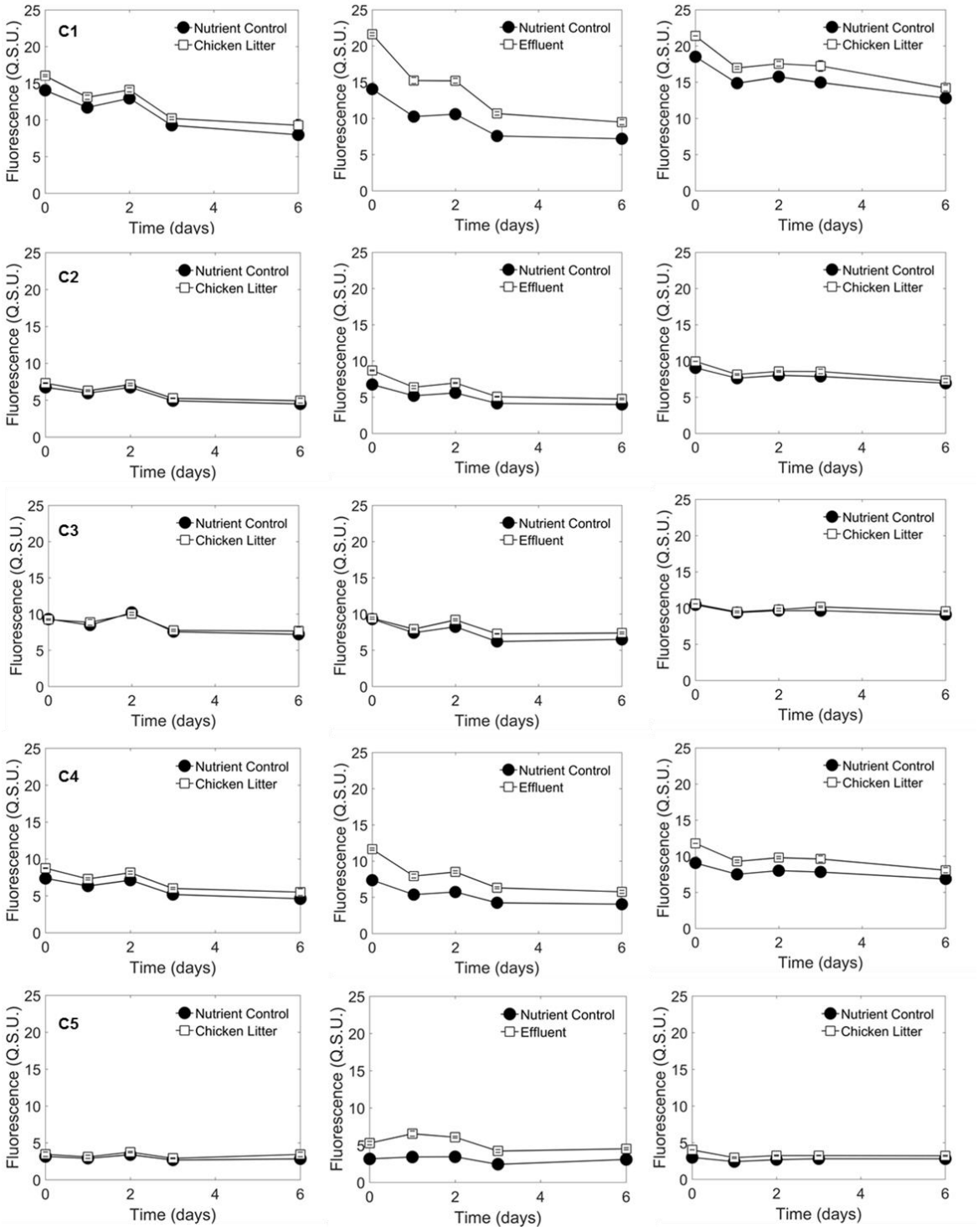

Figure A5.4. Fluorescence of the DOM PARAFAC components (C1, C2, C3, C4, and C5) plotted through the bioassay from day 0 to day 6 for the chicken litter leachate June 2014 treatment (left); effluent, June 2014 (middle); and chicken litter leachate, October 2014 (right). The nutrient addition treatment is displayed in the black circles and the corresponding DOM addition treatment is displayed in the white squares.

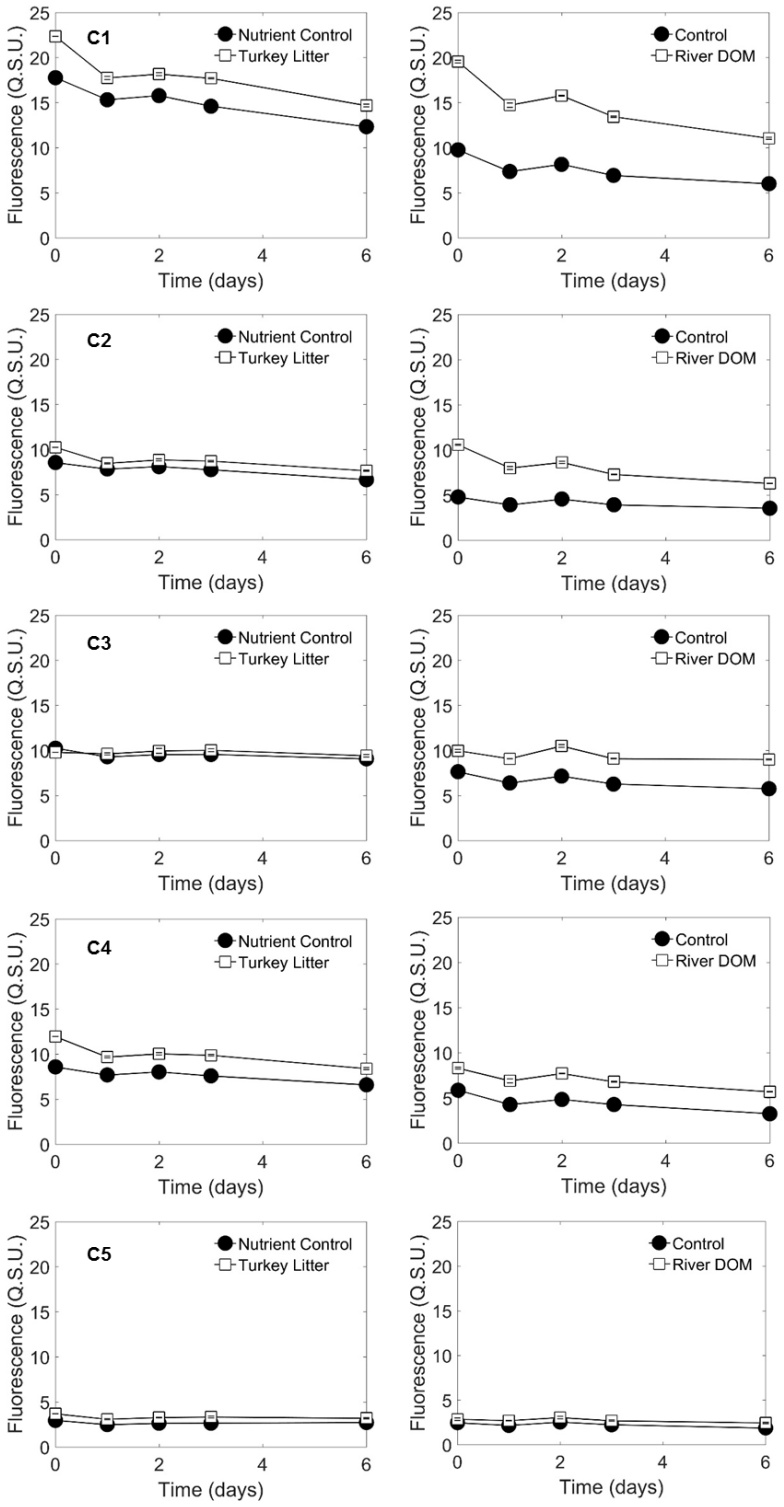

Figure A5.5. Fluorescence of the DOM PARAFAC components (C1, C2, C3, C4, and C5) plotted through the bioassay from day 0 to day 6 for the turkey litter leachate, October 2014 (left) and concentrated River DOM, July 2015 (right). The nutrient addition treatment is displayed in the black circles and the corresponding DOM addition treatment is displayed in the white squares.

Table A5.4. Results from the RM-ANOVA conducted on the coupled DOM addition and inorganic nutrient addition treatments for the five identified EEM-PARAFAC DOM components. Statistically significant p-values ($p < 0.05$) are highlighted in grey. The time column corresponds to differences through time, the treatment column corresponds to differences between the coupled treatments and the time*treatment column corresponds to differences between the two coupled treatments through time. For the October 2014 bioassay (both chicken litter and turkey litter treatments) only Day 1, 2, 3, and 6 were included in the RM-ANOVA as there were not enough replicates on Day 0 for inclusion in the analysis.

	June 2014 Chicken Litter			June 2014 Effluent		
	Time	Treatment	Time*Treatment	Time	Treatment	Time*Treatment
C1	<0.001	<0.001	0.057	<0.001	<0.001	<0.001
C2	<0.001	<0.001	0.459	<0.001	<0.001	<0.001
C3	<0.001	0.277	0.325	<0.001	<0.001	<0.001
C4	<0.001	<0.001	0.119	<0.001	<0.001	<0.001
C5	<0.001	0.006	0.472	<0.001	<0.001	<0.001
	October 2014 Chicken Litter			October 2014 Turkey Litter		
	Time	Treatment	Time*Treatment	Time	Treatment	Time*Treatment
C1	<0.001	<0.001	0.136	<0.001	<0.001	0.004
C2	<0.001	<0.001	0.409	<0.001	<0.001	0.014
C3	<0.001	0.005	0.009	<0.001	<0.001	0.943
C4	<0.001	<0.001	0.087	<0.001	<0.001	0.01
C5	<0.001	<0.001	0.061	<0.001	<0.001	0.119
	July 2015 River DOM					
	Time	Treatment	Time*Treatment			
C1	0.005	<0.001	0.032			
C2	0.004	<0.001	0.128			
C3	0.009	<0.001	0.358			
C4	0.037	<0.001	0.415			
C5	<0.001	0.004	0.185			

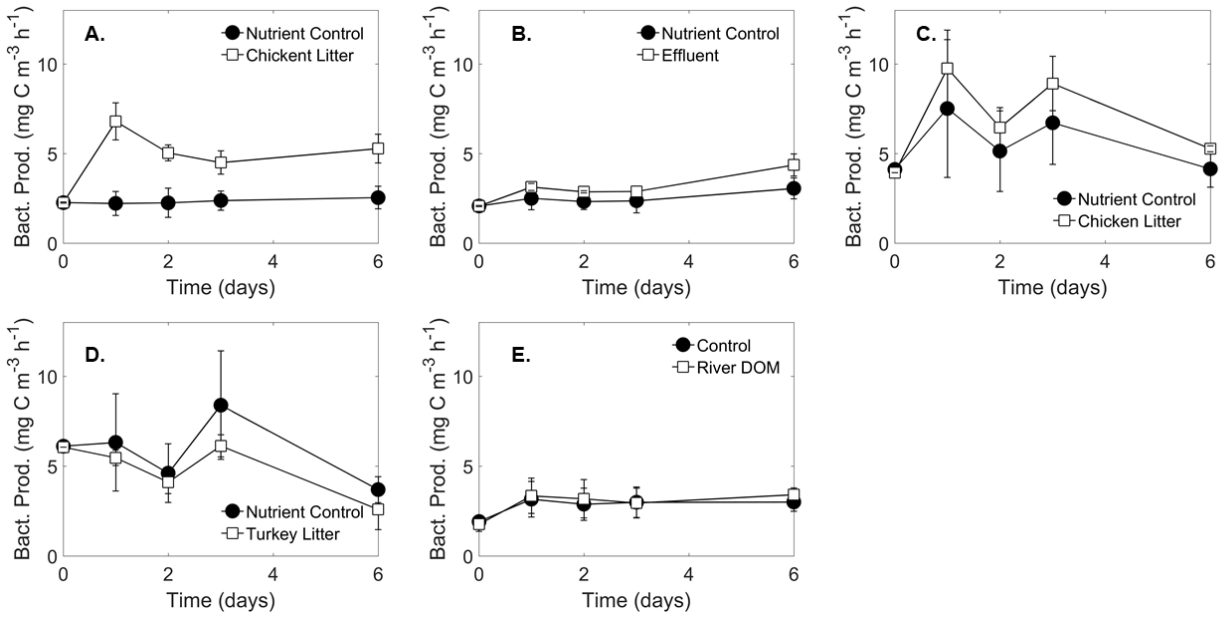

Figure A5.6. Bacterial productivity rates (mg C m^{-3} h^{-1}) plotted for each bioassay treatment. A. June 2014, chicken litter; B. June 2014, effluent; C. October 2014, chicken litter; D. October 2014, turkey litter; and E. July 2015, river DOM. Each nutrient control is plotted in the black circles and each coupled DOM source is plotted in the white squares.

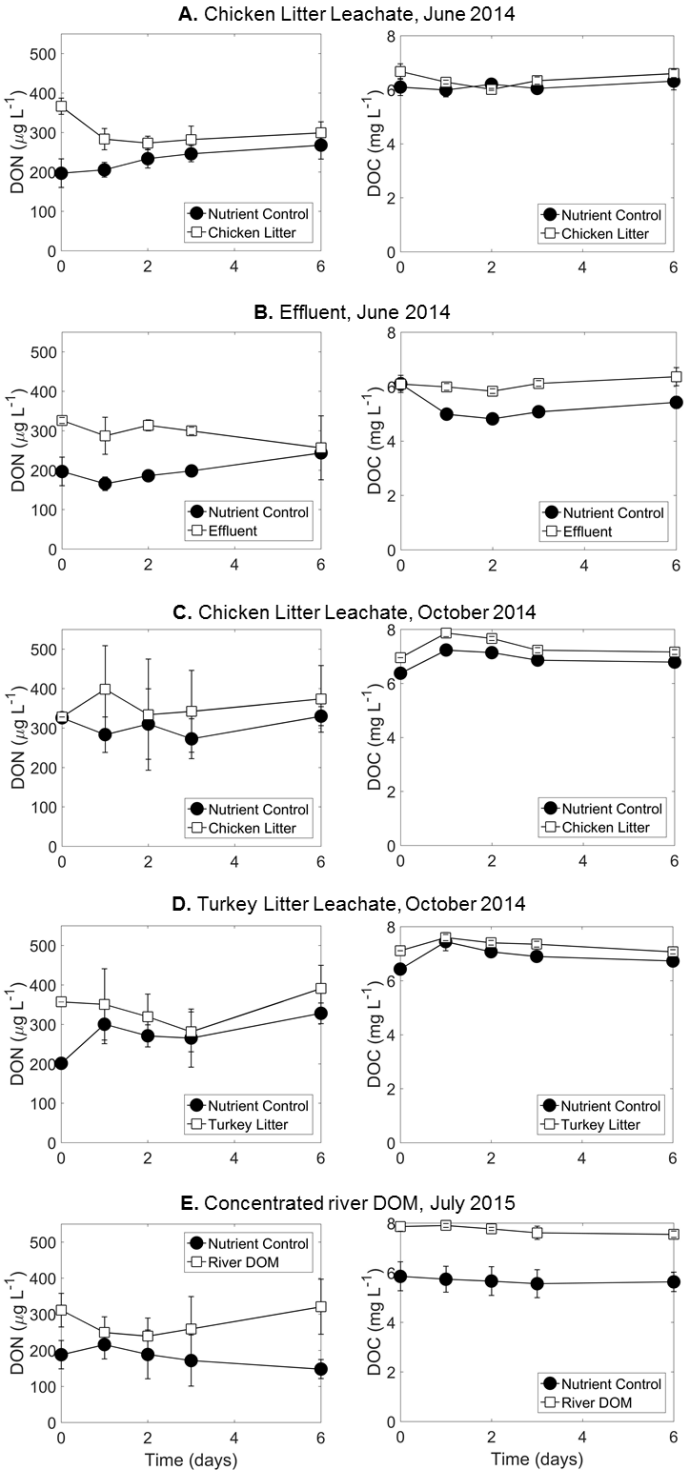

Figure A5.7. DON (µg L^{-1}) and DOC (mg L^{-1}) concentrations plotted for each coupled DOM treatment for A. June 2014, chicken litter; B. June 2014, effluent, C. October 2014, chicken litter, D. October 2014, turkey litter, and E. July 2015, river DOM treatments. Black circles represent the inorganic nutrient addition. The white squares represent the coupled DOM addition treatment.

Table A5.5. Results from the RM-ANOVA conducted on the coupled DOM addition and inorganic nutrient addition treatments for DON and DOC. Statistically significant p-values ($p < 0.05$) are highlighted in grey. The time column corresponds to differences through time, the treatment column corresponds to differences between the coupled treatments and the time*treatment column corresponds to differences between the two coupled treatments through time. For the October 2014 bioassay (both chicken litter and turkey litter treatments) only Day 1, 2, 3, and 6 were included in the RM-ANOVA as there were not enough replicates on Day 0 for inclusion in the analysis.

	June 2014 Chicken Litter			**June 2014 Effluent**		
	Time	Treatment	Time*Treatment	Time	Treatment	Time*Treatment
DON	0.026	0.002	0.001	0.774	0.026	0.001
DOC	0.007	0.029	0.066	<0.001	<0.001	<0.001
	October 2014 Chicken Litter			**October 2014 Turkey Litter**		
	Time	Treatment	Time*Treatment	Time	Treatment	Time*Treatment
DON	0.662	0.661	0.17	0.041	0.869	0.062
DOC	<0.001	0.056	<0.001	<0.001	0.35	<0.001

	July 2015 River DOM		
	Time	Treatment	Time*Treatment
DON	0.773	0.217	0.024
DOC	0.026	0.727	0.002

Table A5.6. Spearman's ρ calculated for each PARAFAC identified DOM component versus DON. All components were statistically, positively correlated with DON concentration.

Bioassay PARAFAC Model	ρ	p
C1	0.501	2.92E-12
C2	0.472	7.20E-11
C3	0.396	8.62E-08
C4	0.547	9.55E-15
C5	0.229	0.003
Residual PARAFAC Model		
C1	0.388	1.60E-07

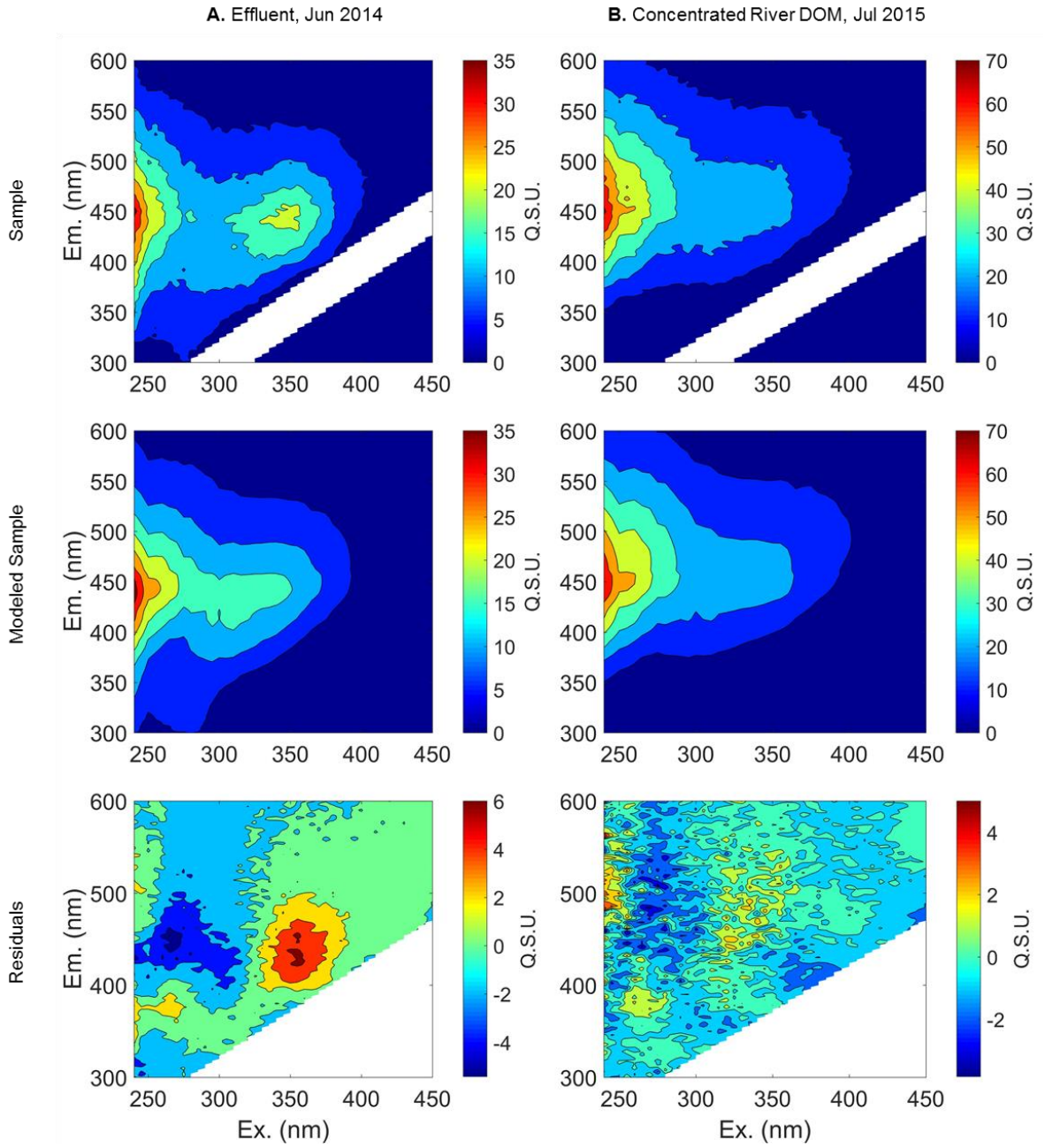

Figure A5.8. Sample EEM (top), PARAFAC modeled EEM (middle), and residual EEM (bottom) for DOM addition sources, A. effluent, June 2014 and B. concentrated river DOM, July 2015. Fluorescence is plotted as Quinine Sulfate Units (Q.S.U.).

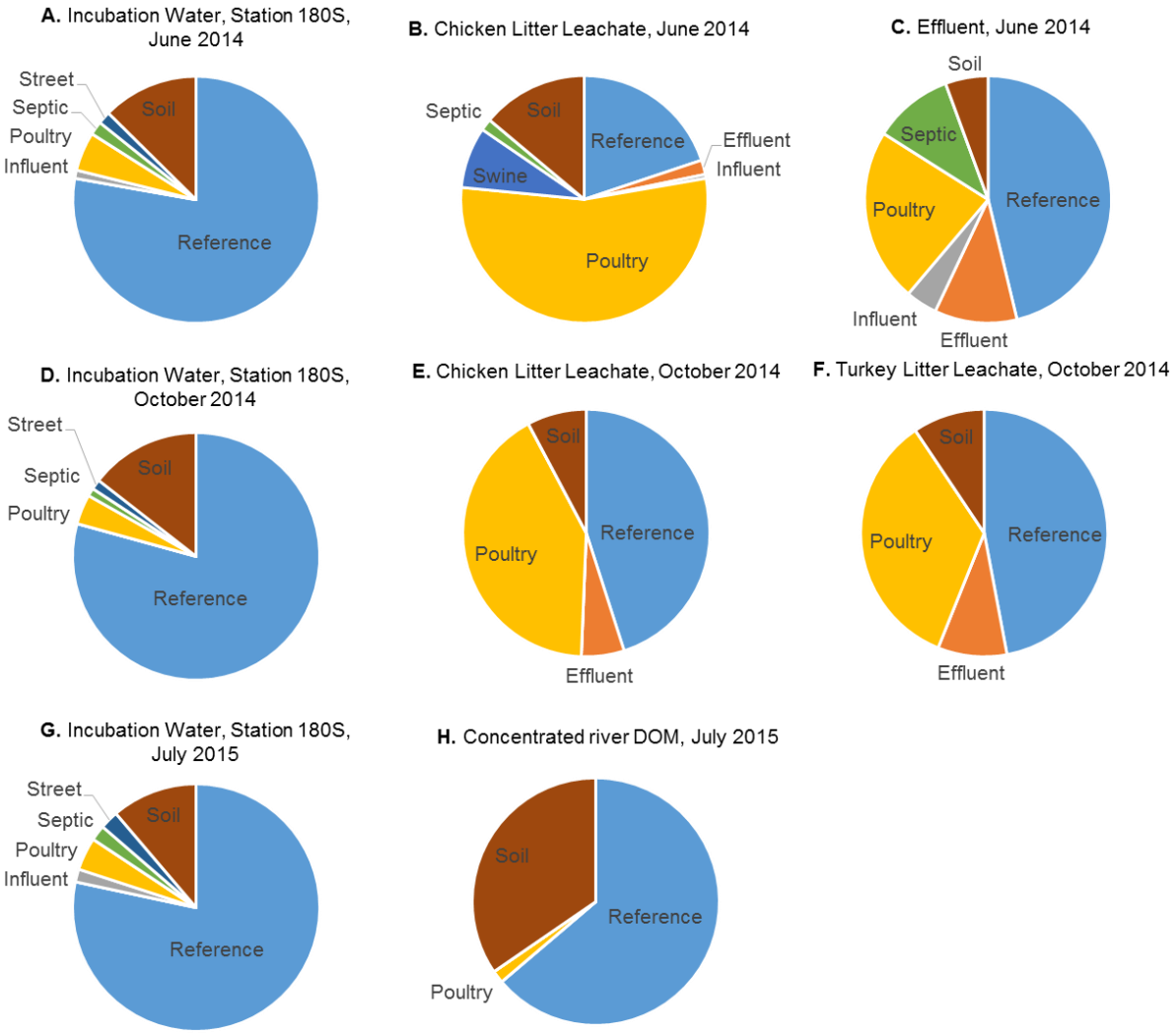

Figure A5.9. Results of FluorMod applied to source samples and incubation water for each bioassay. A. incubation water, Station 180S, June 2014; B. chicken litter leachate, June 2014; C. effluent, June 2014; D. incubation water, Station 180S, October 2014; E. chicken litter leachate, October 2014; F. turkey litter leachate, October 2014; G. incubation water, Station 180S, July 2015; and H. concentrated river DOM, July 2015.

Table A5.7. Results from the RM-ANOVA conducted on the coupled DOM addition and inorganic nutrient addition treatments for the identified residual component. All values were statistically significant. The time column corresponds to differences through time, the treatment column corresponds to differences between the coupled treatments and the time*treatment column corresponds to differences between the two coupled treatments through time. For the October 2014 bioassay (both chicken and turkey litter treatments) only Day 1, 2, 3, and 6 were included in the RM-ANOVA as there were not enough replicates of Day 0 for inclusion in the analysis.

	Residual Component		
	Time	**Treatment**	**Time*Treatment**
J14 Chicken Litter	<0.001	0.002	0.001
J14 Effluent	<0.001	0.03	<0.001
O14 Chicken Litter	<0.001	<0.001	<0.001
O14 Turkey Litter	<0.001	<0.001	0.009
J15 River DOM	0.003	0.023	0.002

REFERENCES

Brym, A., Paerl, H.W., Montgomery, M.T., Handsel, L.T., Ziervogel, K., Osburn, C.L., 2014. Optical and chemical characterization of base-extracted particulate organic matter in coastal marine environments. Marine Chemistry 162, 96–113. https://doi.org/10.1016/j.marchem.2014.03.006

Cawley, K.M., Ding, Y., Fourqurean, J., Jaffe, R., 2012. Characterising the sources and fate of dissolved organic matter in Shark Bay, Australia: a preliminary study using optical properties and stable carbon isotopes. Marine Freshwater Research 63, 1098–1107.

Graeber, D., Gelbrecht, J., Pusch, M.T., Anlanger, C.B, von Schiller, D.C, 2012. Agriculture has changed the amount and composition of dissolved organic matter in Central European headwater streams. Science of the Total Environment 438, 435–446. https://doi.org/10.1016/j.scitotenv.2012.08.087

Guéguen, C., Cuss, C.W., Cassels, C.J., Carmack, E.C., 2014. Absorption and fluorescence of dissolved organic matter in the waters of the Canadian Artic Archipelago, Baffin Bay, and the Labrador Sea. Journal of Geophysical Research: Oceans. 119, 2034–2047. https://doi.org/10.1002/2013JC009173.Received

Kothawala, D.N., Wachenfeldt, E. Von, Koehler, B., Tranvik, L.J., 2012. Selective loss and preservation of lake water dissolved organic matter fluorescence during long-term dark incubations. Science of the Total Environment 433, 238–246. https://doi.org/10.1016/j.scitotenv.2012.06.029

Kowalczuk, P., Cooper, W.J., Durako, M.J., Kahn, A.E., Gonsior, M., Young, H., 2010. Characterization of dissolved organic matter fluorescence in the South Atlantic Bight with use of PARAFAC model: Relationships between fluorescence and its components, absorption coefficients and organic carbon concentrations. Marine Chemistry 118, 22–36. https://doi.org/10.1016/j.marchem.2009.10.002

Lambert, T., Teodoru, C.R., Nyoni, F.C., Bouillon, S., Darchambeau, F., Massicotte, P., Borges, A. V, 2016. Along-stream transport and transformation of dissolved organic matter in a large tropical river. Biogeosciences 13, 2727–2741. https://doi.org/10.5194/bg-13-2727-2016

Murphy, K.R., Bro, R., Stedmon, C.A., 2014. Chemometric Analysis of Organic Matter Fluorescence, in: Aquatic Organic Matter Fluorescence. p. 339. https://doi.org/10.13140/2.1.2595.8080

Osburn, C.L., Handsel, L.T., Mikan, M.P., Paerl, H.W., Montgomery, M.T., 2012. Fluorescence tracking of dissolved and particulate organic matter quality in a river-dominated estuary. Environmental Science & Technology 46, 8628–8636. https://doi.org/10.1021/es3007723

Osburn, C.L., Handsel, L.T., Peierls, B.L., Paerl, H.W., 2016. Predicting Sources of Dissolved Organic Nitrogen to an Estuary from an Agro-Urban Coastal Watershed. Environmental Science & Technology 50, 8473–8484. https://doi.org/10.1021/acs.est.6b00053

Osburn, C.L., Stedmon, C.A., 2011. Linking the chemical and optical properties of dissolved organic matter in the Baltic–North Sea transition zone to differentiate three allochthonous inputs. Marine Chemistry 126, 281–294. https://doi.org/10.1016/j.marchem.2011.06.007

Osburn, C.L., Wigdahl, C.R., Fritz, S.C., Saros, J.E., 2011. Dissolved organic matter composition and photoreactivity in prairie lakes of the U.S. Great Plains. Limnology and Oceanography 56, 2371–2390. https://doi.org/10.4319/lo.2011.56.6.2371

Stedmon, C.A., Markager, S., 2005. Tracing the production and degradation of autochthonous fractions of dissolved organic matter using fluorescence analysis. Limnology and Oceanography 50, 1415–1426. https://doi.org/10.4319/lo.2005.50.5.1415

Stedmon, C.A., Markager, S., Tranvik, L., Kronberg, L., Slätis, T., Martinsen, W., 2007. Photochemical production of ammonium and transformation of dissolved organic matter in the Baltic Sea. Marine Chemistry 104, 227–240. https://doi.org/10.1016/j.marchem.2006.11.005

Walker, S.A., Amon, R.M.W., Stedmon, C., Duan, S., Louchouarn, P., 2009. The use of PARAFAC modeling to trace terrestrial dissolved organic matter and fingerprint water masses in coastal Canadian Arctic surface waters. Journal of Geophysical Research 114, 1–12. https://doi.org/10.1029/2009JG000990

Yamashita, Y., Maie, N., Briceño, H., Jaffé, R., 2010a. Optical characterization of dissolved organic matter in tropical rivers of the Guayana Shield, Venezuela. Journal of Geophysical Research 115, G00F10. https://doi.org/10.1029/2009JG000987

Yamashita, Y., Scinto, L.J., Maie, N., Jaffe, R., 2010b. Dissolved Organic Matter Characteristics Across a Subtropical Wetland's Landscape: Application of Optical Properties in the Assessment of Environmental Dynamics. Ecosystems 13, 1006–1019. https://doi.org/10.1007/s10021-010-9370-1